# NUMERICAL STUDY ON STABILITY OF MAGNETOHYDRODYNAMIC NANOFLUID FLOW THROUGH CHANNEL

by

## MD. SARWAR ALAM

Roll No. 0411094001,

Registration No. 0405409, Session: April 2011

## DOCTOR OF PHILOSOPHY

IN

MATHEMATICS



Department of Mathematics

BANGLADESH UNIVERSITY OF ENGINEERING AND TECHNOLOGY, DHAKA-1000

January 2016

The Thesis entitled

# NUMERICAL STUDY ON STABILITY OF MAGNETOHYDRODYNAMIC NANOFLUID FLOW THROUGH CHANNEL
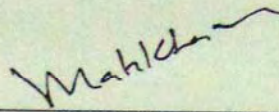
Submitted by

Md. Sarwar Alam

Roll No. 0411094001, Registration No. 0405409, Session: April 2011

has been accepted as satisfactory in partial fulfillment of the requirement for the degree of

**Doctor of Philosophy in Mathematics**

on 23 January, 2016.
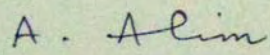
## Board of Examiners

1. _____

   **Dr. Md. Abdul Hakim Khan**                          Chairman

   Professor                                             (Supervisor)

   Department of Mathematics

   BUET, Dhaka-1000.


2. _____

   **Head**                                              Member
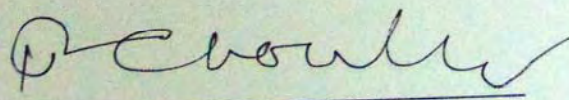
   Department of Mathematics                             (Ex-Officio)

   BUET, Dhaka-1000.


3. _____

   **Dr. Md. Mustafa Kamal Chowdhury**                   Member

   Professor

   Department of Mathematics

   BUET, Dhaka-1000.

4. _A. Alim_

**Dr. Md. Abdul Alim**
Professor
Department of Mathematics
BUET, Dhaka-1000.

Member

5. _Andallah_

**Dr. Laek Sazzad Andallah**
Professor
Department of Mathematics
Jahangirnagar University, Savar, Dhaka.

Member

6. _Rahman_

**Dr. Md. Munsur Rahman**
Professor
IWFM
BUET, Dhaka-1000.

Member

7. _Masheen_

**Dr. Md. Anwar Hossain**
Professor
University Grants Commission of Bangladesh
Agargaon, Sher-e-Banglanagar, Dhaka-1207.

Member
(External)

# Dedication

This work is dedicated to
My Parents

# Author's Declaration

I hereby declare that the work in this thesis was carried out in accordance with the Regulations of the Bangladesh University of Engineering and Technology. The work is original except where indicated by special reference in the text and no part of the dissertation has been submitted for any other degree at any other university or institution other than publications.

_____

Md. Sarwar Alam                                                   23 January, 2016

# Acknowledgements

# Abstract

The stability of steady two-dimensional laminar magnetohydrodynamic flow of viscous incompressible nanofluid through channel has been studied numerically. The basic governing equations in vector form for the flow and thermal field are expressed case by case. The extended governing equations with related boundary conditions are reduced to dimensionless form using appropriate transformations. The resultant nonlinear ordinary differential equations are then solved numerically employing power series with Hermite-Padé approximation scheme.

The effect of temperature dependent thermal conductivity on magnetohydrodynamic radiative flow of Cu-water nanofluid considering viscous dissipation through a vertical parallel channel has been analysed numerically. A stability analysis has been performed for the local rate of heat transfer which specifies the dual solution branch due to thermal conductivity criticality. The influences of the pertinent flow parameters on velocity and temperature profiles are represented graphically. The irreversibility of the system is also displayed in the form of entropy generation rates and Bejan profiles with the effects of flow parameters. A special case study is performed for the pure base water in absence of nanoparticles where the left wall of the channel is taken sliding with a uniform velocity.

The entropy generation on magnetohydrodynamic radiative variable thermal conductivity flow of optically thin viscous water-based three different nanofluids through a vertical porous channel is studied. The effect of porosity parameter together with other physical parameters on velocity and temperature distributions, thermal stability conditions and entropy generation of the system are discussed extensively both numerically and graphically.

The effects of Cu-water nanofluid on the entropy generation of the nonlinear magnetohydrodynamic Jeffery-Hamel flow through divergent channel are analysed. The dominating singularity behaviour of the problem is analysed numerically and graphically. The velocity profiles, temperature distributions and entropy generation rates with Bejan profiles are presented in divergent channel for various values of channel angle, flow Reynolds number along with other flow parameters.

Finally, the effects of three different nanoparticles on the stability of the magnetohydrodynamic nonlinear Jeffery-Hamel flow through convergent-divergent channel have been studied. The dominating singularity behaviour of the problem is analysed numerically and graphically for nanofluid. The alternation in the bifurcation diagram of channel semi-angle and flow Reynolds number due to the effect of various nanoparticles is observed. The critical relationships among the parameters are also performed qualitatively with the effect of different nanoparticles. On the other hand, the irreversibility of the system and the regular behavior of the flow are presented in both convergent and divergent channels for various values of the physical flow parameters.

Comparisons with available results stated in literature review are made and the results show excellent agreement.

# Contents

# Nomenclature

$B_0$          Magnetic field intensity

*Be*          Bejan number

*Br*          Brinkman number

*b*          Length of the parallel vchannel

$c_p$          Specific heat

$\underline{E}$          Electric field vector

*Ec*          Eckert number

$\underline{F}$          Body force per unit volume

*F*          Dimensionless stream function

*f*          Dimensionless velocity

*g*          Acceleration due to gravity

*Gr*          Grashof number

*Ha*          Hartmann number

*Nu*          Local Nusselt number

*N*          Dimensionless pressure gradient

$N_s$          Entropy generation rate

*P*          Dimensional pressure of the fluid

*p′*          Dimensional pressure of the fluid

*p*          Dimensionless pressure of the fluid

*Pr*          Prandtl number

*Pe*          Peclet number

| | |
|---|---|
| $Q$ | Volumetric flow rate |
| $q_r$ | Radiative heat flux per unit time |
| $R$ | Radiation parameter |
| $Re$ | Reynolds number |
| $Rs$ | Porosity parameter |
| $\bar{T}$ | Dimensional temperature of the fluid |
| $T_0$ | Temperature of the ambient fluid |
| $T_a$ | Temperature of the heated surface |
| $u', v'$ | Velocity components in $x', y'$ direction |
| $u, v$ | Dimensionless velocity components in $x, y$ direction |
| $x', y'$ | Cartesian coordinates |
| $x, y$ | Dimensionless Cartesian coordinates |
| $r, \varphi$ | Polar coordinates |

**Greek Symbols**

| | |
|---|---|
| $\alpha$ | Channel semi angle |
| $\beta$ | Co-efficient of thermal expansion |
| $\delta$ | Critical exponent |
| $\phi$ | Nanoparticles solid volume fraction |
| $\varphi$ | Dimensional angle of the channel |
| $\gamma$ | Mean radiation absorption coefficient |
| $\eta$ | Dimensionless angle of the channel |
| $\kappa$ | Thermal conductivity of the fluid |

| $\mu$ | Dynamical viscosity of the fluid |
|-------|----------------------------------|
| $\nu$ | Kinematic viscosity of the fluid |
| $\theta$ | Dimensionless temperature of the fluid |
| $\rho$ | Density of the fluid |
| $\sigma$ | Electrical conductivity of the fluid |
| $\tau$ | Thermal conductivity variation parameter |
| $\psi$ | Dimensional stream function |
| $\Phi$ | Viscous dissipation |

**Subscripts**

| $nf$ | Nanofluid |
|------|-----------|
| $f$ | Base fluid |
| $s$ | Nano-solid particles |

**Superscripts**

Prime (') Differentiation with respect to $\eta$

# Flow Chart of the Thesis

Stability of Magnetohydrodynamic Nanofluid flow through Channel

MHD Radiative flow of variable thermal conductivity Cu-water Nanofluid through vertical parallel channel

MHD Jeffery-Hamel flow through divergent channel with Cu-water Nanofluid

MHD Radiative variable thermal conductivity flow through vertical porous channel with different Nanoparticles

MHD Jeffery-Hamel flow through convergent-divergent channel with different Nanoparticles

Dominating singularity behavior of the problem and irreversibility of the system with regular pattern of the flow are studied

# List of Tables

# List of Figures

*In this chapter, the main terminologies used in the thesis are defined. The hydrodynamic stability and singularity in fluid flow are quantitatively discussed. A detailed review of the magnetohydrodynamics and nanofluids with applications is given. The general idea of the irreversibility in the system is also explained.*

## 1.1  Hydrodynamic Stability

Hydrodynamic stability concerns the stability and instability of motions of fluids according to Drazin (2002).  The concept of stability of a state of a physical or mathematical system was understood in the eighteenth century, and Clerk Maxwell Campbell & Garnett (1882) expressed the qualitative concept clearly in the nineteenth: *When an infinitely small variation of the present state will alter only by an infinitely small quantity the state at some future time, the condition of the system, whether at rest or in motion, is said to be stable; but when an infinitely small variation of the present state may bring about a finite difference in the state of the system in a finite time, the condition of the system is said to be unstable.*

So hydrodynamic stability is an important part of fluid mechanics, because an unstable flow is not observable. An unstable flow being in practice broken down rapidly by some 'small variation' or another. Also unstable flows often evolve into an important state of motion called *turbulence*, with a chaotic three dimensional vorticity field with broad spectrum of small temporal and spatial scales called *turbulence*.

The essential problems of fluid dynamics stability were recognized and formulated in the nineteenth century, notably by Helmholtz, Kelvin, Rayleigh and Reynolds. It is difficult to introduce these problems more clearly than in Osborne Reynolds's (1883) own description of his classic series of experiments on the instability of flow in a pipe. Reynolds went on to show that the laminar flow, the smooth flow through the pipe, breaks down when

$Va/\nu$ exceeds a certain critical value, $V$ being the maximum velocity of the water in the pipe, $a$ the radius of the pipe, and $\nu$ the kinematic viscosity of water at the appropriate temperature. This dimensionless number $Va/\nu$, now called the Reynolds number (*Re*). The series of experiments gave the critical value $\mathrm{Re}_c$ of the Reynolds number as nearly 13000. However, the critical velocity was very sensitive to disturbance in the water before entering the pipes. Different types of instabilities occur around us in daily aspects of life are shown in Figures 1.1-1.3.
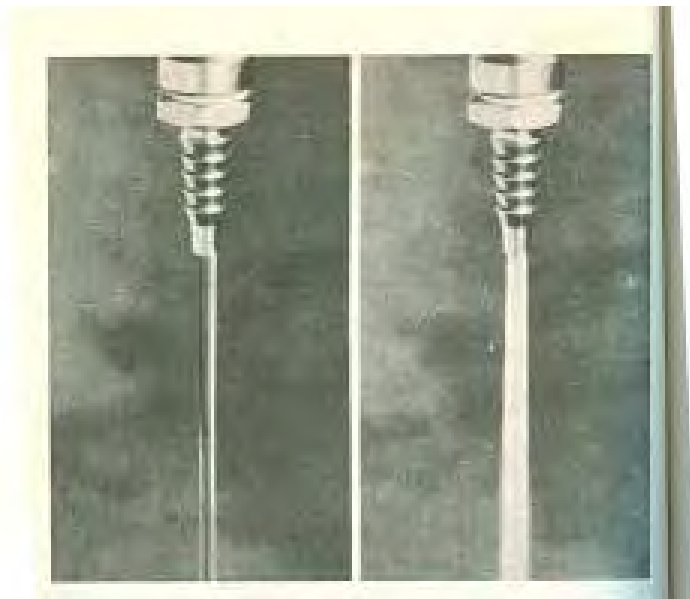


**Figure 1.1**: Water flow from a tap by V. Shankar (2014).

Unstable systems are not observed in nature, they have to be constructed. Usually the unstable systems *explode* and the explosion to occur sooner rather than later. We are interested in when and how laminar flows break down and eventually turn into turbulent flows. Singularities in the solution of problems of fluid dynamics can often be associated to hydrodynamic instability.

The modeling of physical phenomena usually results in nonlinear problems for some unknown function or functions depending on one or many variables. A value of the independent variable for which a function is unbounded or not unique locally is known as a

*singularity* of the function. In this thesis, as is commonly done in the literature, we shall sometimes also use the same word to refer to the *local behavior* of a *function* near a singularity. In the context of mathematical modeling, real singularities often have a physical interpretation. Hence their study is of great practical interest.

Very few nonlinear problems can be solved exactly, but it is sometimes possible to expand a solution in powers of some parameters. The summation of power series is widely used to approximate functions in many areas of mathematics. Particularly in the study of critical phenomena Guttmann (1981), the most valuable and widely used tool has been the calculation and analysis of series. Over the last quarter century, highly specialized techniques have been used to extract the series coefficients, and a variety of methods have been devised for extracting the required information on the singularities from a finite number of series coefficients. Series analysis plays an important role in many areas, particularly in fluid dynamics, where, as mentioned earlier, the presence of real singularities in the solution may reflect some change in the nature of the flow. This is the theme of the thesis.



**Figure 1.2**: Smoke from an incense stick by V. Shankar (2014).

### 1.1.1  Overview of series

Consider a function $u(x)$ which can be represented by a *power series*

$$U(x) = \sum_{i=0}^{\infty} a_i x^i \quad \text{as} \quad x \to 0. \tag{1.1.1}$$

Let us suppose the *Nth* partial sum is

$$U_N(x) = \sum_{i=0}^{N-1} a_i x^i \tag{1.1.2}$$

The series is said to be convergent if the sequence of the partial sums converges. When the series converges, the sum $U(x)$ can be approximated by the partial sum $U_N(x)$ and the error is defined by

$$e_N(x) = U(x) - U_N(x), \tag{1.1.3}$$
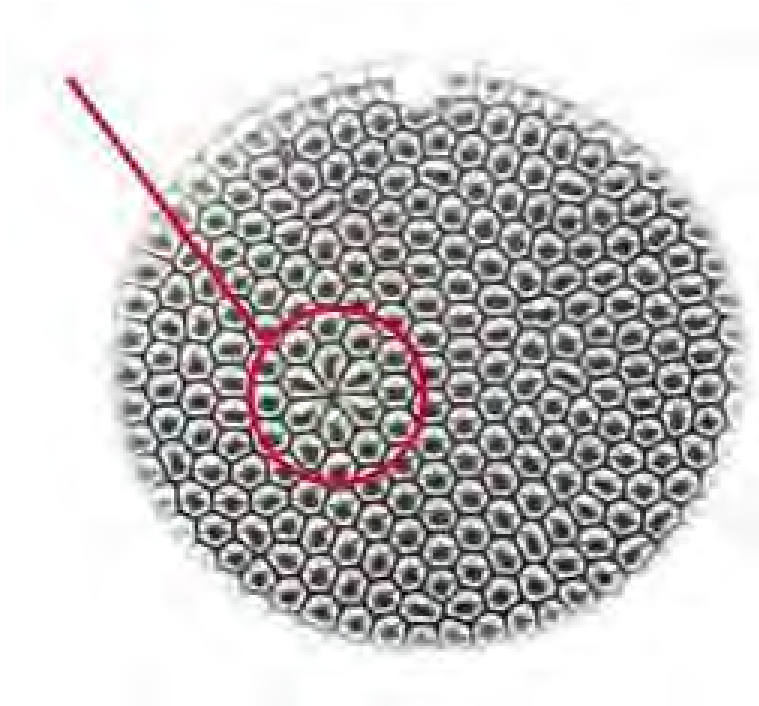


**Figure 1.3**: A layer heated liquid by V. Shankar (2014).

The absolute error is defined by

$$e_N'(x) = \left| \frac{e_N(x)}{U(x)} \right|, \text{ provided } U(x) \neq 0. \tag{1.1.4}$$

The number of accurate decimals for some particular value of $x$ is given by

$$\rho_N = -\log_{10}|e_N|.$$

It is said that the error decays exponentially if there exists a positive constant $\varepsilon$ such that $\varepsilon_N \to \varepsilon$ as $N \to \infty$, where

$$\varepsilon_N = -\frac{\ln|e_N|}{N}. \tag{1.1.5}$$

We say that the error decays superexponentially if there exists a positive constant $\varsigma$ such that $\varsigma_N \to \varsigma$ as $N \to \infty$, where

$$\varsigma_N = -\frac{\ln|e_N|}{N \ln N}. \tag{1.1.6}$$

An important characteristic of a series is its domain of convergence. If the series $U(x)$ converges for some $x_c$ it also converges absolutely in the open disc

$$\{x : x < |x_c|\}$$

with centre at the origin. The largest such disc is called the *disc of convergence* of the series and the radius, say $R$, of the disc is called the *radius of convergence* of the series $U(x)$.

## 1.1.2 Singularity analysis

Singularities are crucial points of a function, because the expansion of a function into a power series depends on the nature of singularities of the function. Several types of singularities may arise in physical (nonlinear) problems. For the purpose of this thesis, we are interested to analyze those functions, which have several types of singularities. Practically, one of these singularities dominates the function. Therefore it is important to know about this singular point to analyze the critical behavior of the function around this point. The rate of convergence of the sequence of partial sums depends crucially on the singularities of the function represented by the series. The *dominating* singularity behavior of the function $u(x)$ represented by a series may be written as

$$u(x) \sim \begin{cases} B + A\left(1 - \dfrac{x}{x_c}\right)^{\delta} & \text{when } \delta \neq 0, 1, 2,..........., \\[4mm] B + A\left(1 - \dfrac{x}{x_c}\right)^{\delta} \ln\left|1 - \dfrac{x}{x_c}\right| & \text{when } \delta = 0, 1, 2,..........., \end{cases} \qquad (1.1.7)$$

as $x \to x_c$, where $A$ and $B$ are some constants and $x_c$ is the *critical point* with the critical exponent $\delta$. If $\delta$ is a negative integer then the singularity is a pole; otherwise if it is a nonnegative rational number then the singularity is a branch point. We can include the correction terms with the dominating part in (1.1.7) to estimate the degree of accuracy of the critical points. It can be as follows

$$u(x) \sim A\left(1 - \frac{x}{x_c}\right)^{\delta}\left[1 + A_1\left(1 - \frac{x}{x_c}\right)^{\delta_1} + A_2\left(1 - \frac{x}{x_c}\right)^{\delta_2} + ...\right], \quad \text{as } x \to x_c \qquad (1.1.8)$$

Where $0 < \delta_1 < \delta_2 < ....$ and $A, A_1, A_2, .....$ are constants. If $\delta_i + \delta \notin N$ for some $i$, then the correction terms are called confluent. Sometimes the correction terms can be logarithmic. e.g.,

$$u(x) \sim A\left(1 - \frac{x}{x_c}\right)^{\delta}\left\{1 + A_1 \ln\left|1 - \frac{x}{x_c}\right|\right\} \quad \text{as} \quad x \to x_c . \qquad (1.1.9)$$

The sign pattern of the series coefficients may indicate the location of the singularity. If all the terms are positive or negative the dominant singular point lies on the positive *x*-axis. If the terms take alternately positive and negative signs then the singular point is on the negative *x*-axis. On the other hand, if the coefficients are periodic with period 4 then the dominant singularity may be on the imaginary x-axis. But in most problems of a physical origin, the series has an aperiodic sign pattern.

### 1.1.3  Elementary bifurcation theory

An investigation of some nonlinear problems in fluid dynamics is made in this thesis. The essences of the general forms of bifurcation, i.e., the common types of change of regime of flow, are introduced in this thesis. And these bifurcations occur where instability occurs will also be shown later. Solutions of nonlinear problems arising in the modeling of physical phenomena, often involve one or more parameters. A *bifurcation* occurs when a small

6

smooth change made to the parameter values (the bifurcation parameters) of a system causes a sudden 'qualitative' or topological change in its behaviour. The bifurcation occurs where the solution set of a nonlinear system alter their qualitative behavior at a certain value of the parameter. In particular, bifurcation theory shows how the number of steady solutions of a system depends on parameters. Examples of bifurcation are: Simple *turning points*, in which two real solutions become complex conjugate solutions, and *pitchforks*, in which the number of real solutions changes discontinuously from one to three (or vice versa). We intend to discuss some basic concepts of bifurcation theory.
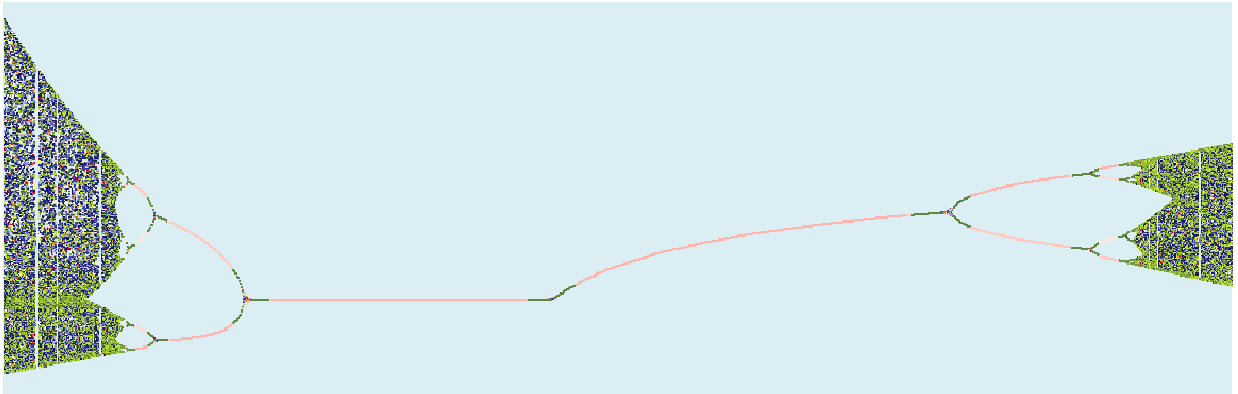


**Figure 1.4**: Period-halving bifurcations (L) leading to order, followed by period doubling bifurcations (R) leading to chaos. (Image source: Wikipedia website)

Consider a functional map $F : \Re \times \Re \to \Re$. We seek for the solutions $u = U(x)$ of

$$F(x, u) = 0. \tag{1.1.10}$$

The solutions can be visualized by means of a *bifurcation diagram* in which the solution curves are drawn in the $(x, u)$-plane. Let $(x_0, u_0)$ be a solution of equation (1.1.10), i.e.

$$F(x_0, u_0) = 0 \tag{1.1.11}$$

then, $F$ can be expanded in a Taylor series about $(x_0, u_0)$ and we can study the solution set in that neighborhood provided that $F$ is smooth. Thus we obtain

$$0 = F(x, u)$$

$$= F(x_0, u_0) + (u - u_0) F_u(x_0, u_0) + (x - x_0) F_x(x_0, u_0) + \frac{1}{2}(u - u_0)^2 F_{uu}(x_0, u_0) + \dots \tag{1.1.12}$$

If, we assume that, $F_u(x_0, u_0) \neq 0$, then

$$u(x) = u_0 - (x - x_0)\frac{F_x(x_0, u_0)}{F_u(x_0, u_0)} + O(x - x_0), \qquad \text{as } x \to x_0. \tag{1.1.13}$$

This gives only one solution curve in the neighborhood of the point $(x_0, u_0)$ in the bifurcation diagram. However, if $(x_0, u_0)$ is replaced with $(x_c, u_c)$, where

$$F(x_c, u_c) = 0, \quad F_u(x_c, u_c) = 0, \tag{1.1.14}$$

then the expansion (1.1.12) shows that there are at least two solution curves in the neighborhood of $(x_c, u_c)$. The point $(x_c, u_c)$ is called a *bifurcation point*. The formation of the bifurcation diagram in the neighbourhood of a bifurcation point depends on the first term of the Taylor series (1.1.12) that does not vanish. Although the solutions cannot be expanded in a Taylor series in that neighbourhood, it is often possible to expand them in a *fractional power series* of the form

$$u = \sum_{n=0}^{\infty} u_n (x - x_c)^\delta \tag{1.1.15}$$

for some $\delta \in Q$

A *period halving bifurcation* is a bifurcation in which the system switches to a new behavior with half the period of the original system. A series of period-halving bifurcations leads the system from chaos to order. A *period doubling bifurcation* is a bifurcation in which a slight change in a parameter value in the system's equations leads to the system switching to a new behavior with twice the period of the original system. Figure 1.4 represents the cases of Phillips curve that period halving bifurcations turning to order and then period doubling bifurcations leading to chaos.

***Example 1.1***: *A turning point.* Consider a simple model problem for descriptive purposes, or 'toy' problem from Drazin (2002), the quadratic equation

$$x - l(V - V_0)^2 = 0,$$

where $x = h(\text{Re} - \text{Re}_c)$, for some constants $h > 0, l \neq 0, V_0$. Here $V$ may be considered as representing a given component of the velocity of the fluid at some point of a steady flow as a function of the Reynolds number $Re$ and $\text{Re}_c$ is the critical value of $Re$. A toy problem can

be helpful to know about a complicated property of fluid motion if the simple toy problem describes that property. Then

$$V = V_0 \pm \sqrt{h(\mathrm{Re}-\mathrm{Re}_c)/l} \ .$$

There are two solutions when $h(\mathrm{Re}-\mathrm{Re}_c)/l > 0,$ one when $\mathrm{Re}=\mathrm{Re}_c,$ and none when $h(\mathrm{Re}-\mathrm{Re}_c)/l < 0.$ In Figure 1.5, the velocity $V$ is plotted against $Re$ for the case $hl > 0.$ It is seen that there is a *simple turning point, fold or a saddle-node bifurcation* at $\mathrm{Re}=\mathrm{Re}_c,$ $V = V_0.$ This is called a *bifurcation point* because the number (and behaviour) of the solutions changes there.
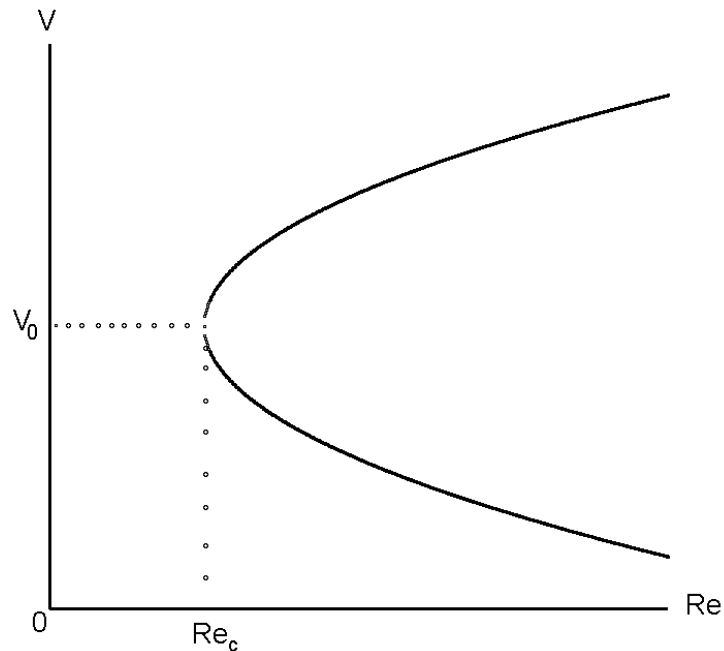


**Figure 1.5**: The bifurcation diagram for the turning point in the (*Re, V*)-plane for the case $l > 0.$

***Example 1.2:*** A *transcritical bifurcation.* As another very simple model of bifurcation of solution of steady flow, the following quadratic equation is considered

$$xV - lV^2 = 0,$$

Then

$$V = 0 \ \text{ or } \ V = x/l = h(\mathrm{Re}-\mathrm{Re}_c)/l \,,$$

Hence there are two solutions for all $\text{Re} \neq \text{Re}_c$. There is a bifurcation at $\text{Re} = \text{Re}_c$, $V = 0$ which is an example of a *transcritical point* shown in Figure 1.6 below.
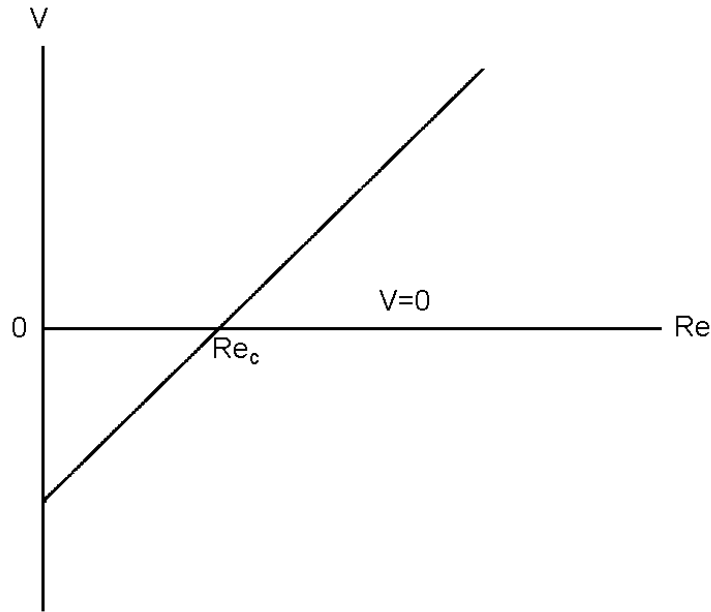


**Figure 1.6**: The bifurcation diagram for the transcritical point in the (*Re, V*)-plane for the case $l > 0$.

***Example 1.3:*** *Pitchfork bifurcation.* Consider the model equation

$$xV - lV^3 = 0,$$

which is typical for the first bifurcation of flows with symmetry in $\pm V$. Then

$$V = 0, \text{ or } V = \pm\sqrt{h(\text{Re}-\text{Re}_c)/l} \text{ if } h(\text{Re}-\text{Re}_c)/l > 0.$$

The bifurcation at $\text{Re} = \text{Re}_c$, $V = 0$ is said to be *pitchfork bifurcation.* It is observed that there is symmetry breaking at $\text{Re} = \text{Re}_c$, in the sense that if $hl > 0$, then there is a unique symmetric solution for $\text{Re} < \text{Re}_c$, but there is also a pair of asymmetric solutions for $\text{Re} > \text{Re}_c$ which is seen in Figure 1.7.
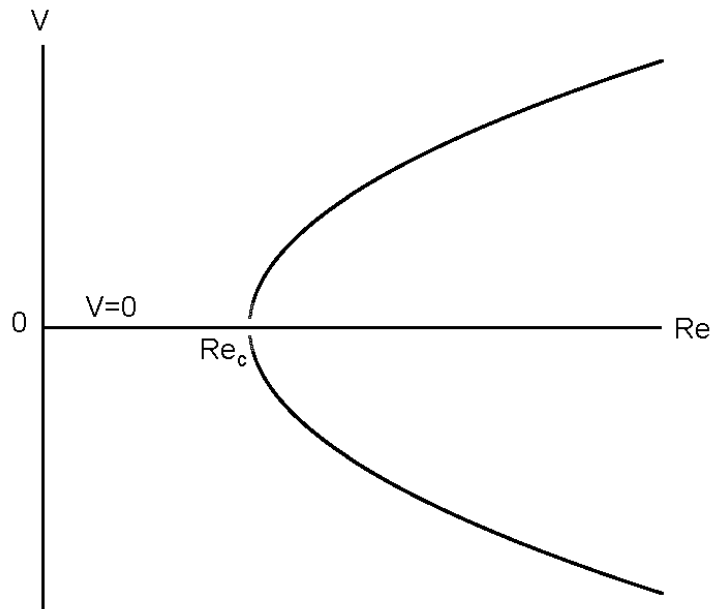
**Figure 1.7**: The bifurcation diagram for the pitchfork in the (*Re, V*)-plane for the case $l > 0$.

## 1.2  Magnetohydrodynamics (MHD)

Magnetohydrodynamics (MHD) is the branch concerned with the dynamics of electrically conducting fluids in a magnetic field. These fluids include salt water, liquid metals (such as Mercury, gallium, molten Iron) and ionized gases or plasmas (such as solar atmosphere). The term MHD is comprised of the words magneto – meaning magnetic, hydro – meaning fluids, and dynamics – meaning movement. The field of MHD was initiated by the Swedish Physicist Hannes Alfvén (1908-1995), who received the Nobel Prize in Physics in 1970 for fundamental work and discoveries in magnetohydrodynamics with fruitful applications in different parts of plasma physics.

Magnetohydrodynamics exhibits the phenomena, where, in an electrically conducting fluid, the velocity field $\underline{V}$ and the magnetic field $\underline{B}$ are coupled. The magnetic field induces an electric current of density $\underline{j}$ in the moving conductive fluid (electromagnetism). The induced current creates forces on the liquid and also changes the magnetic field. Each unit volume of the fluid having magnetic field $\underline{B}$ experiences an MHD force $\underline{j} \times \underline{B}$ known as Lorentz force. This Lorentz force tends to oppose the fluid motion near the leading edge. As

11

the velocity is very small, so that the magnetic force that is proportional to the magnitude of the longitudinal velocity and acts in the opposite direction is also very small. The set of equations which describe MHD flows are a combination of Navier-Stokes equation of fluid dynamics and Maxwell's equations of electromagnetism.

### 1.2.1 Application of MHD

Many natural phenomena and engineering problems are susceptible to MHD analysis. In natural phenomena, since magnetic field exists everywhere in the world, it follows that MHD phenomena must occur whenever conducting fluids are available. Electrically conducting fluids are abundant in nature, although their conductivities vary greatly. On the other hand, MHD is of special technical significance because of its frequent occurrence in many industrial applications such as MHD generators, pumps, cooling of nuclear reactors, geothermal energy extractors, thermal insulators, nuclear waste disposal, heat exchangers, petroleum and polymer technology, and heat transfers involving metallurgical processes.

### 1.3 Heat Transfer

Heat can be defined as the form of energy that is transferred from one system to another as a result of temperature difference. The science that deals with the determination of the *rates* of such energy transfers is the *heat transfer*. Temperature variations may exist within a fluid because of temperature differences between boundaries or between a boundary and an ambient fluid. Temperature variations can also arise from a variety of causes such as radioactivity, absorption of thermal radiation and release of latent heat as fluid vapor condenses. Heat transfer is the generation, exercise, conversion and exchange of thermal energy and heat between the physical systems which occurs as a result of a temperature gradient. Heat transfer is commonly encountered in engineering systems and daily features of life. There are three modes of heat transfer: conduction, convection and radiation. The heat transfer by thermal radiation in the flow through channel is studied in this thesis.
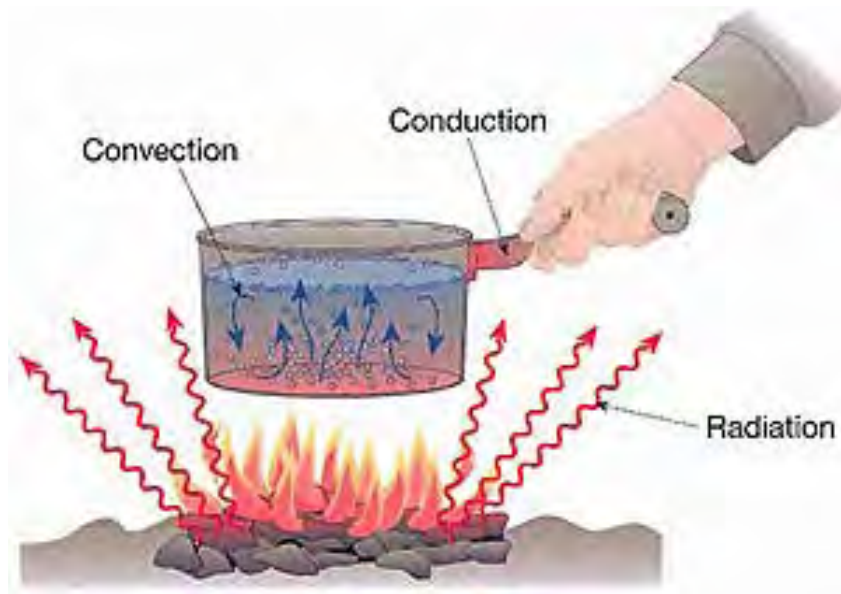
**Figure 1.8:** Combined conduction, convection and radiation heat transfer (Image source: Wikipedia)

### 1.3.1 Thermal Radiation

The theoretical foundation of radiation was established in 1864 by physicist James Clerk Maxwell, who postulated that accelerated charges or changing electric currents give rise to electric and magnetic fields. These rapidly moving fields are called electromagnetic waves. Thermal radiation process by which energy, in the form of electromagnetic waves, is emitted by a heated surface in all directions and travels directly to its point of absorption at the speed of light; thermal radiation does not require an intervening medium to carry it. Also, radiation transfer occurs in solids as well as liquids and gases. Thermal radiation ranges in wavelength from the longest infrared rays through the visible-light spectrum to the shortest ultraviolet rays. The intensity and distribution of radiant energy within this range is governed by the temperature of the emitting surface. The total radiant heat energy emitted by a surface is proportional to the fourth power of its absolute temperature (the Stefan–Boltzmann law).

The rate at which a body radiates (or absorbs) thermal radiation depends upon the nature of the surface as well. Objects that are good emitters are also good absorbers (Kirchhoff's radiation law). A blackened surface is an excellent emitter as well as an excellent absorber. If the same surface is silvered, it becomes a poor emitter and a poor absorber. A blackbody is one that absorbs all the radiant energy that falls on it. Such a perfect absorber would also

be a perfect emitter. The heating of the Earth by the Sun is an example of transfer of energy by radiation. The heating of a room by an open-hearth fireplace is another example. Radiation plays an important role in a variety of heat transfer systems. Combustion processes associated with furnaces, ovens, and internal combustion engines are strongly influenced by radiation heat transfer. Radiation is important in energy production systems, such as boilers and nuclear reactors. Radiation plays a major role in the cooling of electronics in high altitude aircraft, where convection effects are weak due to low air density.

### 1.3.2  Temperature dependent Thermal Conductivity

Thermal conductivity of a material can be defined as the rate of heat transfer through a unit area per unit temperature difference. The thermal conductivity of a material is a measure of the ability of the material to conduct heat. However, it is known that this physical property may change significantly with temperature. When the variation of thermal conductivity with temperature in a particular temperature interval is large, however, it may be necessary to account for this variation to minimize the error. For a liquid, it has been found that the thermal conductivity $\kappa$ varies with temperature in an approximately linear manner in the range from 0 to $400^0$F, as Kay (1966). For example, $\kappa = 0.607$ W/m $^0$C for water and $\kappa = 80.2$ W/m $^0$C for iron at room temperature, which indicates that iron conducts heat more than 100 times faster than water can. Thus it implies that water is a poor heat conductor relative to iron, although water is an excellent medium to store thermal energy. Note that material such as copper and silver that are good electric conductors, and have high values of thermal conductivity. Accounting for the variation of the thermal conductivity with temperature, in general, complicates the analysis. But in simple one-dimensional case, heat transfer relations can be obtained in a straightforward manner.

When the variation of thermal conductivity with temperature $\kappa(T)$ is known, the average value of the thermal conductivity in the temperature range between $T_1$ and $T_2$ can be determined from

$$\kappa_{avg} = \frac{\int_{T_1}^{T_2} \kappa(T)dT}{T_2 - T_1}$$

This relation is based on the requirement that the rate of heat transfer through a medium with constant average thermal conductivity $\kappa_{avg}$ equals the rate of heat transfer through the same medium with variable conductivity $\kappa(T)$. The variation in the thermal conductivity of a material with temperature in the temperature range of interest may often be approximated as a linear function and expressed as

$$\kappa(T) = \kappa_0(1 + \tau T)$$

where $\tau$ is called the temperature coefficient of thermal conductivity.

## 1.4  Nanofluids

Fluid is a substance that deforms continuously under the application of shear stress. Convectional heat transfer fluids such as water, minerals oil and ethylene glycol play an important role in many industrial sectors including power generation, chemical production, air-conditioning, transportation and microelectronics. Although various techniques have been applied to enhance their heat transfer, their performance is often limited by their low thermal conductivities which obstruct the performance enhancement and compactness of heat exchangers.  For example, copper (Cu) has a thermal conductivity 700 times greater water and 3000 times greater than engine oil. With the rising demands of modern technology for process intensification and device miniaturization, there is need to develop new types of fluids that are more effective in terms of heat exchange performance. In order to achieve this, it has been recently proposed to disperse small amounts of nanometer-sized (10-50 nm) solid particles (nanoparticles) in base fluids, resulting into what is commonly known as nanofluids. The term "nanofluid" was coined by Choi (1995) who was working with the group at the Argonne National Laboratory (ANL), USA, in 1995. The nanoparticles used are ultrafine, therefore, nanofluids appear to behave more like a single-phase fluid than a solid-liquid mixture. The commonly used materials for nanoparticles made of chemically stable metals (Al, Cu, Ag, Au, Fe), nonmetals (graphite, carbon nanotubes), oxides ceramics ($Al_2O_3$, CuO, $TiO_2$, $SiO_2$), carbides (SiC), layered (Al+, $Al_2O_3$, Cu+C). The base fluids is

usually a conductive fluid, such as water, (or other coolants), oil (and other lubricants), polymer solutions, bio-fluids and other common fluids, such as paraffin. Some advantages of nanofluids which make them useful are a tiny size, along with a large specific surface area, less clogging and abrasion. Investigations have shown that nanofluids possess enhanced thermophysical properties such as thermal conductivity, thermal diffusivity, viscosity and convective heat transfer coefficients compared to those of base fluids like oil or water done by Choi (2009), Yu et al. (2008), Tyler et al. (2006), Das et al. (2006), Liu et al. (2005), Choi et al. (2004). There are two techniques used in production of nanofluids; the single-step method in which nanoparticles are evaporated directly into the base fluid and the two-step method in which nanoparticles are first prepared by either the inert gas condensation technique or chemical vapor deposition method and then dispersed into the base fluid.

Studies have shown that the particle volume fraction, which is the volumetric concentration of the nanoparticles in the nanofluid has effects on the thermal conductivity of the nanofluid. Experimental results of nanofluids with small nanoparticles volume fractions showed that thermal conductivity significantly increased when compared to the base fluid. Masuda et al. (1993) measured the thermal conductivity of nanofluids containing $Al_2O_3$ (13 nm), $SiO_2$ (12 nm), and $TiO_2$ (27 nm) nanoparticles, with water as the base fluid. They observed an enhancement of 32.4% for the effective thermal conductivity of 4.3% volume of Alumina-water nanofluid at $31.85^\circ C$.

### 1.4.1 Nanoparticles solid volume fraction

The volume fraction $\phi$ is defined as the volume of a nanoparticles divided by the volume of all constituents of the nanofluid. The volume fraction coincides with the volume concentration in ideal solutions where the volumes of the constituents are additive (the volume of the solution is equal to the sum of the volumes of its ingredients).
The sum of all volume fractions of a mixture is equal to 1:

$$\sum_{i=1}^{N} \phi_i = 1$$

**1.4.2 Application of Nanofluids**

Nanofluids have an unprecedented combination of the four characteristic features desired in energy systems (fluid and thermal systems); increased thermal conductivity at low nanoparticle concentrations, Strong temperature dependent thermal conductivity, non-linear increase in thermal conductivity with nanoparticles concentration and increase in boiling critical heat flux. These distinctive features enhance nanofluid's potential applications to improve heat transfer and energy efficiency in industrial and engineering areas including industrial coolants, smart fluids, nuclear reactors coolant, extraction of geothermal power, nanofluids in automobile fuels, brake fluids, car radiator coolant, microelectronics cooling, bio and pharmaceutical industry as Wang and Fan (2010), Kaufui and Omar (2010), Senthilraja et al. (2010).

➢ Generally, industrial coolants are used in public utilities; the oil and gas industry, the food and beverage processing industry, the chemicals and plastics industry, solar energy conversion to electricity and in buildings for heating, ventilation, and air conditioning (HVAC) systems.

➢ In case of energy saving and the widespread use of battery operated devices, such as cell phones and laptops, have accented the necessity for a smart technological handling of energetic resources. Smart materials have one or more properties that can be dramatically altered, eg, smart material with variable viscosity may turn from a fluid which flows easily to a solid. Nanofluids have been demonstrated to be able to handle this role in some instances as a smart fluid.

➢ When extracting energy from the earth's crust that varies in length between 5 to 10 km and temperature between $500^{0}$C and $1000^{0}$C, nanofluids can be employed to cool the pipes exposed to such high temperatures. When drilling, nanofluids can serve in cooling the machinery and equipment working in high friction and high temperature environment.

➢ A principal limitation on developing smaller high density microchips is the heat dissipation problem. Advanced electronic devices face thermal management

challenges from the high level of heat generation and the reduction of available surface area for heat removal. Nanofluids can be used for liquid coolant of computer processors due to their high thermal conductivity and increased heat transfer coefficient.

➢ Nanofluids are been used in automobile for applications such as coolant, fuel additives, lubricant, shock absorber and refrigerant. The current engine oils, automatic transmission fluids, lubricants, and other synthetic high temperature heat transfer fluids found in conventional truck thermal systems radiators, engines heating, ventilation and air-conditioning (HVAC) have inherently poor heat transfer properties. These could benefit from the high thermal conductivity offered by nanofluids.

➢ Cryosurgery is a procedure that uses freezing to destroy undesired tissues. Although, it cannot be regarded as a routine method for cancer treatment, Cryosurgery is becoming a popular alternative to traditional therapies because of its important clinical advantages. According to simulations performed by Yan and Liu (2008), intentional loading of nanoparticles with high thermal conductivity into the target tissues can reduce the final temperature, increase the maximum freezing rate, and enlarge the ice volume obtained in the absence of nanoparticles. The concepts of nanocyrosurgery may offer new opportunities for future tumor treatment.

## 1.5  The second law of Thermodynamics

The first law of thermodynamics provides the basic definition of thermodynamic energy, also called internal energy, associated with all thermodynamic systems, but unknown in classical mechanics, and states the rule of conservation of energy in nature. The concept of energy in the first law does not, however, account for the observation that natural processes have a preferred direction of progress. The first law is symmetrical with respect to the initial and final states of an evolving system. But the second law asserts that a natural process runs only in one sense, and is not reversible. For example, heat always flows spontaneously from hotter to colder bodies, and never the reverse, unless external work is performed on the system. The key concept for the explanation of this phenomenon through the second law of

thermodynamics is the definition of a new physical quantity, the entropy. It also states that all spontaneous processes, both chemical and physical, proceed to maximize entropy, that is, to become more randomized and convert energy into a less available form. A basic corollary of the second law of thermodynamics is the statement that the sum of the entropy change of a system and that of the surroundings will always increase over time and must be positive, i.e., the universe is constrained to become forever more disordered and to proceed towards thermodynamics equilibrium with some absolute maximum value of entropy.

### 1.5.1 Entropy Generation

The idea of *irreversibility* is central to the understanding of *entropy*. Everyone has an intuitive understanding of irreversibility - if one watches a movie of everyday life running forward and in reverse, it is easy to distinguish between the two. The movie running in reverse shows impossible things happening - water jumping out of a glass into a pitcher above it, smoke going down a chimney, water "unmelting" to form ice in a warm room, crashed cars reassembling themselves, and so on. Entropy analysis is a medium to quantify the thermodynamics irreversibility in any fluid flow process. Entropy generation is a measure of the account of irreversibility associated to the real processes. As entropy generation takes place, the quality of energy decreases. According to the second law of thermodynamics the entropy of an isolated system never decreases; such a system will spontaneously evolve toward thermodynamic equilibrium, the configuration with maximum entropy. Systems that are not isolated may decrease in entropy, provided they increase the entropy of their environment by at least that same amount. Since entropy is a state function, the change in the entropy of a system is the same for any process that goes from a given initial state to a given final state, whether the process is reversible or irreversible. However irreversible processes increase the combined entropy of the system and its environment. In order to preserve the quality of energy in a fluid flow process or at least to reduce the entropy generation, it is important to study the distribution of the entropy generation within the fluid volume. The optimal design for any thermal system can be achieved by minimizing entropy generation in the systems. Entropy generation in thermal engineering systems destroys available work and thus reduces its efficiency. Many studies have been published to assess the sources of irreversibility in components and systems. Bejan (1996) studies the

entropy generation for forced convective heat transfer due to temperature gradient and viscosity effect in a fluid. Bejan (1979) also presented various reasons behind entropy generation in applied thermal engineering where the generation of entropy destroys the available work called exergy of a system. The general equation for the entropy generation per unit volume is given by

$$S^m = \frac{\kappa}{T_w^2}(\nabla T)^2 + \frac{\mu}{T_w}\Phi$$

the first term in the equation is the irreversibility due to heat transfer and the second term is the entropy generation due to viscous dissipation. The entropy flowing out of an adiabatic system is always larger than the entropy flowing into the system, the difference arising due to entropy produced by irreversible processes within the system.

## 1.6  Channel Flow

Channel flow constitutes a very important class of flows in fluid dynamics due to its several applications in biological and engineering systems. Therefore, it is necessary to study the characteristics of this flow. We are particularly interested about the stability of the flow through channel by the effects of changing physical properties of the nanofluid. In this respect, we shall consider two types of channel flows, namely parallel flow and convergent-divergent flow. In the late 19th century, Maurice Marie Alfred Couette, a Professor of Physics at the French university of Angers discovered the laminar flow of a viscous fluid in the space between two parallel plates channel, one of which is moving relative to the other. The flow is driven by virtue of viscous drag force acting on the fluid and the applied pressure gradient parallel to the plates named as Couette flow. Steady viscous fluid flow between two parallel stationary plates due to an imposed constant pressure gradient is generally known as Poiseuille flow, since it was first studied experimentally by J.L.M. Poiseuille in 1838. The flow between two planes that meet at an angle was first analyzed by Jeffery (1915) and Hamel (1916), which is called classical Jeffery-Hamel flow through convergent-divergent channel. The study of flows in converging-diverging channel is very important due to its industrial, aerospace, chemical, civil, environmental, mechanical and bio- mechanical engineering applications. Various applications of this type of mathematical model are to understand the flow of rivers and canals, enhancing heat transfer

of heat exchangers for milk flowing, cold drawing operation in polymer industry, extrusion of molten polymers through converging dies and the blood flow in the human body. The theoretical study of MHD channel has been a subject of great interest due to its extensive applications in designing cooling systems with liquid metals, MHD generators, accelerators, pumps, and flow meters (Cha et al. (2002), Tendler (1983)).

## 1.7 Literature Review

The flow and heat transfer between parallel plates channel has been studied by a number of authors Arpaci et al. (2000), Makinde (2008) and Sahin (1999) and occur in many technological applications, such as in biomedical engineering, material processing, as well as the food and petro-chemical industries. In the past few years, several simple flow problems associated with classical hydrodynamics have received new attention within the more general context of magnetohydrodynamics (MHD). A survey of MHD studies in the technological fields can be found in Moreau (1990). The small disturbance stability of MHD plane-Poiseuille flow was investigated by Makinde and Motsa (2001). Makinde (2003) analysed magnetohydrodynamic stability of Plane Poiseuille flow using multideck asymptotic technique. It is observed in his analysis that the magnetic field has a stabilizing effect on the flow and that this stability increases with an increase in Hartmann number. Heat transfer acts a significant role in many fields where the heating and cooling processes involved. Any substance with a temperature above absolute zero transfers heat in the form of radiation. Thermal radiation always exits and can strongly interact with convection in many situations of engineering interest. However, radiative heat transfer has a key impact in high temperature regime. Many technological processes occur at high temperature and good working knowledge of radiative heat transfer plays an instrumental role in designing the relevant equipment. Convection in a channel in the presence of thermal radiation draw the attention because of its importance in many practical applications like a furnace, combustion chamber, cooling tower, rocket engine, and solar collector as Chang *et al* (1983). In Cogley *et al.* (1968), the differential approximation for radiative heat transfer in a nonlinear equation for gray gas near equilibrium was proposed. Chawla and Chan (1980) studied the effect of radiative heat transfer on thermally developing Poiseuille flow with scattering. The

interaction of thermal radiation with conduction and convection in thermally developing, absorbing–emitting, non-gray gas flow in a circular tube was investigated by Tabanfar and Modest (1987). The thermal conductivity of the fluid had been assumed to be constant in many studies. However, it is known that this physical property may change significantly with temperature. For a liquid, it has been found that the thermal conductivity $\kappa$ varies with temperature in an approximately linear manner, as Kay (1966). Yasir *et al* (2011) analyzed the effects of variable viscosity and thermal conductivity on the flow and heat transfer in a laminar liquid film on a horizontal stretching sheet. Pinarbasi *et al*. (2011) investigates the effect of variable viscosity and thermal conductivity of a non-isothermal, incompressible Newtonian fluid flowing under the effect of a constant pressure gradient at constant temperatures in plane Poiseuille flow using Chebyshev pseudospectral method. Sadik *et al*. (2011) studied the effect of variable thermal conductivity and viscosity on single phase convective heat transfer in slip flow. Makinde (2008) studied the steady state solutions for viscous reactive flows through channels with a sliding wall. Patra et al. (2014) examined radiation effect on MHD fully developed mixed convection in a vertical channel with asymmetric heating where they observed that an increase in radiation parameter leads to a decrease in the fluid temperature in the channel. Meanwhile, the thermal boundary layer equation for variable conductivity fluid in the presence of thermal radiation composes a nonlinear problem. The theory of nonlinear differential equations is quite elaborate and their solution remains an extremely important problem of practical relevance in science and engineering. In the last few decades quite a few numerical methods have developed, e. g. finite difference, spectral method, shooting method, etc to tackle this type of problem. Moreover, the models on classical semi-analytical methods have experienced a revival, in connection with the scheme of new hybrid numerical-analytical techniques for nonlinear differential equations, such as Hermite–Padé approximation method, which demonstrated itself as a powerful benchmarking tool and a prospective substitute to traditional numerical techniques in various applications in science and engineering. Makinde (2008) analysed the entropy generation analysis for variable-viscosity channel flow with non-uniform wall temperature. Makinde (2009) investigated the variable viscosity and thermal radiation effects on entropy generation rate in the flow of a temperature dependent variable viscosity optically thin fluid through a channel with isothermal walls using Hermite–Padé semi-

analytical approach. Kwak and Kim (2005) showed that heat transfer efficiency can be improved by increasing the thermal conductivity of the working fluid. Recent advances in nanotechnology have allowed authors to study the next generation heat transfer of nanofluids, a term first introduced by Choi (1995). Nanofluids are engineered dilute colloidal dispersions of nano-sized (less than 100 nm) particles in a base fluid as Das et al. (2007). Nanoparticles have unique chemical and physical properties and have better thermal conductivity with radiative heat transfer compared to the base fluid only as Oztop and Abu-Nada (2008). Mah et al. (2012) studied the entropy generation characteristics in a fully-developed forced convection flow of $Al_2O_3$-water nanofluid in a circular micro-channel. The results showed that when viscous dissipation effects are taken into account, the addition of nanoparticles increases the entropy generation rate and reduces the heat transfer effect since the greater thermal conductivity and viscosity of the nanofluid enhances both the heat transfer irreversibility and the fluid friction irreversibility. Chen et al. (2014) studied heat transfer and entropy generation in fully-developed mixed convection nanofluid flow in vertical channel. They analysed the effects of viscous dissipation on the entropy generation within vertical asymmetrically heated channels containing mixed convection flow.

The flow and heat transfer in porous tubes or channels has been studied by a number of authors (Wernert et al. (2005), Jafari et al. (2009), Goerke (2002)). Berman (1953) described an exact solution of the Navier-Stokes equation for steady two-dimensional laminar flow of a viscous, incompressible fluid in a channel with parallel rigid porous walls driven by uniform suction or injection at the walls. Sheikholeslami (2013) investigated analytically the laminar nanofluid flow in a semi-porous channel in the presence of transverse magnetic field using Homotopy perturbation method. Abiodun et al. (2011) investigated entropy generation in a steady flow of viscous incompressible fluids between two infinite parallel porous plates for two different physical situations Couette flow and pressure-driven Poiseuille flow. Makinde and Eegunjobi (2013) analysed the combined effects of convective heating and suction/injection on entropy generation rate in a channel with permeable walls.

The study of flows in convergent-divergent channel is very important due to its industrial, aerospace, chemical, civil, environmental, mechanical and bio-mechanical engineering applications. Various applications of this type of mathematical model are to understand the

flow of rivers and canals and the blood flow in the human body. Jeffery (1915) and Hamel (1916) first studied the two-dimensional steady motion of a viscous fluid through convergent-divergent channels which is called classical Jeffery-Hamel flow in fluid dynamics. Later, this problem is extensively studied by various researchers. The classical Jeffery-Hamel problem was extended in Axford (1961) to include the effects of external magnetic field on conducting fluid. A survey of information on this problem through divergent channel can be found in Esmaili et al. (2008). Recently, the three analytical methods such as Homotopy analysis method, Homotopy perturbation method and Differential transformation method (DTM) were used by Joneidi et al. (2010) to find the analytical solution of Jeffery-Hamel flow. Motsa et al. (2010) found the solution of the nonlinear equation for the MHD Jeffery-Hamel problem through divergent channel by using novel hybrid spectral-Homotopy analysis method. Moghimi et al. (2011) also solved the Jeffery-Hamel flow problem by using the homotopy perturbation method. Moreover, the effects of magnetic field and nanoparticles on the Jeffery-Hamel flow using a powerful analytical method called the Adomian decomposition method were studied by Sheikholeslami et al. (2012). More recently, Moradi et al. (2013) investigates the effect of three types of nanoparticles Cu, $TiO_2$ and $Al_2O_3$ on Jeffery-Hamel flow using Differential Transformation Method (DTM). They found that the influence of solid volume fraction of nanoparticles on the velocity and skin friction was more enunciated when compared with the type of nanoparticles. Also, the skin friction coefficient for $Al_2O_3$ was observed maximum in comparison to the other two nanoparticles. Fraenkel (1962) investigated the laminar flow in symmetrical channels with slightly curved walls. In his analysis the velocity field of the flow was obtained as a power series in small curvature parameter where the leading term is the Jeffery-Hamel solution. Sobey and Drazin (1986) studied some instabilities and bifurcations of two-dimensional Jeffery-Hamel flows using analytical, numerical and experimental methods. Banks et al. (1988) extended the analysis of perturbation theory of pitchfork bifurcation of the Jeffery-Hamel flows and used as a basis to investigate the spatial development of arbitrary small steady two-dimensional perturbations of Jeffery-Hamel flow both linearly and nonlinearly for nearly plane walls. They found that there is a strong communication between the disturbances up and downstream when the angle between the planes exceeds a critical value, which depends on the value of the Reynolds number.

Moreover, the steady flow of a viscous incompressible fluid in a slightly asymmetrical channel was studied by Makinde (1997). He expanded the solution into a Taylor series with respect to the Reynolds number and performed a bifurcation study. Makinde (2006) investigated the magnetohydrodynamic (MHD) flows in convergent- divergent channels which was an extension of the classical Jeffery-Hamel flows to MHD. He interpreted that the effect of external magnetic field works as a parameter in solution of the MHD flows in convergent - divergent channels. Kayvan et al. (2007) analysed the applicability of magnetic field for controlling hydrodynamic separation in Jeffrey-Hamel flows of viscoelastic fluids. Assuming a purely symmetrical radial flow, they obtained a third-order nonlinear ODE as the single equation governing the MHD flow through converging-diverging channels by similarity analysis. With three physical boundary conditions available, they used Chebyshev collocation-point method to solve this ODE numerically. The effect of magnetic field was found to be more striking such that it is predicted to force fluid elements near the wall to exceed centerline velocity in converging channels and to suppress separation in diverging channels. Makinde (2007) investigated the temporal development of small disturbances in MHD Jeffery-Hamel flows to understand the stability of hydromagnetic steady flows in convergent-divergent channels at very small magnetic Reynolds number *Rm* using Chebyshev spectral collocation method. However, a numerical investigation of the effect of arbitrary magnetic Reynolds number on steady flow of an incompressible conducting viscous liquid in convergent-divergent channels under MHD was presented by Makinde (2008). He solved the non-linear 2D Navier-Stokes equations modeling the flow field using a perturbation technique applying the special type of Hermite-Pade´ approximation method and a bifurcation study was also performed. The increasing values of magnetic Reynolds number cause a general decrease in the fluid velocity around the central region of the channel whereas the flow reversal control is also observed by increasing magnetic field intensity. Alam and Khan (2010) studied the critical behavior of the MHD flow in convergent-divergent channels. The convergence of critical values and the change in bifurcation graph for flow Reynolds number and channel angle by the positive effect of magnetic parameter and the critical relationship among the parameters was discussed in their study. Moreover, the effects of heat transfer and viscous dissipation on the Jeffery-Hamel flow of nanofluids are investigated by Moradi et al. (2015). Finally, Syed et al. (2015)

studied the effects of velocity and temperature slip on the flow between converging and diverging channels using variational iteration and variation of parameters methods.

## 1.8 Significance of the Present Study

Instability of flows and their transition to turbulence are widespread phenomena in engineering, natural environment, and are also important in applied mathematics, astrophysics, biology, geophysics, meteorology, oceanography and physics. Therefore, hydrodynamic stability is an important part of fluid mechanics, because an unstable flow is not observable. Also unstable flows often evolve into an important state of motion called *turbulence*, with a chaotic three dimensional vorticity field with broad spectrum of small temporal and spatial scales. Magnetohydrodynamic stability is a new dimension to hydrodynamic stability considering magnetic effects. Many natural phenomena and engineering problems are susceptible to MHD analysis. In natural phenomena, since magnetic field exists everywhere in the world and magnetohydrodynamics (MHD) occurs whenever conducting fluids are available. MHD is of great significance in the design of many industrial applications such as MHD generators, pumps, flow meters, cooling of nuclear reactors, geothermal energy extractors, nuclear waste disposal, heat exchangers, controlling flows of liquid metals for metallurgical processing and other applications. Further importance of MHD is illustrated by the recent advancement of its application in plasma confinement. The study of MHD flows with heat transfer has also received considerable attention due to its wide application in astrophysical problems. The recent discovery of nanofluids, provides a solution to cooling technology. This is because nanofluids have fascinating features; high thermal conductivity at very low nanoparticles concentration and considerable enhancement of forced convective heat transfer. Nanofluids are also used as coolants for computers and nuclear reactors. Their cooling properties are used in many industrial applications. The main driving force for nanofluids research lies in a wide range of applications. The optimal design for any thermal system can be achieved by minimizing entropy generation in the systems, so it is important to study the distribution of the entropy generation within the fluid volume. However, it is necessary to take into account the variation of thermal radiation and thermal conductivity to obtain a better estimation of

the flow and heat transfer behavior, because these properties must have a significant change with temperature.

## 1.9 Objectives of the Present Study

The objective of this study is to investigate numerically the stability of the magnetohydrodynamic flow and heat transfer in a channel filled with water based nanofluids. Then it is extended considering buoyancy force, viscous dissipation, thermal radiation and temperature dependent thermal conductivity on the flow field. The basic non-linear equations are transformed to dimensionless ordinary differential equations using suitable transformations, which are solved numerically using power series with the aid of Hermite-Padé approximation method. Solutions are obtained and analysed for bifurcation study of the critical parameters, irreversibility analysis of the system, the velocity and temperature profiles for the effect of a set of parameters namely thermal conductivity variation parameter, radiation parameter, magnetic parameter, Grashof number, Brinkman number, nanoparticles volume fraction, porosity parameter, Reynolds number, channel angle, Prandtl number, Eckert number. The major objectives are as follows:

➢ To construct a 2D mathematical model for magnetohydrodynamic flows through channel with water based nanofluids.

➢ To solve the above model for a number of different problems with different boundary conditions using power series with the aid of Hermite- Padé approximation method.

➢ To perform the stability of the solution by showing the dominating singularity behaviour for each of the problems as well as the existence of dual solution branches.

➢ To test the effects of pertinent governing physical parameters (such as: Reynolds number, Radiation parameter, thermal conductivity variation parameter, Hartmann number, channel angle, solid volume fraction, porosity parameter) in each of the problems.

➢ To compare the results of the present investigation with similar available works in the literature.

## 1.10  Organization of the Thesis

In Chapter I, a brief introduction is presented with significances and objectives of the study. This chapter consists of a physical phenomenon of hydrodynamic stability, magnetohydrodynamic, nanofluids, entropy generation, thermal radiation and temperature dependent thermal conductivity with applications. An extensive literature review of the past studies on the above physical facts is included.

The basic governing equations for the flow field and heat transfer are shown in standard vector form and mathematical modeling of the problem for various cases are discussed in Chapter II. The numerical procedures for solving nonlinear dimensionless governing equations are presented in Chapter III.

The radiative heat transfer on the entropy generation of variable thermal conductivity optically thin viscous Cu–water nanofluid with an external magnetic field through a parallel isothermal plate channel has been studied in Chapter IV. The influences of the governing flow parameters namely thermal conductivity variation parameter, radiation parameter, magnetic parameter, Grashof number and Brinkman number on velocity, temperature profiles, and entropy generation with Bejan distribution are discussed quantitatively both numerically and graphically. A stability analysis has been performed for the local rate of heat transfer.

In Chapter V, the entropy generation of the MHD radiative flow of variable thermal conductivity optically thin viscous three different types of nanofluids through a porous parallel channel is investigated. The fluid temperature in the channel varies due to the asymmetric heating of the walls as well as viscous dissipation. The numerical analysis on stability for the local rate of heat transfer is done. Moreover, the entropy generation of the system at the two porous plates is presented with the dominance effect of both the fluid friction and heat transfer irreversibility.

In Chapter VI, the effects of Cu-water nanoparticles on the entropy generation of the nonlinear magnetohydrodynamic Jeffery-Hamel flow are analysed. The velocity profiles, temperature distributions and entropy generation rates with Bejan profiles are presented in divergent channel for various values of nanoparticles solid volume fraction, Hartmann

number, Eckert number, Reynolds number and channel angle. The dominating singularity behavior of the problem is analysed numerically and graphically. The critical relationship between the parameters is studied to observe the instability of the problem for nanofluid.

The effects of three different nanoparticles and magnetic field on the nonlinear Jeffery-Hamel flow through convergent - divergent channel are analysed in Chapter VII. The results are presented in convergent-divergent channels for various values of nanoparticles solid volume fraction, Hartmann number, Prandtl number, Eckert number, Reynolds number and channel angle. The comparison of the present numerical results in tabular form with those obtained by Fraenkel (1962) and Makinde (2008) are also presented. The dominating singularity behavior of the problem is analysed numerically and graphically. The critical relationships among the parameters are studied to observe the instability of the problem for nanofluid.

A summary of major conclusions and some schemes of further work are expressed in Chapter VIII.

The next chapter discusses the basic governing equations of the problem namely continuity, momentum, energy and Maxwell's equations.

Governing Equations of the Problem

*The basic governing equations for the flow and thermal fields in standard vector form and the mathematical modeling of the problem for various cases with different coordinate systems are represented in this chapter.*

## 2.1 Introduction

The basis of computational fluid dynamics is the basic fluid dynamical governing equations; the continuity, momentum (Navier-Stokes equation) and the energy equations. These equations depict the physics of various flows. They are the mathematical statements of the three fundamental laws or principles upon which fluid dynamics is based:

(1) Mass is conserved for a system;

(2) Second law of Newton;

(3) First law of Thermodynamics; Energy is conserved.

## 2.2 Continuity Equation

The continuity equation is based on the mass conservation principle, which states that mass can neither be created nor be destroyed. Conservation of mass is inherent to a control mass system (closed system). The above law is stated mathematically as:

$$\Delta m \big/ \Delta t = 0, \tag{2.2.1}$$

where m = mass of the system.

The equation of continuity in vector form is written as

$$\frac{\partial \rho}{\partial t} + \nabla \cdot (\rho \underline{V}) = 0, \tag{2.2.2}$$

where $\underline{V} = u\,\underline{i} + v\,\underline{j} + w\underline{k}$ is the velocity of the fluid at a point and $\rho$ is the density of the fluid.

For a steady flow, $\dfrac{\partial \rho}{\partial t} = 0,$ thus

$$\nabla \cdot (\rho \underline{V}) = 0. \tag{2.2.3}$$

For incompressible fluid flow, $\rho =$ constant, hence the continuity equation becomes

$$\nabla \cdot \underline{V} = 0. \tag{2.2.4}$$

## 2.3  Momentum Equation (Navier-Stokes Equation)

This equation is formed by applying another fundamental physical principle to a model of the flow, namely Physical principle. Newton's second law on the moving fluid element, states that the net force on the fluid element equals its mass times the acceleration of the element.

$$\underline{F} = m\underline{a} \tag{2.3.1}$$

The momentum equations are called the **Navier-Stokes** equations in honour of two men- the Frenchman M. Navier and the Englishmen G. Stokes, who independently obtained the equations in the first half of the nineteenth century.

The Navier-Stokes equation for viscous incompressible fluid with constant viscosity in vector form is expressed as

$$\rho\left(\frac{\partial \underline{V}}{\partial t} + (\underline{V} \cdot \nabla)\underline{V}\right) = \rho\underline{g} - \nabla p + \mu\nabla^2\underline{V} + \underline{M} \tag{2.3.2}$$

where $\underline{g}$ denote the body force per unit mass acting on the fluid element, p is the pressure, $\mu$ is the viscosity of the fluid and $\underline{M}$ is the other external force.

## 2.4  Energy Equation

The energy equation is obtained from the first law of thermodynamics which states that the amount of heat added to a system $dQ$ is equal to change in internal energy $dE$ plus the amount of energy lost due to work done on the system $dW$. This implies that energy can neither be created nor destroyed; it can only change in form.

The energy equation under the first law of thermodynamics in vector form is

$$\rho c_p \left( \frac{\partial T}{\partial t} + \underline{V} \cdot \nabla T \right) = \kappa \nabla^2 T + \Phi - \nabla.q_r \qquad (2.4.1)$$

Here $\Phi$ is the dissipation function, $T$ is the temperature of the fluid, $\kappa$ is the thermal conductivity of the fluid, $q_r$ is the radiative heat flux and $c_p$ be the specific heat at constant volume.

## 2.5 The Governing equations in Cartesian coordinate system

The governing equations (2.2.2), (2.3.2) and (2.4.1) in vector form are transformed into the following equations in Cartesian form.

**Mass Conservation (Continuity) equation**

$$\frac{\partial \rho}{\partial t} + \frac{\partial (\rho u)}{\partial x} + \frac{\partial (\rho v)}{\partial y} + \frac{\partial (\rho w)}{\partial z} = 0$$

For incompressible steady fluid flow;

$$\frac{\partial u}{\partial x} + \frac{\partial v}{\partial y} + \frac{\partial w}{\partial z} = 0$$

**Momentum (Navier-Stokes) Equations**

x-direction: $\quad \rho \left( \frac{\partial u}{\partial t} + u \frac{\partial u}{\partial x} + v \frac{\partial u}{\partial y} + w \frac{\partial u}{\partial z} \right) = -\frac{\partial p}{\partial x} + \mu \left( \frac{\partial^2 u}{\partial x^2} + \frac{\partial^2 u}{\partial y^2} + \frac{\partial^2 u}{\partial z^2} \right) + \rho g_x$

y-direction: $\quad \rho \left( \frac{\partial v}{\partial t} + u \frac{\partial v}{\partial x} + v \frac{\partial v}{\partial y} + w \frac{\partial v}{\partial z} \right) = -\frac{\partial p}{\partial y} + \mu \left( \frac{\partial^2 v}{\partial x^2} + \frac{\partial^2 v}{\partial y^2} + \frac{\partial^2 v}{\partial z^2} \right) + \rho g_y$

z-direction: $\quad \rho \left( \frac{\partial w}{\partial t} + u \frac{\partial w}{\partial x} + v \frac{\partial w}{\partial y} + w \frac{\partial w}{\partial z} \right) = -\frac{\partial p}{\partial z} + \mu \left( \frac{\partial^2 w}{\partial x^2} + \frac{\partial^2 w}{\partial y^2} + \frac{\partial^2 w}{\partial z^2} \right) + \rho g_z$

**Energy Equation**

$$\rho c_p \left( \frac{\partial T}{\partial t} + u \frac{\partial T}{\partial x} + v \frac{\partial T}{\partial y} + w \frac{\partial T}{\partial z} \right) = \kappa \left( \frac{\partial^2 T}{\partial x^2} + \frac{\partial^2 T}{\partial y^2} + \frac{\partial^2 T}{\partial z^2} \right) + \Phi$$

where $\Phi = \mu \left[ 2 \left\{ \left( \frac{\partial u}{\partial x} \right)^2 + \left( \frac{\partial v}{\partial y} \right)^2 + \left( \frac{\partial w}{\partial z} \right)^2 \right\} + \left( \frac{\partial u}{\partial y} + \frac{\partial v}{\partial x} \right)^2 + \left( \frac{\partial v}{\partial z} + \frac{\partial w}{\partial y} \right)^2 + \left( \frac{\partial w}{\partial x} + \frac{\partial u}{\partial z} \right)^2 \right]$

and $u, v$ and $w$ are the velocity components in the $x, y, z$ directions respectively.

## 2.6 The Governing equations in Cylindrical coordinate system

The del operator in cylindrical coordinate system is defined as

$$\nabla \rho = \frac{1}{r}\frac{\partial}{\partial r}(\rho r) + \frac{1}{r}\frac{\partial}{\partial \theta}(\rho) + \frac{\partial}{\partial z}(\rho)$$

The governing equations (2.2.2), (2.3.2) and (2.4.1) in vector form are transformed into the following equations in cylindrical coordinate system.

### Mass Conservation (Continuity) equation

$$\frac{\partial \rho}{\partial t} + \frac{1}{r}\frac{\partial}{\partial r}(\rho v_r\, r) + \frac{1}{r}\frac{\partial}{\partial \theta}(\rho v_\theta) + \frac{\partial}{\partial z}(\rho v_z) = 0.$$

For incompressible steady fluid flow;

$$\frac{\partial v_r}{\partial r} + \frac{v_r}{r} + \frac{1}{r}\frac{\partial v_\theta}{\partial \theta} + \frac{\partial v_z}{\partial z} = 0.$$

where $v_r, v_\theta$ and $v_z$ be the velocity components in the $r, \theta, z$ directions respectively.

### Momentum (Navier-Stokes) Equations

$$\rho\left(\frac{\partial v_r}{\partial t} + v_r\frac{\partial v_r}{\partial r} + \frac{v_\theta}{r}\frac{\partial v_r}{\partial \theta} - \frac{v_\theta^2}{r} + v_z\frac{\partial v_r}{\partial z}\right) = -\frac{\partial p}{\partial r} + \mu\left(\frac{\partial^2 v_r}{\partial r^2} + \frac{1}{r}\frac{\partial v_r}{\partial r} - \frac{v_r}{r^2} + \frac{1}{r^2}\frac{\partial^2 v_r}{\partial \theta^2} - \frac{2}{r^2}\frac{\partial v_\theta}{\partial \theta} + \frac{\partial^2 v_r}{\partial z^2}\right) + \rho g_r$$

$$\rho\left(\frac{\partial v_\theta}{\partial t} + v_r\frac{\partial v_\theta}{\partial r} + \frac{v_\theta}{r}\frac{\partial v_\theta}{\partial \theta} + \frac{v_r v_\theta}{r} + v_z\frac{\partial v_\theta}{\partial z}\right) = -\frac{1}{r}\frac{\partial p}{\partial \theta} + \mu\left(\frac{\partial^2 v_\theta}{\partial r^2} + \frac{1}{r}\frac{\partial v_\theta}{\partial r} - \frac{v_\theta}{r^2} + \frac{1}{r^2}\frac{\partial^2 v_\theta}{\partial \theta^2} + \frac{2}{r^2}\frac{\partial v_r}{\partial \theta} + \frac{\partial^2 v_\theta}{\partial z^2}\right) + \rho g_\theta$$

$$\rho\left(\frac{\partial v_z}{\partial t} + v_r\frac{\partial v_z}{\partial r} + \frac{v_\theta}{r}\frac{\partial v_z}{\partial \theta} + v_z\frac{\partial v_z}{\partial z}\right) = -\frac{\partial p}{\partial z} + \mu\left(\frac{\partial^2 v_z}{\partial r^2} + \frac{1}{r}\frac{\partial v_z}{\partial r} + \frac{1}{r^2}\frac{\partial^2 v_z}{\partial \theta^2} + \frac{\partial^2 v_z}{\partial z^2}\right) + \rho g_z$$

where, $g_r, g_\theta$ and $g_z$ are the components of the body force in the $r, \theta, z$ directions respectively.

### Energy Equation

$$\rho c_p\left(\frac{\partial T}{\partial t} + v_r\frac{\partial T}{\partial r} + \frac{v_\theta}{r}\frac{\partial T}{\partial \theta} + v_z\frac{\partial T}{\partial z}\right) = \kappa\left(\frac{1}{r}\frac{\partial}{\partial r}\left[r\frac{\partial T}{\partial r}\right] + \frac{1}{r^2}\frac{\partial^2 T}{\partial \theta^2} + \frac{\partial^2 T}{\partial z^2}\right) + \Phi$$

where,

$$\Phi = \mu\left[2\left\{\left(\frac{\partial v_r}{\partial r}\right)^2 + \left(\frac{1}{r}\frac{\partial v_\theta}{\partial \theta} + \frac{v_r}{r}\right)^2 + \left(\frac{\partial v_z}{\partial z}\right)^2\right\} + \left(r\frac{\partial}{\partial r}\left(\frac{v_\theta}{r}\right) + \frac{1}{r}\frac{\partial v_r}{\partial \theta}\right)^2 + \left(\frac{1}{r}\frac{\partial v_z}{\partial \theta} + \frac{\partial v_\theta}{\partial z}\right)^2 + \left(\frac{\partial v_r}{\partial z} + \frac{\partial v_z}{\partial r}\right)^2\right]$$

## 2.7  Maxwell's Equations

Magnetohydrodynamic equations are the ordinary electromagnetic and hydrodynamic equations modified to take account of the interaction between the motion of the fluid and the electromagnetic field. Formulation of the electromagnetic theory is known as Maxwell's equations. Maxwell's basic equations show the relation of basic field quantities and their construction. The *Maxwell's* equations are:

Charge continuity

$$\nabla \cdot \underline{D} = \rho_e \tag{2.7.1}$$

Current continuity

$$\nabla \cdot \underline{J} = -\frac{\partial \rho_e}{\partial t} \tag{2.7.2}$$

Magnetic field continuity

$$\nabla \cdot \underline{B} = 0 \tag{2.7.3}$$

Ampere's Law

$$\nabla \times B_0 = \underline{J} + \frac{\partial \underline{D}}{\partial t} \tag{2.7.4}$$

Faraday's Law

$$\nabla \times \underline{E} = -\frac{\partial \underline{B}}{\partial t} \tag{2.7.5}$$

Constitutive equations for $\underline{D}$ and $\underline{B}$

$$\underline{D} = \varepsilon \underline{E} \text{ and } \underline{B} = \mu_e B_0 \tag{2.7.6}$$

Total current density flow

$$\underline{J} = \sigma(\underline{E} + \underline{V} \times \underline{B}) + \rho_e \underline{V} \tag{2.7.7}$$

The equations (2.7.1) to (2.7.7) are Maxwell's equations where $\underline{D}$ is the electron displacement, $\rho_e$ is the charge density, $\underline{E}$ is the electric field, $\underline{B}$ is the magnetic field, $B_0$ is the magnetic field intensity, $\underline{J}$ is the current density, $\frac{\partial \underline{D}}{\partial t}$ is the displacement current density, $\varepsilon$ is the electric permeability of the medium, $\mu_e$ is the magnetic permeability of the medium, $\underline{V}$ is the velocity vector, $\sigma$ is the electrical conductivity and $\rho_e \underline{V}$ is the convection current due to charge moving with the field.

In MHD, a fluid is considered as grossly neutral. Then the charge density $\rho_e$ in Maxwell's equations is interpreted as an excess charge density, which is generally not large. If the excess charge density is ignored, then the displacement current is also ignored. In most problems the current due to convection of the excess charge are small. Therefore, the electromagnetic equations can be reduced to the following form:

Charge continuity

$$\nabla \cdot \underline{D} = 0 \tag{2.7.8}$$

Current continuity

$$\nabla \cdot \underline{J} = 0 \tag{2.7.9}$$

Ampere's Law

$$\nabla \times B_0 = \underline{J} \tag{2.7.10}$$

Total current density flow

$$\underline{J} = \sigma(\underline{E} + \underline{V} \times \underline{B}) \tag{2.7.11}$$

## 2.8  General Equations Governing Magnetohydrodynamic Nanofluid flow

### 2.8.1  The Continuity Equation

The MHD continuity equation for viscous incompressible electrically conductive nanofluid remains as that of usual continuity equation

$$\nabla \cdot \underline{V} = 0 \tag{2.8.1}$$

### 2.8.2  The Momentum (Navier-Stokes) Equation

The equation of momentum (2.3.2) governing the flow of a nanofluid is expressed as

$$\rho_{nf}\left[ \frac{\partial V}{\partial t} + (\underline{V} \cdot \nabla)\underline{V} \right] = -\nabla p + \mu_{nf}\nabla^2\underline{V} + \rho_{nf}\,\underline{g} + \underline{M} \tag{2.8.2}$$

where $\underline{M}$ is other external forces acting on the flow.

Taking into account the force due to gravity, thermal expansion and the force per unit volume when an electric current density $\underline{J}$ flows through the fluid i.e. the Lorentz force $\underline{J} \times \underline{B}$ due to the presence of magnetic field, the Navier-Stokes equation (2.8.2) becomes,

$$\frac{\partial V}{\partial t} + (\underline{V} \cdot \nabla)\underline{V} = \frac{1}{\rho_{nf}}\left[ -\nabla p + \mu_{nf}\nabla^2\underline{V} \right] + \underline{g}\beta_{nf}\Delta T + \frac{1}{\rho_{nf}}(\underline{J} \times \underline{B}) \tag{2.8.3}$$

35

where $\underline{V}$ is velocity vector, p is pressure, $\rho_{nf}$ is the density of the nanofluid, $\mu_{nf}$ is the dynamic viscosity of the nanofluid and $\beta_{nf}$ is the thermal expansion coefficient of nanofluid.

### 2.8.3  The Energy Equation

The energy equation (2.4.1) for a viscous incompressible nanofluid can be written as:

$$\left(\rho c_p\right)_{nf}\left(\frac{\partial T}{\partial t}+\underline{V}\cdot\nabla T\right)=\kappa_{nf}\,\nabla^2 T-\nabla q+\Phi \tag{2.8.4}$$

where $\underline{V}$ is velocity vector, T is local temperature of the nanofluid, $\left(\rho c_p\right)_{nf}$ is heat capacitance of the nanofluid, $\kappa_{nf}$ is the thermal conductivity of the nanofluid, $\Phi$ is viscous dissipation and $\nabla q$ is radiative heat flux.

Following Sheikholeslami et al. (2012), the relationship between the thermophysical properties of the nanofluid and the conventional base fluid together with nanoparticles are given as:

$$\mu_{nf}=\frac{\mu_f}{(1-\phi)^{2.5}}, \quad \rho_{nf}=(1-\phi)\rho_f+\phi\rho_s, \quad \beta_{nf}=(1-\phi)\beta_f+\phi\beta_s,$$

$$k_{nf}=k_f\,\frac{k_s+2k_f-2\phi(k_f-k_s)}{k_s+2k_f+\phi(k_f-k_s)}, \quad \left(\rho c_p\right)_{nf}=(1-\phi)\left(\rho c_p\right)_f+\phi\left(\rho c_p\right)_s \tag{2.8.5}$$

$$\frac{\sigma_{nf}}{\sigma_f}=1+\left[3\left(\frac{\sigma_s}{\sigma_f}-1\right)\phi\Big/\left(\left(\frac{\sigma_s}{\sigma_f}+2\right)-\left(\frac{\sigma_s}{\sigma_f}-1\right)\phi\right)\right]$$

where $\rho_f$ density of the base fluid, $\rho_s$ is density of the nanoparticles, $\phi$ is the volume fraction of the nanoparticles, $\beta_f$ is the base fluid thermal expansion coefficient, $\beta_s$ is the nanoparticles thermal expansion coefficient, $\mu_f$ is the dynamic viscosity of base fluid, $\kappa_f$ is the thermal conductivity of the base fluid, $\sigma_f$ is the electric conductivity of the base fluid, $\kappa_s$ is the thermal conductivity of the nanoparticles, $\sigma_s$ is the electric conductivity of the nanoparticles, $\left(\rho c_p\right)_f$ is heat capacitance of the base fluid, $\left(\rho c_p\right)_s$ is heat capacitance of the nanoparticles.

# Chapter III

# Approximant Methods

---

*The numerical procedures as Approximant method for solving nonlinear dimensionless governing equations of the problems are presented in this chapter.*

## 3.1 Introduction

This thesis is concerned with the techniques for summing power series that can be described collectively as *approximant* methods to reveal the local behavior of a series around its singular point and the critical relationship among the solution parameters.

The approximation methods are widely used to approximate functions in many areas of applied mathematics. A function is said to be approximant for a given series if its Taylor series expansion reproduces the first few terms of the series.

Padé (1892) and Hermite (1893) introduced a very efficient solution method, known as Hermite-Padé approximants. Blanch (1964) evaluated continued fractions numerically. Brezinski (1990) studied history of continued fraction and Padé approximants. Also the applications of continued fractions and their generalizations to problems in approximation theory have been studied by Khovanskii (1963). Baker and Graves-Morris (1996) studied Padé approximants and its properties. Algebraic and Differential approximants (1978) are some useful generalizations of Padé approximants. Khan (2001) analysed singularity behavior by summing power series. Khan (2002) also introduced a new model of Differential approximant for single independent variable for the summation of power series called High-order differential approximant (HODA). The method is a special type of Hermite-Padé class and it is one of the best methods of singularity analysis for the problems of single independent variable. High-order partial differential approximants discussed in Rahman (2004) is a multivariable differential approximants.

## 3.2 Hermite- Padé Approximants

The entire one variable approximants that are used or discussed throughout this thesis belong to the Hermite- Padé class. In its most general form, this class is concerned with the simultaneous approximation of several independent series and there is some advantage in first describing the Hermite- Padé class from that point of view.

Let $d \in N$ and let the $(d+1)$ power series

$$U_0(x), U_1(x), ..., U_d(x)$$

are given. We say that the $(d+1)$-tuple of polynomials

$$\{P_N^{[0]}, P_N^{[1]}, ..., P_N^{[d]}\},$$

where

$$\deg P_N^{[0]} + \deg P_N^{[1]} + ... + \deg P_N^{[d]} + d = N, \tag{3.2.1}$$

is a Hermite- Padé form of these series if

$$\sum_{i=0}^{d} P_N^{[i]}(x) U_i(x) = O(x^N) \qquad \text{as} \quad x \to 0. \tag{3.2.2}$$

Here $U_0(x), U_1(x), ..., U_d(x)$ may be independent series or different form of a unique series. We need to find the polynomials $P_N^{[i]}$ that satisfy the equations (3.2.1) and (3.2.2). These polynomials are completely determined by their coefficients. So, the total number of unknowns in equation (3.2.2) is

$$\sum_{i=0}^{d} \deg P_N^{[i]} + d + 1 = N + 1 \tag{3.2.3}$$

Expanding the left hand side of equation (3.2.2) in powers of $x$, it is found that equation (3.2.2) is equivalent to equating the first $N$ terms in the expansion to zero. We get a system of N linear homogeneous equations for the unknown coefficients of the polynomials. To calculate the coefficients of the Hermite- Padé polynomials we require some sort of normalization, such as

$$P_N^{[i]}(0) = 1 \text{ for some } 0 \le i \le d. \tag{3.2.4}$$

The equation (3.2.3) simply ensures that the coefficient matrix associated with the system is square. One way to construct the Hermite- Padé polynomials is to solve the system of linear

equations by any standard method such as Gaussian elimination or Gauss-Jordan elimination. The computational complexity of this approach is

$$O(N^3) \text{ (work)}, \ O(N^2) \text{ (storage) as } N \to \infty.$$

It is important to emphasize that the only input required for the calculation of the Hermite-Padé polynomials are the first $N$ coefficients of the series $U_0, U_1, ..., U_d$.

## 3.3  Padé Approximants

Padé approximant is a technique for summing power series that is widely used in applied mathematics as Van Dyke (1975). In the Padé method, the approximant is sought in the class of *rational* functions. Padé approximant can be described from the Hermite- Padé class in the following sense.

In the Hermite- Padé class, let $d = 1$ and the polynomials $P_N^{[0]}$ and $P_N^{[1]}$ satisfy equations (3.2.1) and (3.2.2). One can define an approximant $u_N(x)$ of the series $U(x)$ by

$$P_N^{[1]} u_N - P_N^{[0]} = 0, \tag{3.3.1}$$

Where, $U_1 = U$ and $U_0 = -1$.

Then we select the polynomials

$$P_N^{[0]}(x) = \sum_{i=0}^{n} b_i x^i \text{ and } P_N^{[1]}(x) = \sum_{i=0}^{m} c_i x^i . \tag{3.3.2}$$

Such that $(n + m) \leq N$, the constants $b_i$'s and $c_i$'s are unknowns to be determined. So that,

$$u_N(x) P_N^{[1]}(x) - P_N^{[0]}(x) = O\left(x^{n+m+1}\right). \tag{3.3.3}$$

Equating the first $(n + m)$ equations of (3.3.3) equal to zero and the normalization condition in equation (3.2.4), we find the values of $b_i$'s and $c_i$'s. Then, the rational approximant known as Padé approximant denoted as

$$u_N(x) = \frac{P_N^{[0]}(x)}{P_N^{[1]}(x)}, \tag{3.3.4}$$

Padé approximants have often been used to obtain information about the singularity structure of a function from its series coefficients. The main idea is to examine the behaviour of the zeros of the denominator $P_N^{[1]}$. The Padé approximants also have been used

39

in tackling slowly convergent, divergent and asymptotic series. The zeroes of the denominator $P_N^{[1]}$ give the singular point such as pole of the function $u(x)$ if it exists. If a sequence of zeroes approaches a limit as $N$ increases, then the limit is almost certainly a singularity of $U(x)$.

## 3.4 Algebraic Approximants

Algebraic approximant is a special type of Hermite- Padé approximants. In the Hermite-Padé class, we take

$$d \geq 1, \quad U_0 = 1, \ U_1 = U, \ ...... \ U_d = U^d.$$

An Algebraic approximant $u_N(x)$ of the series $U(x)$ can be defined as the solution of the equation

$$P_N^{[0]}(x) + P_N^{[1]}(x)u_N(x) + P_N^{[2]}(x)u_N^2(x) + ... + P_N^{[d]}(x)u_N^d(x) = 0 \qquad (3.4.1)$$

Since the equation (3.4.1) is a polynomial of the partial sum $u_N(x)$ in degree $d$, the Algebraic approximant $u_N(x)$, is in general a multivalued function with $d$ branches. At first this may appear to be an undesirable feature of the method, in that case we have the problem of identifying the particular branch that approximates $U(x)$. On the other hand, the series $U(x)$ is the expansion of a particular type of function $u(x)$ that is itself multivalued. For Algebraic approximants, one uses the partial sum $u_N(x)$ to construct the $(d+1)$ polynomials

$$\{P_N^{[0]}(x), \ P_N^{[1]}(x), \ ....., \ P_N^{[d]}(x)\}$$

such that

$$\sum_{i=0}^{d} P_N^{[i]}(x)u_N^i(x) = O(x^N) \qquad (3.4.2)$$

and $\displaystyle\sum_{i=0}^{d} \deg P_N^{[i]} + d = N$ .

The total number of unknowns in the equation (3.4.2) is

$$\sum_{i=0}^{d} \deg P_N^{[i]}(x) + d + 1 = N + 1.$$  (3.4.3)

In order to determine the coefficients of the polynomials $P_N^{[i]}$ one can set $P_N^{[0]}(0) = 1$ for normalization, without loss of generality. The discriminant of the equation (3.4.1) approximates the singularity of function $u(x)$.

## 3.5 Drazin -Tourigney Approximants

As it is seen in the previous section that if the function has a countable infinity of branches, then the error of Algebraic approximation converges to zero faster with increasing $d$. So it might be a good idea to let $d$ increase with $N$, rather than keeping it fixed as $N \to \infty$. Drazin and Tourigney in (1996) implemented the idea that $d = O(\sqrt{N})$ as $N \to \infty$. Their method is simply a particular kind of Algebraic approximant, satisfying the equation (3.4.1). In this method they considered

$$\deg P_N^{[i]} = d - i$$  (3.5.1)

and

$$N = \frac{1}{2}\left(d^2 + 3d - 2\right).$$  (3.5.2)

There is a recurrence relation for the calculation of the Drazin-Tourigny polynomials, but its order increases with $N$ (see Drazin and Tourigney (2000)). At present, nothing is known about the convergence of these approximants. However, Drazin and Tourigney (2000) presents some numerical results that suggest that the error for the series of (3.4.1) decays superexponentially.

Drazin and Tourigney initial motivation in (1996) was to solve boundary value problems for nonlinear systems of ordinary and partial differential equations.

## 3.6 Differential Approximants

Differential approximants is an important member of the Hermite- Padé class. It is obtained by taking

$$d \geq 2, \quad U_0 = 1, \quad U_1 = U, \quad U_2 = DU \;\ldots\ldots U_d = D^{d-1}U \;,$$  (3.6.1)

where $D \equiv \dfrac{d}{dx}$ is the differential operator, a differential approximant $u_N(x)$ of the series

$U(x)$ can be defined as the solution of the differential equation

$$P_N^{[0]} + P_N^{[1]}u_N + P_N^{[2]}Du_N + ... + P_N^{[d]}D^{d-1}u_N = 0.$$ (3.6.2)

A popular variant is obtained by taking

$$d \geq 1, \quad U_0 = U, \quad U_1 = DU, \quad U_2 = D^2U \;........\; U_d = D^d U,$$ (3.6.3)

instead of (3.6.1). This gives the homogeneous linear differential equation

$$P_N^{[0]}u_N + P_N^{[1]}Du_N + P_N^{[2]}D^2u_N + ... + P_N^{[d]}D^d u_N = 0$$ (3.6.4)

for the approximant.

*In this thesis, unless otherwise stated, the name "differential approximant" will refer to the non-homogeneous form of the method, i.e. Equations (3.6.1) and (3.6.2).*

Here (3.6.2) is a linear differential equation of order $(d-1)$ with polynomial coefficients. There are $(d-1)$ linearly independent solutions, but only one of them has the same first few Taylor coefficients as the given series $U(x)$. When $d > 2$, the usual method for solving such an equation is to construct a series solution.

Differential approximants are used chiefly for series analysis. They are powerful tools for locating the singularities of a series and for identifying their nature. In this respect, the key is to note that it is not necessary to *solve* the differential equation (3.6.2) in order to find the singularities of $u_N(x)$. The only singularities of $U(x)$ are located at the zeroes of the leading polynomial $P_N^{[d]}(x)$. Hence, some of the zeroes of $P_N^{[d]}(x)$ may provide approximations of the singularities of the series $U(x)$. For instance, if $u_N(x)$ has a singularity at $\lambda = \lambda_{c,N}$ of the algebraic type

$$u_N \sim u_{0,N} + u_{1,N}(\lambda - \lambda_{c,N})^{\alpha_N},$$

then the exponent $\alpha_N$ is given by the simple formula

$$\alpha_N = d - 2 - \frac{P_N^{(d-1)}(\lambda_{c,N})}{DP_N^{(d)}(\lambda_{c,N})}$$

## 3.7 High-Order Differential Approximants (HODA)

Khan (2002) introduced an extension of differential approximant, which he mentioned as High-order differential approximant. When the function has a countable infinity of branches, then the fixed low-order differential approximants may not be useful. So, for these cases he considered $d$ increase with $N$. It leads to a particular kind of differential approximant $u_N(x)$, satisfying equation (3.6.2), i.e.

$$P_N^{[0]} + P_N^{[1]}u_N + P_N^{[2]}Du_N + \ldots + P_N^{[d]}D^{d-1}u_N = 0$$

where

$$N = \frac{1}{2}d(d+3) \tag{3.7.1}$$

and

$$\deg P_N^{[i]} = i. \tag{3.7.2}$$

From (3.7.2) he deduced that there are

$$\sum_{i=0}^{d}(i+1) = \sum_{i=1}^{d+1}i = \frac{1}{2}(d+1)(d+2)$$

unknown parameters in the definition of the Hermite- Padé form. In order to determine those parameters, the N equations are used that follow from (3.2.2)

$$P_N^{[0]}(x) + \sum_{i=1}^{d} P_N^{[i]}(x)D^{i-1}U(x) = O(x^N) \text{ as } x \to 0.$$

In addition one can normalize by setting $P_N^{[d]}(0) = 1$. Then there remain as many equations as unknowns. One of the roots, say $x_{c,N}$, of the coefficient of the highest derivative, i.e.

$$P_N^{[d]}(x_{c,N}) = 0,$$

gives an approximation of the dominant singularity $x_c$ of the series $U$. If the singularity is of algebraic type, then the exponent $\alpha$ may be approximated by

$$\alpha_N = d - 2 - \frac{P_N^{[d-1]}(x_{c,N})}{DP_N^{[d]}(x_{c,N})}. \tag{3.7.3}$$

It is worth noting that the formulae for the location and the exponent of the dominant singularity involve only the coefficients of the highest derivatives in the differential equation

43

that defines the approximant. This motivates the choice (3.7.2) with its emphasis on those very coefficients.

## 3.8  High-Order Partial Differential Approximants (HPDA)

Consider the function $f(x, y)$ of two independent variables, represented by its power series

$$U(x, y) = \sum_{i=0}^{\infty} \sum_{j=0}^{\infty} c_{ij} x^i y^j \qquad (x, y) \to (0,0) \tag{3.8.1}$$

and the partial sum

$$U_N(x, y) = \sum_{i=0}^{N-1} \sum_{j=0}^{N-1} c_{ij} x^i y^j \tag{3.8.2}$$

By using that partial sum, the following $(2d+1)$ polynomials can be constructed

$$P_{[0,0]}, \ P_{[1,0]}, \ P_{[0,1]} \ldots \ldots \ldots, P_{[d,0]}, P_{[0,d]} \tag{3.8.3}$$

in $x$ and $y$ such that

$$P_{[0,0]} U_N + P_{[1,0]} \frac{\partial U_N}{\partial x} + P_{[0,1]} \frac{\partial U_N}{\partial y} + \ldots \ldots + P_{[d,0]} \frac{\partial^d U_N}{\partial x^d} + P_{[0,d]} \frac{\partial^d U_N}{\partial y^d} = \sum_{i=0}^{\infty} \sum_{j=0}^{\infty} e_{ij} x^i y^j$$

$$\tag{3.8.4}$$

Where $\qquad\qquad e_{ij} = 0 \quad$ for $i + j < N = 3d - 1$ $\qquad\qquad$ (3.8.5)

By equating the coefficients of the variables and their powers from (3.8.5), one can obtain a total of

$$N_e = \frac{3d(3d-1)}{2} \tag{3.8.6}$$

equations to determine the unknown coefficients of the polynomials in (3.8.3), the normalization condition can be imposed

$$P_{[0,0]} = 1, \ \text{ or } \ P_{[d,0]} = 1 \text{ or } \ P_{[0,d]} = 1 \text{ for } (x, y) = (0,0). \tag{3.8.7}$$

Thus the remaining unknowns

$$N_u = \frac{1}{3} d(d^2 + 6d + 11) \tag{3.8.8}$$

must be found by the use of $N_e$ equations.

It would be helpful to write the system of linear equations $e_{i,j} = 0$ into the matrix form with the $N_u \times 1$ unknown matrix $\underline{x}$.

Thus the non-homogeneous system of $N_e$ linear equations with $N_u$ unknowns can be written in matrix form as

$$A\underline{x} = \underline{b} \tag{3.8.9}$$

where A is $N_e \times N_u$ matrix and $\underline{b}$ is the non-zero column matrix of order $N_e \times 1$. Thus system will be solvable if

$$N_e \leq N_u. \tag{3.8.10}$$

However, the system may be consistent or inconsistent. If the system is consistent, then the system can be solved by converting the augmented matrix $[A|\underline{b}]$ to row echelon or reduced row echelon form by using the Gaussian elimination or Gauss-Jordan elimination. It is to note that, there will exist some free variables. Naturally the values of the free variables in the multivariable approximant methods can be chosen at random. There is no particular reason to pick up these particular numbers. It might for instance seek a solution such that the polynomials in (3.8.3) have as few high-order terms as possible. Usually the accuracy of the method does not depend critically on the particular choice made. Once the polynomials (3.8.3) have been found, it is more practical to find the singular points by solving either of the polynomials coefficients of the highest derivatives

$$P_{[d,0]}(x, y) = 0 \quad \text{or} \quad P_{[0,d]}(x, y) = 0 \text{ or both simultaneously.}$$

The effects of thermal radiation and variable thermal conductivity on entropy generation of MHD nanofluid flow through vertical channel are analysed in the next chapter.

# Entropy Generation Analysis for MHD Radiative Variable Thermal Conductivity Nanofluid Flow through Vertical Channel[1]

*In this chapter the radiative heat transfer on the entropy generation of variable thermal conductivity optically thin viscous Cu–water nanofluid with an external magnetic field through a vertical parallel isothermal plate channel has been studied. Here the approach uses the power series from the governing non-linear differential equations for small values of thermal conductivity variation parameter which are then analysed by various generalizations of Hermite- Padé approximation method. The influences of the pertinent flow parameters on velocity, temperature, thermal conductivity criticality conditions and entropy generation of the system are discussed quantitatively graphically. A stability analysis has been performed for the local rate of heat transfer which signifies that the lower solution branch is stable and physically acceptable, whereas the upper solution branch is unstable.*

## 4.1 Introduction

The flow and heat transfer between parallel plates channel has been studied by a number of authors (Arpaci et al. (2000), Makinde (2008), Sahin (1999)) and occur in many technological applications. Heat transfer plays a major role in many fields where the heating and cooling processes are involved. Any substance with a temperature above absolute zero transfers heat in the form of radiation. Thermal radiation always exits and can strongly interact with convection in many situations of engineering interest. However, radiative heat

---

transfer has a key impact in high temperature regime. Many technological processes occur at high temperature and good working knowledge of radiative heat transfer plays an instrumental role in designing the relevant equipment. In Cogley *et al.* (1968), the differential approximation for radiative heat transfer in a nonlinear equation for gray gas near equilibrium was proposed. The thermal conductivity of the fluid had been assumed to be constant in many studies. However, it is known that this physical property may change significantly with temperature. Pinarbasi *et al.* (2011) investigates the effect of variable viscosity and thermal conductivity of a non-isothermal, incompressible Newtonian fluid flowing under the effect of a constant pressure gradient at constant temperatures in plane Poiseuille flow using Chebyshev pseudospectral method. Sadik *et al.* (2011) studied the effect of variable thermal conductivity and viscosity on single phase convective heat transfer in slip flow.

Studies of electrically conducting viscous fluids within channels or ducts are important from a practical point of view in MHD generators and accelerators. Moreau (1990) studies a survey of MHD in the technological fields. The small disturbance stability of MHD plane-Poiseuille flow was investigated by Makinde and Motsa (2001). Makinde (2003) analysed magnetohydrodynamic stability of Plane Poiseuille flow using multideck asymptotic technique. It is observed in his analysis that the magnetic field has a stabilizing effect on the flow and that this stability increases with an increase in Hartmann number. Patra et al. (2014) examined radiation effect on MHD fully developed mixed convection in a vertical channel with asymmetric heating where they observed that an increase in radiation parameter leads to a decrease in the fluid temperature in the channel.

Kwak and Kim (2005) showed that heat transfer efficiency can be improved by increasing the thermal conductivity of the working fluid. Due to heat transfer mostly used fluids such as water, ethylene glycol, and engine oil have relatively low thermal conductivities compared to the thermal conductivity of solids. High thermal conductivity of solids can be used to increase the thermal conductivity of a fluid by adding small solid particles to that fluid. The feasibility of the usage of such suspensions of solid particles with sizes on the order of millimeters or micrometers was investigated by various researchers. Recent advances in nanotechnology have allowed authors to study the next generation heat transfer nanofluids, a term first introduced by Choi (1995). Nanofluids are engineered dilute

colloidal dispersions of nano-sized (less than 100 nm) particles in a base fluid as Das et al. (2007). Nanoparticles have unique chemical and physical properties in Oztop and Abu-Nada (2008) and have better thermal conductivity and radiative heat transfer compared to the base fluid only.

Entropy generation provides a measure of the amount of irreversibility associated with real process. Bejan (1996) studied the entropy-generation for forced convective heat transfer due to temperature gradient and viscosity effects in a fluid. Bejan (1979) also presented various reasons for entropy generation in applied thermal engineering where the generation of entropy destroys the available work of a system. The effect of thermal radiation and variable viscosity on entropy generation rate in the flow of optically thin fluid through channel was analysed by Makinde (2009) using Hermite–Padé approximation method. Mah et al. (2012) studied the entropy generation characteristics in a fully-developed forced convection flow of $Al_2O_3$-water nanofluid in a circular micro-channel. The results showed that when viscous dissipation effects are taken into account, the addition of nanoparticles increases the entropy generation rate and reduces the heat transfer effect, since the greater thermal conductivity and viscosity of the nanofluid enhances both the heat transfer irreversibility and the fluid friction irreversibility. Chen et al. (2014) studied heat transfer and entropy generation in fully-developed mixed convection nanofluid flow in vertical channel. They analysed the effects of viscous dissipation on the entropy generation within vertical asymmetrically heated channels containing mixed convection flow.

The main objective of this chapter is to investigate numerically the effect of variable thermal conductivity and thermal radiation on entropy generation rate in the flow of MHD conducting viscous nanofluid through a channel with non-uniform wall temperature applying Hermite- Padé approximation scheme. A stability analysis is also performed to show the physically realizable solution branch in practice of local Nusselt number due to thermal conductivity criticality. Confining the analysis to optically thin limit, results of the velocity, temperature, volumetric entropy generation rate and Bejan number for various values of the involved parameters are presented graphically.

## 4.2. Model Configuration

Consider the steady laminar magnetohydrodynamic variable thermal conductivity flow of an electrically conducting incompressible optically thin viscous Cupper-water nanofluid through an open-ended vertical channel. A uniform magnetic field $B_0$ is acting in the direction normal to the right wall at a distance 2b apart from the left wall. The origin is taken at the centre of the channel and the axis of $x'$ in the direction to the plates.
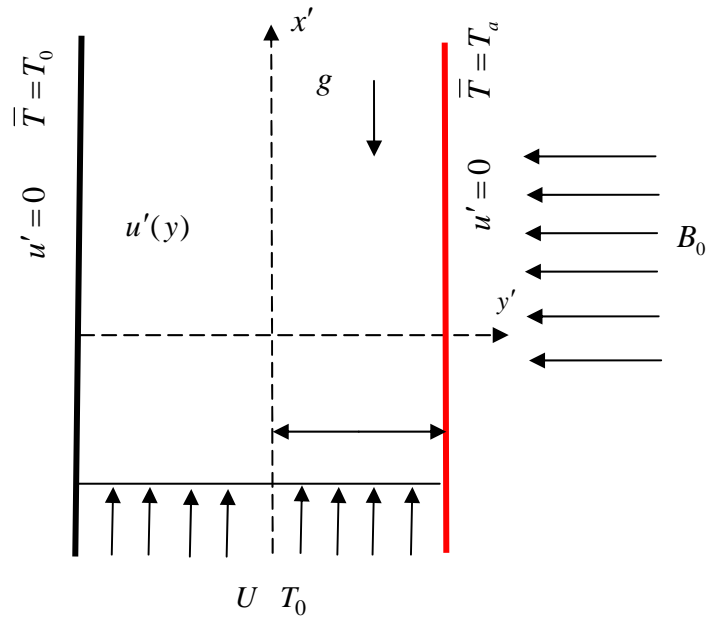


**Figure 4.1:** Geometry of the problem

A two-dimensional Cartesian coordinate system is used and the flow is chosen along the $x'$-direction under constant pressure gradient. The left and right wall temperatures are non-uniform under radiative heat transfer and the fluid has constant properties except the density changes which produce buoyancy force.

## 4.3 Mathematical Formulation

The equations of continuity, momentum and energy considering viscous dissipation and buoyancy force for the problem are

$$\frac{\partial u'}{\partial x'} + \frac{\partial v'}{\partial y'} = 0$$

(4.3.1)

$$u'\frac{\partial u'}{\partial x'} + v'\frac{\partial u'}{\partial y'} = -\frac{1}{\rho_{nf}}\frac{\partial p'}{\partial x'} + \nu_{nf}\left(\frac{\partial^2 u'}{\partial x'^2} + \frac{\partial^2 u'}{\partial y'^2}\right) - \frac{\sigma_{nf}B_0^2}{\rho_{nf}}u' + g\beta(\overline{T} - T_0)$$

(4.3.2)

$$u'\frac{\partial v'}{\partial x'} + v'\frac{\partial v'}{\partial y'} = -\frac{1}{\rho_{nf}}\frac{\partial p'}{\partial y'} + \nu_{nf}\left(\frac{\partial^2 v'}{\partial x'^2} + \frac{\partial^2 v'}{\partial y'^2}\right)$$

(4.3.3)

$$(\rho c_p)_{nf}\left(u'\frac{\partial \overline{T}}{\partial x'} + v'\frac{\partial \overline{T}}{\partial y'}\right) = \kappa_{nf}\left(\frac{\partial^2 \overline{T}}{\partial x'^2} + \frac{\partial^2 \overline{T}}{\partial y'^2}\right) + \mu_{nf}\left(\frac{\partial u'}{\partial y'}\right)^2 - \frac{\partial q_r}{\partial y'}$$

(4.3.4)

Where, according to Kay (1966), the variable thermal conductivity is expressed as

$$\kappa_{nf} = \kappa_{\infty}\left[1 + \tau\frac{\overline{T} - T_a}{T_a - T_0}\right],$$

(4.3.5)

and $k_{\infty}$ is the thermal conductivity at the ambient temperature $T_0$, $\tau$ is defined by

$$\tau = \frac{1}{\kappa_{nf}}\left(\frac{\partial \kappa}{\partial \overline{T}}\right)_{nf}.$$

$(u', v')$ are the velocity components of the nanofluid in the $(x', y')$ directions respectively, $p'$ is the fluid pressure. The dynamic viscosity $\mu_{nf}$, effective density $\rho_{nf}$, effective thermal conductivity $\kappa_{nf}$, heat capacity $(\rho c_p)_{nf}$ and effective electrical conductivity $\sigma_{nf}$ of the nanofluid are defined by equation (2.8.5) in chapter 2.

Since the velocity is only along $x'$-direction and $v' = 0$.

Eq. (4.3.1) reduces to $\frac{\partial u'}{\partial x'} = 0$, which implies that $u'$ depends on $y'$ only.

For simplicity $\frac{\partial \overline{T}}{\partial x'} = 0, \quad \frac{\partial^2 \overline{T}}{\partial x'^2} = 0$. Equations (4.3.2) and (4.3.4) takes the form

$$\frac{d^2 u'}{dy'^2} - \frac{1}{\mu_{nf}}\frac{dp'}{dx'} - \frac{\sigma_{nf}B_0^2}{\mu_{nf}}u' + \frac{g\beta(\overline{T} - T_0)}{\nu_{nf}} = 0$$

(4.3.6)

$$\frac{1}{(\rho c_p)_{nf}}\left[\kappa_{nf}\frac{d^2 \overline{T}}{dy'^2} - \frac{dq_r}{dy'} + \mu_{nf}\left(\frac{du'}{dy'}\right)^2\right] = 0$$

(4.3.7)

The boundary conditions are:

$$y' = -b: \ u' = 0, \ \overline{T} = T_0$$
$$y' = b: \ u' = 0, \ \overline{T} = T_a$$

(4.3.8)

An algebraic approximation is usually used for the differential radiative flux term $\partial q_r / \partial y'$, since, it can be very complex to physical model. Cogley *et al.* (1968) established a compact and numerically agreeable expression for non-gray fluid. They confirmed that in the optically thin limit, the fluid is not self-absorbing but will absorb radiation emitted by the confining boundaries (i.e. right vertical wall) and the radiative flux gradient near equilibrium can be approximated as

$$\frac{dq_r}{dy'} = 4\gamma^2 (\overline{T} - T_a)$$

(4.3.9)

where $\gamma^2$ is the intensity parameter and is given by the following integral

$$\gamma^2 = \int_0^{y'} K_{\lambda a} \left( \frac{\partial e_{b\lambda}}{\partial \overline{T}} \right)_a d\lambda$$

where $K_{\lambda a}$ is the radiation absorption coefficient, $\lambda$ is the wave length and $e_{b\lambda}$ is the Planks' function.

The following transformations are considered

$$x = \frac{x'}{b}, \quad y = \frac{y'}{b}, \quad u = \frac{u'}{U}, \quad p = \frac{b \, p'}{U}, \quad \theta = \frac{\overline{T} - T_0}{T_a - T_0}, \quad Ha'^2 = \frac{\sigma_f B_0^2 b^2}{\mu_f}, \quad Gr' = \frac{g\beta(T_a - T_0)b^2}{v_f \, U},$$

$$R' = \frac{4\gamma^2 b^2}{\kappa_\infty}, \quad Br' = \frac{\mu_f U^2}{\kappa_\infty (T_a - T_0)}, \quad N = -\frac{1}{\mu_f} \frac{dp}{dx}, \quad \kappa = \frac{\kappa_{nf}}{\kappa_\infty}, \quad \kappa = 1 + \tau\theta$$

(4.3.10)

where U is the mean velocity, $R'$ is radiation parameter, $Ha'$ is Hartmann number, $Gr'$ is Grashof number, $Br'$ is Brinkman number and $\tau$ is thermal conductivity variation parameter. The non-dimensional form of the Esq. (4.3.6)-(4.3.7) is

$$\frac{d^2 u}{dy^2} - C(A \, Ha'^2 u - B \, Gr'\theta - N) = 0$$

(4.3.11)

$$[1 + \tau\theta]\frac{d^2\theta}{dy^2} - R'\theta + \frac{Br'}{C}\left(\frac{du}{dy}\right)^2 = 0$$

(4.3.12)

Where, $A = 1 + \left[ 3\left(\frac{\sigma_s}{\sigma_f} - 1\right)\phi \Big/ \left( \left(\frac{\sigma_s}{\sigma_f} + 2\right) - \left(\frac{\sigma_s}{\sigma_f} - 1\right)\phi \right) \right]$, $B = 1 - \phi + \phi\frac{\rho_s}{\rho_f}$, $C = (1 - \phi)^{2.5}$

and $\phi$ is the nanoparticles solid volume fraction.

The boundary conditions in dimensionless form

$$y = -1: \quad u = 0, \quad \theta = 0$$
$$y = 1: \quad u = 0, \quad \theta = 1$$

(4.3.13)

For simplicity of calculation we rescale by considering,

$$Gr = \frac{Gr'}{\tau}, \quad Ha^2 = \frac{Ha'^2}{\tau}, \quad R = \frac{R'}{\tau}, \quad Br = \frac{Br'}{\tau}.$$

Then the dimensionless equations (4.3.11) – (4.3.12) take the form

$$\frac{d^2u}{dy^2} - C(A\,Ha^2\tau u - B\,Gr\tau\,\theta - N) = 0$$

(4.3.14)

$$\frac{d^2\theta}{dy^2} + \tau\theta\frac{d^2\theta}{dy^2} - R\tau\theta + \frac{Br}{C}\tau\left(\frac{du}{dy}\right)^2 = 0$$

(4.3.15)

Esq. (4.3.14)-(4.3.15) will be solved using both power series and Hermite- Padé approximation method.

The local Nusselt number $Nu$ and heat transfer rate are

$$Nu = \frac{q_w\big|_{y'=b}}{\kappa_f \Delta\overline{T}}, \quad q_w = -\kappa_{nf}\left(\frac{\partial\overline{T}}{\partial y'}\right)$$

(4.3.16)

From equations (4.3.10) and (4.3.16), the Nusselt number results in the following form

$$Nu = -\frac{\kappa_{nf}}{\kappa_f}\theta'(1)$$

(4.3.17)

## 4.4  Series Analysis

The following power series expansions are considered in terms of the parameter $\tau$ as equation (4.3.15) is non-linear for temperature field

$$\theta = \sum_{i=0}^{\infty} \theta_i\tau^i, \quad u = \sum_{i=0}^{\infty} u_i\tau^i, \quad |\tau| < 1$$

(4.4.1)

The non-dimensional governing equations (4.3.14) and (4.3.15) are then solved into series solutions by substituting the Eq. (4.4.1) and equating the coefficients of powers of $\tau$. With the help of algebraic programming language MAPLE, we have computed the first 18 coefficients for the series of the temperature $\theta(\tau)$ and velocity $u(\tau)$ in terms

52

of $\tau, Ha, R, Gr, Br, N, A, B, C$ respectively. The first few coefficients of the series for $\theta(\tau)$ and $u(\tau)$ are as follows:

$$\theta(y;\tau,R,Ha,Br,Gr,N) = \frac{1}{2} + \frac{1}{2}y - \frac{1}{12}(y-1)(y+1)(Br\,C\,N^2\,y^2 - R\,y - 3R + Br\,C\,N^2)\tau - \frac{1}{720}$$
$$(y-1)(y+1)(2R\,y^4\,Br\,C\,N^2 + 8Br\,C^2\,N^2\,y^4\,A\,Ha^2 - 18Br\,C\,N^2\,y^3 - 3y^3R^2 + 18Br\,C\,N\,y^3\,B\,Gr$$
$$-30Br\,C\,N^2\,y^2 - 15y^2R^2 + 60Br\,C\,N\,y^2\,B\,Gr + 15y^2R - 52Br\,C^2\,N^2\,y^2\,A\,Ha^2 + 2Br\,C\,N^2\,y^2\,R$$
$$-18Br\,C\,N^2\,y + 60R\,y + 7R^2\,y - 2Br\,C\,N\,y\,B\,Gr - 28Br\,C\,N^2\,R - 30Br\,C\,N^2 + 105R + 75R^2$$
$$+60Br\,C\,N\,B\,Gr - 52Br\,C^2\,N^2\,A\,Ha^2)\tau^2 + O(\tau^3) \tag{4.4.2}$$

$$u(y;\tau,R,Ha,Br,Gr,N) = -\frac{1}{2}N\,C(y-1)(y+1) - \frac{1}{24}C(y-1)(y+1)(A\,Ha^2\,C\,N\,y^2 - 5A\,Ha^2\,C\,N$$
$$+2B\,Gr\,y + 6B\,Gr)\tau - \frac{1}{720}C(y-1)(y+1)(A^2\,Ha^4\,C^2\,N\,y^4 - 2B\,Gr\,y^4\,Br\,C\,N^2 + 3A\,Ha^2\,C\,y^3\,B\,Gr$$
$$+3B\,Gr\,y^3\,R - 14A^2\,Ha^4\,C^2\,N\,y^2 + 15A\,Ha^2\,C\,y^2\,B\,Gr + 15B\,Gr\,R\,y^2 - 2C\,y^2\,B\,Gr\,Br\,N^2$$
$$-7A\,Ha^2\,C\,B\,Gr\,y - 7B\,Gr\,R\,y + 28B\,Gr\,Br\,C\,N^2 + 61A^2\,Ha^4\,C^2\,N - 75A\,Ha^4\,C\,B\,Gr - 75B\,Gr\,R)\tau^2$$
$$+O(\tau^3) \tag{4.4.3}$$

The obtained power series solutions are valid for very small values of $\tau$. Therefore, the series are analysed applying Hermite- Padé approximation method.

## 4.5  Entropy Generation

Flow properties inside a channel with isothermal walls in the presence of thermal radiation and MHD effect are irreversible. The exchange of energy and momentum within the fluid and at solid boundaries causes inequilibrium conditions which leads to continuous entropy generation. Following Bejan (1996) the volumetric entropy generation rate is given as

$$E_G = \frac{\kappa_{nf}}{T_0^2}\left(\frac{d\overline{T}}{dy'}\right)^2 + \frac{\mu_{nf}}{T_0}\left(\frac{du'}{dy'}\right)^2 \tag{4.5.1}$$

Where the first term on the right side of equation (4.5.1) is the irreversibility due to heat transfer and the second term is the irreversibility due to viscous dissipation. The entropy generation number can be expressed in dimensionless form as

$$N_S = \frac{T_0{}^2 b^2 E_G}{\kappa_f (T_a - T_0)^2} = \frac{\kappa_{nf}}{\kappa_f}\left(\frac{d\theta}{dy}\right)^2 + \frac{Br}{\Omega(1-\phi)^{2.5}}\left(\frac{du}{dy}\right)^2 \qquad (4.5.2)$$

Where $\Omega = \dfrac{(T_a - T_0)}{T_0}$ is the temperature difference parameter and

$$N_1 = \frac{\kappa_{nf}}{\kappa_f}\left(\frac{d\theta}{dy}\right)^2, \quad N_2 = \frac{Br}{\Omega(1-\phi)^{2.5}}\left(\frac{du}{dy}\right)^2$$

In general, the entropy generation number $N_s$ given in Eq. (4.5.2) provides a useful means of producing entropy generation profiles. However, it gives no indication as to the relative contributions of the fluid heat transfer and fluid friction effects. Thus, the parameter, Bejan number $Be$ is commonly used in its place.

The Bejan number is given as $Be = \dfrac{N_1}{N_S}$

It is noteworthy that the Bejan number ranges from 0 to 1 and $Be = 0$ is the limit where the irreversibility is dominated by fluid friction effects. $Be = 1$ is the limit where the irreversibility due to heat transfer dominates the flow system because of finite temperature differences. The contributions of heat transfer and fluid friction to entropy generation are equal when $Be = \dfrac{1}{2}$.

## 4.6 Results and Discussion

In this chapter we focus on the combined effect of thermal radiation and temperature dependent variable thermal conductivity on the entropy generation of MHD nanofluid flow in a channel. The minimum entropy conditions provide the possibility of achieving the maximum available work.

In the present study, the nanoparticle volume fraction is specified in the range of $\phi = 0\% - 10\%$, where a value of $\phi = 0$ indicates the pure base fluid. In addition, the thermal conductivity variation parameter is assigned in the range of $-0.1 \le \tau \le 0.9$, the radiation parameter $0 \le R \le 10$, the Brinkman number $1 \le Br \le 50$, the Hartmann number $0 \le Ha \le 4$. The Grashof number and dimensionless pressure gradient are kept fixed at

$Gr = 1$, $N = 1$. Table 4.1 represents the thermo physical properties of the pure base water and Cu-nanoparticles respectively.

**Table 4.1** Thermo physical properties of base water and Cu-nanoparticles as Sheikholeslami (2013).

| Physical properties | Base fluid (water) | Cu |
|---|---|---|
| $\rho$ | 998.1 | 8933 |
| $C_p$ | 4179 | 385 |
| $\kappa$ | 0.613 | 401 |
| $\sigma$ | 0.05 | $5.96 \times 10^7$ |

### 4.6.1 Stability Analysis

For the analysis, we choose the series (4.4.2) for the following functional form

$$Nu = -\frac{\kappa_{nf}}{\kappa_f}\left[\frac{d\theta}{dy}\right]_{y=1}$$

which is related to the local rate of heat transfer at the right hot wall of the channel. The singularities have the form

$$Nu \sim A + B(\tau - \tau_c)^\delta$$

where A, B are constants and $\delta$ represents the critical exponent of the singular point $\tau_c$. Table 4.2 represents that the critical values of the thermal conductivity variation parameter $\tau_c$ increase with a positive increase in the values of radiation parameter $R$ and the values of $\delta$ indicate that $\tau_c$ is a branch point. Therefore, it is significant to notice from the table that as the radiation effect increases, the progress of thermal runaway enhances and the thermal instability in the system improves. While the negative values of radiation parameter may lessen the value of the criticality parameter and reduce thermal runaway in the system. However, in presence of nanofluid ($\phi = 5\%$), both the rate of heat transfer $Nu$ and $\tau_c$ enhances as $R$ increases. This implies that the heat transfer performance is higher in

nanofluid than base fluid. Finally the values of $\tau_c$ in Table 4.2 give an idea about the onset of thermal instability and its nature numerically.

**Table 4.2** Numerical calculations showing thermal conductivity criticality for different parameter values using High-order Differential Approximants at $Br = 1, Gr = 1, Ha = 1, N = 1$.

| $R$ | $\phi$ | $\tau_c$ | $\delta$ | $Nu$ |
|-----|--------|----------|----------|------|
| 0.5 | 0 | -0.72295638183 | 0.489985004 | -0.1897709072 |
| 1 | 0 | -0.53565727924 | 0.464278610 | 0.1864302964 |
| 2 | 0 | -0.37733219733 | 0.449667446 | 0.5561558067 |
| 5 | 0 | -0.21641937233 | 0.456544910 | 1.130723424 |
| 2 | 0.05 | -0.37328441444 | 0.449147585 | 0.6115499181 |
| 5 | 0.05 | -0.21567016329 | 0.453808805 | 1.154478277 |

A segment of bifurcation diagram for different values of $d$ in the $(\tau, Nu)$ plane is noticed in Figure 4.2(a) using Drazin-Tourigny Approximants. We say that there is a *simple turning point, fold or a saddle-node bifurcation* at $\tau = \tau_c$. It is interesting to notice that there are two solution branches (I and II) of Nusselt number when $\tau > \tau_c$, one solution when $\tau = \tau_c$, and no solution when $\tau < \tau_c$, where $\tau_c$ is the critical value of $\tau$ for which the solution exists. A stable solution is denoted by a continuous curve and an unstable solution by a broken curve. The stability analysis indicates that the lower solution branch (II) is stable and physically realizable. For different values of $d$, the upper solution branch (I) is unstable and physically unacceptable as shown in Figure 4.2(a). Figure 4.2(b) represents the effect of radiation parameter $R$ on the bifurcation diagram in the way that the bifurcating point increases as $R$ increases uniformly and produces more instability to the upper solution branch (I). The numerical values in Table 4.2 are also consistent with the lower solution branch of $Nu$ as $R$ increases for negative values of $\tau$ in Figure 4.2(b). Moreover, the local

rate of heat transfer decreases very slowly in lower solution (II) as $R$ increases due to radiative heat loss for positive increase of $\tau$ .
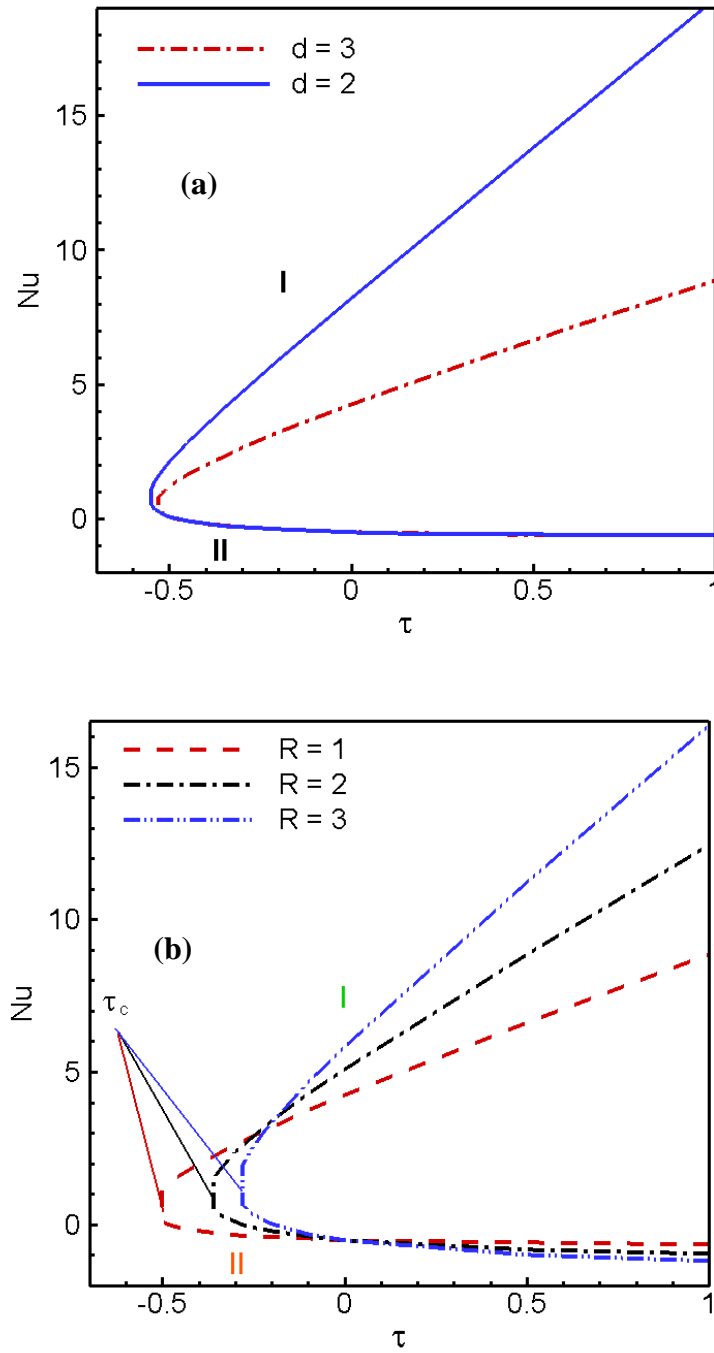


**Figure 4.2:** Approximate bifurcation diagrams against $\tau$ in the $(\tau, \ Nu(1))$ plane (a) for different $d$ and (b) for different $R$ obtained by Drazin-Tourigny method (1996) for $N = 1, Gr = 1, Br = 1, Ha = 1, R = 1, d = 3$.

### 4.6.2 Effect of Thermal Conductivity variation parameter

Figures 4.3-4.4 represent the effects of thermal conductivity variation parameter on velocity profiles, temperature distribution, entropy generation rate $N_s$ and distribution of Bejan number *Be* respectively. It is observed in Figure 4.3(a) that increasing value of $\tau$ results in slow increment in fluid velocity and for nanofluid there is a significant improvement in fluid motion approximately by $20\%$ along the centerline region as $\tau$ increases. As the thermal conductivity increases, the heat is more readily transferred particularly in nanofluid which leads to enhancement of fluid velocity within the centerline. A decrease in the fluid temperature around the central region of the channel is observed in Figure 4.3(b) due to the escalating values of $\tau$. The increases of thermal conductivity variation parameter produce more heat transfer within the channel centerline region and reduce dimensionless temperature distribution. Furthermore, due to the higher thermal conductivity coefficient of the nanofluid, the heat is more keenly transferred. Generally, the value of $N_2$ i.e., the entropy generated by fluid friction is larger than that of $N_1$ i.e., the entropy produced by fluid heat transfer. As a result, $N_S$ is contributed mainly by $N_2$ throughout the entire flow field. However, in the areas of the flow field characterized by a faster flow rate, the velocity gradient is reduced, and thus $N_2$ also reduces. In the present parallel channel, $N_S$ gradually reduces to zero at $y = -0.5$ as shown in Figure 4.4(a). In this particular region of the flow field, the velocity gradient becomes less, and thus $N_S$ is contributed mainly by $N_1$. Figure 4.4(a) illustrates the entropy generation rate when $\tau$ is increasing and other parameters remain constant. The entropy production number $N_S$ closely similar from left wall to centerline and then to the right wall for lesser values of $\tau$, but for rising values of $\tau$, $N_S$ increases rapidly in base fluid and further in nanofluid in the region from the centerline to the hot wall. However, in the region from the centerline to the cold wall $N_S$ decreases as $\tau$ increases, because the dominant effect of heat transfer occurs at the right hot wall. Figure 4.4(b) displays the distribution of the Bejan number (*Be*) versus the channel width for thermal conductivity variation parameter $\tau$. It is noticed that *Be* has a value of less than 1 on either side of the channel since, as discussed previously, the velocity

gradient is increased at the cold and hot sides of the channel, and hence $N_S$ is contributed initially by $N_2$.
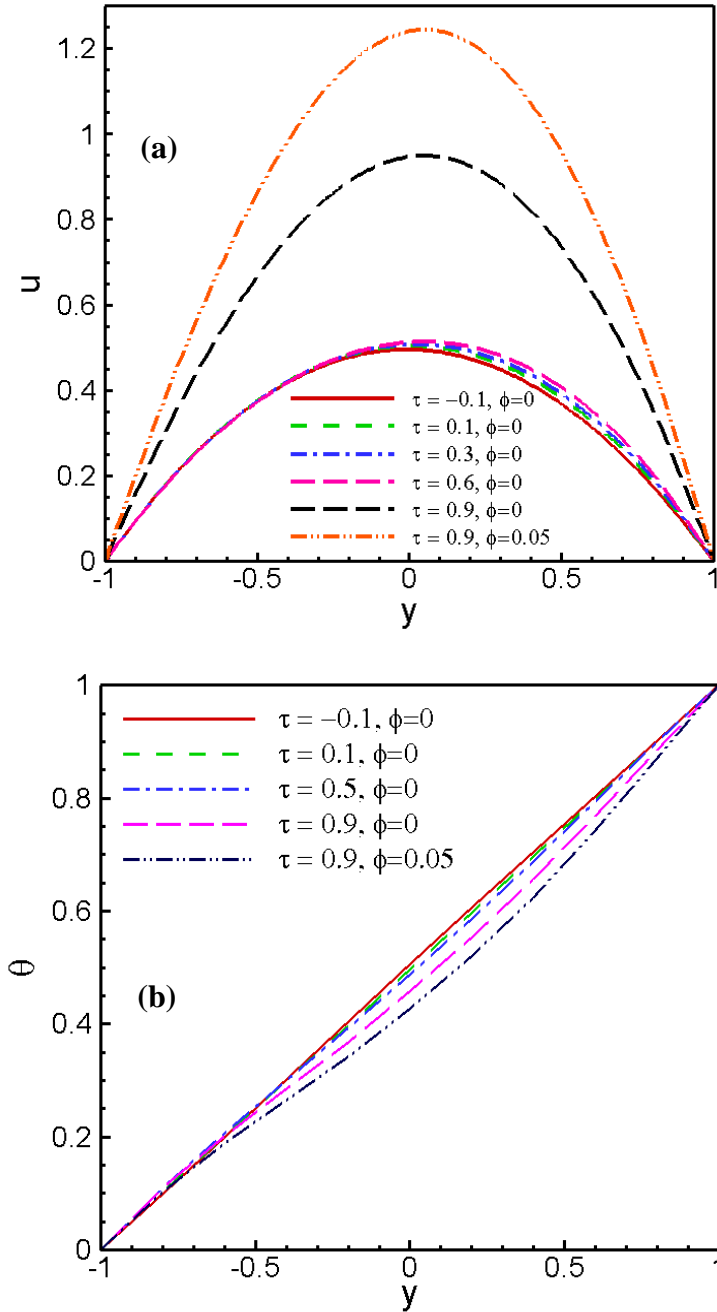


**Figure 4.3** (a) Velocity profiles (b) Temperature profiles for different values of $\tau$ at

$$R = 1, N = 1, Gr = 1, Br = 1, Ha = 1.$$
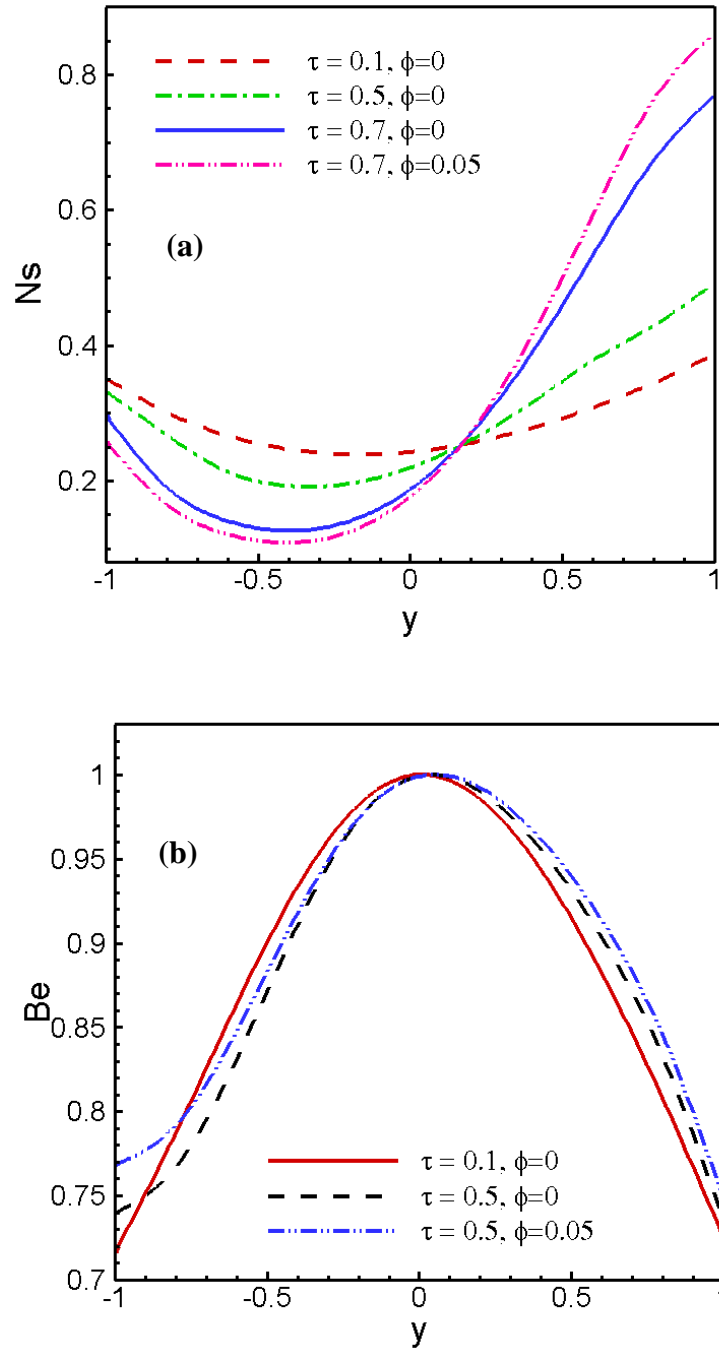
**Figure 4.4** (a) Entropy generation rates (b) Bejan number for different values of $\tau$ :

$$N = 1, Gr = 1, Br = 1, Ha = 1, R = 1.$$

In the central region of the flow field, *Be* increases to a maximum value of 1 due to the reduction in the velocity gradient and the corresponding increase in the contribution of $N_1$ to the overall entropy generation. It is to be seen that the heat transfer irreversibility dominates

the flow process within the channel centerline region, while the little influence of fluid friction irreversibility can be observed at the walls. It is also seen in Figure 4.4(b) that from left cold wall to centerline region $Be$ decreases as $\tau$ increases and conversely from centerline region to right hot wall $Be$ increases as $\tau$ increases.

### 4.6.3 Effect of Radiation parameter

The influences of radiation parameter on velocity profiles, temperature distribution, entropy generation rate $N_s$ and distribution of Bejan number $Be$ are depicted in Figures.4.5-4.6. Figure 4.5(a) shows that the velocity slowly decreases as $R$ increases and a decrement of nearly $12\%$ in the velocity at centerline is seen for nanofluid when $R$ increases due to radiative heat loss. The temperature decrease is further strengthened with rising values of the radiation parameter $R$ for base fluid and nanofluid shown in Figure 4.5(b). As $R$ increases, the rate of heat loss accelerates around the center of the channel that generates the reduction of the temperature profiles. As nanofluid exhibits higher rate of heat transfer, the reduction of the temperature profile becomes faster in nanofluid as shown in Figure 4.5(b). Figure 4.6(a) depicts the similar conjecture for $N_S$ as $\tau$ when $R$ increases except the reduction of $N_S$ in nanofluid around the right hot wall due to the lesser viscous dissipation effect. It is to be noted from Figure 4.6(b) that heat transfer irreversibility dominates the flow process within the channel centerline region, while the little influence of fluid friction irreversibility can be observed at the walls. It is also seen in Figure 4.6(b) that from left cold wall to centerline region $Be$ decreases as $R$ increases and conversely from centerline region to right hot wall $Be$ increases as $R$ increases.

### 4.6.4 Effect of Hartmann number

Figures 4.7(a, b, c) represent the flow characteristics with entropy generation due to the effect of Hartmann number. In Figure 4.7(a) it is depicted that the velocity decreases for the positive changes of $Ha$ and a reduction of around $40\%$ in centerline velocity is found for the variation of $Ha = 0$ to $Ha = 4$. The variation of $Ha$ leads to the variation of the Lorentz force due to magnetic field and the Lorentz force produces more resistance to the fluid velocity. It is seen from Figure 4.7(b) that Hartmann number $Ha$ acts to reduce the entropy generation

rate uniformly and $N_S$ is lowest within the channel centerline that increases towards the both walls particularly more at the right wall.
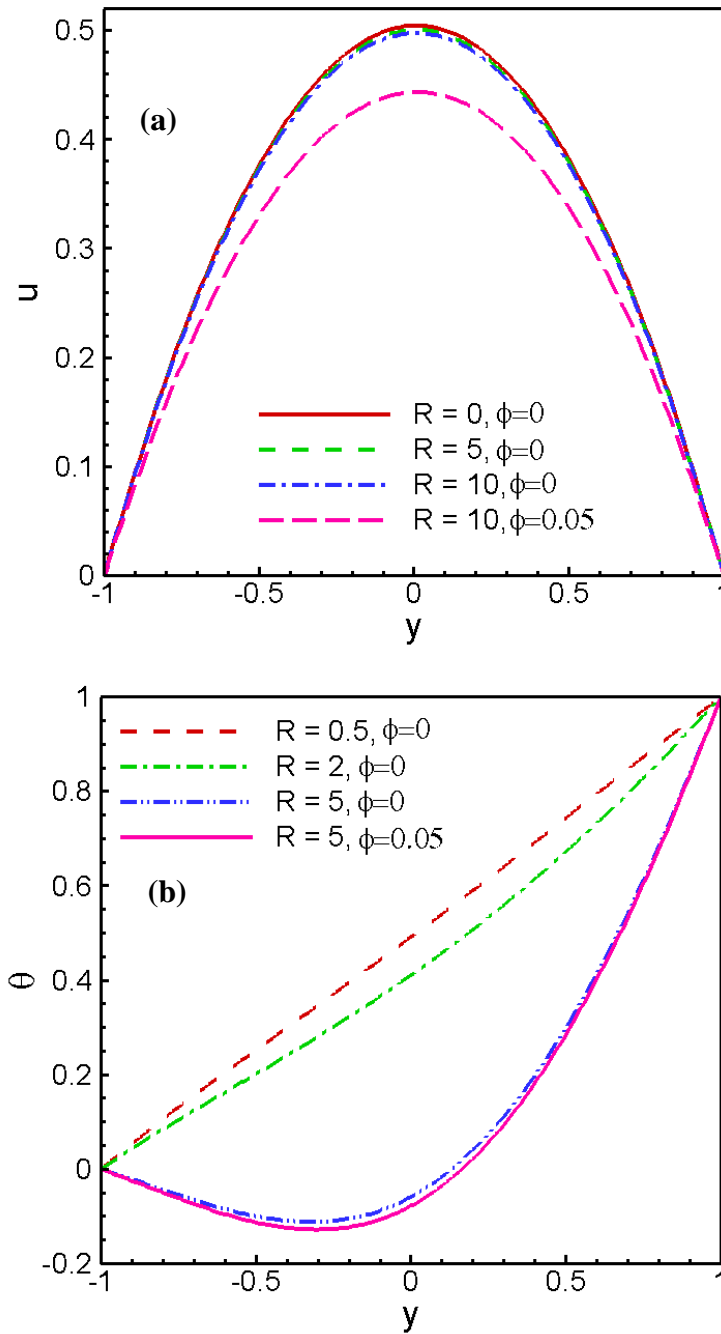


**Figure 4.5** (a) Velocity profiles (b) Temperature profiles for different values of $R$

at $N = 1, Gr = 1, Br = 1, Ha = 1, \ \tau = 0.1$.

Figure 4.7(c) demonstrates that as Hartmann number *Ha* increases, the fluid friction irreversibility at the walls decreases significantly and further in nanofluid. The Lorentz force due to magnetic field produces more resistance to the fluid friction irreversibility and hence enhances the dominance effect of heat transfer irreversibility.
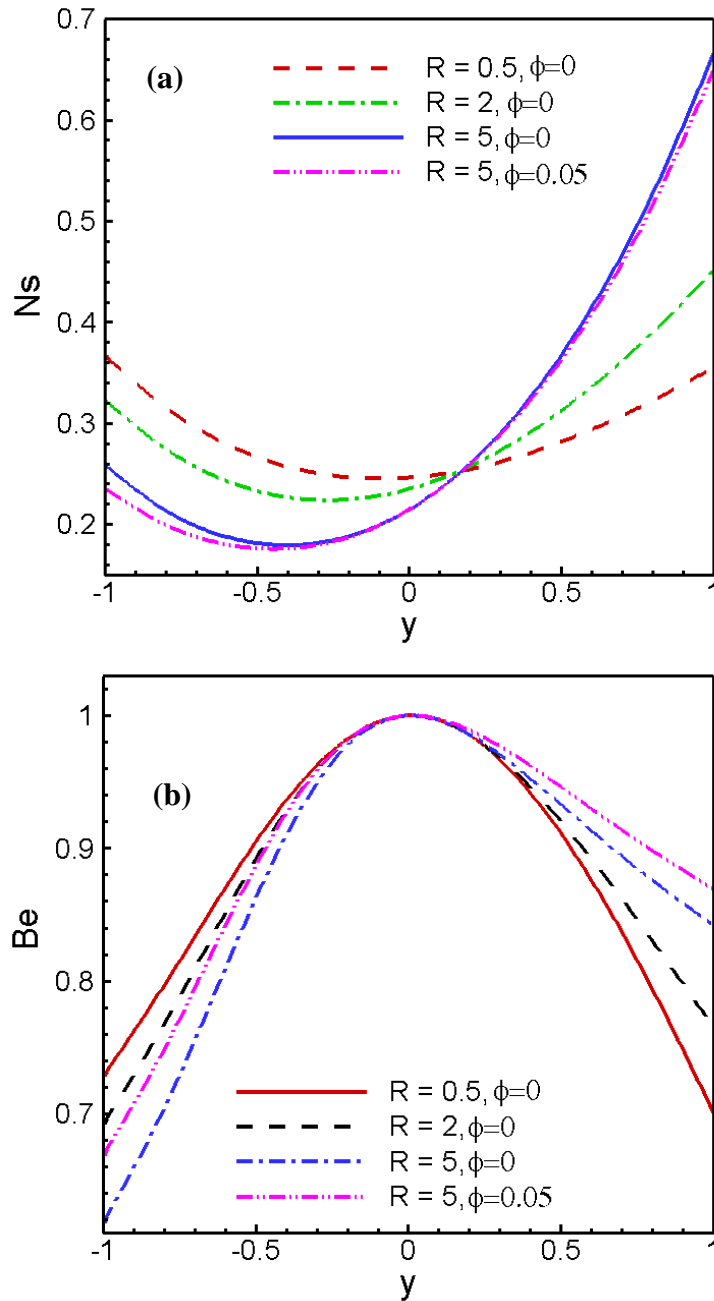


**Figure 4.6** (a) Entropy generation rates (b) Bejan number for different values of *R*

at $N = 1, Gr = 1, Br = 1, Ha = 1, \tau = 0.1$.
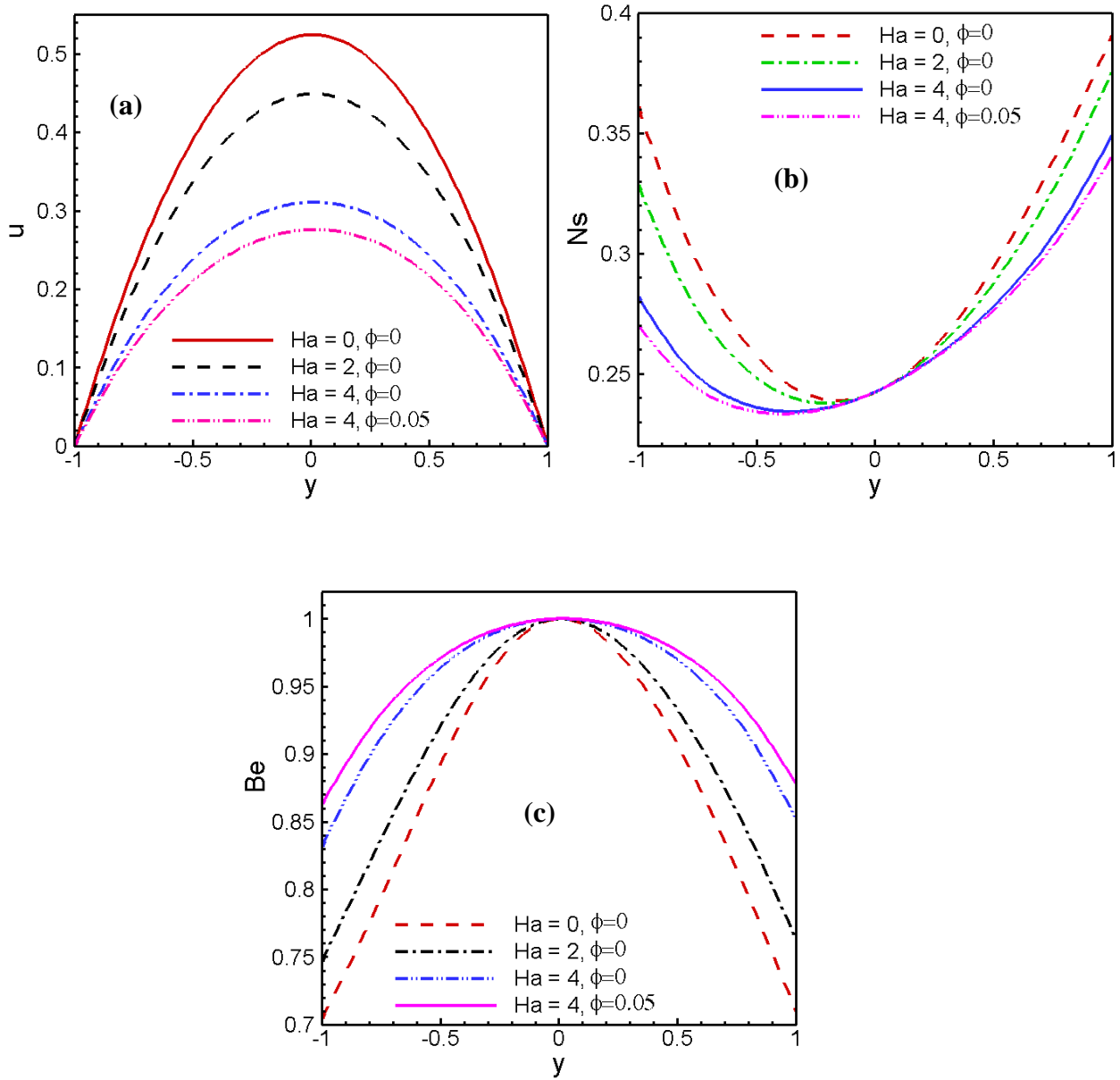
**Figure 4.7** (a) Velocity profiles (b) Entropy generation rates and (c) Bejan number for different values of *Ha* at $N = 1, Gr = 1, Br = 1, R = 1, \tau = 0.1$.

### 4.6.5 Effect of Nanoparticles solid volume fraction

The control of nanoparticles volume fraction on flow field and entropy generation are presented in Figures 4.8 (a, b, c). In Figure 4.8 (a), a uniform reduction in fluid velocity is observed as $\phi$ increases. The equivalent thermal expansion coefficient of the nanofluid is less than that of base water. As a result, the buoyancy force acting on the nanofluid is also less than that acting on the pure water, and hence the dimensionless velocity is reduced. In addition, since the density and viscosity of the nanofluid are greater than those of base water, the velocity distribution within the channel is more uniform for nanofluid. Figure 4.8(b) shows the effect of an increase in volume fraction of nanoparticles on entropy generation rate. A uniform reduction is observed at the walls to $N_S$ when $\phi$ increases. Therefore, nanofluid is suitable to reduce the entropy generation rate and to enhance the efficiency of the system. The mounting values of $\phi$ causes an identical increment of *Be* at the two walls symmetrically indicating governance effect of heat transfer irreversibility for nanofluid as shown in Figure 4.8(c).

### 4.6.6 Effect of Brinkman number

The dimensionless velocity distribution of the flow field has a direct effect on the dimensionless temperature distribution as the effects of viscous dissipation are taken into consideration in the present problem. It is noticed from Figure 4.9 that the fluid temperature increases with increasing parametric values of viscous heating parameter *Br* but a minor reduction is seen in presence of nanoparticles. The velocity gradient of the pure working fluid is greater than that of the nanofluid due to the lower viscosity which results in more viscous dissipation effect. Furthermore, due to the higher thermal conductivity coefficient of the nanofluid, the heat is more intensely transferred. Hence, the dimensionless temperature of the nanofluid is less than that of the base fluid in Figure 4.9.
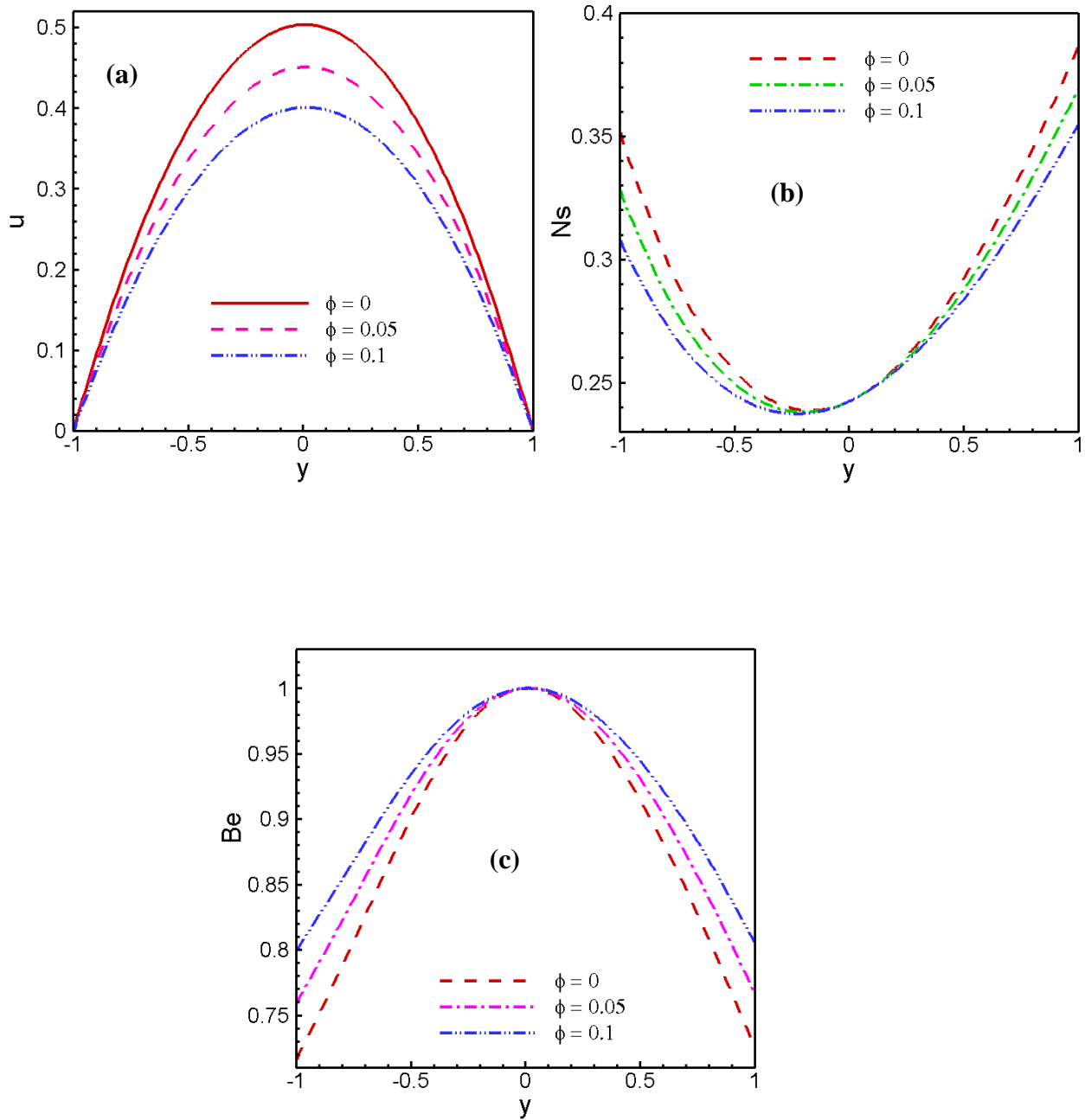
**Figure 4.8** (a) Velocity profiles (b) Entropy generation rates and (c) Bejan number for different values $\phi$ at $N = 1, Gr = 1, Br = 1, Ha = 1, \tau = 0.1, R = 1.$
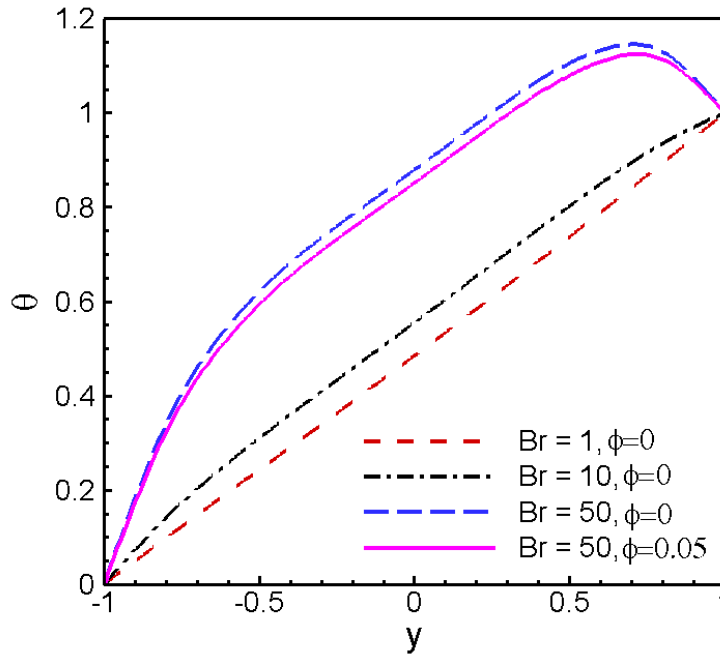
**Figure 4.9** Temperature profiles for different values of *Br*

at $Ha = 1, N = 1, Gr = 1, R = 1, \tau = 0.1$.

Thus thermal radiation and variable thermal conductivity play an imperative role to fluid friction and heat transfer irreversibility in modeling boundary layer flows with nanofluids through a channel. Physically the variation of thermal conductivity controls the rate of heat transfer. Moreover, the point of existence of two solution branches of which the lower one is physically acceptable, is determined by temperature dependent variable thermal conductivity. Finally, thermal radiation in presence of nanofluids has a key impact on the physical solution.

## 4.7. Conclusion

A numerical investigation is performed to the radiative heat transfer performance, temperature varied thermal conductivity effects and entropy generation characteristics of MHD Cu-water nanofluid flow through a channel with asymmetric heated wall applying Hermite-Padé approximants method. The dominating singularity behaviour due to the thermal conductivity variation parameter and the thermal stability conditions for two

67

solution branches are analysed with the effect of Radiation parameter. An increase in the thermal conductivity variation parameter advances fluid velocity along centerline and reduces temperature distribution. Radiation parameter reduces both the fluid velocity and temperature distribution due to faster heat loss. Increasing Hartmann number and nanoparticles solid volume fraction cause the reduction of fluid velocity near the centerline uniformly because of the acting of Lorentz force and reduction of buoyancy force respectively. For regions of the flow field at a greater velocity gradient, i.e., adjacent to the hot and cold walls, the total entropy generation rate is dominated by the effects of fluid friction. Conversely, in the regions of the flow field at a higher and more uniform velocity distribution, i.e., the central region of the channel, the total entropy generation rate is dominated by the effects of fluid heat transfer.

In the next section, a case study regarding MHD radiative flow through a channel with left sliding wall is represented.

**4.8 A Special Case Study: MHD Radiative Flow of Variable Thermal Conductivity Fluid through Vertical Channel with a sliding wall[2]**

*The combined effect of variable thermal conductivity and radiative heat transfer on steady flow of a conducting optically thin viscous fluid through a vertical channel with left sliding wall and non-uniform wall temperatures under the influence of an externally applied homogeneous magnetic field are analyzed in this study. The similarity transformation reduces the governing equations for momentum and thermal energy into a set of coupled ordinary differential equations which are solved using power series together with Hermite-Padé approximation. The dimensionless velocity profiles, temperature profiles and thermal criticality conditions are presented numerically and graphically to interpret the effect of various physical parameters of the problem.*

### 4.8.1 Mathematical Model

Consider a steady two-dimensional laminar incompressible flow of electrically conducting non-gray optically thin viscous fluid through a vertical channel with the left sliding wall. An externally homogeneous magnetic field is applied in normal direction to the right wall of the channel and the wall temperatures are non-uniform under radiative heat transfer. A Cartesian coordinate system is used and the flow is chosen along the $x'$-direction under constant pressure gradient which is driven solely by uniform velocity at the left wall, i.e. the velocity profile is linear with zero at the right fixed wall and maximum value at the left moving wall. Consider all the physical properties of the fluid constant except the thermal conductivity and density which varies linearly with temperature. The reduced momentum and energy equations considering buoyancy force and neglecting the viscous dissipation are as follows:

---

[2] *This work consists of a Journal paper*: Md. S. Alam, M. A. H. Khan, "Hermite- Padé projection to thermal radiative and variable conductivity MHD flows through channel with a sliding wall", *International Journal of Engineering, Science and Technology*, Vol. 6, No. 1, pp. 88-97, (2014).

$$v\frac{d^2u'}{dy'^2} - \frac{1}{\rho}\frac{dp'}{dx'} - \frac{\sigma_e B_0^2}{\rho}u' + g\beta(\overline{T} - T_0) = 0 \qquad (4.8.1)$$

$$\frac{\overline{\kappa}}{\rho c_p}\frac{d^2\overline{T}}{dy'^2} - \frac{1}{\rho c_p}\frac{dq_r}{dy'} = 0 \qquad (4.8.2)$$

The appropriate boundary conditions of the problem are

$$u' = u_1, \quad \overline{T} = T_0 \text{ at } y' = 0, \qquad (4.8.3)$$

$$u' = 0, \quad \overline{T} = T_a \quad \text{at } y' = b \qquad (4.8.4)$$
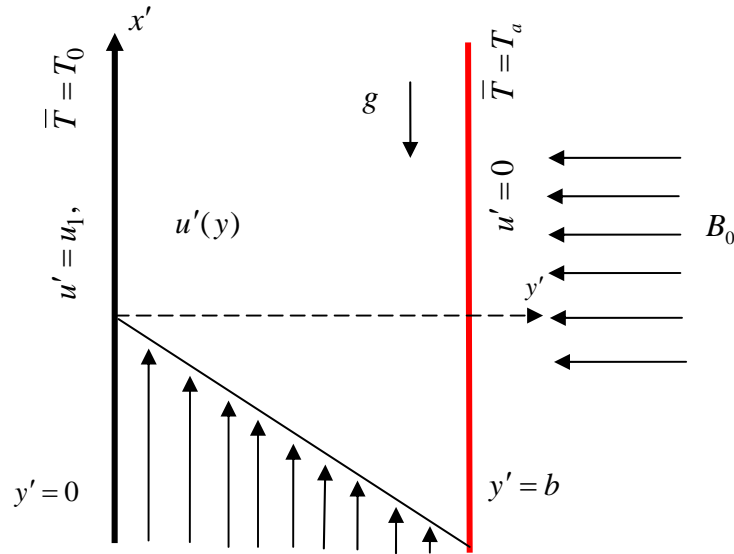


**Figure 4.8.1** Geometry of the problem

According to Cogley et al. (1968), the radiative heat flux for optically thin fluid is given by

$$\frac{dq_r}{dy'} = 4\gamma^2(\overline{T} - T_a) \qquad (4.8.5)$$

$$\gamma^2 = \int_0^{y'} K_{\lambda a}\left(\frac{\partial e_{b\lambda}}{\partial \overline{T}}\right)_a d\lambda$$

where $K_{\lambda a}$ is the radiation absorption coefficient, $\lambda$ is the wave length and $e_{b\lambda}$ is the Planks' function. Following Kay (1966), the variable thermal conductivity can be written as

$$\overline{\kappa} = \kappa_\infty\left[1 + \tau\frac{\overline{T} - T_a}{T_a - T_0}\right], \qquad (4.8.6)$$

and $k_\infty$ is the thermal conductivity at the ambient temperature $T_0$, $\tau$ is defined by

$$\tau = \frac{1}{\overline{\kappa}}\left(\frac{\partial\overline{\kappa}}{\partial\overline{T}}\right).$$

Dimensionless quantities and parameters are initiated in the problem as follows

$$y = \frac{y'}{b}, \quad x = \frac{x'}{b}, \quad u = \frac{u'}{u_1}, \quad \kappa = \frac{\overline{\kappa}}{\kappa_\infty}, \quad p = \frac{bp'}{u_1}, \quad N = -\frac{1}{\mu}\frac{dp}{dx}, \quad \theta = \frac{\overline{T} - T_0}{T_a - T_0}$$ (4.8.7)

$$\overline{R} = \frac{4\gamma^2 b^2}{\kappa_\infty}, \quad \overline{Ha} = \sqrt{\frac{b^2 \sigma B_0{}^2}{\mu}}, \quad Gr = \frac{g\beta(T_a - T_0)b^2}{\nu u_1}, \quad \kappa = 1 + \tau\theta$$

The governing equations (4.8.1) and (4.8.2) are reduced to the following dimensionless form

$$\frac{d^2 u}{dy^2} - \tau\, Ha^2 u + Gr\theta + N = 0$$ (4.8.8)

$$\frac{d^2\theta}{dy^2} + \tau\left[\theta\frac{d^2\theta}{dy^2} - R\theta\right] = 0$$ (4.8.9)

Where $\kappa = 1 + \tau\,\theta$, $R = \dfrac{\overline{R}}{\tau}$, $Ha^2 = \dfrac{\overline{Ha}^2}{\tau}$,

The dimensionless form of the corresponding boundary conditions is

$$u = 0, \quad \theta = 1, \quad \text{at} \quad y = 1$$ (4.8.10)

$$u = 1, \quad \theta = 0, \quad \text{at} \quad y = 0$$

### 4.8.2 Series Analysis

The following power series expansions are considered in terms of the parameter $\tau$ as equations (4.8.8) and (4.8.9) are non-linear for velocity field and temperature distribution

$$u = \sum_{i=0}^{\infty} u_i\tau^i, \quad \theta = \sum_{i=0}^{\infty} \theta_i\tau^i$$ (4.8.11)

The non-dimensional governing equations are then solved into series solutions by substituting the Eq. (4.8.11) into Eqs. (4.8.8) and (4.8.9) and equating the coefficients of powers of $\tau$.

Order zero $(\tau^0)$

$$\frac{d^2 u_0}{dy^2} + Gr\theta_0 + N = 0, \quad \frac{d^2\theta_0}{dy^2} = 0$$ (4.8.12)

$$u_0 = 0, \quad \theta_0 = 1 \qquad \text{at} \quad y = 1$$ (4.8.13)

$$u_0 = 1, \quad \theta_0 = 0 \qquad \text{at} \quad y = 0$$ (4.8.14)

Order one $(\tau^1)$

$$\frac{d^2u_1}{dy^2} - Ha^2u_0 + Gr\theta_1 = 0, \qquad \frac{d^2\theta_1}{dy^2} + \theta_0\frac{d^2\theta_0}{dy^2} - R\theta_0 = 0 \tag{4.8.15}$$

$$u_1 = 0, \quad \theta_1 = 0 \qquad \text{at} \quad y = 1 \tag{4.8.16}$$

$$u_1 = 0, \quad \theta_1 = 0 \qquad \text{at} \quad y = 0 \tag{4.8.17}$$

With the help of MAPLE, we have computed the first 18 coefficients for the series of the velocity $u$ and temperature field $\theta$ in terms of $\tau$, $Ha$, $R$, $Gr$, $N$. The first few coefficients of the series for $u$ and $\theta$ are as follows:

$$u(y;Gr,R,Ha,N,\tau) = -\frac{1}{6}(y-1)(Gry^2 - 3yN + Gry + 6) - \frac{1}{360}y(y-1)(3Ha^2Gry^3 + 3GrRy^3$$

$$-15Ha^2y^2N + 3y^2Ha^2Gr + 3y^2GrR - 7GrRy + 15Ha^2yN - 7Ha^2Gr\,y + 60Ha^2y - 7Ha^2\,Gr$$

$$-120Ha^2 - 180N + 15Ha^2N - 7GrR)\tau + O(\tau^2) \tag{4.8.18}$$

$$\theta(y;R,\tau) = y + \frac{1}{6}Ry(y-1)(y+1)\tau + \frac{1}{360}Ry(y-1)(3y^3R - 30y^2 + 3y^2R - 7yR - 30y - 7R$$

$$-30)\tau^2 + O(\tau^3) \tag{4.8.19}$$

### 4.8.3  Results and Discussion

The main objective of the study is to analyze the singularity behaviour of MHD radiative variable thermal conductivity viscous incompressible flow through the parallel plate channel using Hermite-Padé approximants. The regular effect of the governing physical parameters namely thermal conductivity variation parameter, Radiation parameter, Hartmann number and Grashof number on the dimensionless velocity and temperature profiles are depicted graphically. A stability analysis as dual solution branch for the local rate of heat transfer is also performed.

#### 4.8.3.1  Stability Analysis
For the analysis, we choose the series (4.8.19) for the following functional form

$$Nu = -\left.\frac{d\theta}{dy}\right|_{y=1} \tag{4.8.20}$$

which is related to the local rate of heat transfer at the right hot wall of the channel The singularities have the form

$$Nu \sim A + B(\tau - \tau_c)^\delta$$

where A, B are constants and $\delta$ represents the critical exponent of the singular point $\tau_c$.

Table 4.8.1 displays that the critical thermal conductivity variation parameter $\tau_c$ increases uniformly for the increases of radiation parameter R with $Ha = 0$ at $d = 4$ taking $N = 18$. On the other hand, the values of $\delta$ confirm that $\tau_c$ is a branch point using HODA. The values of $\tau_c$ in Table 4.8.1 (neglecting viscous dissipation) and Table 4.2 (considering viscous dissipation) both at $R = 1$ for pure base fluid are $-0.53565727924$ and $-0.8095725031$ respectively. By considering the effect of viscous dissipation, the dimensionless velocity distribution of the flow field has a direct effect on the dimensionless temperature distribution. As a result, there occur early thermal runaway and progress of thermal instability in the system. Employing the algebraic approximation method to the series (4.8.20) we have obtained the bifurcation diagram against $\tau$ in Figure 4.8.2 It is interesting to notice again as in Figure 4.2 at the previous section that there are two solution branches (I and II) of local Nusselt number when $\tau > \tau_c$, one solution when $\tau = \tau_c$, and no solution when $\tau < \tau_c$, where $\tau_c$ is the critical value of $\tau$ for which the solution exists.

**Table 4.8.1** Numerical values of thermal conductivity criticality $\tau_c$ and corresponding exponent $\delta$ at various values of R at $Ha = 0$ .

| R | $\tau_c$ | $\delta$ |
|---|---|---|
| 1 | -0.8095725031 | 0.4976501741 |
| 2 | -0.6702408724 | 0.4926654350 |
| 4 | -0.5160126951 | 0.4995668656 |
| 6 | -0.4281462458 | 0.4996975550 |
| 8 | -0.3694196308 | 0.4985993397 |
| 10 | -0.3270367744 | 0.4995634864 |
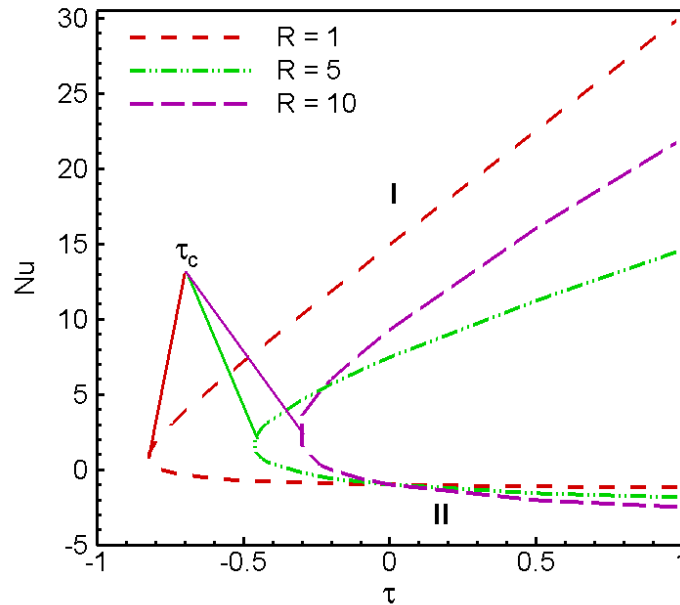
**Figure 4.8.2** Approximate bifurcation diagram against $\tau$ in the $(\tau - Nu)$ plane for different values of $R$ with $d = 4$ at $Ha = 0$ .

As the values of $R$ increase, the bifurcation points increase uniformly shown in Figure 4.8.2. The conjecture of Figure 4.8.2 is consistent with the results shown in Table 4.8.1 using differential approximation.

### 4.8.3.2 Effect of Thermal Conductivity variation parameter

Figures 4.8.3 (a)-(b) illustrate the effect of thermal conductivity variation parameter $\tau$ on temperature distributions and velocity profiles respectively. It is observed from the Figure 4.8.3(a) that an increase in the thermal conductivity variation parameter $\tau$ leads to decrease in the temperature field across the center line region particularly for $\tau > 1$ due to more rapidly heat transfer. The velocity profile by the effect of $\tau$ is observed in Figure 4.8.3(b) generally with maximum value at the left sliding wall and minimum value along the right fixed wall. It is clear that an increasing presence of $\tau$ gives a minor and uniform reduction in the fluid velocity as demonstrated particularly around the left cold wall. In the vicinity of $y = 0$, the fluid contacts the low temperature wall and shrinks accordingly, and in absence of viscous dissipation effect, the density increases, while the buoyancy force reduces.
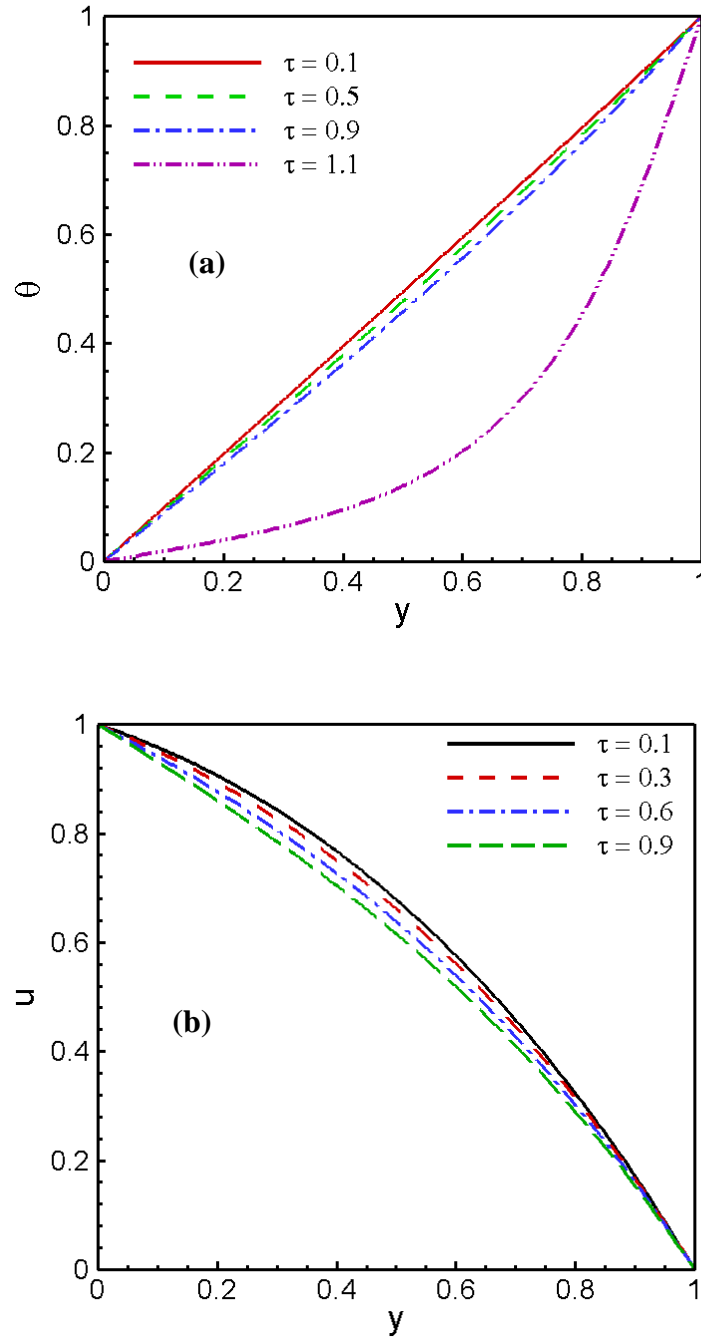
**Figure 4.8.3** (a) Temperature distributions and (b) Velocity profiles for different values of $\tau$ at $R = 1, N = 1, Ha = 1, Gr = 1$.

### 4.8.3.3 Effect of Radiation parameter

A significant influence of Radiation parameter on velocity and temperature field is depicted in Figures 4.8.4(a-b). We observe from Figure 4.8.4(a) that the fluid temperature decreases around the centerline region of the channel with increasing values of $R$ as a result of

radiative heat loss. Meanwhile, the minimum temperature is generally seen along the channel centerline and then increases gradually to the prescribed value at the right wall.
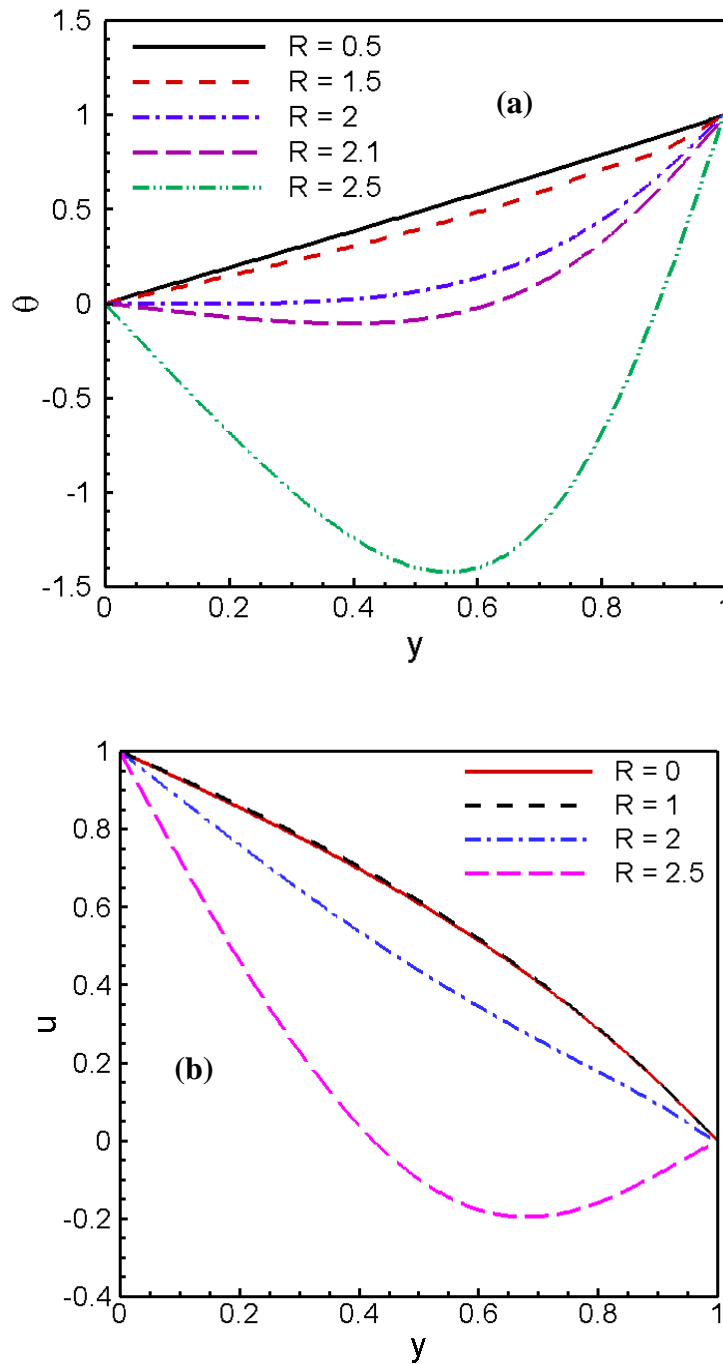


**Figure 4.8.4** (a) Temperature distributions and (b) Velocity profiles for different values of R at

$$\text{Ha} = 1, \text{N} = 1, \tau = 1, \text{Gr} = 1.$$

As *R* increases, the rate of heat loss accelerates around the center of the channel that generates the reduction of the velocity profiles which is seen in Figure 4.8.4(b).

### 4.8.3.4  Effect of Hartmann number
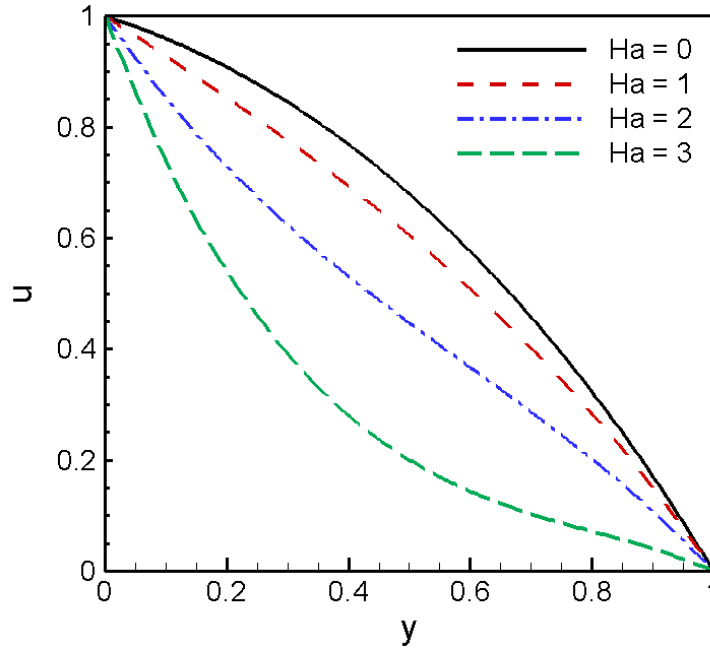


**Figure 4.8.5** Velocity profiles for different values of *Ha* at $N = 1, R = 1, \tau = 1, Gr = 1$.

It is seen from Figure 4.8.5, a uniform reduction in the centerline velocity at the positive variation of Hartman number *Ha*. The presence of magnetic field decreases the dimensionless velocity due to Lorentz force.

### 4.8.3.5  Effect of Grashof number

There is a significant and uniform incretion is seen to the fluid velocity around the channel centerline in Figure 4.8.6 when the Grashof number *Gr* increases. The pure water with low density has more thermal expansion coefficient than other fluids. As a consequence, it is more affected by the higher buoyancy force in the flow region, and thus the velocity increases as *Gr* increases.
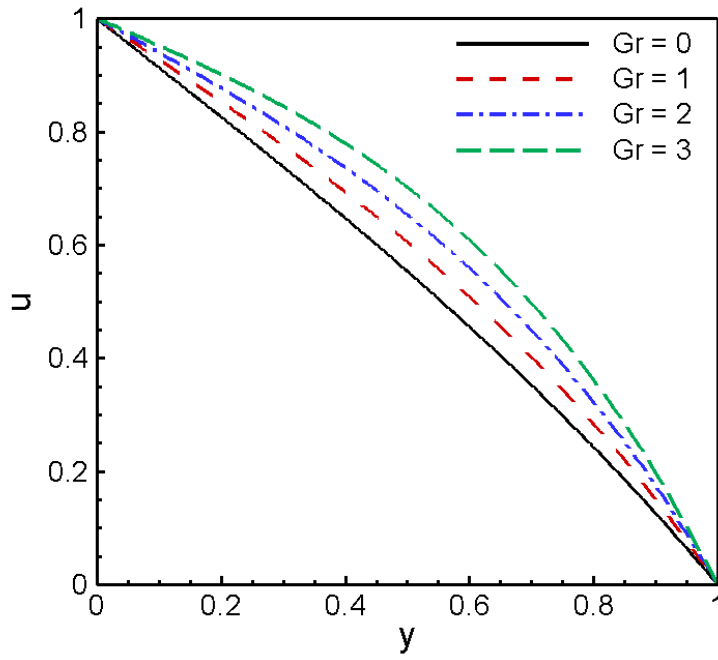
**Figure 4.8.6** Velocity profiles for different values of $Gr$ at $N = 1, R = 1, \tau = 1, Ha = 1$.

### 4.8.3.6 Effect of Pressure Gradient parameter
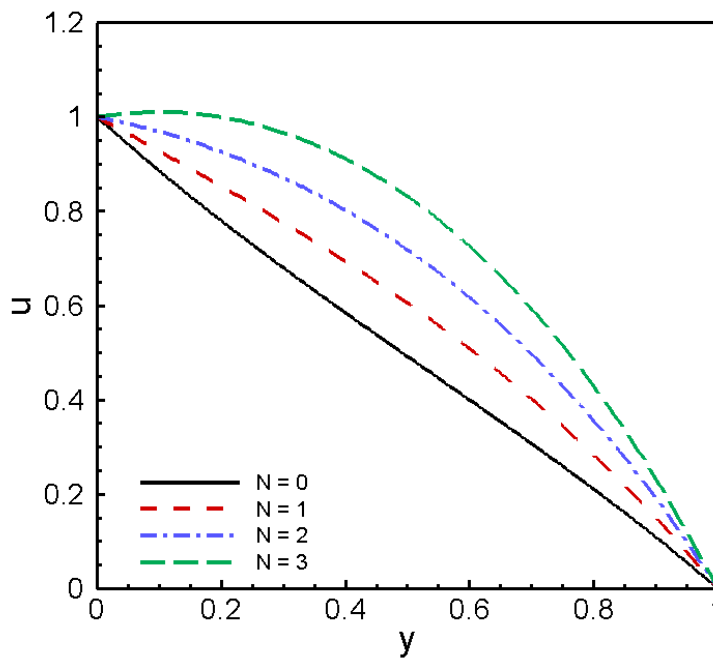


**Figure 4.8.7** Velocity profiles for different values of $N$ at $Ha = 1, R = 1, \tau = 1, Gr = 1$.

From Figure 4.8.7, it is noticed that the velocity profile exhibits significant increments along the centerline region at every increasing values of *N*. As *N* increases, the pressure gradient and viscosity of the fluid decreases which leads to enhancement of fluid velocity in the channel.

## 4.8.4 Conclusion

The influences of thermal radiation on MHD flow of an optically thin variable thermal conductivity viscous incompressible fluid through a vertical channel with sliding wall of non-uniform wall temperatures are investigated using a special type of Hermite-Pade′ approximation technique. The dominating singularity behaviour of the solution of the problem is analysed with the effect of variable thermal conductivity and radiation. The velocity and temperature profiles are obtained analytically to observe the effect of the parameters of the solution. Our results generally represent that increasing thermal radiation and conductivity reduces centerline velocity and temperature field while increasing magnetic parameter causes decrease in the magnitude of centerline dimensionless velocity.

The next chapter investigates the entropy generation of MHD radiative flow of different nanofluids through a porous channel.

# Entropy Generation for MHD Radiative Variable Thermal Conductivity Flow in Porous Channel with different Nanoparticles[3]

*The entropy generation on radiative heat transfer performance in the flow of variable thermal conductivity optically thin viscous water-based nanofluid with an external magnetic field through a porous vertical channel is investigated in this chapter. Three types of nanoparticles as Cu, TiO$_2$ and Al$_2$O$_3$ are used to observe their performance. The fluid temperature in the channel varies due to the asymmetric heating of the walls as well as viscous dissipation. Here the approach uses the power series from the governing non-linear differential equations for small values of thermal conductivity variation parameter which are then analysed by various generalizations of Hermite- Padé approximation method. The influences of the pertinent governing flow parameters on velocity, temperature, thermal conductivity criticality conditions and entropy generation are discussed extensively both numerically and graphically. A stability analysis has been performed for the local rate of heat transfer which signifies that the lower solution branch is stable and physically realizable, whereas the upper solution branch is unstable. It is interesting to remark that the entropy generation of the system increases at the two porous plates whereas the fluid friction irreversibility is dominant there.*

## 5.1 Introduction

The flow and heat transfer of magnetohydrodynamic nanofluid flow in porous tubes or channels has various applications in biomedical engineering, material processing, as well as the food and petro-chemical industries. These include; magnetics drug targeting, MHD blood flow meters, production of magneto-rheostatic (MR) materials known as smart fluids.

---

In recent years, we find several applications in polymer industries, cooling of metallurgical materials, cooling of microchips in computers and other electronics which use microfluidic applications, cooling of automobile engine, wire drawing. The nanofluid containing magnetic nanoparticles also acts as a super-paramagnetic fluid, which, in an alternating electromagnetic field, absorbs energy and produces a controllable hyperthermia. Berman (1953) described an exact solution of the Navier-Stokes equation for steady two-dimensional laminar flow of a viscous, incompressible fluid in a channel with parallel rigid porous walls driven by uniform suction or injection at the walls.

Heat transfer efficiency can be improved by increasing the thermal conductivity of the working fluid as Kwak and Kim (2005). Due to heat transfer mostly used fluids such as water, ethylene glycol, and engine oil have relatively low thermal conductivities compared to the thermal conductivity of solids. High thermal conductivity of solids can be used to increase the thermal conductivity of a fluid by adding small solid particles to that fluid. The feasibility of the usage of such suspensions of solid particles with sizes on the order of millimeters or micrometers was investigated by various researchers. Recent advances in nanotechnology have allowed authors to study the next generation heat transfer nanofluids, a term first introduced by Choi (1995). Nanoparticles have unique chemical and physical properties Oztop and Abu-Nada (2008) and have better thermal conductivity and radiative heat transfer compared to the base fluid only. Nanofluids are engineered dilute colloidal dispersions of nano-sized (less than 100 nm) particles in a base-fluid Das et al. (2007). Sheikholeslami (2013) investigated analytically the laminar nanofluid flow in a semi-porous channel in the presence of transverse magnetic field using Homotopy perturbation method.

However, the thermal boundary layer equation for variable thermal conductivity fluids in the presence of thermal radiation construct a nonlinear problem and the solution behavior will present a looming into physical process of thermal instability in the system. Abiodun et al. (2011) investigated entropy generation in a steady flow of viscous incompressible fluids between two infinite parallel porous plates for two different physical situations Couette flow and pressure-driven Poiseuille flow. Makinde and Eegunjobi (2013) analysed the combined effects of convective heating and suction/injection on entropy generation rate in a channel with permeable walls.

81

Taking into account the significance of variable thermal conductivity and thermal radiation effect on entropy generation rate in the flow of MHD conducting viscous nanofluid through a porous channel with non-uniform wall temperature is studied applying Hermite- Padé approximation method. A stability analysis is also performed to show the physically realizable solution in practice of local Nusselt number due to thermal conductivity criticality. Results for the velocity, temperature, volumetric entropy generation rate and Bejan profile for various values of the solution parameters are presented graphically.

## 5.2. Physical Model

A two-dimensional steady, incompressible and laminar variable thermal conductivity flow for three different nanofluids in a porous vertical channel is considered. The left and right walls of the channel at a distance of 2b apart are assumed to be porous as injection and suction respectively so that $\vec{V} = (u', v', 0)$ where $u'$ and $v'$ are the horizontal and vertical (injection/suction) components of velocity respectively. The flow is chosen along the $x'$-direction under constant pressure gradient and depends on $y'$ alone. The left and right wall temperatures are non-uniform under radiative heat transfer and an externally homogeneous magnetic field is applied in normal direction to the right hot wall.
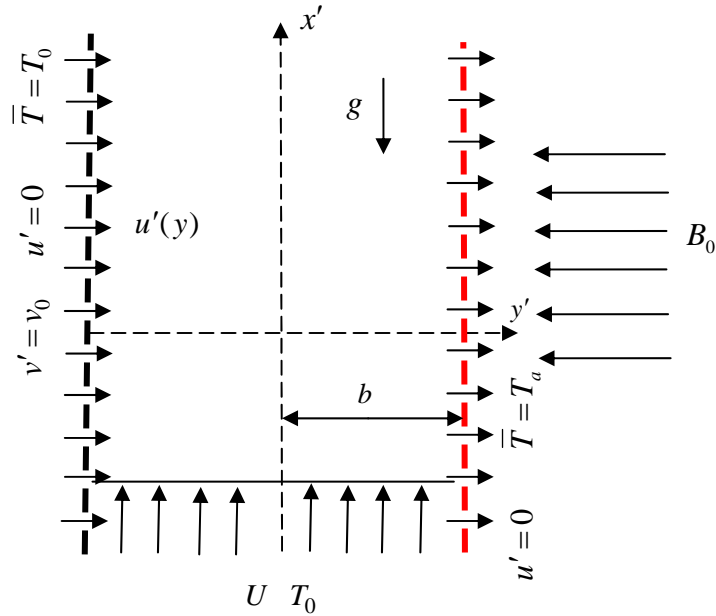


**Figure 5.1** Schematic diagram of the problem

82

The fluid has constant properties except the thermal conductivity and density changes which produce buoyancy force.

## 5.3 Formulation of Mathematical Equations

The basic equations of the problem considering viscous dissipation and buoyancy force are

$$\frac{\partial u'}{\partial x'} + \frac{\partial v'}{\partial y'} = 0 \tag{5.3.1}$$

$$u'\frac{\partial u'}{\partial x'} + v'\frac{\partial u'}{\partial y'} = -\frac{1}{\rho_{nf}}\frac{\partial p'}{\partial x'} + \nu_{nf}\left(\frac{\partial^2 u'}{\partial x'^2} + \frac{\partial^2 u'}{\partial y'^2}\right) - \frac{\sigma_{nf} B_0^{\;2}}{\rho_{nf}}u' + g\beta(\overline{T} - T_0) \tag{5.3.2}$$

$$\left(\rho c_p\right)_{nf}\left(u'\frac{\partial \overline{T}}{\partial x'} + v'\frac{\partial \overline{T}}{\partial y'}\right) = \kappa_{nf}\left(\frac{\partial^2 \overline{T}}{\partial x'^2} + \frac{\partial^2 \overline{T}}{\partial y'^2}\right) + \mu_{nf}\left(\frac{\partial u'}{\partial y'}\right)^2 - \frac{\partial q_r}{\partial y'} \tag{5.3.3}$$

Where $p'$ is the fluid pressure. The dynamic viscosity $\mu_{nf}$, effective density $\rho_{nf}$, effective thermal conductivity $\kappa_{nf}$, heat capacity $(\rho c_p)_{nf}$ and effective electrical conductivity $\sigma_{nf}$ of the nanofluid are defined by equation (2.8.5) in chapter 2.

As the velocity is only along $x'$-direction, it is assumed that

$$\frac{\partial u'}{\partial x'} = 0, \; \frac{\partial \overline{T}}{\partial x'} = 0, \; \frac{\partial^2 \overline{T}}{\partial x'^2} = 0.$$

By integrating Eqn (5.3.1) reduces to $v' = v_0$. Equations (5.3.2) and (5.3.3) then take the form

$$\frac{d^2 u'}{dy'^2} - \frac{v_0}{\nu_{nf}}\frac{du'}{dy'} - \frac{1}{\mu_{nf}}\frac{dp'}{dx'} - \frac{\sigma_{nf} B_0^{\;2}}{\mu_{nf}}u' + \frac{g\beta(\overline{T} - T_0)}{\nu_{nf}} = 0 \tag{5.3.4}$$

$$\frac{1}{\left(\rho c_p\right)_{nf}}\left[\kappa_{nf}\frac{d^2 \overline{T}}{dy'^2} - \left(\rho c_p\right)_{nf} v_0 \frac{d\overline{T}}{dy'} - \frac{dq_r}{dy'} + \mu_{nf}\left(\frac{du'}{dy'}\right)^2\right] = 0 \tag{5.3.5}$$

Eqs. (5.3.4)- (5.3.5) are subjected to the boundary conditions are:

$$\begin{aligned} y' = -b: \; u' = 0, \; \overline{T} = T_0 \\ y' = b: \; u' = 0, \; \overline{T} = T_a \end{aligned} \tag{5.3.6}$$

The radiative heat flux gradient of optically thin non-gray fluid near equilibrium according to Cogley (1968) is given by

$$\frac{dq_r}{dy'} = 4\gamma^2(\overline{T} - T_a) \tag{5.3.7}$$

$$\gamma^2 = \int_0^{y'} K_{\lambda a}\left(\frac{\partial e_{b\lambda}}{\partial \overline{T}}\right)_a d\lambda$$

where $K_{\lambda a}$ is the radiation absorption coefficient, $\lambda$ is the wave length and $e_{b\lambda}$ is the Planks' function.

According to Kay (1966), the variable thermal conductivity is

$$\kappa_{nf} = \kappa_\infty\left[1 + \tau\,\frac{\overline{T} - T_a}{T_a - T_0}\right],$$

and $k_\infty$ is the thermal conductivity at the ambient temperature $T_0$, $\tau$ is defined by

$$\tau = \frac{1}{\kappa_{nf}}\left(\frac{\partial \kappa}{\partial \overline{T}}\right)_{nf}.$$

Introduce the following transformations to seek for a similarity solution of Eqs. (5.3.4)-(5.3.5)

$$x = \frac{x'}{b},\ \ y = \frac{y'}{b},\ u = \frac{u'}{v_0},\ \ p = \frac{b\,p'}{\mu_f v_0},\ \ \theta = \frac{\overline{T} - T_0}{T_a - T_0},\ \ Ha'^2 = \frac{\sigma_f B_0{}^2 b^2}{\mu_f},\ Gr' = \frac{g\beta(T_a - T_0)b^2}{v_f v_0},$$

$$R' = \frac{4\gamma^2 b^2}{\kappa_\infty},\ Br' = \frac{\mu_f v_0{}^2}{\kappa_\infty(T_a - T_0)},\ N = -\frac{dp}{dx},\ Rs' = \frac{v_0 b}{v_f},\ Pe' = \frac{v_0 b(\rho c_p)_f}{\kappa_\infty},\ \kappa = \frac{\kappa_{nf}}{\kappa_\infty},\ \kappa = 1 + \tau\theta$$

(5.3.8)

where $Rs'$ is the porosity parameter, $Ha'$ is Hartmann number, $Gr'$ is Grashof number, $R'$ is radiation parameter, $Pe'$ is Peclet number and $Br'$ is Brinkman number.

Equations (5.3.4)-(5.3.5) reduced in non-dimensional form are as follows

$$\frac{d^2 u}{dy^2} - BC\,Rs'\frac{du}{dy} - C(A\ Ha'^2 u - B\,Gr'\theta - N) = 0 \qquad (5.3.9)$$

$$[1 + \tau\theta]\frac{d^2\theta}{dy^2} - B\,Pe'\frac{d\theta}{dy} - R'\theta + \frac{Br'}{C}\left(\frac{du}{dy}\right)^2 = 0 \qquad (5.3.10)$$

Where, $A = 1 + \left[3\left(\frac{\sigma_s}{\sigma_f} - 1\right)\phi \middle/ \left(\left(\frac{\sigma_s}{\sigma_f} + 2\right) - \left(\frac{\sigma_s}{\sigma_f} - 1\right)\phi\right)\right]$, $B = 1 - \phi + \phi\frac{\rho_s}{\rho_f}$ and $C = (1 - \phi)^{2.5}$

and $\phi$ is the nanoparticles solid volume fraction.

The boundary conditions in Eqn (5.3.6) reduce to following dimensionless form

$$y = -1: \quad u = 0, \quad \theta = 0$$
$$y = 1 \quad : \quad u = 0, \quad \theta = 1$$

(5.3.11)

Because of simplicity in calculation, the dimensionless numbers in Eqs (5.3.9)-(5.3.10) are

rescaled as $\quad Gr = \dfrac{Gr'}{\tau}, \quad Ha^2 = \dfrac{Ha'^2}{\tau}, \quad R = \dfrac{R'}{\tau}, \quad Br = \dfrac{Br'}{\tau}, \quad Rs = \dfrac{Rs'}{\tau}, \quad Pe = \dfrac{Pe'}{\tau}.$ (5.3.12)

The dimensionless Eqs (5.3.9)-(5.3.10) now get the form

$$\frac{d^2u}{dy^2} - BC\,Rs\,\tau\frac{du}{dy} - C(A\,Ha^2\,\tau u - B\,Gr\tau\,\theta - N) = 0$$

(5.3.13)

$$\frac{d^2\theta}{dy^2} + \tau\theta\frac{d^2\theta}{dy^2} - B\,Pe\,\tau\frac{d\theta}{dy} - R\tau\,\theta + \frac{Br}{C}\tau\left(\frac{du}{dy}\right)^2 = 0$$

(5.3.14)

The local Nusselt number $Nu$ and heat transfer rate are

$$Nu = \frac{q_w\big|_{y'=b}}{\kappa_f\,\Delta\bar{T}}, \quad q_w = -\kappa_{nf}\left(\frac{\partial\bar{T}}{\partial y'}\right)$$

(5.3.15)

From equations (5.3.8) and (5.3.15), the Nusselt number results in the following form

$$Nu = -\frac{\kappa_{nf}}{\kappa_f}\theta'(1)$$

(5.3.16)

## 5.4 Series Analysis

The power series expansions are considered in terms of the parameter $\tau$ as equations (5.3.13) and (5.3.14) are non-linear for velocity field and temperature distribution

$$u = \sum_{i=0}^{\infty} u_i\tau^i, \quad \theta = \sum_{i=0}^{\infty} \theta_i\tau^i, \quad |\tau| < 1$$

(5.4.1)

The non-dimensional governing equations (5.3.13) and (5.3.14) are then solved into series solutions by substituting the Eq. (5.4.1) and equating the coefficients of powers of $\tau$. The first 12 coefficients for the series of the temperature $\theta(\tau)$ and velocity $u(\tau)$ in terms of $\tau, Ha, R, Gr, Br, N, Rs, Pe, A, B, C$ are computed respectively. The first few coefficients of series for $\theta(\tau)$ is given below:

85

$$\theta(y;\tau,R,Rs,Pe,N,Gr,Br,Ha,A,B,C) = \frac{1}{2} + \frac{1}{2}y - \frac{1}{12}(y-1)(y+1)(BrCN^2y^2 - Ry - 2BPe - 3R$$

$$+ BrCN^2)\tau - \frac{1}{720}(y-1)(y+1)(105R - 30BrCN^2 + 30yBPe + 90BPeR - 60B^2Pe^2y + 75R^2 + 60Ry$$

$$+ 90BPe + 15Ry^2 - 3R^2y^3 - 15R^2y^2 + 7R^2y - 18BrCN^2y - 18BrCN^2y^3 - 30BPeRy^2 - 60BPeRy$$

$$- 28BrCN^2R - 30BrCN^2y^2 + 12BPeBrCN^2y + 2RBrCN^2y^2 + 12BPeBrCN^2y^3 + 2RBrCN^2y^4$$

$$+ 8ABrC^2N^2Ha^2y^4 + 36BrC^2N^2BRs\,y^3 - 52ABrC^2N^2Ha^2y^2 + 18BrCNGrBy^3 + 60BrCNGrBy^2$$

$$- 2BrCNGrBy - 4BrC^2N^2BRs\,y - 52BrC^2N^2AHa^2 + 60BrCNBGr)\tau^2 + O(\tau^3) \qquad (5.4.2)$$

The above power series solutions are valid for very small values of $\tau$. Therefore, the series are analysed applying Hermite- Padé approximation method.

## 5.5. Irreversibility Analysis

The characteristics of the flow field inside a porous channel with isothermal walls in the presence of thermal radiation with viscous dissipation and MHD effect are irreversible. The exchange of energy and momentum within the fluid and at the boundaries causes inequilibrium conditions which leads to continuous entropy generation. Following Bejan (1996) the volumetric entropy generation rate is given as

$$E_G = \frac{\kappa_{nf}}{T_0^{\,2}}\left(\frac{d\overline{T}}{dy'}\right)^2 + \frac{\mu_{nf}}{T_0}\left(\frac{du'}{dy'}\right)^2 \qquad (5.5.1)$$

Where the first term on the right side of equation (5.5.1) is the irreversibility due to heat transfer and the second term is the irreversibility due to viscous dissipation. The entropy generation number can be expressed in dimensionless form as,

$$N_S = \frac{T_0^{\,2}b^2E_G}{\kappa_f(T_a - T_0)^2} = \frac{\kappa_{nf}}{\kappa_f}\left(\frac{d\theta}{dy}\right)^2 + \frac{Br}{\Omega(1-\phi)^{2.5}}\left(\frac{du}{dy}\right)^2 \qquad (5.5.2)$$

Where $\Omega = \frac{(T_a - T_0)}{T_0}$ is the temperature difference parameter and

$$N_1 = \frac{\kappa_{nf}}{\kappa_f}\left(\frac{d\theta}{dy}\right)^2, \quad N_2 = \frac{Br}{\Omega(1-\phi)^{2.5}}\left(\frac{du}{dy}\right)^2$$

In general, the entropy generation number $N_s$ given in Eq. (5.5.2) provides a useful means of producing entropy generation profiles. However, it gives no indication as to the relative contributions of the fluid heat transfer and fluid friction effects. Thus, the parameter, Bejan number $Be$ is commonly used in its place.

The Bejan number is given as $Be = \dfrac{N_1}{N_S}$

It is noteworthy that the Bejan number ranges from 0 to 1 and $Be = 0$ is the limit where the irreversibility is dominated by fluid friction effects. $Be = 1$ is the limit where the irreversibility due to heat transfer dominates the flow system because of finite temperature differences. The contributions of heat transfer and fluid friction to entropy generation are equal when $Be = \frac{1}{2}$. In the present work, second law analysis is investigated between a porous channel.

## 5.6. Results and Discussion

The influences of thermal radiation and temperature dependent variable thermal conductivity on the entropy generation of nanofluid flow through a porous channel under viscous dissipation effect in the presence of uniform magnetic field is studied in this chapter. The numerical computations of series for the temperature $\theta(\tau)$ and velocity $u(\tau)$ are carried out at various values of the physical parameters *Pr, R, Br, Gr, Rs, Pe, Ha* and $\tau$ to obtain the condition under which the dual (upper and lower branch) solutions may exist. The minimum entropy conditions provide the possibility of achieving the maximum available work. In the present study, the nanoparticle volume fraction is specified in the range of $\phi = 0\% - 5\%,$ where a value of $\phi = 0$ indicates the pure base fluid. In addition, the thermal conductivity variation parameter is assigned in the range of $-0.1 \leq \tau \leq 0.2$, the porosity parameter $0 \leq Rs \leq 8$, the radiation parameter $0 \leq R \leq 10$, the Brinkman number $1 \leq Br \leq 100$, the Hartmann number $0 \leq Ha \leq 5$. The Grashof number and dimensionless pressure gradient are kept fixed at $Gr = 1, N = 1$. Table 5.1 shows the comparison of our results with those of Makinde and Eegunjobi (2013) with $Br = 0, Ha = 0, Gr = 0, Rs = 1, N = 1$ for pure base fluid. The results in Table 5.1 imply that there is a good agreement of the values of velocity profile between the present study and

Makinde and Eegunjobi (2013) from the left injected wall ($y = -1$) towards the centerline ($y = 0$) and then to the right suctioned wall ($y = 1$) of the channel.

**Table 5.1** Comparison of numerical values for velocity with available literature when $Br = 0, Ha = 0, Gr = 0, \phi = 0, Rs = 1, N = 1$.

| $y$ | Present Study | Makinde and Eegunjobi (2013) | Relative Difference |
|---|---|---|---|
| -1.0 | 0 | 0 | |
| -0.8 | 0.03894655 | 0.03879297 | 0.4% |
| -0.6 | 0.07258247 | 0.07114875 | 1.3% |
| -0.4 | 0.09765518 | 0.09639032 | 2% |
| -0.2 | 0.11658237 | 0.11376948 | 2.4% |
| 0 | 0.12939390 | 0.12245933 | 5.3% |
| 0.2 | 0.12553130 | 0.12154600 | 3.2% |
| 0.4 | 0.11508405 | 0.11001953 | 4.4% |
| 0.6 | 0.09134248 | 0.08676372 | 5% |
| 0.8 | 0.05172775 | 0.05054498 | 2.3% |
| 1.0 | 0 | 0 | |

### 5.6.1 Stability Analysis

Table 5.2 displays that the critical values of thermal conductivity variation parameter $\tau_c$ increase with a positive increase in the values of radiation parameter $R$ in absence of suction/injection parameter and the values of $\delta$ indicates that $\tau_c$ is a branch point. On the other hand, the presence of porosity parameter ($Rs = 3$) increases $\tau_c$ positively. Therefore, it is significant to notice from the table that the progress of thermal runaway enlarges and develops thermal instability in the system when radiation effect enhances in porous walls. Moreover, the rate of heat transfer $Nu$ enhances as $R$ increases. Finally the values of $\tau_c$ in Table 5.2 give an idea about the onset of thermal instability and its nature numerically. A segment of bifurcation diagram for different values of $R$ in the $(\tau, Nu)$ plane is noticed in

Figure 5.2(a) using Drazin-Tourigny Approximants at $Rs = 0$. A *simple turning point, fold or a saddle-node bifurcation* at $\tau = \tau_c$ is shown in Figure 5.2. It is interesting to notice that there are two solution branches (I and II) of Nusselt number when $\tau > \tau_c$, one solution when $\tau = \tau_c$, and no solution when $\tau < \tau_c$, where $\tau_c$ is the critical value of $\tau$ for which the solution exists. The stability analysis indicates that the lower solution branch (II) is stable and physically realizable. For different values of *R,* the upper solution branch (I) is unstable and physically unacceptable shown in Figure 5.2(a).

**Table 5.2** Numerical calculations showing thermal conductivity criticality for different parameter values using High-order Differential Approximants at $Br = 1, Gr = 1, \phi = 0, Ha = 1, N = 1$ for $d = 3$.

| $R$ | $Rs$ | $\tau_c$ | $\delta$ | $Nu$ |
|-----|------|----------|----------|------|
| 1 | 0 | -0.53565727924096 | 0.4642786109 | 0.1864302965 |
| 2 | 0 | -0.37733219733189 | 0.4496674465 | 0.5561558070 |
| 5 | 0 | -0.21641937233523 | 0.4565449106 | 1.130723424 |
| 1 | 3 | 0.008001204075356 | 0.4566547116 | 5.920689257 |
| 5 | 3 | 0.009206845176432 | 0.4487675475 | 6.014179785 |

Meanwhile, the positive variation of thermal conductivity parameter slowly decreases the rate of heat transfer and as *R* increases the bifurcating point increases and produces more instability to the upper solution branch (I). The numerical values in Table 5.2 are also consistent with the lower solution branch of *Nu* as *R* increases in Figure 5.2(a). Figure 5.2(b) represents the effect of three different nanoparticles on the bifurcation diagram in such a way at $\phi = 0.1, Rs = 2$ that the bifurcating points almost coincide. However, they produce instability to the upper solution branch (I) and the value of Nusselt number decreases in Cu-nanoparticles than $TiO_2$ and $Al_2O_3$-nanopaticles.
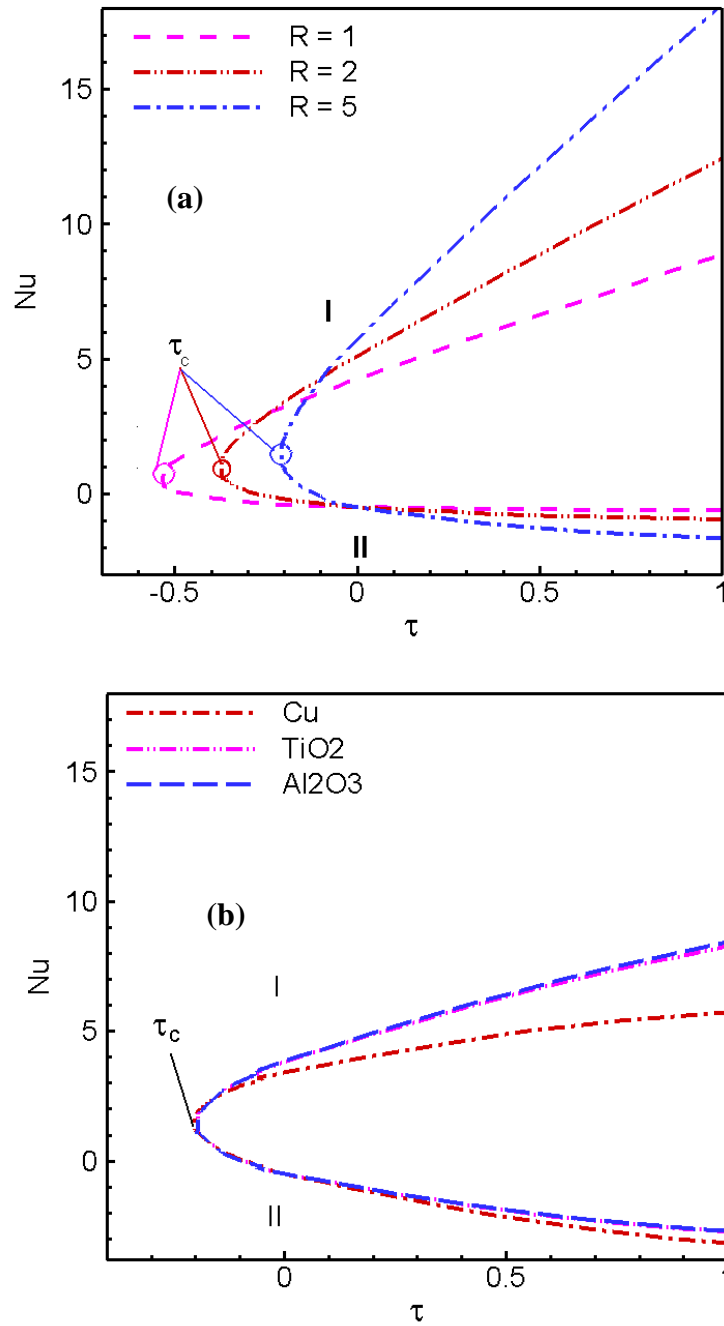
**Figure 5.2** Approximate bifurcation diagrams against $\tau$ in the $(\tau,\ Nu(1))$ plane (a) for different values of $R$ with $\phi = 0, Rs = 0$ and (b) for different nanoparticles with $\phi = 0.1, Rs = 2$ obtained by Drazin-Tourigny method (1996) at $d = 3, N = 1, Ha = 1, Gr = 1, Br = 1$.

### 5.6.2 Effect of Porosity parameter

Figures 5.3(a, b), 5.4(a, b) describes the effect of porosity parameter on flow characteristics with entropy generation within the channel. Figure 5.3(a) reveals that the velocity decreases with an increase in injection parameter as $Rs$ near the left wall $(y = -1)$ and the maximum velocity also develops towards the right wall when $Rs$ increases due to suction.
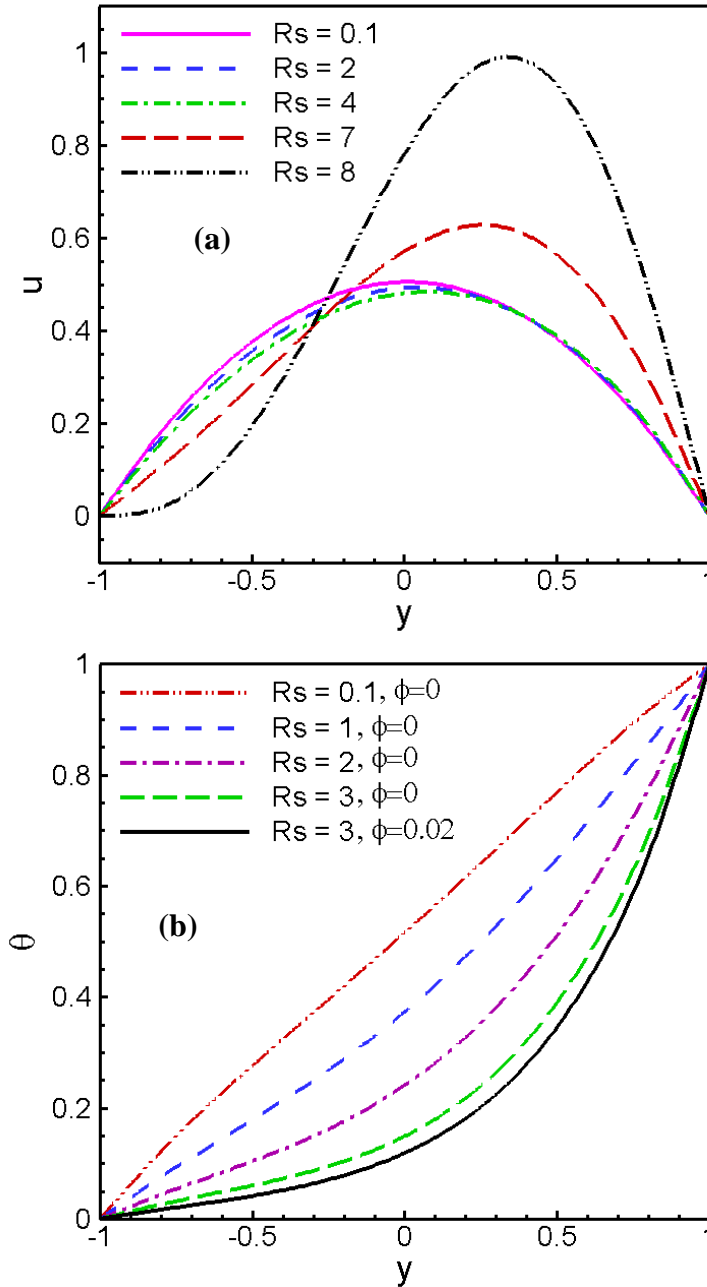


**Figure 5.3** Effect of porosity parameter on (a) velocity profiles and (b) temperature distributions respectively at $Br = 7.1, Gr = 1, \tau = 0.1, \ N = 1, \Pr = 7.1, Ha = 1, R = 1.$

91
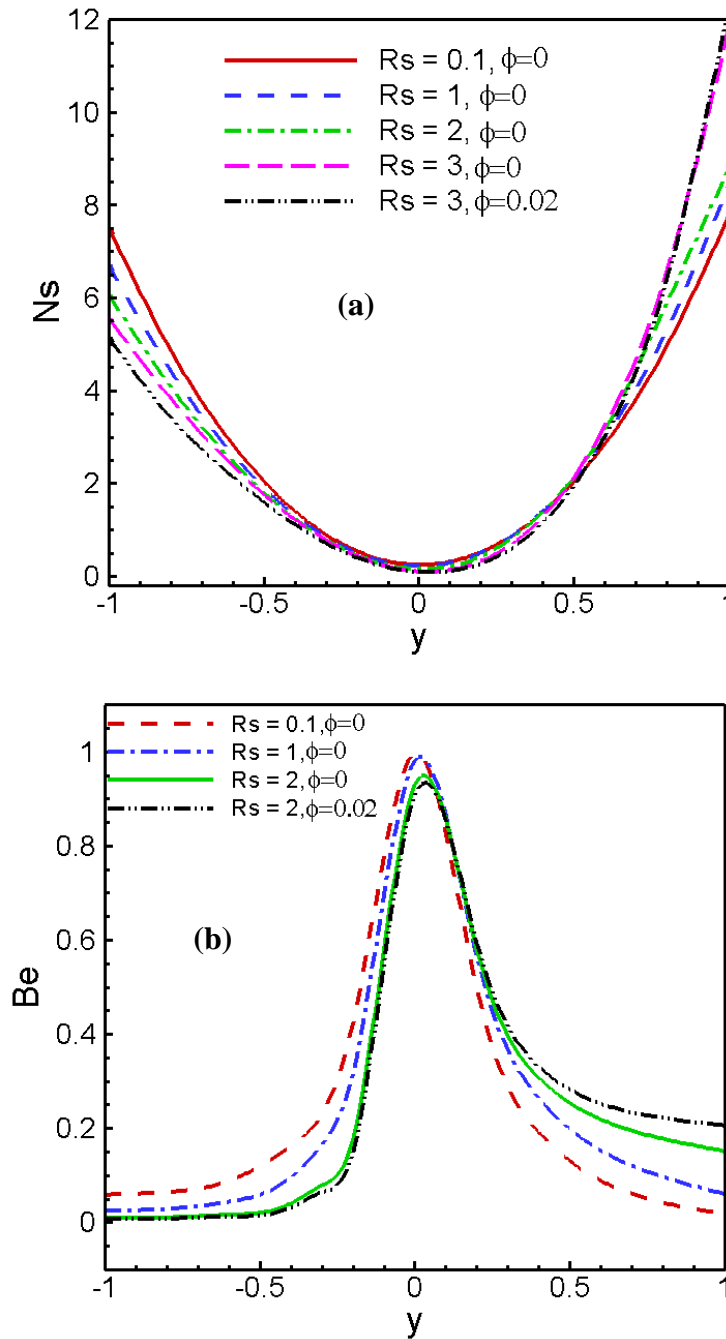
**Figure 5.4** Effect of porosity parameter on (a) entropy generation rates and (b) Bejan profiles respectively at $\Pr = 7.1, Gr = 1, Br = 7.1, \ N = 1, R = 1, Ha = 1, \tau = 0.1.$

In absence of suction/injection parameter $(Rs = 0)$, the velocity profile is parabolic and symmetrically distributed inside the channel; it however becomes skewed with increase in suction/injection parameter. Meanwhile, there occur backflow at the left porous wall for

large values of *Rs*. Figure 5.3(b) demonstrates a significant reduction in fluid temperature inside the channel when suction/injection parameter as *Rs* increases. This is physically true since injection of fluid increases the fluid velocity around centerline thereby increases the heat transfer rate within the channel. Generally, the value of $N_2$ i.e., the entropy generated by fluid friction is larger than that of $N_1$ i.e., the entropy produced by fluid heat transfer. As a result, $N_S$ is contributed mainly by $N_2$ throughout the entire flow field. However, in the areas of the flow field characterized by a faster flow rate, the velocity gradient is reduced, and thus $N_2$ also reduces. In the present porous channel, $N_S$ gradually reduces to zero at $y = 0$ as shown in Figure 5.4(a). In this particular region of the flow field, fluid friction effects play only a minor role, and thus $N_S$ is contributed mainly by $N_1$. The figure reveals a minor decrease in $N_s$ when *Rs* increase near the cold porous wall, whereas $N_S$ increases rapidly in base fluid and further in nanofluid in the region above the centerline to the right hot porous wall. Since the dominant effect of heat transfer occurs at the right hot wall. Figure 5.4(b) displays the distribution of the Bejan number (*Be*) versus the channel width for porosity parameter. It is noticed that *Be* has a value of zero at the left cold wall and close to zero at the right hot wall of the channel since, as discussed previously, the velocity gradient is increased at the walls due to suction/injection, and hence $N_S$ is contributed mainly by $N_2$. In the central region of the flow field, *Be* increases to a maximum value of 1 due to the reduction in the velocity gradient and the corresponding increase in the contribution of $N_1$ to the overall entropy generation. It is to be seen that the heat transfer irreversibility dominates the flow process within the channel centerline region, while the influence of fluid friction irreversibility can be observed at the two porous walls.

### 5.6.3 Effect of Thermal Conductivity variation parameter

The influences of thermal conductivity variation parameter on temperature distribution, entropy generation rate $N_s$ and distribution of Bejan number *Be* are depicted in Figures 5.5(a, b, c). A decrease in the fluid temperature around the central region of the channel is observed in Figure 5.5(a) due to the positive escalating values of $\tau$. The temperature profile is further decreased in nanofluid than base fluid as $\tau$ increases.

**Figure 5.5** Effect of thermal conductivity variation parameter on (a) temperature profiles, (b) entropy generation rates and (c) Bejan profiles respectively at $\Pr = 7.1, Gr = 1, Br = 7.1, \ N = 1, Rs = 1, Ha = 1, R = 1.$

The increases of thermal conductivity variation parameter produce more heat transfer within the channel centerline region and reduce dimensionless temperature distribution.

Furthermore, due to the higher thermal conductivity coefficient of the nanofluid, the heat is more keenly transferred. Figure 5.5(b) indicates the effect of thermal conductivity variation parameter on entropy generation number inside the channel. From this figure, it is observed that near the cold porous wall, $N_s$ decreases slightly with the increase of $\tau$ while it increases with the increase of $\tau$ toward the hot porous wall. The influence of thermal conductivity variation parameter on Bejan profile is seen in Figure 5.5(c). It can be noted from this figure that fluid friction irreversibility dominates entropy generation near the porous walls while heat transfer irreversibility is the dominant contributor near the channel centerline. It is observed that as $\tau$ increases, the dominance of heat transfer irreversibility near the hot wall increases especially for nanofluid while the dominance of fluid friction irreversibility near the cold porous wall is insensitive to change in $\tau$ .

### 5.6.4 Effect of Radiation parameter

Figures 5.6(a, b, c) represent the thermal field with entropy generation due to the effect of Radiation parameter. The effect of Radiation parameter $R$ on fluid temperature in Figure 5.6(a) shows that temperature near the channel centre line reduces uniformly by the positive increase of $R$ due to radiative heat loss. Also nanofluid enhances the rate of heat transfer which leads to more reduction in temperature as reflect in Figure 5.6(a). Entropy generation due to the effect of radiation parameter $R$ is shown in Figure 5.6(b). The figure reveals a small decrease in $N_s$ when $R$ increase near the cold porous wall, whereas $N_s$ increases significantly toward the hot porous wall because of the sole contribution of heat transfer effect. Figure 5.6(c) displays the distribution of Bejan number for different values of Radiation parameter $R$. The figure instructed that as $R$ increases, there is enhanced dominance of heat transfer irreversibility near the hot porous wall where nanofluid exhibits the maximum. There is an absolute dominance of heat transfer irreversibility $(Be = 1)$ for varying values of $R$ near the centerline of the channel while there absolute dominance of fluid friction irreversibility $(Be = 0)$ near the cold porous wall.

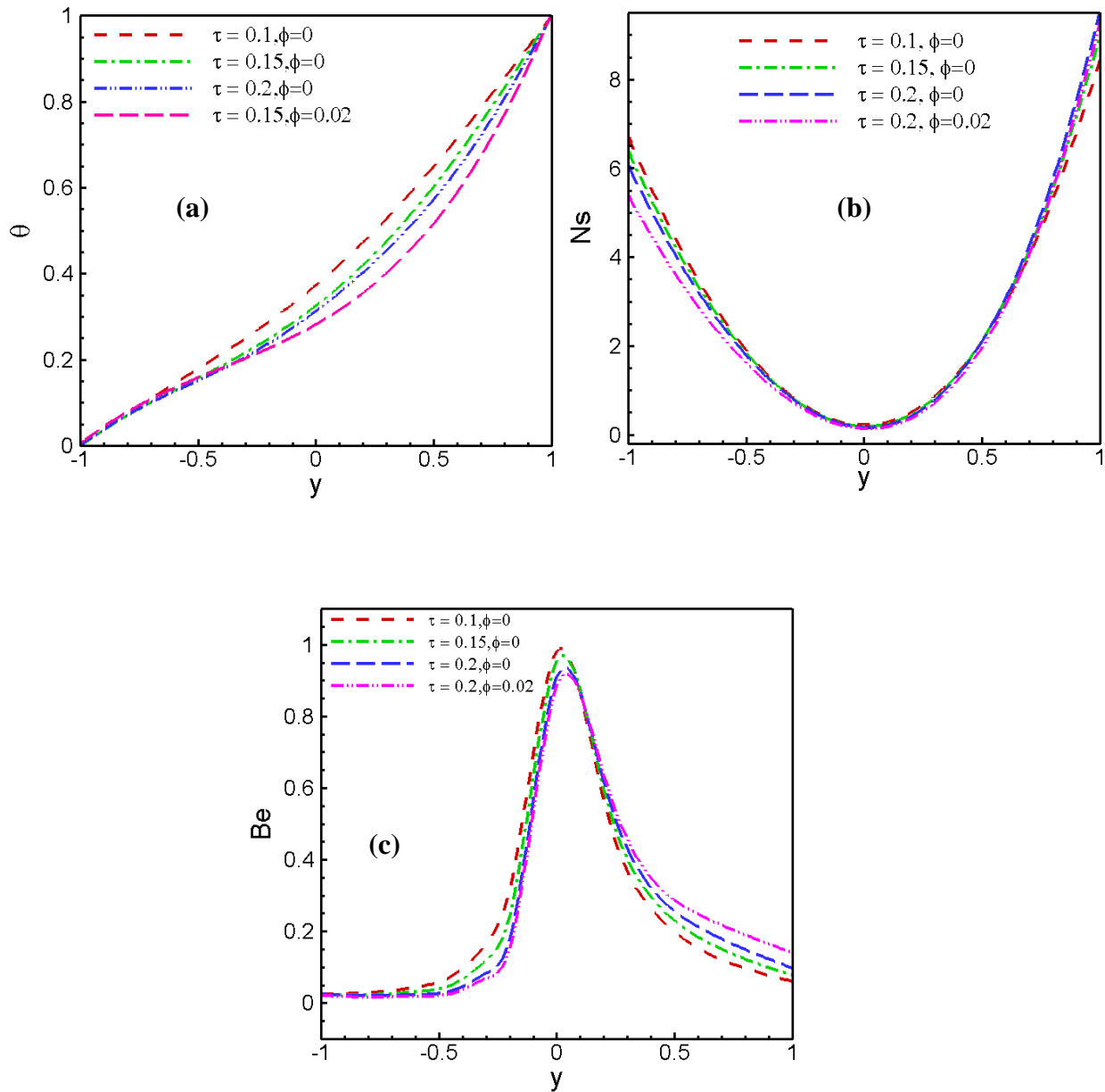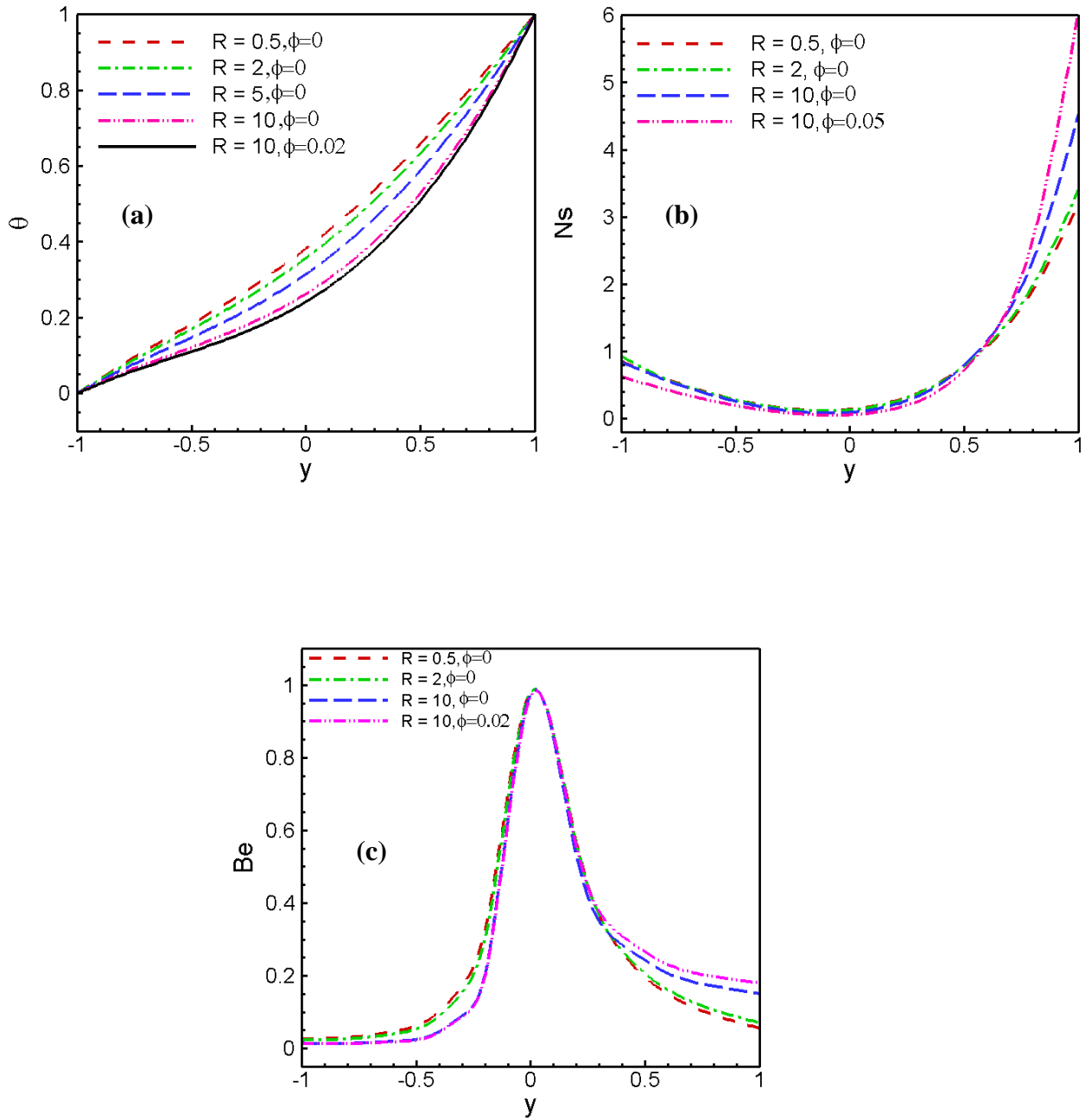**Figure 5.6** Effect of Radiation parameter on (a) temperature profiles, (b) entropy generation rates and (c) Bejan profiles respectively at $\mathrm{Pr} = 7.1, Gr = 1, Br = 7.1, \ N = 1, Rs = 1, Ha = 1, \tau = 0.1.$

### 5.6.5 Effect of Prandtl number

The effects of Prandtl number on temperature distribution, entropy generation rate $N_s$ and distribution of Bejan number *Be* are depicted in Figures 5.7(a, b, c). Prandtl number is the ratio of viscous force and thermal force. Therefore, increasing values of *Pr* increases viscosity and decreases thermal action of the fluid. The dimensionless temperature of fluid inside the channel decreases rapidly for base water and further in Cu-water nanofluid than air or other gases due to higher thermal conductivity coefficient as observed in Figure 5.7(a). The effect of Prandtl number *Pr* on entropy generation rate is noticed in Figure 5.7(b). The figure reveals an increase in $N_s$ as *Pr* increases near the porous walls. This is due to the increase in temperature gradient as *Pr* increases which is also further in nanofluid. In Figure 5.7(c), Bejan number is represented for various values of Prandtl number *Pr*. It is noticed from the figure that the dominance effect of both fluid friction and heat transfer irreversibilities near the two walls almost similar. On the other hand, the dominance effect of fluid friction irreversibility is absolute near the porous walls and the dominance of heat transfer irreversibility decreases as *Pr* increases for base water and Cu-water nanofluid. The conjecture of Figures 5.7 (b, c) has a good agreement with those results of Abiodun et al. (2011).

### 5.6.6 Effect of Hartmann number

Figure 5.8 represents that in absence of magnetic field velocity achieves its maximum value, while increasing values of *Ha* produces reduction of the velocity near the channel centerline region. The variation of *Ha* leads to the variation of the Lorentz force due to magnetic field and the Lorentz force produces more resistance to the fluid velocity.

### 5.6.7 Effect of nanoparticles volume fraction

The influence of nanoparticles volume fraction $\phi$ on velocity is depicted in Figure 5.9 at $Rs = 1$. In Figure 5.9, a uniform reduction in fluid velocity is observed as $\phi$ increases. The equivalent thermal expansion coefficient of the nanofluid is less than that of base water. As a result, the buoyancy force acting on the nanofluid is also less than that acting on the pure water, and hence the dimensionless velocity is reduced. In addition, since the density and

viscosity of the nanofluid are greater than those of base water, the velocity distribution within the channel is more uniform.
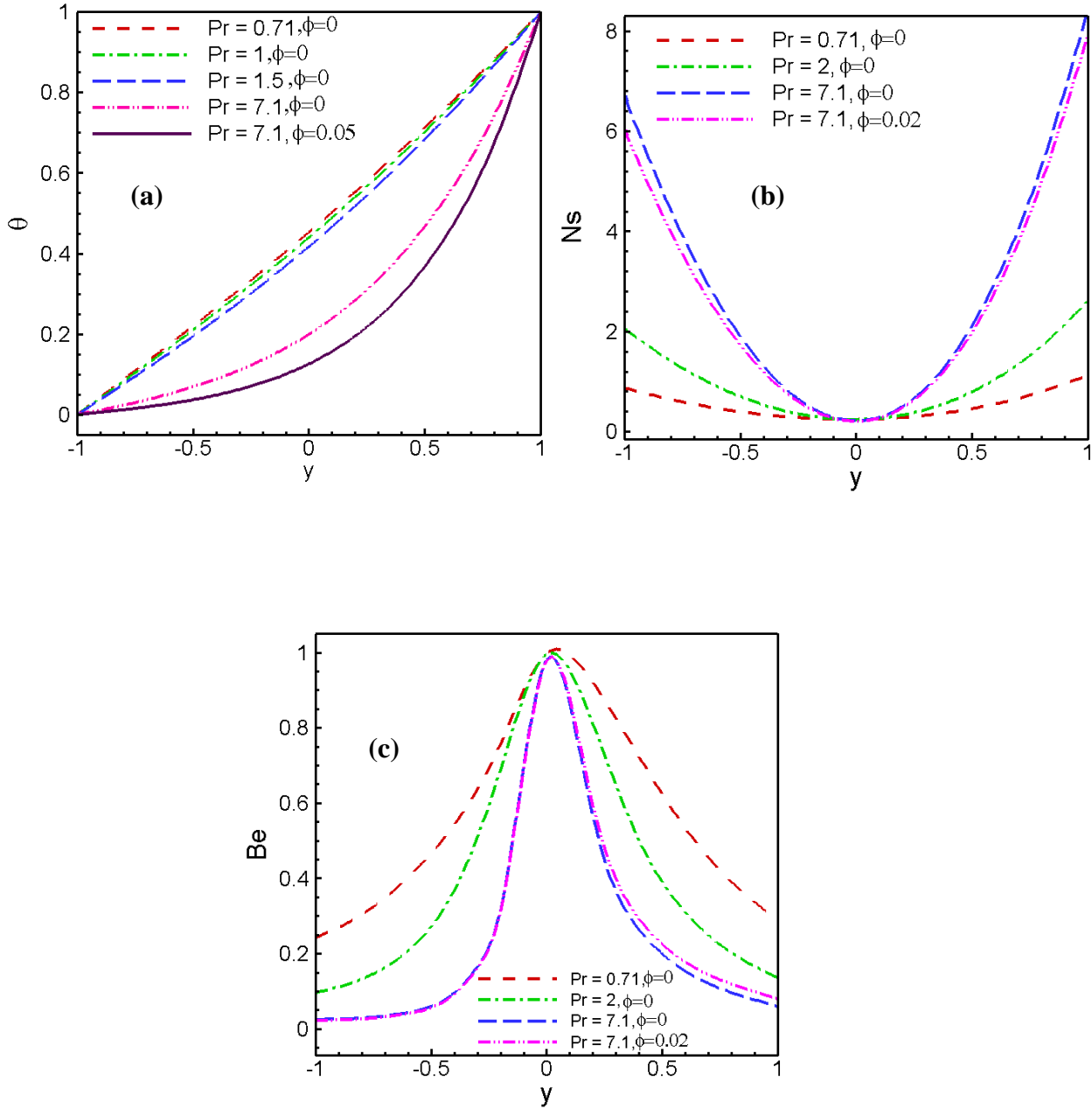


**Figure 5.7** Effect of Prandtl number on (a) temperature profiles, (b) entropy generation rates and (c) Bejan profiles respectively at $R = 1, Gr = 1, Br = 7.1, \ N = 1, Rs = 1, Ha = 1, \tau = 0.1.$
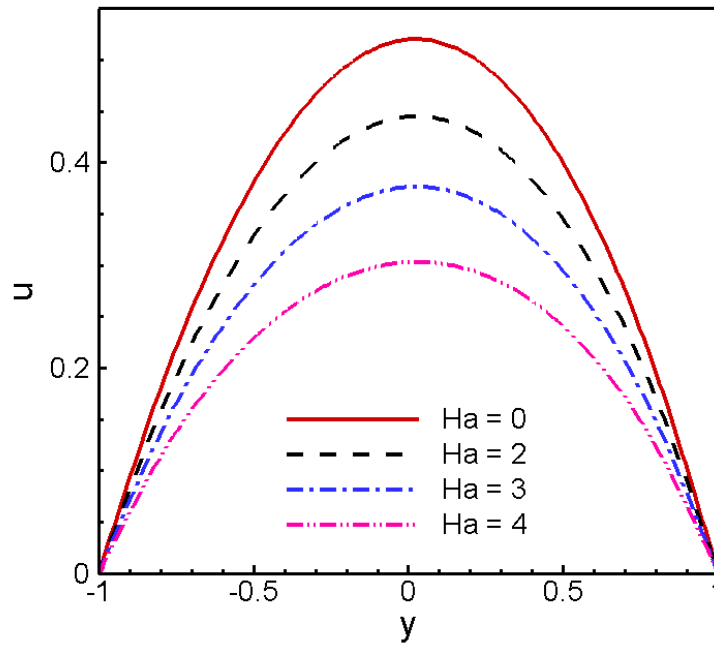
**Figure 5.8** Effect of Hartmann number on velocity profiles at $Br = 7.1, Gr = 1, \tau = 0.1,$
$Rs = 1, R = 1, \Pr = 7.1, \phi = 0.$
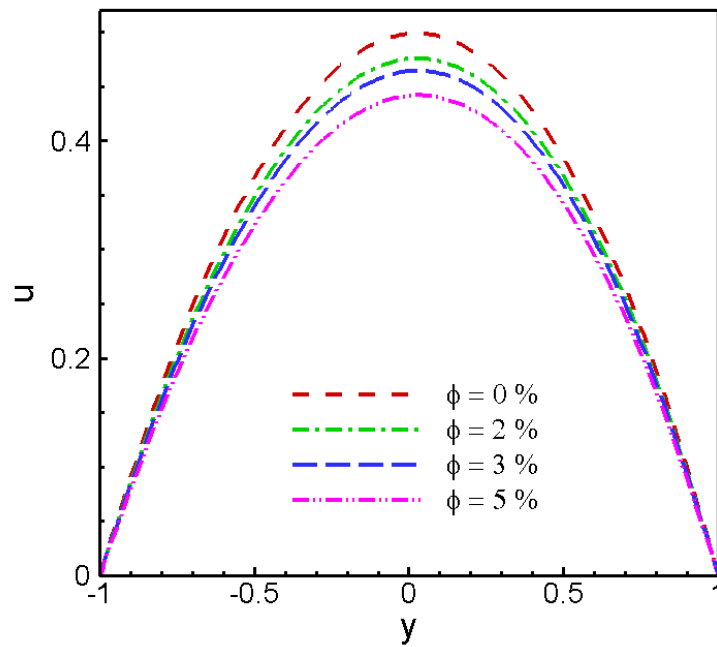


**Figure 5.9** Effect of nanoparticles volume fraction on velocity profiles at
$Br = 7.1, Gr = 1, \tau = 0.1, \quad Rs = 1, R = 1, \Pr = 7.1, Ha = 1.$

### 5.6.8 Effect of Brinkman number

The dimensionless velocity distribution of the flow field has a direct effect on the dimensionless temperature distribution as the effects of viscous dissipation are taken into consideration in the present problem. It is noticed from Figure 5.10 that the fluid temperature increases with increasing parametric values of viscous heating parameter *Br* but a minor reduction is seen in presence of nanoparticles. The velocity gradient of the pure working fluid is greater than that of the nanofluid due to the lower viscosity which results in more viscous dissipation effect. Furthermore, due to the higher thermal conductivity coefficient of the nanofluid, the heat is more intensely transferred. Hence, the dimensionless temperature of the nanofluid is less than that of the base fluid in Figure 5.10.
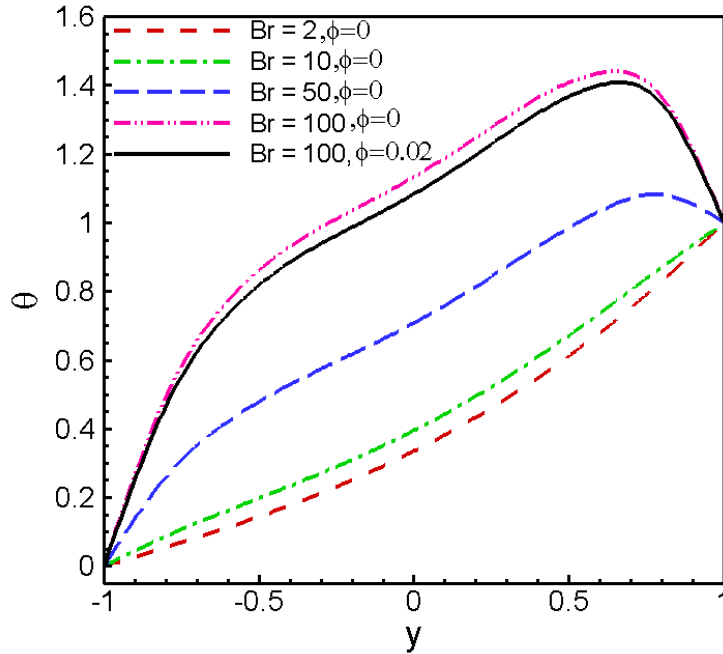


**Figure 5.10** Effect of Brinkman number on temperature profiles at $Rs = 1, Ha = 1, \tau = 0.1$.
$R = 1, Gr = 1, \ N = 1, \Pr = 7.1$

### 5.7. Conclusion

In this chapter we investigate the entropy generation of a steady laminar radiative variable thermal conductivity flow and heat transfer with viscous dissipation of three various nanofluids through a vertcal porous channel in the presence of transverse magnetic field.

The numerical simulation is carried out applying Hermite- Padé approximation method to examine the dominating singularity behaviour of the problem as well as the existence of the dual solutions of the rate of heat transfer. It is observed that suction/injection of fluid exerts a significant influence on the velocity and temperature distribution, which transitively affects the entropy generation within the channel. The major conclusions of the present problem are

➢ For $\tau > \tau_c$, the solution of local rate of heat transfer has two branches, namely, an upper branch and a lower branch. It is found that at the lower solution branch which is physically acceptable, the value of Nusselt number decreases with the increase of radiation parameter.

➢ At the region of the left porous wall, there occur backflow as the porosity parameter *Rs* increases. An increase in the thermal conductivity variation parameter and Radiation parameter reduces temperature distribution due to faster heat loss. Increasing Hartmann number and nanoparticles solid volume fraction cause the reduction of fluid velocity near the centerline uniformly because of the acting of Lorentz force and reduction of buoyancy force.

➢ For regions of the flow field at a greater velocity gradient, i.e., adjacent to the porous walls, the total entropy generation rate is dominated by the effects of fluid friction. Moreover, in the regions of the flow field at a higher and more uniform velocity distribution, i.e., the central region of the channel, the total entropy generation rate is dominated absolutely by the effects of fluid heat transfer.

The stability of MHD Jeffery-Hamel nanofluid flow through divergent channel is studied in the next chapter.

# Stability of Magnetohydrodynamic Jeffery-Hamel Nanofluid Flow through Divergent Channel[4]

*The effects of Cu-water nanofluid on the entropy generation of the nonlinear magnetohydrodynamic Jeffery-Hamel flow through divergent channel are analyzed in the present study. The basic governing equations are solved into series solution using a semi-numerical analytical technique called Hermite- Padé approximation. The velocity profiles, temperature distributions and entropy generation rates with Bejan profiles are presented in divergent channel for various values of nanoparticles solid volume fraction, Hartmann number, Eckert number, Reynolds number and channel angle. The dominating singularity behavior of the problem is analysed numerically and graphically. The critical relationship between the parameters is studied to observe the instability of the problem for nanofluid.*

## 6.1 Introduction

The study of flows through non parallel walls, inclined at an angle, i.e., in convergent-divergent channel is very important due to its industrial, aerospace, chemical, civil, environmental, mechanical and bio- mechanical engineering applications. Jeffery (1915) and Hamel (1916)  first studied the two-dimensional steady motion of a viscous fluid through convergent-divergent channels which is called classical Jeffery-Hamel flow in fluid dynamics.

The theory of MHD is inducing current in a moving conductive fluid in the presence of magnetic field; such induced current results force on ions of the conductive fluid. Damping and controlling of electrically conducting fluid can be achieved by means of an electromagnetic body force (Lorentz force), which is produced by the interaction of an

---

[4] *Part of this chapter appears as a published paper: International Journal of Engineering, Transaction A, Vol. 28, No.4, pp. 599-607(2015).*

applied magnetic field and an electric current that is usually externally supplied. The theoretical study of MHD channel has been a subject of great interest due to its extensive applications in designing cooling systems with liquid metals, MHD generators, accelerators, pumps, and flow meters (Cha et al. (2002), Tendler(1983)). The classical Jeffery-Hamel problem was extended in Axford (1961) to include the effects of external magnetic field on conducting fluid. Motsa et al. (2010) found the solution of the nonlinear equation for the MHD Jeffery-Hamel problem by using novel hybrid spectral-homotopy analysis method. Moghimi et al. (2011) also solved the Jeffery-Hamel flow problem by using the homotopy perturbation method. Taking into account the rising demands of modern technology, including chemical production, power station, and microelectronics, there is a need to develop new types of fluids that will be more effective in terms of heat exchange performance. The term 'nanofluid' was envisioned to describe a fluid in which nanometer-sized particles were suspended in conventional basic fluids by Choi (1995). These nanoparticles are good conductors of heat and enable the base fluids to enhance their thermal properties. The effects of magnetic field and nanoparticles on the Jeffery-Hamel flow using a powerful analytical method called the Adomian decomposition method were studied by Sheikholeslami et al. (2012). Moradi et al. (2013) investigate the effect of three types of nanoparticles Cu, $TiO_2$ and $Al_2O_3$ on Jeffery-Hamel flow using Differential Transformation Method (DTM). Moreover, the effects of heat transfer and viscous dissipation on the Jeffery-Hamel flow of nanofluids are investigated by Moradi et al. (2015). Finally, a study of velocity and temperature slip effects on flow of water based nanofluids in converging and diverging channels was done by Syed et al. (2015).

For any thermal system, as the entropy generation increases, the energy decreases. Thus, to enhance the efficiency of the system, the rate of entropy generation must be effectively controlled. Bejan (1996) studied the entropy generation for forced convective heat transfer due to temperature gradient and viscosity effects in a fluid. Bejan (1979) also presented various reasons for entropy-generation in applied thermal engineering where the generation of entropy destroys the available work of a system.

In this study, our objective is to investigate the stability and entropy generation on magnetohydrodynamic Jeffery-Hamel nanofluid flow through divergent channel considering viscous dissipation effect. Using an appropriate similarity transformation, the well-known

governing partial differential equations are reduced to ordinary differential equations. The resulting equations are solved applying the power series along with Hermite–Padé approximation (HPA). The effects of various thermophysical parameters on velocity field, temperature distributions, entropy generation rate with Bejan profiles are discussed in detail. The change in singular points for channel angle and flow Reynolds number by the effect of nanofluids and the critical relationship between the parameters is an extension of the available literature. A comparative study between the previously published results and the present results in a limiting sense reveals excellent agreement between them.

## 6.2 Physical Configuration

Consider a steady two-dimensional laminar incompressible flow of electrically conducting viscous Cu-water nanofluid from a source or sink between two channel walls intersect at an angle $2\alpha$ in the axis of $z$. A cylindrical coordinate system $(r, \varphi, z)$ is used and assume that the velocity is purely radial and depends on $r$ and $\varphi$ so that there is no change in the flow parameter along the z-direction.
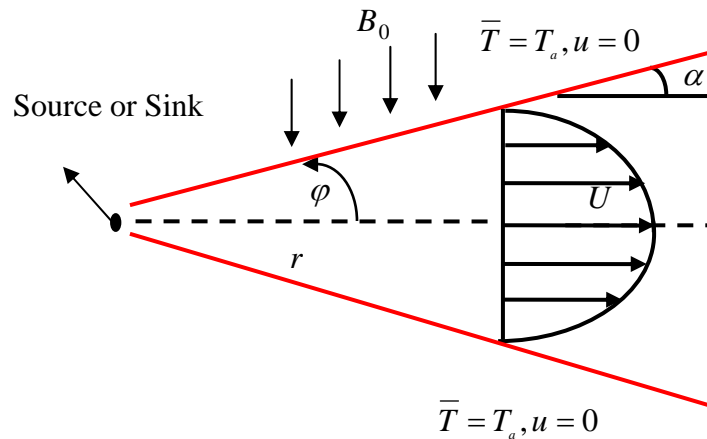


**Figure 6.1** Geometry of the problem

The top and bottom walls of the channel are heated with uniform temperature $T_a$. It is presumed that there is a magnetic field acting in the vertical downward direction to the top wall of the channel.

104

## 6.3 Mathematical Formulation

The continuity equation, the Navier-Stokes equation and energy equation considering viscous dissipation in reduced polar coordinates are

$$\frac{\rho_{nf}}{r}\frac{\partial}{\partial r}(ru(r,\varphi)) = 0, \tag{6.3.1}$$

$$u(r,\varphi)\frac{\partial u(r,\varphi)}{\partial r} = -\frac{1}{\rho_{nf}}\frac{\partial p}{\partial r} + v_{nf}\left(\frac{\partial^2 u(r,\varphi)}{\partial r^2} + \frac{1}{r}\frac{\partial u(r,\varphi)}{\partial r} + \frac{1}{r^2}\frac{\partial^2 u(r,\varphi)}{\partial \theta^2} - \frac{u(r,\varphi)}{r^2}\right)$$
$$- \frac{\sigma B_0^2}{\rho_{nf}r^2}u(r,\varphi), \tag{6.3.2}$$

$$\frac{1}{\rho_{nf}r}\frac{\partial p}{\partial \varphi} - \frac{2v_{nf}}{r^2}\frac{\partial u(r,\varphi)}{\partial \varphi} = 0, \tag{6.3.3}$$

$$u(r,\varphi)\frac{\partial \overline{T}(r,\varphi)}{\partial r} = \frac{\kappa_{nf}}{\left(\rho c_p\right)_{nf}}\left(\frac{\partial^2 \overline{T}(r,\varphi)}{\partial r^2} + \frac{1}{r}\frac{\partial \overline{T}(r,\varphi)}{\partial r} + \frac{1}{r^2}\frac{\partial^2 \overline{T}(r,\varphi)}{\partial \varphi^2}\right)$$
$$+ \frac{\mu_{nf}}{\left(\rho c_p\right)_{nf}}\left(4\left(\frac{\partial u(r,\varphi)}{\partial r}\right)^2 + \frac{1}{r^2}\left(\frac{\partial u(r,\varphi)}{\partial \varphi}\right)^2\right) \tag{6.3.4}$$

Where $B_0$ is the electromagnetic induction, $\sigma$ is the conductivity of the fluid, $u(r,\varphi)$ is the velocity along radial direction, $\overline{T}$ is the dimensional temperature, $p$ is the fluid pressure.

The boundary conditions are as follows:

At the centerline of the channel: $\varphi = 0$

$$\frac{\partial u(r,\varphi)}{\partial \varphi} = 0, \frac{\partial \overline{T}(r,\varphi)}{\partial \varphi} = 0, \ u(r,\varphi) = U$$

At the boundary of the channel: $\varphi = \alpha$

$$u(r,\varphi) = 0, \overline{T} = T_a$$

The effective density $\rho_{nf}$, the effective dynamic viscosity $\mu_{nf}$, and the kinematic viscosity $\nu_{nf}$ of the nanofluid are given as Sheikholeslami et al. (2013)

$$\rho_{nf} = \rho_f(1-\phi) + \rho_s\phi, \quad \mu_{nf} = \frac{\mu_f}{(1-\phi)^{2.5}}, \quad \nu_{nf} = \frac{\mu_{nf}}{\rho_{nf}}, \tag{6.3.5}$$

Here $\phi$ is the solid volume fraction.

The corresponding effective thermal conductivity and heat capacity of nanofluid are

$$k_{nf} = k_f \frac{k_s + 2k_f - 2\phi(k_f - k_s)}{k_s + 2k_f + \phi(k_f - k_s)}, \quad (\rho c_p)_{nf} = (1-\phi)(\rho c_p)_f + \phi(\rho c_p)_s \tag{6.3.6}$$

Considering purely radial flow, the continuity Eq. (6.3.1) implies that

$$f(\varphi) = ru(r,\varphi) \tag{6.3.7}$$

The dimensionless form of the velocity and temperature can be obtained according to Hamel (1916) as

$$f(\eta) = \frac{f(\varphi)}{f_{max}}, \ f_{max} = rU, \ \theta(\eta) = \frac{\overline{T}}{T_a}, \ \eta = \frac{\varphi}{\alpha} \tag{6.3.8}$$

Where $\alpha$ is the channel angle and $\varphi$ is any angle.

Substituting Eqn. (6.3.8) into Eqns. (6.3.2-6.3.4) and eliminating the pressure term $p$, the nonlinear ordinary differential equations in terms of velocity profile $f(\eta)$ and temperature field $\theta(\eta)$ can be written as

$$f'''(\eta) + 2\alpha \operatorname{Re} A_1(1-\phi)^{2.5} f(\eta)f'(\eta) + (4 - (1-\phi)^{1.25} Ha)\alpha^2 f'(\eta) = 0, \tag{6.3.9}$$

$$\theta''(\eta) + \frac{A_2 Ec \operatorname{Pr}}{A_3(1-\phi)^{2.5}}\left[4\alpha^2 f^2(\eta) + (f'(\eta))^2\right] = 0, \tag{6.3.10}$$

Using (6.3.7) and (6.3.8) the boundary conditions become

$$f(0) = 1, \ f'(0) = 0, \ f(1) = 0,$$
$$\theta(1) = 1, \ \theta'(0) = 0 \tag{6.3.11}$$

$$\operatorname{Pr} = \frac{(\mu c_p)_f}{\kappa_f}, \quad Ec = \frac{f_{max}^2}{(c_p)_f T_a}, \quad Ha = \sqrt{\frac{\sigma B_0^2}{\rho_f \nu_f}},$$

$$\operatorname{Re} = \frac{f_{max}\alpha}{\nu_f} = \frac{Ur\alpha}{\nu_f} \begin{pmatrix} \text{divergent channel}: \alpha > 0, \ f_{max} > 0 \\ \text{convergent channel}: \alpha < 0, \ f_{max} < 0 \end{pmatrix} \tag{6.3.12}$$

Where Prandtl number *Pr*, Eckert number *Ec*, Hartmann number *Ha*, Reynolds number *Re* and channel angle $\alpha$.

$$A_1 = (1-\phi) + \frac{\rho_s}{\rho_f}\phi, \quad A_2 = (1-\phi) + \frac{(\rho c_p)_s}{(\rho c_p)_f}\phi$$

$$A_3 = \frac{k_s + 2k_f - 2\phi(k_f - k_s)}{k_s + 2k_f + \phi(k_f - k_s)} \quad \text{are the constants.}$$

The local Nusselt number Nu and heat transfer rate are

$$Nu = \frac{rq_w|_{\varphi=\alpha}}{\kappa_f T_a}, \quad q_w = -\kappa_{nf}\left(\frac{1}{r}\frac{\partial \overline{T}}{\partial \varphi}\right) \tag{6.3.13}$$

From equations (6.3.8) and (6.3.13), the Nusselt number results in the following form

$$Nu = -\frac{1}{\alpha}\frac{\kappa_{nf}}{\kappa_f}\theta'(1) \tag{6.3.14}$$

## 6.4 Series Analysis

The following power series expansions are considered in terms of the parameter $\alpha$ as equations (6.3.9) and (6.3.10) are non-linear for velocity and temperature fields.

$$f(\eta) = \sum_{i=0}^{\infty} f_i(\eta)\alpha^i, \quad \theta(\eta) = \sum_{i=0}^{\infty} \theta_i(\eta)\alpha^i, \quad |\alpha| < 1 \tag{6.4.1}$$

The non-dimensional governing equations are then solved into series solutions by substituting the series (6.4.1) into Eqns. (6.3.9), (6.3.10) and the boundary conditions (6.3.11) and equating the coefficients of powers of $\alpha$. With the help of MAPLE, we have computed the first 42 coefficients for the series of the velocity $f(\eta)$ and temperature $\theta(\eta)$ in terms of $\alpha$, *Ha*, *Re*, *Pr*, *Ec*, $\phi$, $A_1$, $A_2$, $A_3$. The first few coefficients of the series for $f(\eta)$ and $\theta(\eta)$ are as follows:

$$f(\eta,\alpha,Ha,\text{Re},\phi,A_1) = 1 - \eta^2 - \frac{1}{30}\eta^2(\eta-1)(\eta+1)(\eta-2)(\eta+2)\text{Re }A_1(1-\phi)^{2.5}\alpha + \frac{1}{12}\eta^2(\eta-1)$$

$$(\eta+1)(4-(1-\phi)^{1.25}Ha)\alpha^2 + \frac{1}{5040}\eta^2(\eta-1)(\eta+1)(5\eta^4 - 9\eta^2 - 9)\text{Re}(1-\phi)^{2.5}A_1(4-$$

$$(1-\phi)^{1.25}Ha)\alpha^3 + O(\alpha^4) \tag{6..4.2}$$

$$\theta(\eta,\alpha,Ha,\mathrm{Re},\phi,Ec,\mathrm{Pr},A_1,A_2,A_3) = 1 + \frac{A_2 Ec\,\mathrm{Pr}}{3A_3(1-\phi)^{2.5}}(1-\eta^4) -$$

$$\frac{A_2 Ec\,\mathrm{Pr}\,\mathrm{Re}\,A_1(\eta-1)(\eta+1)(9\eta^6 - 47\eta^4 + 9\eta^2 + 9)}{630A_3}\alpha$$

$$+ O(\alpha^2) \tag{6.4.3}$$

The obtained power series solutions are valid for very small values of $\alpha$. Then, the series are analysed applying Hermite- Padé approximation method.

## 6.5 Entropy Generation

The flow characteristics within the channel with isothermal walls in the presence of magnetic field and viscous dissipation are irreversible. The exchange of energy and momentum within the fluid and at solid boundaries causes inequilibrium conditions which leads to continuous entropy generation. Following Bejan (1996), the volumetric entropy generation rate for fully developed flow in cylindrical coordinates is given as

$$E_G = \frac{\kappa_{nf}}{T_a^2}\left(\frac{d\overline{T}}{d\varphi}\right)^2 + \frac{\mu_{nf}}{T_a}\left(\frac{du}{d\varphi}\right)^2 \tag{6.5.1}$$

Where the first term on the right side of equation (6.5.1) is the irreversibility due to heat transfer and the second term is the irreversibility due to viscous dissipation. The entropy generation number can be expressed in dimensionless form as,

$$N_S = \frac{\alpha^2 E_G}{\kappa_f} = \frac{\kappa_{nf}}{\kappa_f}\left(\frac{d\theta}{d\eta}\right)^2 + \frac{A_2\,\mathrm{Pr}\,Ec}{A_3(1-\phi)^{2.5}}\left(\frac{df}{d\eta}\right)^2 \tag{6.5.2}$$

Where $N_1 = \dfrac{\kappa_{nf}}{\kappa_f}\left(\dfrac{d\theta}{d\eta}\right)^2$, $N_2 = \dfrac{A_2\,\mathrm{Pr}\,Ec}{A_3(1-\phi)^{2.5}}\left(\dfrac{df}{d\eta}\right)^2$

The Bejan number is given as $Be = \dfrac{N_1}{N_S}$

It is noteworthy that the Bejan number ranges from 0 to 1 and $Be = 0$ is the limit where the irreversibility is dominated by fluid friction effects. $Be = 1$ is the limit where the irreversibility due to heat transfer dominates the flow system because of finite temperature

differences. The contributions of heat transfer and fluid friction to entropy generation are equal when $Be = \frac{1}{2}$.

## 6.6 Results and Discussion

The main objective of the current study is to analyze the effect of nanoparticles and magnetic field on the irreversibility of Jeffery-Hamel flow of viscous incompressible conducting fluid by using Hermite-Pade' approximants. The effects of pertinent physical parameters namely nanoparticles volume fraction $\phi$, channel angle $\alpha$, Prandtl number $Pr$, Eckert $Ec$, Reynolds number $Re$ and Hartman number $Ha$ on velocity and temperature field are discussed quantitatively.

**Table 6.1** Comparison of numerical values of local Nusselt number $\alpha Nu$
at $Ha = 0$, $Pr = 6.2$, $Ec = 0.4$.

| | $\phi = 0.1$ | | | $\phi = 0.2$ | | |
|---|---|---|---|---|---|---|
| $Re$ | Present study | Moradi et al. (2013) | Relative Difference | Present study | Moradi et al. (2013) | Relative Difference |
| 10 | 4.11539 | 4.11857 | 0.08 % | 5.40418 | 5.50722 | 1.9 % |
| 30 | 3.77336 | 3.77626 | 0.08 % | 4.93999 | 5.03454 | 1.9 % |
| 50 | 3.65216 | 3.655 | 0.08 % | 4.82152 | 4.91475 | 1.9 % |

Table 6.1 represents a comparison of the local Nusselt number obtained in the present work for different volume fractions of nanofluids with $Ha = 0$, $Pr = 6.2$, $Ec = 0.4$ and obtained by Moradi et al. (2013) which indicated that there is an excellent agreement between these two results. In order to validate the accuracy of our numerical procedure, the velocity in absence of nanofluids and magnetic field effects is considered as shown in Table 6.2. Our results

agreed perfectly with the one reported by Sheikholeslami et al. (2012) at $\text{Re} = 25, \ \alpha = 5^\circ$

and Motsa et al. (2010) at $\text{Re} = 50, \ \alpha = 5^\circ$ respectively.

**Table 6.2** Comparison of numerical values for velocity obtained in the present work with available literature when $\phi = 0, Ha = 0$

| $\eta$ | $\text{Re} = 25, \ \alpha = 5^\circ$ | | | $\text{Re} = 50, \ \alpha = 5^\circ$ | | |
|---|---|---|---|---|---|---|
| | Present Study | Sheikholeslami et al. (2012) | Relative Difference | Present Study | Motsa et al. (2010) | Relative Difference |
| 0.0 | 1.000000 | 1.000000 | 0 % | 1.000000 | 1.000000 | 0 % |
| 0.1 | 0.986667 | 0.986637 | 0.003 % | 0.982427 | 0.982431 | 0.0004 % |
| 0.2 | 0.947244 | 0.947127 | 0.012 % | 0.931211 | 0.931225 | 0.0015 % |
| 0.3 | 0.883391 | 0.883146 | 0.028 % | 0.850581 | 0.850609 | 0.0033 % |
| 0.4 | 0.797654 | 0.797259 | 0.05 % | 0.746745 | 0.746788 | 0.0058 % |
| 0.5 | 0.693175 | 0.692638 | 0.078 % | 0.626890 | 0.626945 | 0.0088 % |
| 0.6 | 0.573358 | 0.572716 | 0.11 % | 0.498170 | 0.498231 | 0.012 % |
| 0.7 | 0.441526 | 0.440850 | 0.15 % | 0.366903 | 0.366964 | 0.017 % |
| 0.8 | 0.300617 | 0.300013 | 0.2 % | 0.238071 | 0.238122 | 0.021 % |
| 0.9 | 0.152943 | 0.152552 | 0.25 % | 0.115120 | 0.115151 | 0.027 % |
| 1.0 | 0.000000 | 0.000000 | 0 % | 0.000000 | 0.000000 | 0 % |

## 6.6.1 Singularity Analysis

For the analysis, we choose the series (6.4.2) for the functional form as follows

$$f\left(\eta = \frac{1}{2}\right)$$

which is related to the centerline velocity of the divergent channel. From the results shown in Table 6.3 it appears that there is a pair of complex conjugate singularities along the imaginary axis in the complex $\alpha$ plane. The singularities have the form

$$f\left(\eta = \frac{1}{2}\right) \sim A + B(\alpha \pm \alpha_c)^{\delta}$$

with, $\delta = 1/2$. The values of $\delta$ confirm that $\alpha_c$ is a branch point using HODA. Moreover, it is seen from Table 6.4 that the critical channel semi-angle $\alpha_c$ decreases uniformly for the increasing values of nanoparticles volume fraction $\phi$.

A similar phenomenon is observed in Table 6.5 that there is a pair of complex conjugate singularities of the flow Reynolds number along the imaginary axis in the complex $\mathrm{Re}$ plane and it is a branch point verified by the values of $\delta$. Table 6.6 represents that $\mathrm{Re}_c$ also diminishes rapidly for the rising values of $\phi$ with $Ha = 1$. Hence, nanofluids act in a similar manner for both types of singular points, i.e., the enhancement of nanoparticles volume fraction reduces the magnitudes of the singular points.

The High-order Differential Approximant (2002) is applied to the series (6.4.2) in order to determine the critical relationship between the parameters $\alpha$ and $\mathrm{Re}$. Figure 6.2 displays the critical relation between the channel angular width $\alpha$ and flow Reynolds number $\mathrm{Re}$ for various values of $\phi$. It is found that as $\alpha$ increases then $\mathrm{Re}$ decreases and conversely $\mathrm{Re}$ increases when $\alpha$ decreases. This implies that both channel angle and Reynolds number are inversely proportional to each other which is an excellent agreement with the classical Jeffery-Hamel flow when $\phi = 0$. There is a notable variation in the curves at $\phi = 0.1$ and $\phi = 0.2$ than in the curve at $\phi = 0$. Therefore, nanofluid has a significant impact on the stability of Jeffery-Hamel flow.

**Table 6.3** Estimates of critical angles $\alpha_c$ and corresponding exponent $\delta$ at $\mathrm{Re} = 20,\ Ha = 1,\ \phi = 0$.

| d | N | $\alpha_c$ | $|\alpha_c|$ | $\delta$ |
|---|---|---|---|---|
| 2 | 7 | $0.3182866 \pm 0.6584999\ i$ | $0.73138813$ | $0.466261 \pm 0.114586\ i$ |
| 3 | 12 | $0.3251003 \pm 0.6026430\ i$ | $0.68473998$ | $0.499587 \pm 0.007775\ i$ |
| 4 | 18 | $0.3259369 \pm 0.6006401\ i$ | $0.68337648$ | $0.500438 \pm 0.001907\ i$ |

**Table 6.4** Variation of critical angles $\alpha_c$ and corresponding exponent $\delta$ for different $\phi$ at $\mathrm{Re} = 20,\ Ha = 1$.

| $\phi$ | $\alpha_c$ | $|\alpha_c|$ | $\delta$ |
|---|---|---|---|
| 0 | $0.3259369 \pm 0.6006401\ i$ | $0.68337648$ | $0.500438 \pm 0.001907\ i$ |
| 0.05 | $0.2568848 \pm 0.4944919\ i$ | $0.55723614$ | $0.496772 \pm 0.004736\ i$ |
| 0.1 | $0.2259055 \pm 0.4426434\ i$ | $0.49695731$ | $0.495870 \pm 0.005297\ i$ |
| 0.15 | $0.2122295 \pm 0.4187484\ i$ | $0.46945887$ | $0.495435 \pm 0.005544\ i$ |

**Table 6.5** Estimates of critical Reynolds number $\mathrm{Re}_c$ and corresponding exponent $\delta$ at $\alpha = 0.1,\ Ha = 1, \phi = 0$.

| d | N | $\mathrm{Re}_c$ | $|\mathrm{Re}_c|$ | $\delta$ |
|---|---|---|---|---|
| 2 | 7 | $57.144629 \pm 133.678372\ i$ | $145.380245$ | $0.66719 \pm 0.36868\ i$ |
| 3 | 12 | $58.149392 \pm 123.844527\ i$ | $136.816734$ | $0.48726 \pm 0.00667\ i$ |
| 4 | 18 | $58.425688 \pm 124.067525\ i$ | $137.136107$ | $0.48691 \pm 0.00297\ i$ |

**Table 6.6** Numerical values of critical $\mathrm{Re}_c$ and corresponding exponent $\delta$ at $\alpha = 0.1,\ Ha = 1$ for different values of $\phi$.

| $\phi$ | $\mathrm{Re}_c$ | $\left|\mathrm{Re}_c\right|$ | $\delta$ |
|--------|-----------------|------------------------------|----------|
| 0 | $58.425688 \pm 124.067525\ i$ | $137.136107$ | $0.48691 \pm 0.00297\ i$ |
| 0.05 | $47.524761 \pm 100.923388\ i$ | $111.553275$ | $0.47691 \pm 0.00297\ i$ |
| 0.1 | $42.353306 \pm 89.944903\ i$ | $99.417745$ | $0.47690 \pm 0.00298\ i$ |
| 0.15 | $39.998962 \pm 84.948378\ i$ | $93.894323$ | $0.47690 \pm 0.00299\ i$ |
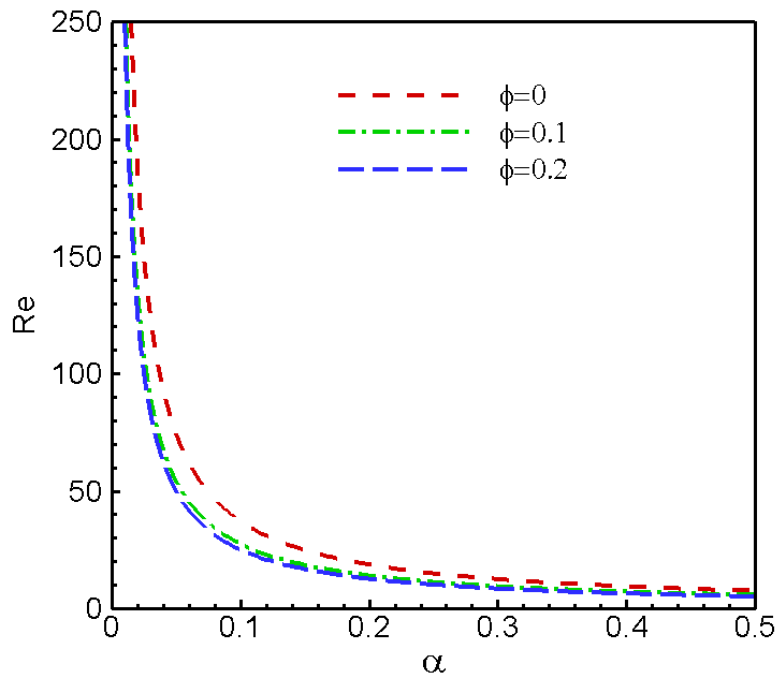


**Figure 6.2** Critical relation between $\alpha$ and *Re* for different values of $\phi$ at $Ha = 1$ obtained by HODA for $d = 7$.

### 6.6.2 Effect of Channel Angle

The combined effects of channel angle and magnetic field on velocity profiles are observed in Figure 6.3. Figure 6.3 (a) exhibits no significant change in the velocity curve due to the increase of Hartmann number for lower channel angle. For increasing values in opening channel angle in Figure 6.3 (b), the boundary layer thickness increases and the velocity near

113

the upper wall increases minorly when *Ha* increases. However, the backflow occur in diverging channel for higher values of $\alpha = 10^0$ at a fixed Reynolds number when $Ha = 0$ seen in Figure 6.3(c). Whereas to diminish the backflow an increased *Ha* is required. It can be concluded from Figure 6.3 (c) that as channel angle increases, the variation of velocity is observed more with the changing values of *Ha*.
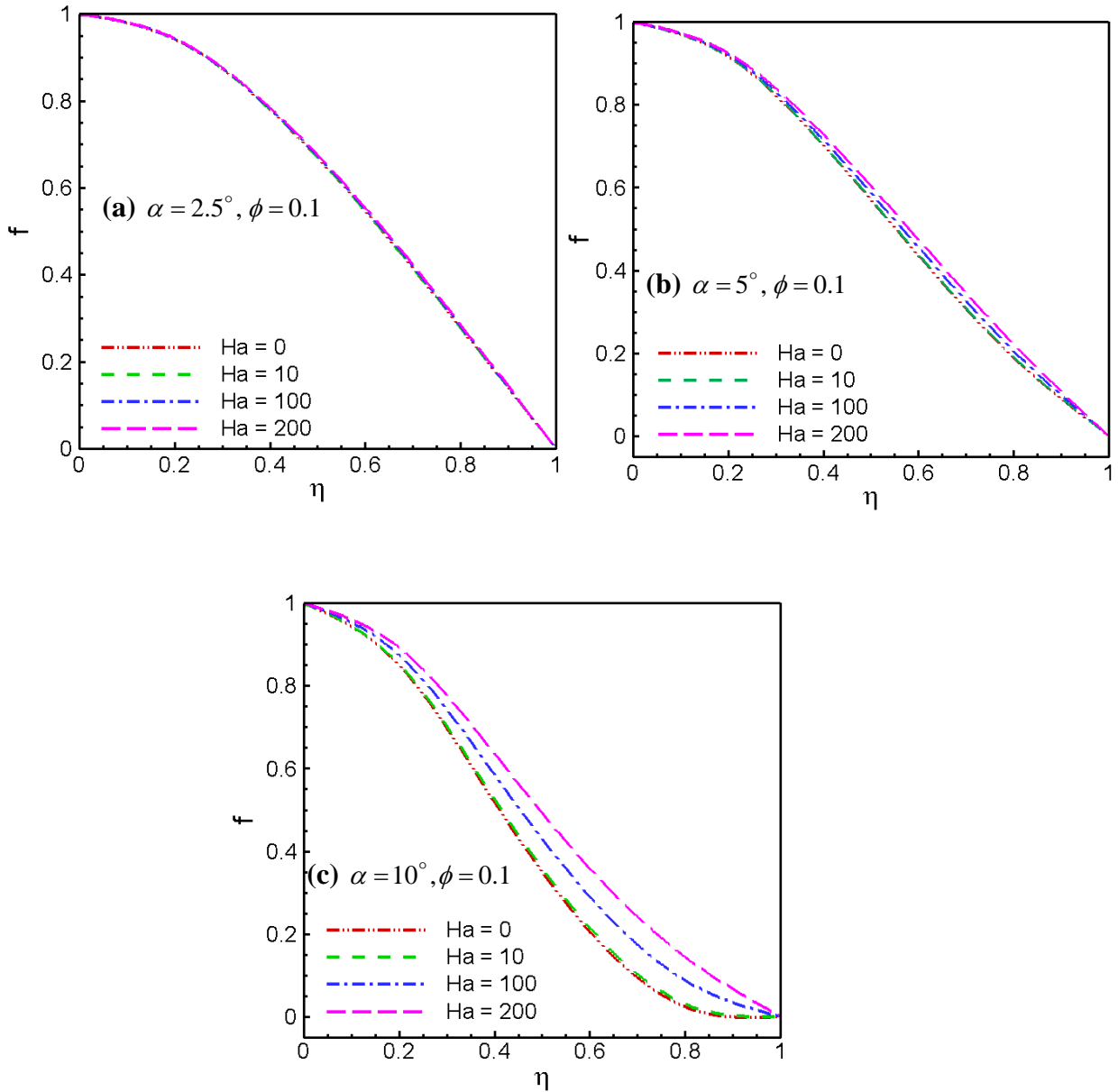


**Figure 6.3** Velocity profiles in divergent channel with different values of $\alpha$ and *Ha* at $Re = 50$.
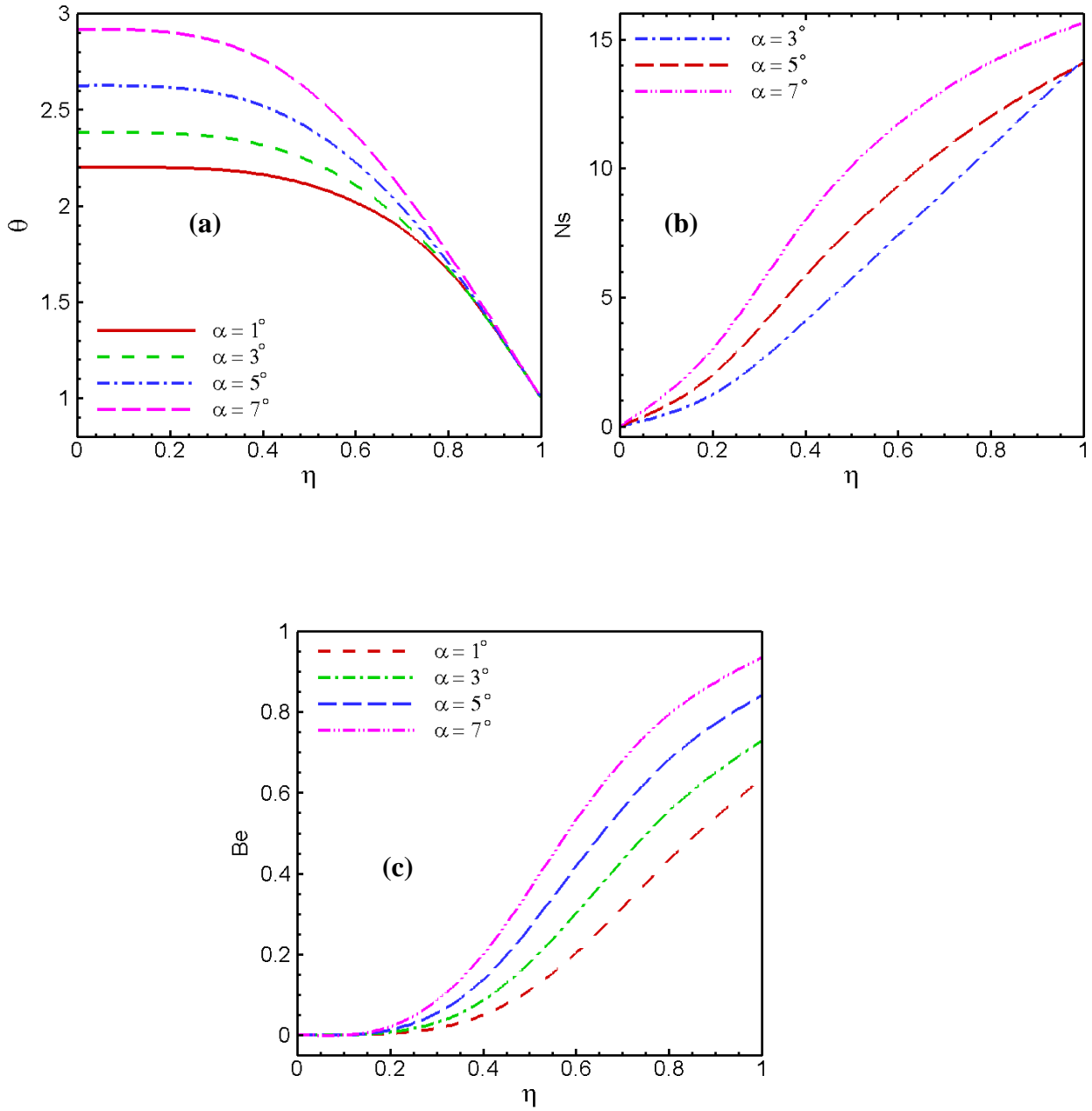
**Figure 6.4** Effect of channel angle on (a) temperature distributions, (b) Entropy rates, (c) Bejan profiles respectively at $Ec = 0.5, \text{Pr} = 7.1,\ \phi = 0.1,\ \text{Re} = 50,\ Ha = 100$ .

The velocity curves show that the rate of alteration is significantly reduced with the increase of Hartmann number. Thus, the transverse magnetic field opposes the alteration phenomena

clearly. As the variation of *Ha* leads to the variation of the Lorentz force due to magnetic field and the Lorentz force produces more resistance to the alternation phenomena. Figure 6.4 represents the consequences of channel angle on temperature distribution, entropy generation rate and Bejan number respectively. As we are taking water as the base fluid, therefore, the value of Prandtl number *Pr* is fixed as 7.1. Figure 6.4 (a) is sketched to see the effects of increasing angle $\alpha$ on temperature field. Because of an increase in the gap between the walls, the temperature of the fluid is seen to be getting higher. This increase is major at the centreline of the channel. Also, the temperature is seen to be higher for nanofluid and the larger value of thermal conductivity coefficient is a major cause for this increment in temperature. The entropy generated by fluid friction $N_2$ is usually more than that of $N_1$, the entropy produced by fluid heat transfer. Thus, $N_S$ is contributed mainly by $N_2$ throughout the entire flow field. However, in the areas of the flow field characterized by a faster flow rate, the velocity gradient reduces and hence $N_2$ also decreases. Figure 6.4 (b) illustrates the entropy generation rate with the effect of increasing angle $\alpha$, where $N_s$ is close to zero at centerline of the channel as discussed above, but $N_s$ increases gradually to the upper hot wall. Moreover, as $\alpha$ increases, $N_s$ increases at the hot wall due to the rising of temperature as discussed in Figure 6.4 (a). Figure 6.4(c) displays the distribution of Bejan number (*Be*) with the effect of $\alpha$. It is noticed from the figure that *Be* has a value of zero at the channel centerline region since, as discussed previously, fluid friction irreversibility is dominant there because of faster flow rate. At the top heated wall, *Be* increases to a maximum value of approximately 1 due to the increase in the contribution by $N_1$ to the overall entropy generation. It is to be seen that the heat transfer irreversibility dominates the flow process at the hot wall of the channel and *Be* increases uniformly as $\alpha$ increases at that region.

### 6.6.3  Effect of flow Reynolds number

Figure 6.5 represents the effect of Reynolds number on velocity profiles at $\alpha = 5^\circ, \phi = 0.1$ with different values of Hartmann number. In Figure 6.5(a) for $Re = 50$, the velocity increases gradually when Hartmann number increases and no backflow is observed.  It can be seen from Figure 6.5(b) that backflow starts when magnetic field is

116

absent at $\mathrm{Re} = 100$ and these properties are reduced with the rising values of Hartmann number. The backflow enlarges at high Reynolds number and hence the larger magnetic field is required to abolish it.



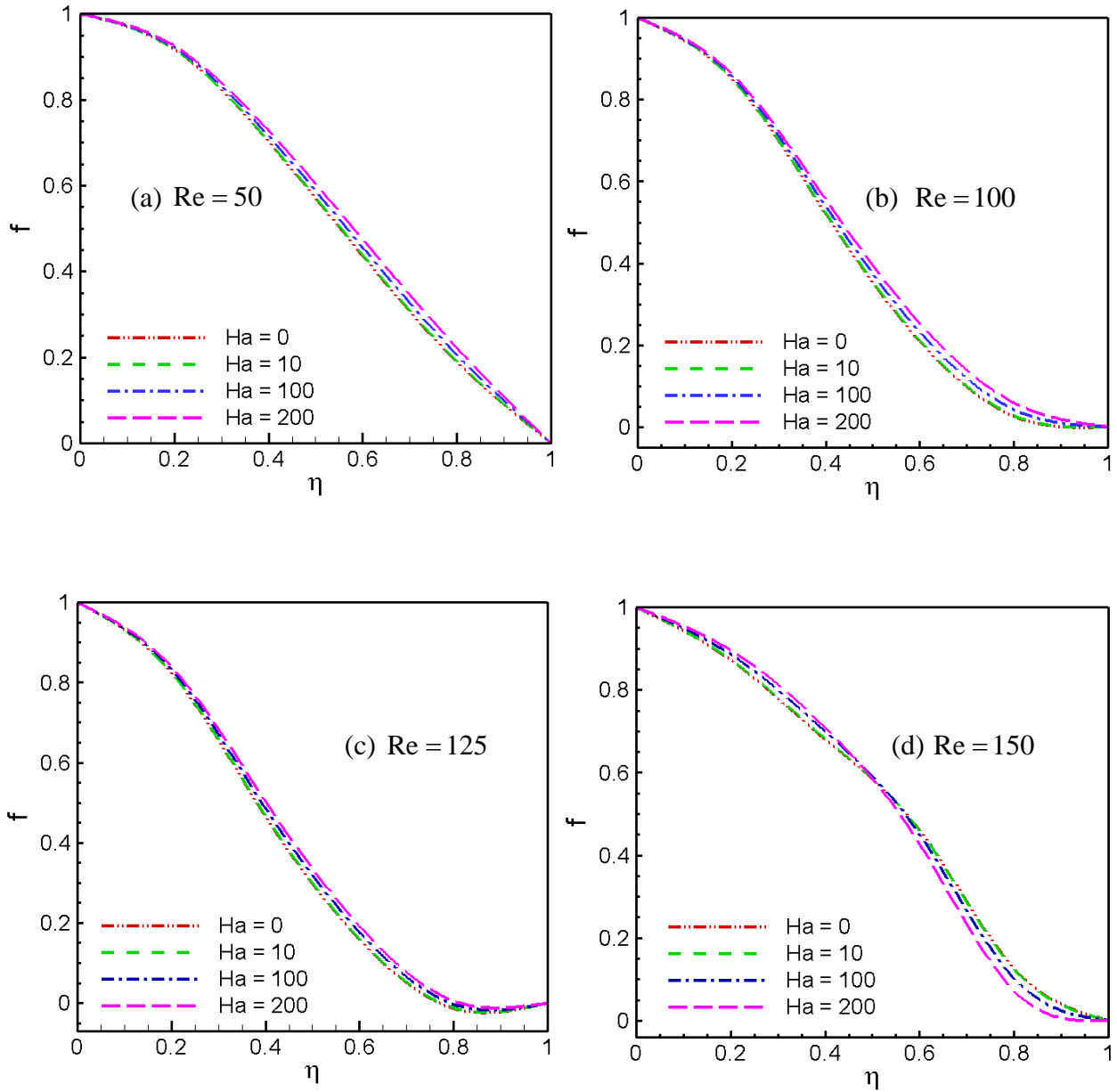**Figure 6.5** Velocity profiles in divergent channel with different values of *Re* and *Ha* at

$$\alpha = 5^{\circ}, \phi = 0.1.$$

Moreover, it is detected from Figure 6.5(c) at $\mathrm{Re} = 125$ that the backflow is lessened at $Ha = 200,$ whereas there occurs backflow for each values of Hartmann number. A reverse

phenomenon is observed in Figure 6.5(d) beyond the critical Reynolds number at $\eta = 0.5$, such that the back flow enlarges due to the increasing values of *Ha* which is contradictory to the previous cases. The effect of Reynolds number on temperature field is shown in Figure 6.6(a) in such a way that an increase in the values of *Re* generates enhancement of the temperature of the fluid particularly more at the centreline of the channel. It implies that the increase of viscous force is also responsible for an increase in the temperature. On the other hand, in the areas of the flow field characterized by a faster flow rate, the velocity gradient reduces and hence entropy generate rate $N_s$ also decreases. Figure 6.6 (b) demonstrates that the entropy generation rate reduces to zero at the centerline with the increasing values of *Re* as mentioned above, whereas $N_s$ increases gradually to the upper hot wall. It is remarkable to notice that the behaviour of $N_s$ is irregular at $\mathrm{Re} = 150$ which is beyond the critical Reynolds number. Almost identical behavior for the Bejan number is observed in Figure 6.6(c) for rising Re like channel angle $\alpha$ . The fluid friction irreversibility is dominant at the centerline whereas the heat transfer irreversibility is dominant at the hot wall of the channel.

### 6.6.4  Effect of Nanoparticles volume fraction

A Cu-water nanofluid flow is considered and the effects of nanoparticles volume fraction on velocity and temperature distributions, irreversibility of the system are analysed in this section. It is assumed that the base fluid and the nanoparticles are in thermal equilibrium and no slip occurs between them. Figure 6.7 deal with the effect of nanoparticles volume fraction ($\phi = 0, 0.05, 0.1, 0.2$) on the velocity profiles with the variation of channel angle ($\alpha = 2.5^\circ, 5^\circ$) and Reynolds number ($\mathrm{Re} = 100, 150$).The equivalent thermal expansion coefficient of the nanofluid is less than that of base water. As a result, the buoyancy force acting on the nanofluid is also less than that acting on the pure water, and hence the velocity decreases as nanoparticles volume fraction increases. In addition, since the density and viscosity of the nanofluid are greater than those of base water, the velocity distribution within the channel is more uniform for nanofluid. The characteristics of velocity profiles are similar as $\phi$ increases in both Figure 6.7 (a, b) at fixed Reynolds number $\mathrm{Re} = 100$ in absence of magnetic field, although there occurs back flow at increasing values of $\alpha$ as

118

noted in Figure 6.7 (b) and this back flow extended for increasing values of $\phi$. Whereas there observed an irregular behaviour of the velocity field in Figure 6.7 (c) at $\text{Re} = 150$ just exceeding the critical values of *Re* with the increasing values of $\phi = 0.1, 0.2$.



**Figure 6.6** Effect of Reynolds number on (a) temperature distributions, (b) Entropy rates, (c) Bejan profiles respectively at $Ec = 0.5, \Pr = 7.1, \alpha = 5^0, \quad Ha = 100, \phi = 0.1$.
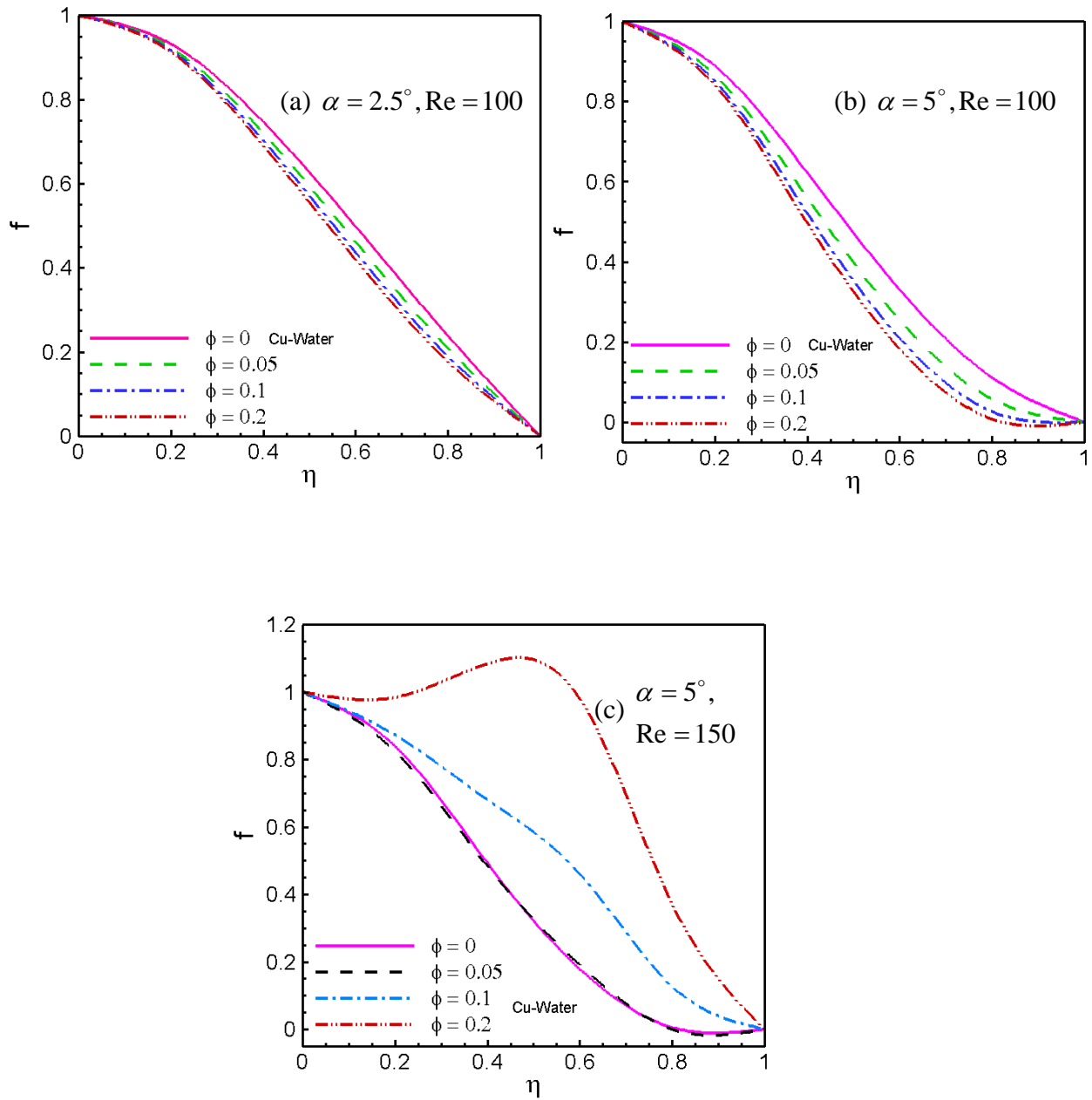
**Figure 6.7** Effects of nanoparticles volume fraction on velocity profiles for various values of $\alpha$ and *Re* at $Ha = 0$.

Therefore, increasing volume fraction of nanoparticles in the nanofluid forms instability in the fluid flow at high Reynolds number.
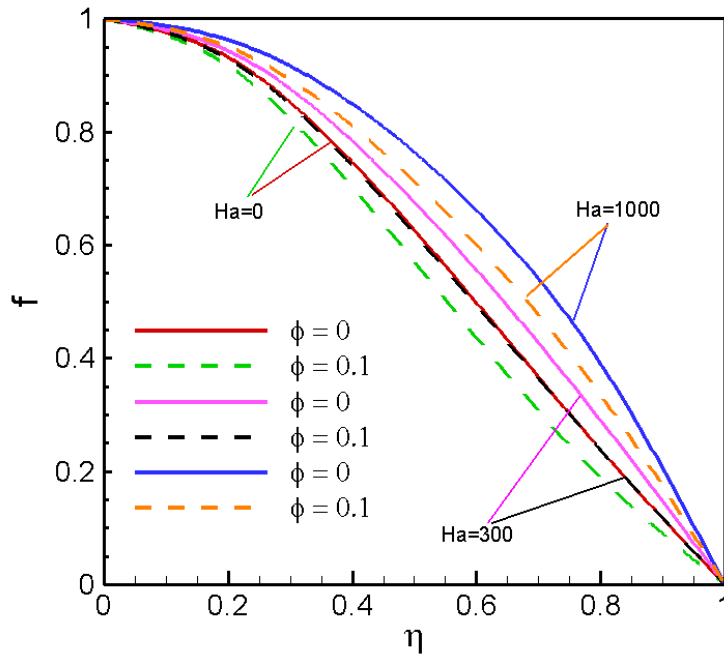
**Figure 6.8** Velocity profiles for several values of Hartmann number and solid volume fraction

at $\alpha = 5^{\circ}, \mathrm{Re} = 50$.

Figure 6.8 predicts the combined effects of magnetic field and nanoparticles volume fraction on the velocity field for divergent channel with fixed Reynolds number. The figure represents a sensible increases in the velocity with rising Hartmann number for both viscous and nanofluid near the wall that coincide with those results of Sheikholeslami et al. (2012). It is also observed that for all Hartmann numbers there is no backflow in the viscous fluid $\phi = 0$, nevertheless backflow starts for nanofluid with $Ha = 0$ at $\alpha = 5^{\circ}, \mathrm{Re} = 50$ and this phenomenon is reduced with the rising values of Hartmann number. Figures 6.9 (a, b, c) illustrate the effect of nanoparticles volume fraction $\phi$ on the development of temperature distribution, entropy generation rate and Bejan profiles respectively which are plotted for Prandtl number $\mathrm{Pr} = 7.1$, Reynolds number $\mathrm{Re} = 50$, Hartmann number $Ha = 100$ and angle $\alpha = 5^{\circ}$. From Figure 6.9 (a), it is seen that an increase in the nanoparticles volume fraction leads to an homogeneous increase in the temperature field across the centerline region of the channel. The entropy generation rate $N_s$ is almost linear in pure base fluid while there is an identically minor increases of $N_s$ for the escalating values of $\phi$ as shown in

Figure 6.9 (b). The Bejan profiles in Figure 6.9 (c) depict that the dominant effect of heat transfer irreversibility at the heated wall improves by the increases of $\phi$. The thermal conductivity of nanofluid is higher than base water and it becomes more by the increases of $\phi$, which enhances the dominant effect of heat transfer irreversibility.
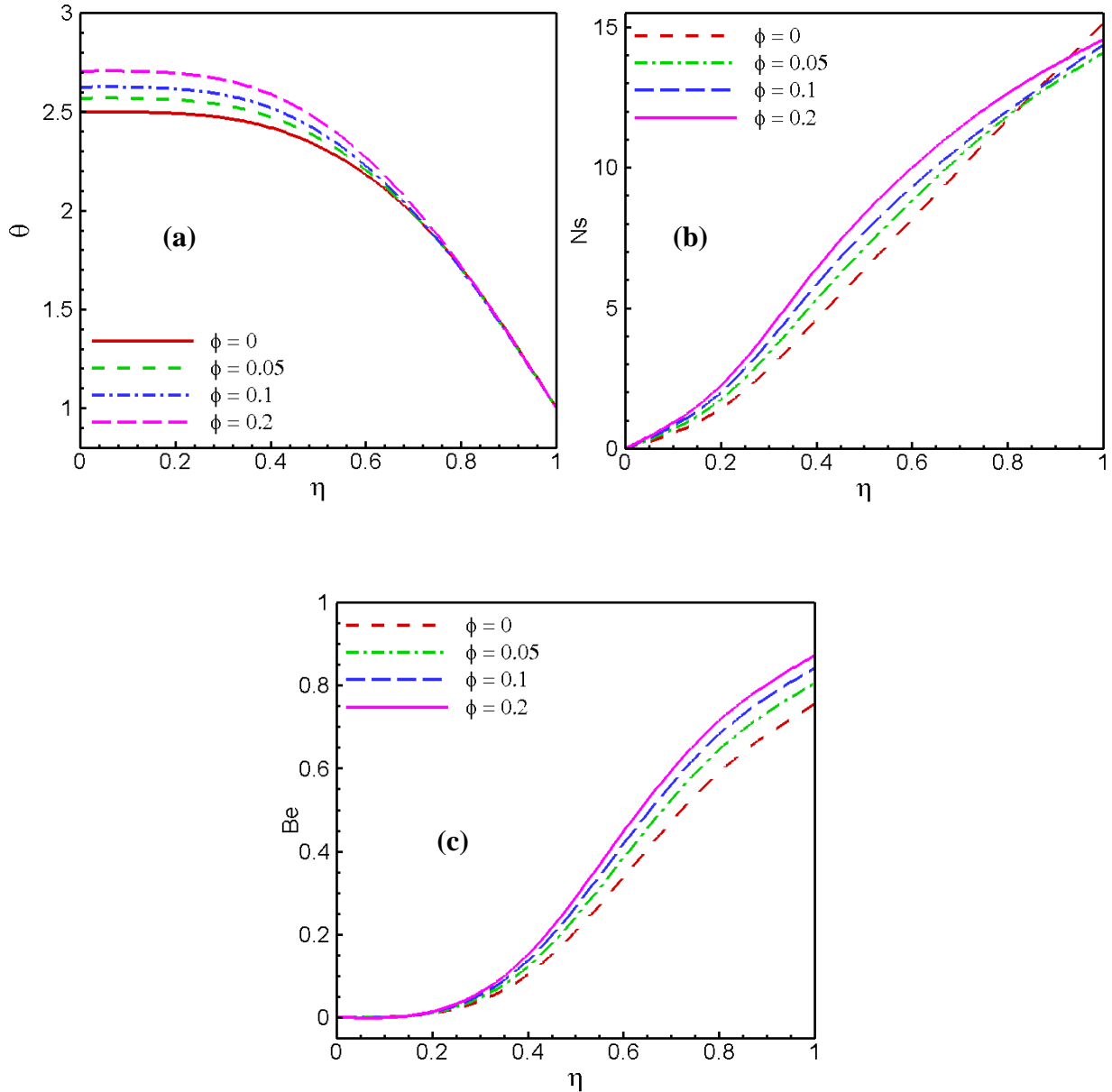


**Figure 6.9** Effect of nanoparticles volume fraction on (a) temperature distributions, (b) Entropy rates, (c) Bejan profiles respectively at $\alpha = 5^0, \mathrm{Pr} = 7.1, \mathrm{Re} = 50, \ Ha = 100$ .

### 6.6.5 Effect of Eckert number

The temperature profiles and entropy generation with Bejan profiles are plotted against channel half width in divergent channel for different values of Eckert number $Ec$ with $\Pr = 7.1, \alpha = 5^0, \mathrm{Re} = 50$ and $Ha = 100$ in Figure 6.10.
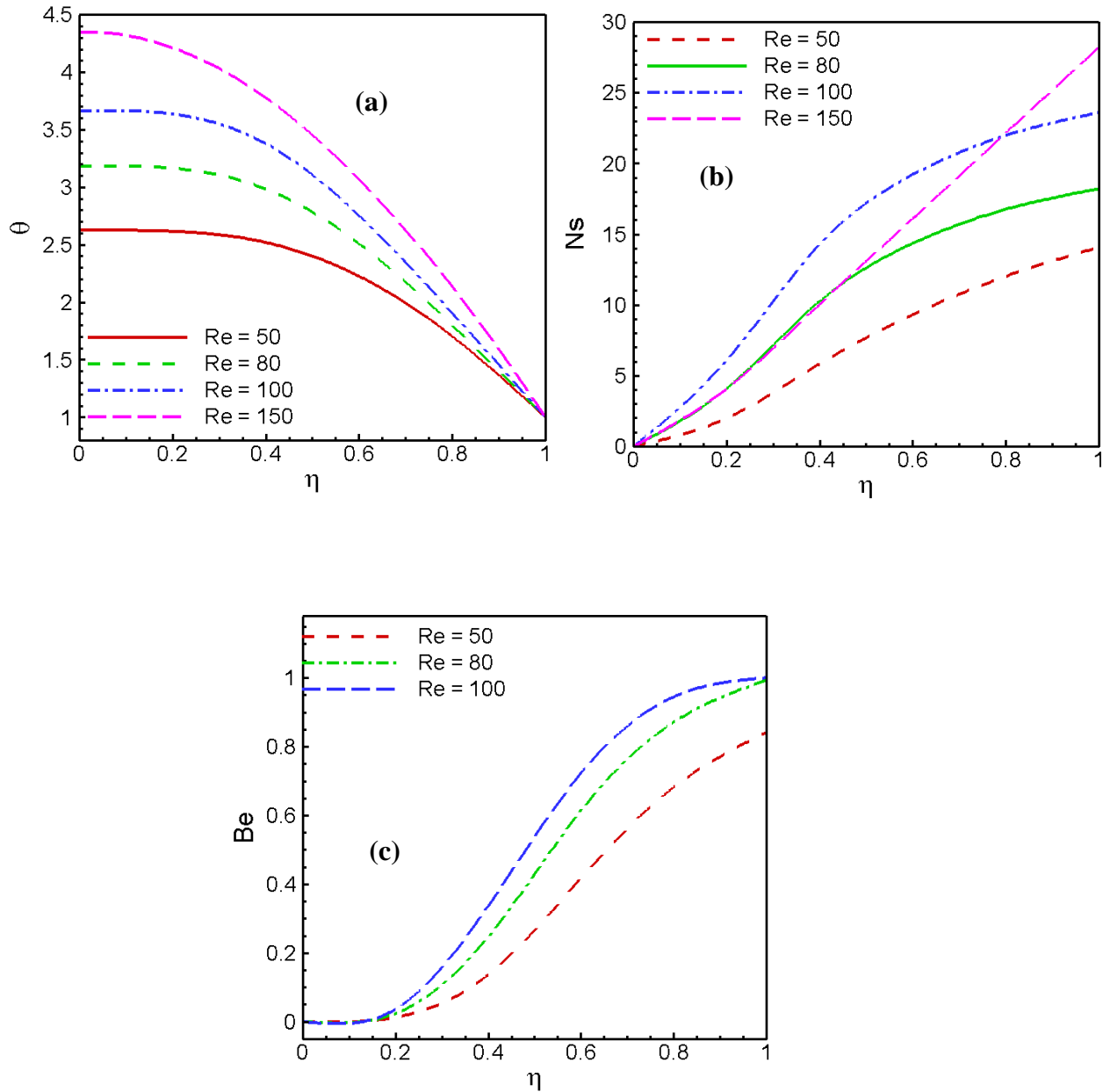


**Figure 6.10** Effect of Eckert number on (a) temperature distributions, (b) Entropy rates, (c) Bejan profiles respectively at $\Pr = 7.1, \alpha = 5^0, \phi = 0.1, \mathrm{Re} = 50, Ha = 100$ .
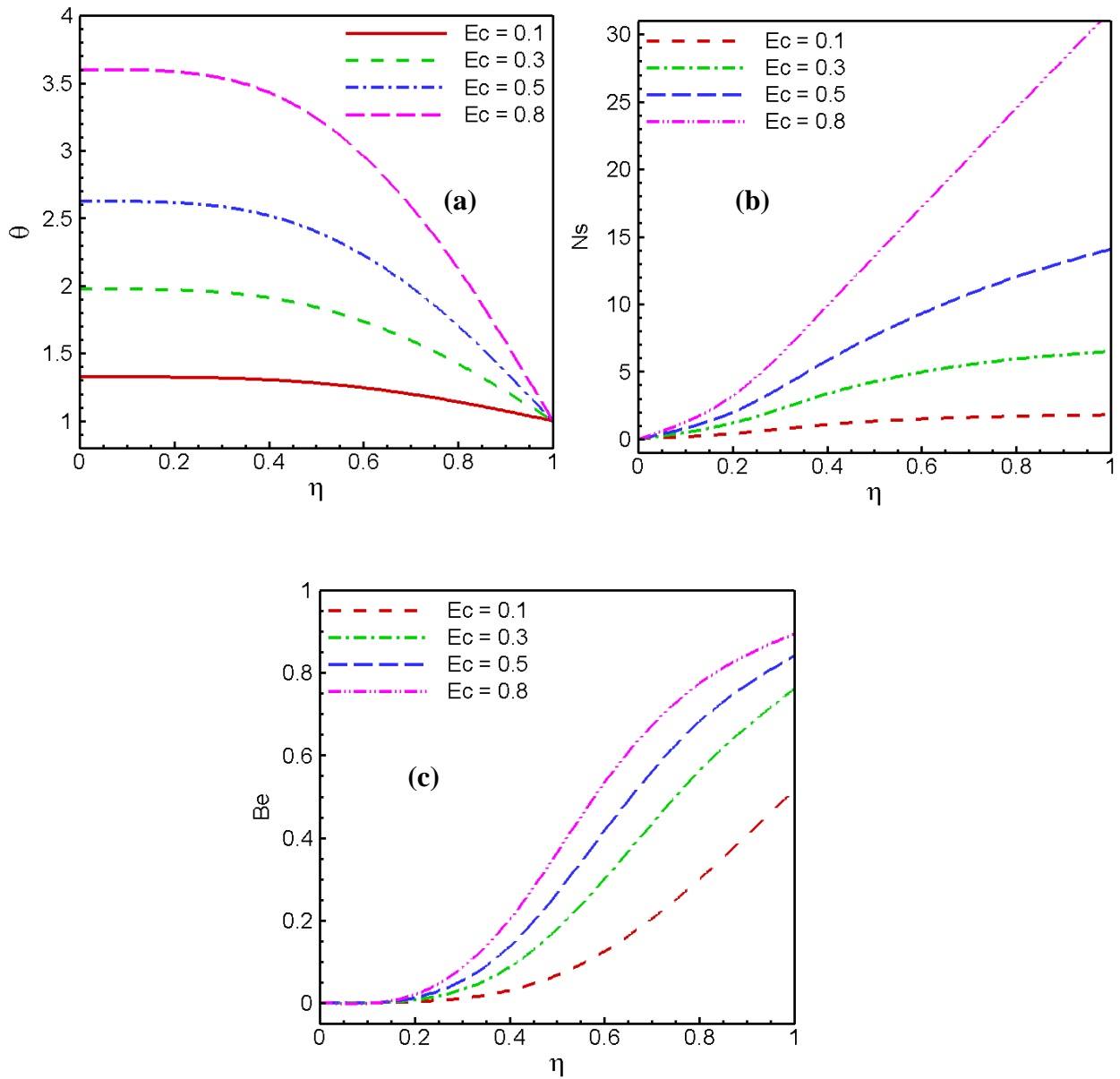
The temperature field is affected directly by the dimensionless velocity distribution of the flow field when the effects of viscous dissipation are taken into consideration. It is noticed from Figure 6.10 (a) that the fluid temperature increases with increasing parametric values of viscous heating parameter $Ec$. The entropy generate rate raises rapidly towards the hot wall of the channel as Eckert number increases noticed in Figure 6.10 (b) which is expected as mentioned above. Also, the value of Bejan number is higher at the hot wall by the increases of $Ec$ in Figure 6.10 (c) indicates the dominance of heat transfer irreversibility.

## 6.7 Conclusion

The entropy generation of magnetohydrodynamic Jeffry-Hamel flow with nanofluid is investigated using a special type of Hermite-Padé approximation technique. A comparison is made between the available results and the present approximate solutions.The accurate numerical approximation of the critical parameters of the flow is obtained. The numerical study indicates that HPA is a powerful approach for solving this problem. The influences of various physical parameters on the velocity field, temperature distribution and entropy generation rate with Bejan profile are discussed in detail. The basic conclusions are as follows:

➢ The dominating singularity behaviour of the wall divergence semi-angle and flow Reynolds number is analysed with the effect of nanoparticles volume fraction. The critical relationship between the parameters with the effect of nanoparticles coincides with the conjecture of classical Jeffery-Hamel flow.

➢ Increasing channel angle and Reynolds number leads to backflow near the wall of the channel. Increasing Hartmann number produces to backflow reduction. High Hartmann number is required to decline of backflow for larger angles or Reynolds numbers. The velocity decreases as nanoparticles volume fraction increases.

➢ The increasing values of the pertinent physical parameters namely channel angle, flow Reynolds number, Eckert number enhances temperature field along the channel centerline region. Also temperature increases uniformly as nanoparticles volume fraction increases.

➢ Entropy generation is higher near the hot solid wall in comparison to the channel centerline. Fluid friction irreversibility dominates the entropy generation near the channel centerline while heat transfer irreversibility dominates near the hot solid wall. Fluid friction

irreversibility is the sole contributor to the total entropy generation along the channel's centerline. Nanofluid enhances the dominant effect of heat transfer irreversibility in entropy generation of the system.

The following chapter discusses the stability of magnetohydrodynamic flow through convergent-divergent channel for different nanofluids.

# Stability of Magnetohydrodynamic Jeffery-Hamel Flow through Convergent-Divergent Channel with different Nanoparticles[5]

*The effects of three different nanoparticles and magnetic field on the entropy generation of the nonlinear Jeffery-Hamel flow through convergent-divergent channel are analyzed in the present study. A similarity transform has been employed to reduce the nonlinear partial differential equations to a system of nonlinear ordinary differential equations which are then solved using power series coupled with a semi-numerical analytical technique called Hermite- Padé approximation. The velocity profiles, temperature distributions and entropy generation rates with Bejan profiles are presented in convergent-divergent channels for various values of nanoparticles solid volume fraction, Hartmann number, Eckert number, Reynolds number and channel angle. The dominating singularity behavior of the problem is analysed numerically and graphically for nanofluid. The critical relationships among the parameters are also performed qualitatively with the effect of different nanoparticles.*

## 7.1 Introduction

The two dimensional flow of a viscous, incompressible fluid between converging/diverging channels separated by a fixed angle and driven by a source or sink at the apex is known as the classical Jeffery-Hamel flow which was studied first by Jeffery (1915) and Hamel (1916). It has important applications particularly in fluid mechanics, chemical, mechanical and bio-mechanical engineering.

Many available studies have considered different properties related to this problem and have tried to investigate the flow characteristics by varying the angle between the walls

---

(Rosenhead (1940), Batchelor (1967), Sadri (1997), Hamadiche (1994)). These flows have discovered similarity solutions of the Navier-Stokes equations depending on two non-dimensional parameters, the flow Reynolds number and channel angular width. Fraenkel (1962) then investigated the laminar flow in symmetrical channels with slightly curved walls. In his analysis the velocity field of the flow was obtained as a power series in small curvature parameter where the leading term is the Jeffery-Hamel solution. Sobey and Drazin (1986) studied some instabilities and bifurcations of two-dimensional Jeffery-Hamel flows using analytical, numerical and experimental methods. Moreover, the steady flow of a viscous incompressible fluid in a slightly asymmetrical channel was studied by Makinde (1997). He expanded the solution into a Taylor series with respect to the Reynolds number and performed a bifurcation study.

Meanwhile, the study of electrically conducting viscous fluid flowing through convergent/divergent channels under the influence of an external magnetic field is not only fascinating theoretically, but also finds applications in mathematical modelling of several industrial and biological systems. Clearly, the motion in the region with intersecting walls may represent a local transition between two parallel channels with different cross-sections, an expansion or a contraction of the flow. Makinde (2006) investigated the MHD flows in convergent- divergent channels which was an extension of the classical Jeffery-Hamel flows to MHD. He interpreted that the effect of external magnetic field works as a parameter in solution of the MHD flows in convergent - divergent channels. Makinde (2007) investigated the temporal development of small disturbances in MHD Jeffery-Hamel flows to understand the stability of hydromagnetic steady flows in convergent-divergent channels at very small magnetic Reynolds number $Rm$ using Chebyshev spectral collocation method. However, a numerical investigation of the effect of arbitrary magnetic Reynolds number on steady flow of an incompressible conducting viscous liquid in convergent-divergent channels under MHD was presented by Makinde (2008). He solved the non-linear 2D Navier-Stokes equations modeling the flow field using a perturbation technique applying the special type of Hermite-Pade´ approximation method and a bifurcation study was also performed. The increasing values of magnetic Reynolds number cause a general decrease in the fluid velocity around the central region of the channel whereas the flow reversal control is also observed by increasing magnetic field intensity.

Presently there is an increasing attention of the researchers in the analysis of nanofluids. The word nanofluid was introduced by Choi (1995). In fact a nanofluid is a dilute suspension of solid nanoparticles with the average size below 100 nm in a base fluid, such as: water, oil and ethylene glycol. These nanoparticles are good conductors of heat and enable the base fluids to enhance their thermal properties. The effects of magnetic field and nanoparticles on the Jeffery-Hamel flow using a powerful analytical method called the Adomian decomposition method were studied by Sheikholeslami et al. (2012). Moreover, the effects of heat transfer and viscous dissipation on the Jeffery-Hamel flow of nanofluids are investigated by Moradi et al. (2015). Finally, a study of velocity and temperature slip effects on flow of water based nanofluids in converging and diverging channels was done by Syed et al. (2015).

The purpose of this study is to investigate the stability and entropy generation analysis on magnetohydrodynamic Jeffery-Hamel nanofluid flow through convergent - divergent channel considering viscous dissipation effect. The resulting problem is solved applying the power series along with Hermite–Padé approximation (HPA). The effects of various thermophysical parameters namely nanoparticles volume fraction $\phi$, Hartmann number *Ha,* Eckert number *Ec* and channel angle on velocity fields, temperature distributions, entropy generation rates with Bejan profiles are discussed in detail. The critical values and bifurcation diagrams of channel angle and flow Reynolds number with the effect of $\phi$ for $Cu, TiO_2, Al_2O_3$-nanoparticles are studied numerically and graphically. The critical relationships among the parameters are also shown to interpret the effect of nanoparticles solid volume fraction as an extension of the available literature. A comparative study between the previously published results and the present results in a limiting sense reveals excellent agreement between them.

## 7.2 Derivation of Mathematical Equation

Consider a steady two-dimensional laminar incompressible viscous nanofluid flow from a source or sink between two channel walls intersect at an angle $2\alpha$. A cylindrical coordinate system $(r, \varphi, z)$ is used and assumed that the velocity is purely radial depends on $r$ and $\varphi$ so that there is no change in the flow parameter along the z-direction. Further it is presumed

128

that there is an external magnetic field acting vertically downward to the top wall. Let $\alpha$ be the semi-angle and the domain of the flow be $-|\alpha| < \varphi < |\alpha|$. The continuity equation, the Navier-Stokes equations and energy equation considering viscous dissipation in reduced polar coordinates are

$$\frac{\rho_{nf}}{r} \frac{\partial}{\partial r}(ru(r,\varphi)) = 0, \tag{7.2.1}$$

$$u(r,\varphi)\frac{\partial u(r,\varphi)}{\partial r} = -\frac{1}{\rho_{nf}}\frac{\partial p}{\partial r} + v_{nf}\left(\frac{\partial^2 u(r,\varphi)}{\partial r^2} + \frac{1}{r}\frac{\partial u(r,\varphi)}{\partial r} + \frac{1}{r^2}\frac{\partial^2 u(r,\varphi)}{\partial \varphi^2} - \frac{u(r,\varphi)}{r^2}\right)$$
$$- \frac{\sigma B_0^2}{\rho_{nf} r^2} u(r,\varphi), \tag{7.2.2}$$

$$\frac{1}{\rho_{nf} r}\frac{\partial p}{\partial \varphi} - \frac{2v_{nf}}{r^2}\frac{\partial u(r,\varphi)}{\partial \varphi} = 0, \tag{7.2.3}$$

$$u(r,\varphi)\frac{\partial \overline{T}(r,\varphi)}{\partial r} = \frac{\kappa_{nf}}{(\rho c_p)_{nf}}\left(\frac{\partial^2 \overline{T}(r,\varphi)}{\partial r^2} + \frac{1}{r}\frac{\partial \overline{T}(r,\varphi)}{\partial r} + \frac{1}{r^2}\frac{\partial^2 \overline{T}(r,\varphi)}{\partial \varphi^2}\right)$$
$$+ \frac{\mu_{nf}}{(\rho c_p)_{nf}}\left(4\left(\frac{\partial u(r,\varphi)}{\partial r}\right)^2 + \frac{1}{r^2}\left(\frac{\partial u(r,\varphi)}{\partial \varphi}\right)^2\right) \tag{7.2.4}$$
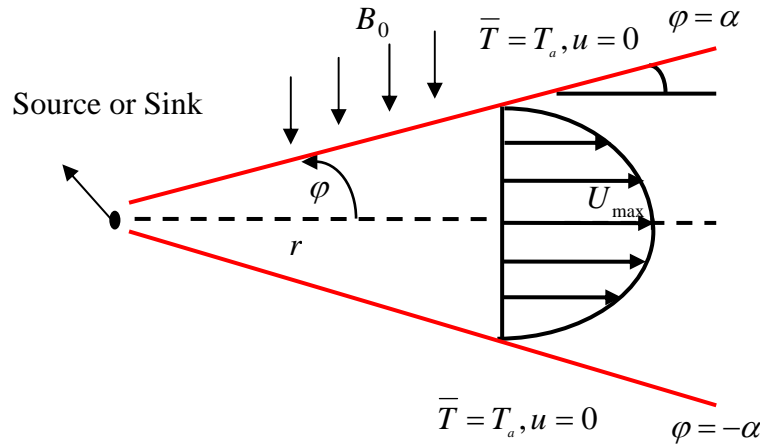


**Figure 7.1** Geometry of the problem

129

The flow is assumed to be symmetrically radial, so that $v = 0$. Then the volumetric flow rate through the channel is

$$Q = \int_{-\alpha}^{\alpha} ur\, d\varphi \qquad (7.2.5)$$

The boundary conditions are

$$u(r, \varphi) = 0, \quad \overline{T} = T_a \quad \text{at} \quad \varphi = \pm\alpha \qquad (7.2.6)$$

Where $B_0$ is the electromagnetic induction, $\sigma$ is the conductivity of the fluid, $u$ is the velocity along radial direction and p is the fluid pressure. The effective density $\rho_{nf}$, the effective dynamic viscosity $\mu_{nf}$, and the kinematic viscosity $v_{nf}$ of the nanofluid are given as Sheikholeslami et al. (2013).

$$\rho_{nf} = \rho_f (1 - \phi) + \rho_s \phi, \quad \mu_{nf} = \frac{\mu_f}{(1 - \phi)^{2.5}}, \quad v_{nf} = \frac{\mu_{nf}}{\rho_{nf}}, \qquad (7.2.7)$$

The corresponding effective thermal conductivity and heat capacity of nanofluid are

$$k_{nf} = k_f \frac{k_s + 2k_f - 2\phi(k_f - k_s)}{k_s + 2k_f + \phi(k_f - k_s)}, \quad (\rho c_p)_{nf} = (1 - \phi)(\rho c_p)_f + \phi(\rho c_p)_s \qquad (7.2.8)$$

Here, $\phi$ is the solid volume fraction of the nanoparticles.

If it requires $Q \geq 0$, then for $\alpha > 0$ the flow is diverging from a source at $r = 0$.

Let $\psi = \psi(r, \varphi)$ be the stream function, then

$$\frac{\partial \psi}{\partial \varphi} = ur, \quad \frac{\partial \psi}{\partial r} = 0$$

Introducing the dimensionless variables

$$\eta = \frac{\varphi}{\alpha}, \quad F(\eta) = \frac{\psi(\varphi)}{Q}, \quad \theta(\eta) = \frac{\overline{T}}{T_a}$$

The governing equations (7.2.2-7.2.4) reduce to the following ordinary differential equations

$$F^{(iv)} + 2\alpha \operatorname{Re} A_1 (1 - \phi)^{2.5} F'F'' + (4 - (1 - \phi)^{1.25} Ha)\alpha^2 F'' = 0, \qquad (7.2.9)$$

$$\theta'' + \frac{A_2 Ec \operatorname{Pr}}{A_3 (1 - \phi)^{2.5}} \left[ 4\alpha^2 F'^2 + (F'')^2 \right] = 0, \qquad (7.2.10)$$

The boundary conditions are reduced as follows:

$$F = \pm 1, \quad F' = 0, \quad \theta = 1 \quad \text{at} \quad \eta = \pm 1 \qquad (7.2.11)$$

$$Re = \frac{Q}{v_f}, \quad Pr = \frac{(\mu c_p)_f}{\kappa_f}, \quad Ec = \frac{U_{max}^2}{(c_p)_f T_a}, \quad Ha = \sqrt{\frac{\sigma B_0^2}{\rho_f v_f}}, \tag{7.2.12}$$

Where Reynolds number *Re*, Prandtl number *Pr*, Eckert number *Ec*, Hartmann number *Ha* and channel angle $\alpha$. Here

$$A_1 = (1-\phi) + \frac{\rho_s}{\rho_f}\phi, \quad A_2 = (1-\phi) + \frac{(\rho c_p)_s}{(\rho c_p)_f}\phi$$

$$A_3 = \frac{k_s + 2k_f - 2\phi(k_f - k_s)}{k_s + 2k_f + \phi(k_f - k_s)} \quad \text{are the constants.}$$

## 7.3 Series Analysis

The following power series expansions are considered in terms of the parameter $\alpha$ as equations (7.2.9-7.2.10) are non-linear for stream function and temperature profile

$$F(\eta) = \sum_{i=0}^{\infty} F_i(\eta)\alpha^i, \quad \theta(\eta) = \sum_{i=0}^{\infty} \theta_i(\eta)\alpha^i, \text{ as } |\alpha| < 1 \tag{7.3.1}$$

The non-dimensional governing equations are then solved into series solution by substituting the Eq. (7.3.1) into Eqs. (7.2.9) and (7.2.10) with boundary conditions (7.2.11) and equating the coefficients of powers of $\alpha$.

Order zero $(\alpha^0)$:

$$\frac{d^4 F_0}{d\eta^4} = 0, \qquad \theta_0'' + \frac{A_2 \, Ec \, Pr}{A_3(1-\phi)^{2.5}}(F_0'')^2 = 0, \tag{7.3.2}$$

$$F_0(\pm 1) = \pm 1, \ F_0'(\pm 1) = 0, \ \theta_0(\pm 1) = 1 \tag{7.3.3}$$

Order one $(\alpha^1)$:

$$\frac{d^4 F_1}{d\eta^4} + 2\,Re\,A_1(1-\phi)^{2.5}\frac{dF_0}{d\eta}\frac{d^2 F_0}{d\eta^2} = 0, \quad \theta_1'' + \frac{A_2 \, Ec \, Pr}{A_3(1-\phi)^{2.5}}(2F_0''F_1'') = 0, \tag{7.3.4}$$

$$F_1(\pm 1) = 0, \ F_1'(\pm 1) = 0, \ \theta_1(\pm 1) = 0 \tag{7.3.5}$$

With the help of algebraic programming language MAPLE, we have computed the first 18 coefficients for the series of the stream function $F(\eta)$ and temperature $\theta(\eta)$ in terms

131

of $\alpha$, $Ha$, $Re$, $Pr$, $Ec$, $\phi$, $A_1$, $A_2$, $A_3$. The first few coefficients of the series for $F(\eta)$ and $\theta(\eta)$ are as follows:

$$F(\eta; \alpha, \mathrm{Re}, Ha, \phi, A_1) = \frac{3}{2}\eta - \frac{1}{2}\eta^3 - \frac{3}{280}\mathrm{Re}\, A(1-\phi)^{(5/2)}\eta(\eta^2 - 5)(\eta - 1)^2(\eta + 1)^2\alpha + \frac{1}{431200}\eta(\eta - 1)^2$$

$$(\eta + 1)^2(43120 + 9590\eta^4\,\mathrm{Re}^2\,A_1^2\phi^2 - 9590\eta^4\,\mathrm{Re}^2\,A_1^2\phi^3 + 4795\eta^4\,\mathrm{Re}^2\,A_1^2\phi^4 - 959\eta^4\,\mathrm{Re}^2\,A_1^2\phi^5$$

$$- 4795\eta^4\,\mathrm{Re}^2\,A_1^2\phi - 24720\eta^2\,\mathrm{Re}^2\,A_1^2\phi^2 + 24720\eta^2\,\mathrm{Re}^2\,A_1^2\phi^3 - 12360\eta^2\,\mathrm{Re}^2\,A_1^2\phi^4 + 2472\eta^2\,\mathrm{Re}^2\,A_1^2\phi^5$$

$$+ 12360\eta^2\,\mathrm{Re}^2\,A_1^2\phi - 980\eta^6\,\mathrm{Re}^2\,A_1^2\phi^2 + 980\eta^6\,\mathrm{Re}^2\,A_1^2\phi^3 - 490\eta^6\,\mathrm{Re}^2\,A_1^2\phi^4 + 98\eta^6\,\mathrm{Re}^2\,A_1^2\phi^5$$

$$+ 490\eta^6\,\mathrm{Re}^2\,A_1^2\phi + 2875\,\mathrm{Re}^2\,A_1^2 - 10780Ha(1-\phi)^{(1/4)} + 28750\,\mathrm{Re}^2\,A_1^2\phi^2 - 28750\,\mathrm{Re}^2\,A_1^2\phi^3 - 98\eta^6\,\mathrm{Re}^2\,A_1^2$$

$$- 2472\eta^2\,\mathrm{Re}^2\,A_1^2 + 959\eta^4\,\mathrm{Re}^2\,A_1^2 + 10780Ha(1-\phi)^{(1/4)}\phi - 2875\,\mathrm{Re}^2\,A_1^2\phi^5 - 14375\,\mathrm{Re}^2\,A_1^2\phi$$

$$+ 14375\,\mathrm{Re}^2\,A_1^2\phi^4)\alpha^2 + O(\alpha^3)\dots\dots\dots\dots\dots\dots\dots\dots\dots\dots\dots\dots\dots\dots\dots\dots\dots\dots\dots\dots \quad (7.3.6)$$

$$\theta(\eta; \alpha, \mathrm{Re}, Ha, \phi, Ec, \mathrm{Pr}, A_1, A_2, A_3) = 1 - \frac{3A_2\,Ec\,\mathrm{Pr}}{A_3(1-\phi)^{2.5}}(1 - \eta^4) -$$

$$\left( \frac{3A_2\,Ec\,\mathrm{Pr}\,\mathrm{Re}\,A_1}{560A_3}(9\eta^4 - 38\eta^2 - 19(\eta - 1)^2(\eta + 1)^2 \right)\alpha + O(\alpha^2)$$

$$(7.3.7)$$

Applying differential and algebraic approximant methods to the series above, we determine the comparison between the present and previous published results and the changes in bifurcation graphs for the channel angle and flow Reynolds number by the positive effect of nanoparticles volume fraction. The effect of magnetic field and nanofluid on velocity field, temperature profile and entropy generation are also shown graphically using differential approximant method.

## 7.4 Irreversibility of the System

The properties of flow in a convergent-divergent channel with isothermal walls in the presence of magnetic field and viscous dissipation are irreversible. The inequilibrium conditions arise due to the exchange of energy and momentum within the fluid and at solid boundaries which produces continuous entropy generation. Following Bejan (1996), the volumetric entropy generation rate for fully developed flow in cylindrical coordinates is given as

$$E_G = \frac{\kappa_{nf}}{T_a^2}\left(\frac{d\overline{T}}{d\varphi}\right)^2 + \frac{\mu_{nf}}{T_a}\left(\frac{du}{d\varphi}\right)^2 \tag{7.4.1}$$

Where the first term on the right side of equation (7.4.1) is the irreversibility due to heat transfer and the second term is the irreversibility due to viscous dissipation. The entropy generation number can be expressed in dimensionless form as,

$$N_S = \frac{\alpha^2 E_G}{\kappa_f} = \frac{\kappa_{nf}}{\kappa_f}\left(\frac{d\theta}{d\eta}\right)^2 + \frac{A_2 \Pr Ec}{A_3(1-\phi)^{2.5}}\left(\frac{d^2 F}{d\eta^2}\right)^2 \tag{7.4.2}$$

Where $N_1 = \frac{\kappa_{nf}}{\kappa_f}\left(\frac{d\theta}{d\eta}\right)^2$, $N_2 = \frac{A_2 \Pr Ec}{A_3(1-\phi)^{2.5}}\left(\frac{d^2 F}{d\eta^2}\right)^2$

The Bejan number is given as $Be = \dfrac{N_1}{N_S}$

It is notable that the Bejan number ranges from 0 to 1 and $Be = 0$ is the limit where the irreversibility is dominated by fluid friction effects. The irreversibility due to heat transfer dominates the flow system at the limit $Be = 1$ because of finite temperature differences. The contributions of heat transfer and fluid friction to entropy generation are equal when $Be = \frac{1}{2}$.

## 7.5 Results and Discussion

The current work analyzed the stability and irreversibility analysis of Jeffery-Hamel flow of viscous incompressible nanofluid with the effect of an external magnetic field using Hermite-Padé approximants. Three different types of nanoparticles are considered namely Cu, $TiO_2$, $Al_2O_3$-nanoparticles. The understanding of the flow physics is achieved through a combination of numerical studies. There are six parameters of interest in the present problem, the effects of nanoparticles volume fraction $\phi$, channel angle $\alpha$, Prandtl number $Pr$, Eckert $Ec$, Reynolds number $Re$ and Hartman number $Ha$.

### 7.5.1 Stability Analysis

As mentioned earlier, we have computed for investigation the centre line axial velocity and radial velocity as two series in powers of $\alpha$, $Re$, $\phi$, $A_1$ and $Ha$ by differentiating series (7.3.6) at $\eta = 0$ and for all $\eta$ respectively in the following functional form.

$$F'(\eta = 0; \alpha, \text{Re}, Ha, \phi, A_1) \tag{7.5.1}$$

$$F'(\eta; \alpha, \text{Re}, Ha, \phi, A_1) \tag{7.5.2}$$

The dominating singularity behavior of the function $F'(\alpha)$ represented by a series (7.5.1) may be written as

$$F'(\alpha) \sim \begin{cases} B + A\left(1 - \dfrac{\alpha}{\alpha_c}\right)^{\delta} & \text{when } \delta \neq 0, 1, 2, \ldots, \\[4mm] B + A\left(1 - \dfrac{\alpha}{\alpha_c}\right)^{\delta} \ln\left|1 - \dfrac{\alpha}{\alpha_c}\right| & \text{when } \delta = 0, 1, 2, \ldots, \end{cases} \tag{7.5.3}$$

as $\alpha \to \alpha_c$, where $A$ and $B$ are some constants and $\alpha_c$ is the critical point with the critical exponent $\delta$. If $\delta$ is a negative integer then the singularity is a pole; otherwise it represents a branch point singularity.

The series (7.5.1) is analyzed by High-order differential approximant method (2002) to show the comparison between present results and the results of Fraenkel (1962) in Tables 7.1-7.2 and the variation in the critical values $\alpha_c$ and $\text{Re}_c$ with critical exponent $\delta$ for various values of nanoparticles solid volume fraction significantly. Table 7.1 exhibits the decreases of critical channel semi-angle $\alpha_c$ for four different increasing values of $\phi = 0$, 0.05, 0.1, 0.2 as Cu-nanoparticles with water is the base fluid by considering $d = 4$ and $N = 18$. The values of $\delta$ confirm that $\alpha_c$ is a branch point using HODA. Moreover, Table 7.2 implies that $\text{Re}_c$ decreases as significantly and uniformly for different increasing values of $\phi$ and $\text{Re}_c$ is a branch point verified by the values of $\delta$. The results of Tables 7.1-7.2 show a good agreement with those results of Fraenkel (1962) and Makinde (2008) for $\phi = 0$. Hence the obtained results indicate that the presence of nanofluids forms early development in the instability of the flow process.

**Table 7.1** Numerical values of critical angles $\alpha_c$ and corresponding exponent $\delta$ at $Re = 20$ and $Ha = 1$ for various values of $\phi$.

| Present study | | | Fraenkel (1962) | Makinde (2008) |
|---|---|---|---|---|
| $\phi$ | $\alpha_c$ | $\delta$ | $\alpha_c$ | $\alpha_c$ |
| 0 | 0.2691819115000 | 0.49515872313 | 0.269 | 0.269162 |
| 0.05 | 0.2122678984825 | 0.49785814583 | _ | _ |
| 0.1 | 0.1963360739593 | 0.50387522948 | _ | _ |
| 0.2 | 0.1828175409234 | 0.49803815751 | _ | _ |

**Table 7.2** Numerical values of critical $Re_c$ and corresponding exponent $\delta$ at $\alpha = 0.1$ and $Ha = 1$ for various values of $\phi$.

| Present study | | | Fraenkel (1962) | Makinde (2008) |
|---|---|---|---|---|
| $\phi$ | $Re_c$ | $\delta$ | $Re_c$ | $Re_c$ |
| 0 | 54.47285679258 | 0.5071160433 | 54.61 | 54.4717 |
| 0.05 | 44.31499529952 | 0.4985570114 | _ | _ |
| 0.1 | 39.49239826450 | 0.4996886803 | _ | _ |
| 0.2 | 36.73956809792 | 0.4990504907 | _ | _ |

It is seen from Table 7.3 that the values of $\alpha_c$ increases uniformly for $Cu, TiO_2$ and $Al_2O_3$ nanoparticles respectively with different values of volume fraction as the nanoparticles are arranged in descending order of density. The similar behavior of the above three nanoparticles are observed in Table 7.4 for critical Reynolds number $Re_c$.

**Table 7.3** Variation of critical angles $\alpha_c$ and corresponding exponent $\delta$ at $\mathrm{Re} = 20$ and $Ha = 1$ for different types of nanoparticles.

| | $\alpha_c$ | | | $\delta$ |
|---|---|---|---|---|
| $\phi$ | Cu | $TiO_2$ | $Al_2O_3$ | |
| 0 | 0.2691819115000 | 0.2691819115000 | 0.2691819115000 | 0.49515872313 |
| 0.05 | 0.2199306158629 | 0.2632195331417 | 0.2661882689428 | 0.49785814583 |
| 0.1 | 0.1963360739593 | 0.2641976761310 | 0.2697502648509 | 0.50387522948 |
| 0.2 | 0.1828175409234 | 0.2839251923510 | 0.2935579643072 | 0.49803815751 |

**Table 7.4** Variation of critical $\mathrm{Re}_c$ and corresponding exponent $\delta$ at $\alpha = 0.1$ and $Ha = 1$ for different types of nanoparticles.

| | $\mathrm{Re}_c$ | | | $\delta$ |
|---|---|---|---|---|
| $\phi$ | Cu | $TiO_2$ | $Al_2O_3$ | |
| 0 | 54.47285679258 | 54.47285679258 | 54.47285679258 | 0.5071160433 |
| 0.05 | 44.31499529952 | 53.25377222292 | 53.90465402042 | 0.4985570114 |
| 0.1 | 39.49239826450 | 53.46867304615 | 54.60503673870 | 0.4996886803 |
| 0.2 | 36.73956809792 | 57.61325087441 | 59.63881039190 | 0.4990504907 |

Employing the algebraic approximation method to the series (7.5.1) we have obtained the bifurcation graphs of $\alpha$ and $Re$. Figure 7.2(a) shows the bifurcation diagram of $\alpha$ with the effect of Cu-water nanofluid. We say that there is a *simple turning point, fold or a saddle-node bifurcation* at $\alpha = \alpha_c$. It is interesting to notice that there are two solution branches of velocity when $\alpha < \alpha_c$, one marginal solution when $\alpha = \alpha_c$, and no solution when $\alpha > \alpha_c$, where $\alpha_c$ is the critical value of $\alpha$ for which the solution exists. It can be also noted here that the bifurcation points change from $\alpha \approx 0.2691819115$ to $\alpha \approx 0.2122678984$ and

then to $\alpha \approx 0.1963360739$ for different values of nanoparticles volume fraction respectively at $\mathrm{Re} = 20$, $Ha = 1$.
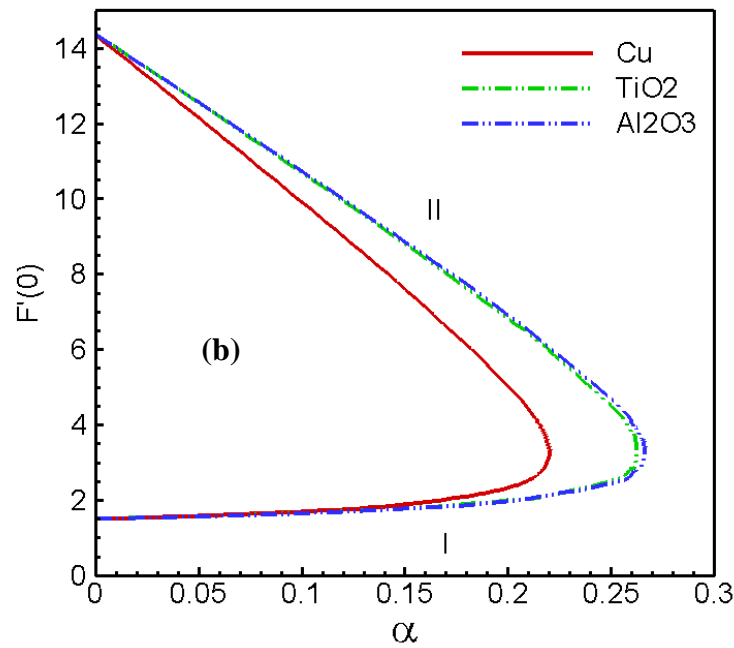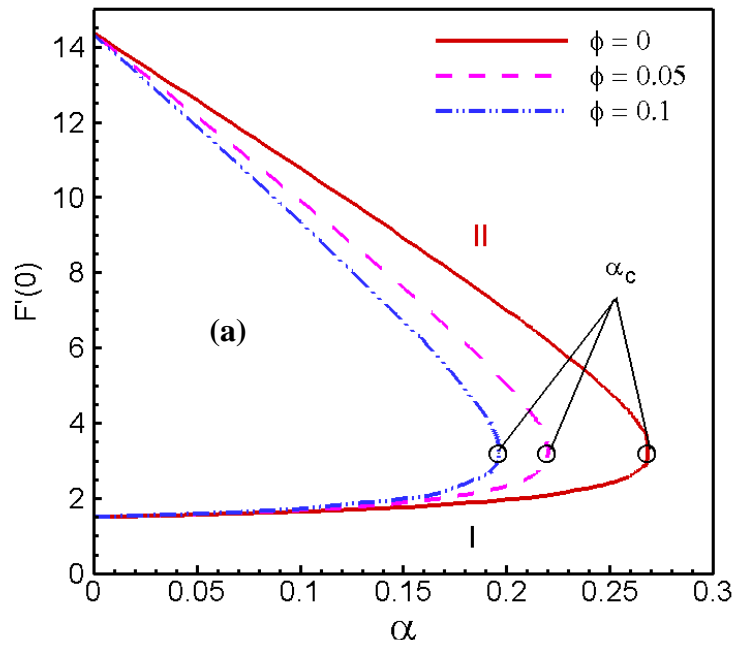


**Figure 7.2** Approximate bifurcation diagrams against $\alpha$ in the $(\alpha, F'(0))$ plane at $Ha = 1$, $\mathrm{Re} = 20$ (a) with different values of $\phi$ for Cu-water nanofluid and (b) for various types of nanoparticles at $\phi = 0.05$ obtained by Drazin-Tourigny method (1996) for $d = 4$.

**Figure 7.3** Approximate bifurcation diagrams against $\mathrm{Re}$ in the $(\mathrm{Re},\, F'(0))$ plane at $Ha = 1,\, \alpha = 0.1$ (a) with different values of $\phi$ for Cu-water nanofluid and (b) for various types of nanoparticles at $\phi = 0.05$ obtained by Drazin-Tourigny method (1996) for $d = 4$.
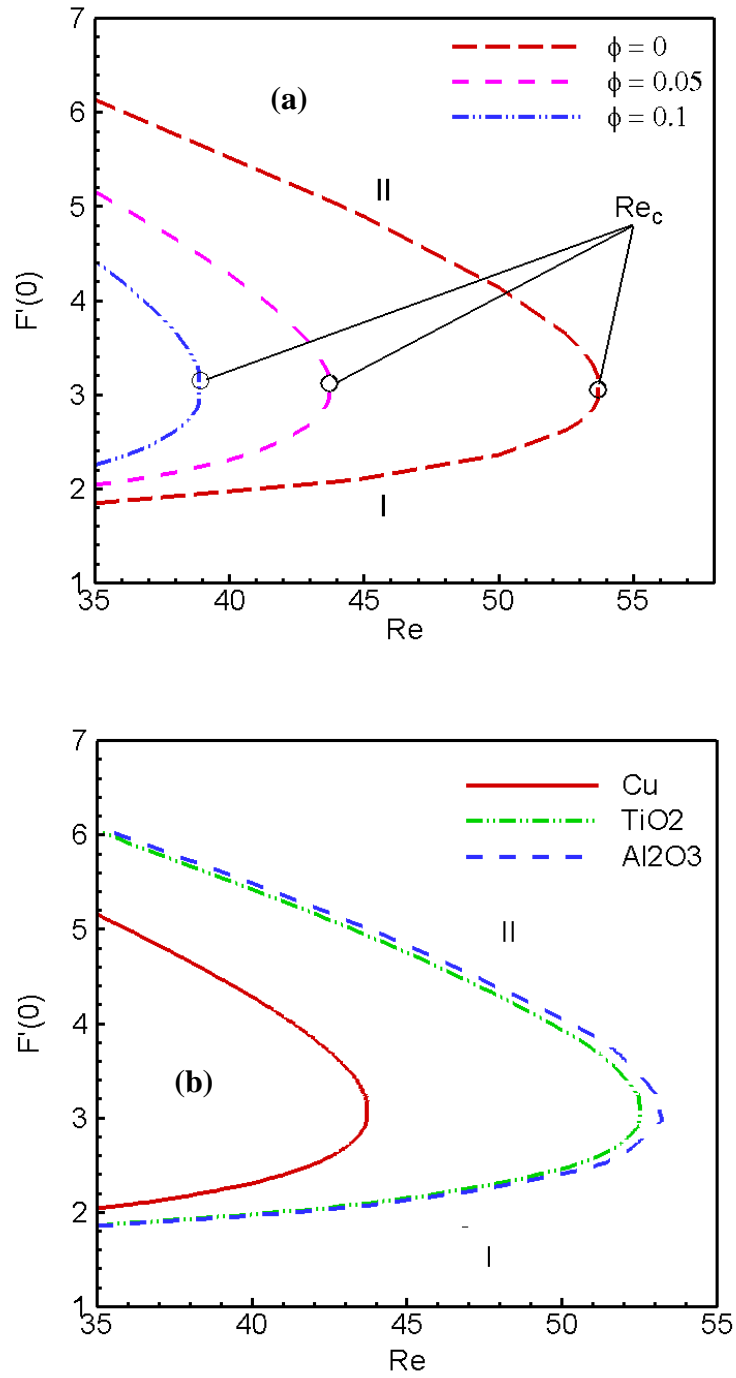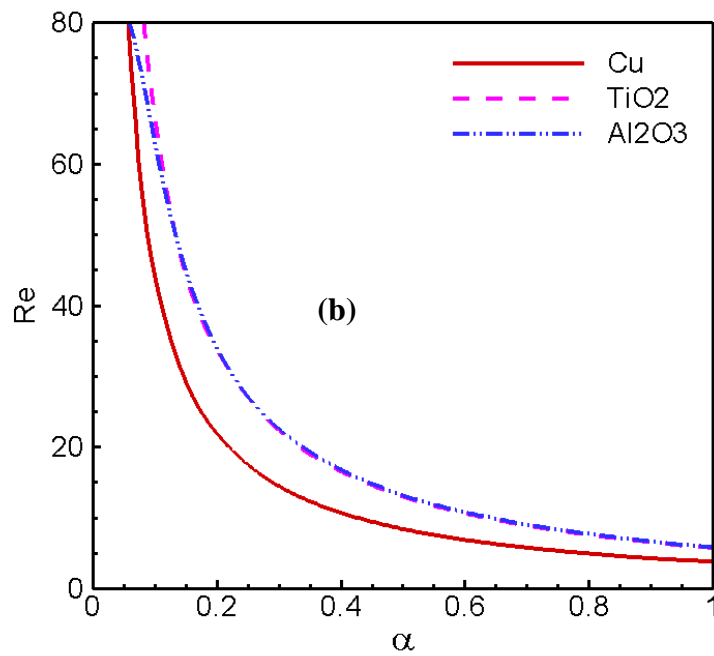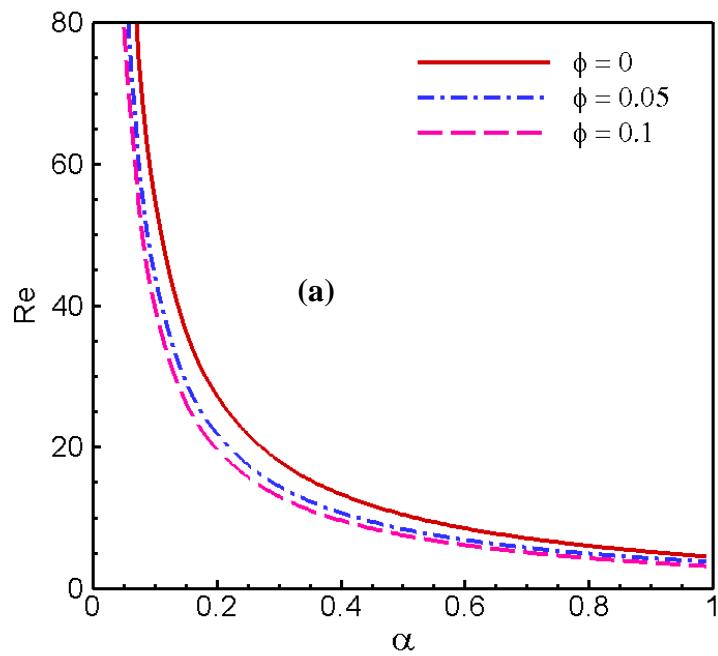
**Figure 7.4** Critical relation between $\alpha$ and *Re* at $Ha = 1$ (a) for different values of $\phi$ for Cu-water nanofluid and (b) for various types of nanoparticles at $\phi = 0.05$ obtained by HPDA (2004) for $d = 5$.
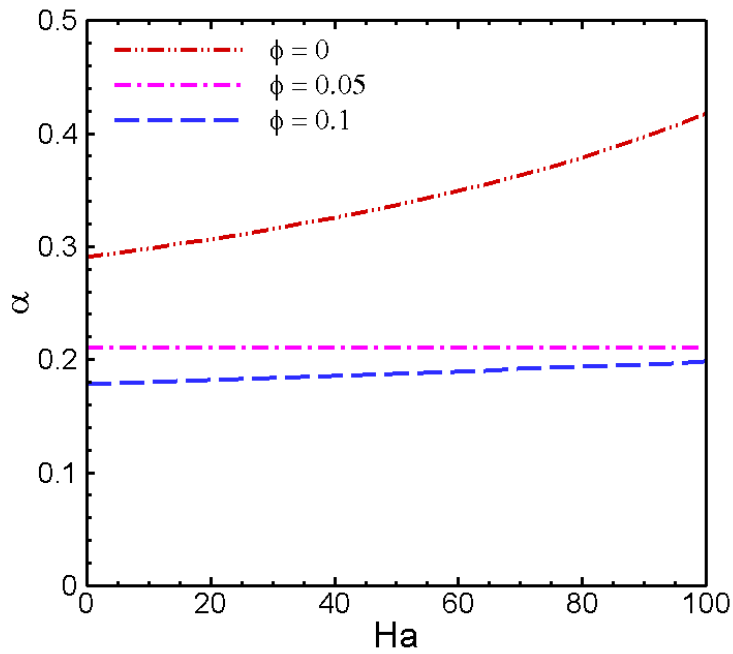
**Figure 7.5** Critical relation between $\alpha$ and *Ha* for different values of $\phi$ at $\mathrm{Re} = 20$ obtained by
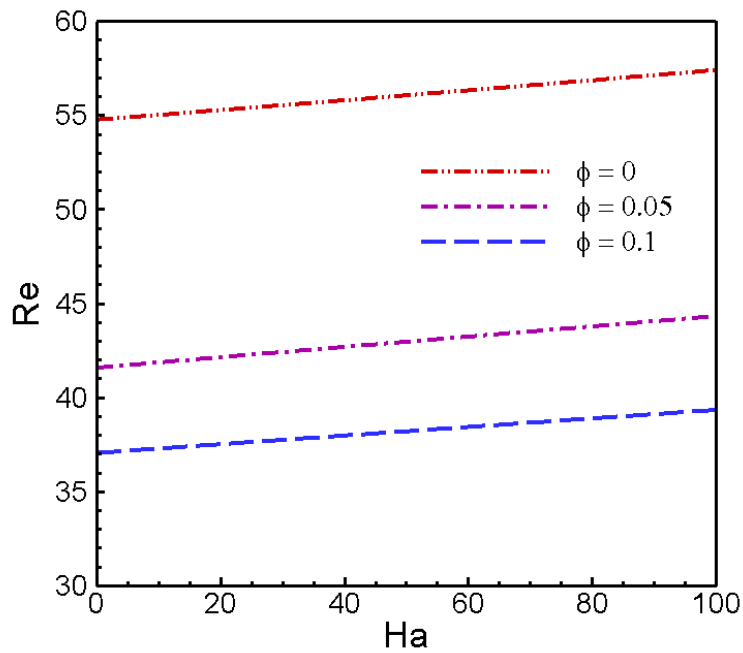
HPDA (2004) for $d = 4$.



**Figure 7.6** Critical relation between $\mathrm{Re}$ and *Ha* for different values of $\phi$ at $\alpha = 0.1$ obtained by

HPDA (2004) for $d = 4$.

On the other hand, it is noticed from Figure 7.2(b) that the bifurcation curves of $TiO_2$ and $Al_2O_3$-nanoparticles almost coincide whereas there is a significant variation for Cu-nanoparticles due to higher respective densities. Moreover, from Figure 7.3 (a) it is observed that the flow also bifurcates at $Re = Re_c$. Moreover, the bifurcation points decreases uniformly for three different values of nanoparticles volume fraction at $\alpha = 0.1, Ha = 1$. Figure 7.3(b) represents the effect of three different nanoparticles on the bifurcation diagram of $Re$ remarkably. The conjecture of Figures 7.2 and 7.3 is consistent with the results shown in Tables 7.1 - 7.4 using differential approximation. One major finding is that, as nanoparticles volume fraction increases the critical channel angle and flow Reynolds number decreases. The temporal and spatial complexity of the observed flows changes in a succession of bifurcations until the onset of instability. Each bifurcation is marked by the onset of instability of one flow and followed by equilibrium to another stable flow.

The High-order partial Differential Approximant HPDA (2004) is applied to the series (7.5.1) in order to determine the critical relationships among the parameters $\alpha$, $Ha$ and $Re$ with the effect of nanofluid. Figure 7.4 (a) displays the critical relation between the channel angular width $\alpha$ and flow Reynolds number $Re$ for three various values of Cu-nanoparticles volume fraction. It is found that as $\alpha$ increases then $Re$ decreases and conversely $Re$ increases when $\alpha$ decreases. This implies that both channel angle and Reynolds number are inversely proportional to each other which is an excellent agreement with the previously established results obtained by Fraenkel (1962) for $\phi = 0$ in classical Jeffery-Hamel flow. A significant variation is observed in the relationship curves for Cu-nanoparticles at $\phi = 0.05$ & $\phi = 0.1$. Moreover, from Figure 7.4(b) it is found that Cu-nanoparticles produce a clear difference in the relationship curve than $TiO_2$ and $Al_2O_3$-nanoparticles due to the effective densities. Figure 7.5 depicts the relationship between $\alpha$ and Hartmann number $Ha$ with different volume fraction of Cu-nanoparticles in divergent channel. It is seen from the figure that $\alpha$ increases as $Ha$ increases and the rate of increase is lower in Cu-water nanofluid than pure base fluid. Also, $\alpha$ decreases as $\phi$ increases. Finally, in Figure7.6, the flow Reynolds number $Re$ increases with rising $Ha$ in absence of nanofluid

but then the tendency of increase becomes slower for $\phi = 0.05$ & $\phi = 0.1$. The conjecture of both the Figures 7.5 and 7.6 coincides with those results of Alam and Khan (2010) at $\phi = 0$. Therefore, nanofluid diminishes the alternation phenomenon in the relationship graphs among the parameters. Series analysis plays an important role in many areas, particularly in fluid dynamics, where, as mentioned earlier, the presence of real singularities in the solution may reflect some changes in the nature of the flow. The criticality of channel angle and flow Reynolds number lead to instability in the fluid flow with a significant effect of nanofluid.

### 7.5.2 Effect of Channel Angle

Figures 7.7(a, b) show the effect of channel angle on the velocity profiles in divergent channel for both base fluid and nanofluid respectively. It is seen from Figure 7.7(a) that the velocity increases moderately at the centerline of the channel whereas decreases gradually near the two walls with a rising values of $\alpha$ at $Re = 7, Ha = 1$ for base fluid $(\phi = 0)$ but the differences between the velocity profiles are more noticeable at larger angles. However, the backflow is detected in diverging channel for higher values of $\alpha = \pi/4$. In Figure 7.7(b), the presence of Cu-nanoparticles $(\phi = 0.05)$ accelerates the increment of centerline velocities more rapidly, while there occurs major backflow near the walls at large value of $\alpha = \pi/4$. The flow breaks the symmetry, with most of the fluid going in a thin layer along the walls as channel angle increases. The fluid is prevented from utilizing the whole area of the expanding channel by a recirculation vortex which blocks the exit. In addition, secondary instabilities driven by this vertical motion develop in this flow. The effect of increasing $\alpha$ on the temperature of the fluid is seen in the Figure 7.8 (a) in a way that the temperature rises massively at the centerline of the channel due to the faster flow rate. The entropy generation rate $N_s$ by the effect of $\alpha$ is shown in Figure 7.8 (b) such that the irreversibility of the system is absolutely zero at center of the channel whether symmetrically increases towards the fixed two hot walls. The maximum velocity at the center leads to approximately zero velocity gradient, also the temperature distribution observed in Figure 7.8 (a) is very high at the center which turns the temperature gradient to zero. As a result, the contribution of both fluid friction $N_2$ and heat transfer $N_1$ to the total entropy $N_s$ become zero at the center of

the channel. Moreover, the increasing values of $\alpha$ accelerates $N_s$ near the walls because of the formation of back flow over there.
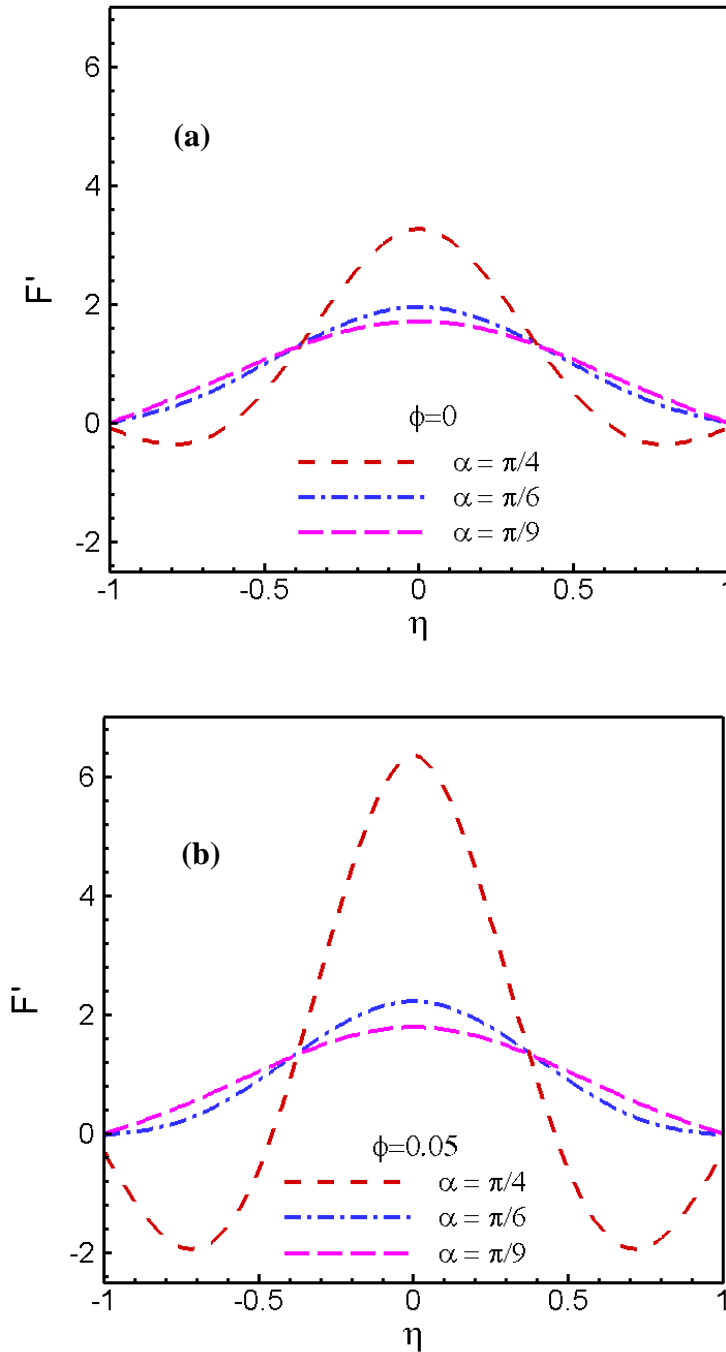


**Figure 7.7** Velocity profiles in divergent channel with different values of $\alpha$ at $\text{Re} = 7$, $Ha = 1$ for (a) base fluid and (b) Cu-water nanofluid.

143

For the same reason it is noticed from Figure 7.8 (c) in the Bejan profile that fluid friction irreversibility is dominant at the center and heat transfer irreversibility is dominant at the two hot walls. Increases of $\alpha$ has a significant influence on the dominance effect of heat transfer irreversibility at the walls.
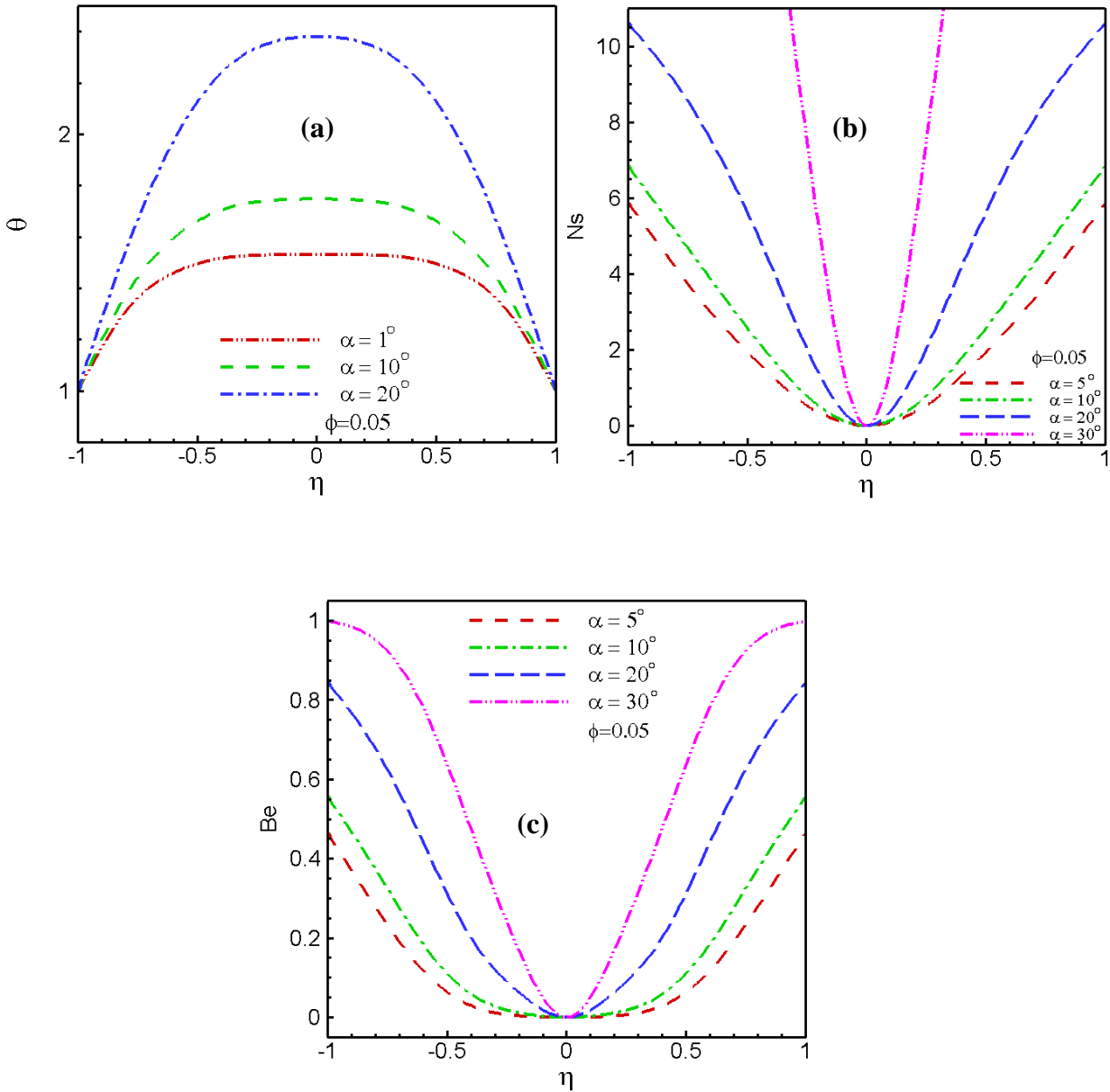


**Figure 7.8** Effect of channel angle on (a) temperature distributions, (b) Entropy rates, (c) Bejan profiles respectively at $Ec = 0.1, \text{Pr} = 7.1, \text{Re} = 7, \text{and } Ha = 1$ .

### 7.5.3 Effect of Reynolds Number

The influences of flow Reynolds number on velocity profile is presented in Fgure 7.9(a, b) significantly for both divergent and convergent channels. A similar characteristic in the velocity profile is observed for divergent channel ($\alpha = 10^\circ$) in Figure 7.9(a) as in Figure 7.7 (a) for channel angle when the flow Reynolds number $Re$ increases. The velocity along the centerline increases rapidly when $Re$ increases, because the volumetric flow rate accelerates which faster the maximum velocity at the center of the channel. On the other hand, flow reversal forms and then enlarges at the two walls when $Re$ increases. Figure 7.9(b) shows the velocity profile in convergent channel ($\alpha = -10^\circ$) with the effect of Reynolds number. A symmetrical but contrary phenomenon is seen in the convergent channel such that the velocity deceases at the center of the channel and increases at the walls when $Re$ increases because of the negative volumetric flow rate towards the sink at $r = 0$. At larger values of Reynolds number, back flow produces at the centerline of the channel, which we have seen in Figure 7.9(a) at the walls for divergent channel. The effect of Reynolds number on temperature distribution is noticed in Figure 7.10 (a) that the temperature at the center of the channel increases rapidly with increases of $Re$ due to the faster flow rate at that region. It is seen from figure 7.10 (b) for divergent channel that the entropy generation rate goes faster at the two walls for the rising values of $Re$, which is consistent with the results shown in Figure 7.9 (a) that flow reversal produces at that region. A symmetrical behaviour of Bejan profile for Reynolds number is observed in Figure 7.10 (c) in comparison of channel angle that the dominance of fluid friction irreversibility occurs at the centerline whereas the heat transfer irreversibility is dominant at the two hot walls.

### 7.5.4 Effect of Hartmann number

The velocity curves in Figure 7.11(a) show that the rate of alteration is significantly and uniformly reduced with increase of Hartmann number $Ha$ in absence of nanoparticles $(\phi = 0)$. The transverse magnetic field opposes the alteration phenomena clearly. The variation of $Ha$ leads to the variation of the Lorentz force due to magnetic field and the Lorentz force produces more resistance to the alternation phenomena within the channel. It can be noted also from Figure 7.11(b) that the centerline velocity decreases

reasonably with rising *Ha* in presence of nanofluid $(\phi = 0.05)$ at a large angle $\alpha = \pi/4$ with $\text{Re} = 7$. Figure 7.12 predicts the combined effects of magnetic field and nanoparticles volume fraction on the velocity field for divergent channel with fixed Reynolds number.
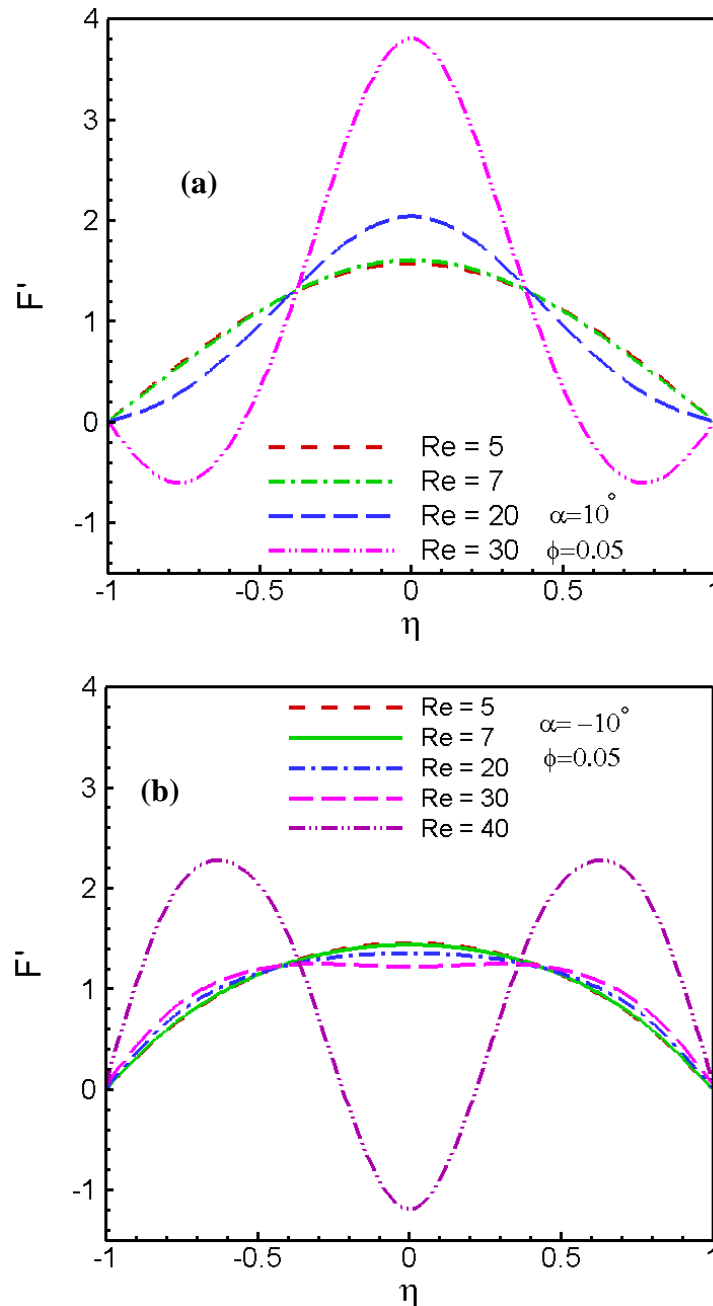


**Figure 7.9** Velocity profiles in (a) divergent channel and (b) convergent channel with different values of *Re* at $Ha = 1$ for Cu-water nanofluid.

**Figure 7.10** Effect of Reynolds number on (a) temperature distributions, (b) Entropy rates, (c) Bejan profiles respectively at $Ec = 0.1, \Pr = 7.1, \alpha = 10^\circ,$ and $Ha = 1$ .

**Figure 7.11** Velocity profiles in divergent channel with different values of $Ha$ at $\mathrm{Re} = 7$, $\alpha = \pi/4$ for

(a) base fluid and (b) Cu-water nanofluid.
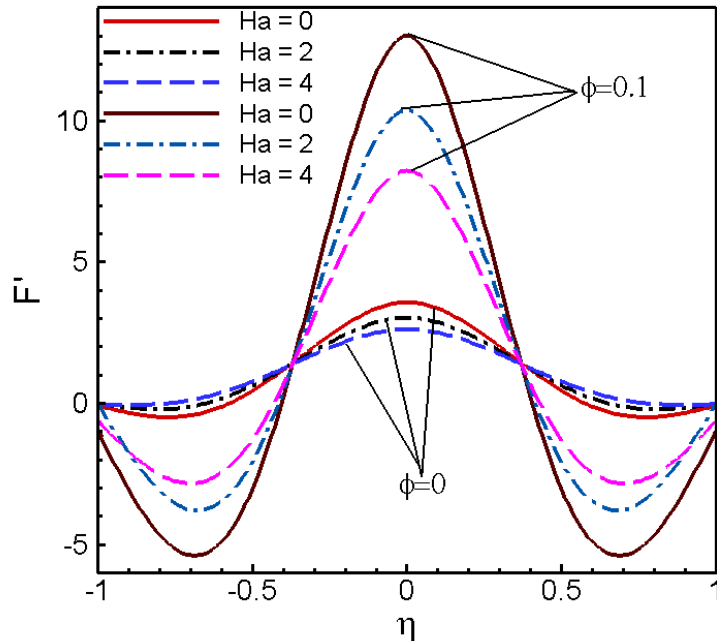
**Figure 7.12** Combined effects of Hartmann number and solid volume fraction of Cu-nanoparticles on velocity profile for $\alpha = \pi/4, \mathrm{Re} = 7$.

The figure represents sensible decreases in the centerline velocity with rising Hartmann number for both base fluid and nanofluid that coincide with those results of Sheikholeslami et al. (2012). It is also observed that for all values of Hartmann number there is no backflow in the base fluid $(\phi = 0)$, nevertheless backflow starts for nanofluid with $Ha = 0$ at $\alpha = \pi/4, \mathrm{Re} = 7$ and this phenomenon is decreased with the rising values of Hartmann number.

### 7.5.4 Effect of Nanoparticles volume fraction

Figure 7.13 represents the consequences of solid volume fraction on velocity profiles at fixed Reynolds number in both convergent-divergent channels. In Figure 7.13(a) at $\alpha = \pi/4$ for divergent channel as $\phi$ increases, the center line velocity increases and on the other side the backflow is observed near the walls. Conversely, Figure 7.13(b) for convergent channel $(\alpha = -\pi/4)$ represents that backflow starts at the centerline when $(\phi = 0.05)$ whether there is no sign of backflow in absence of nanoparticles $(\phi = 0)$ and

these properties are enhanced with rising values of $\phi = 0.1$. Therefore, the state of backflow in convergent channel is completely opposite in comparison to divergent channel.
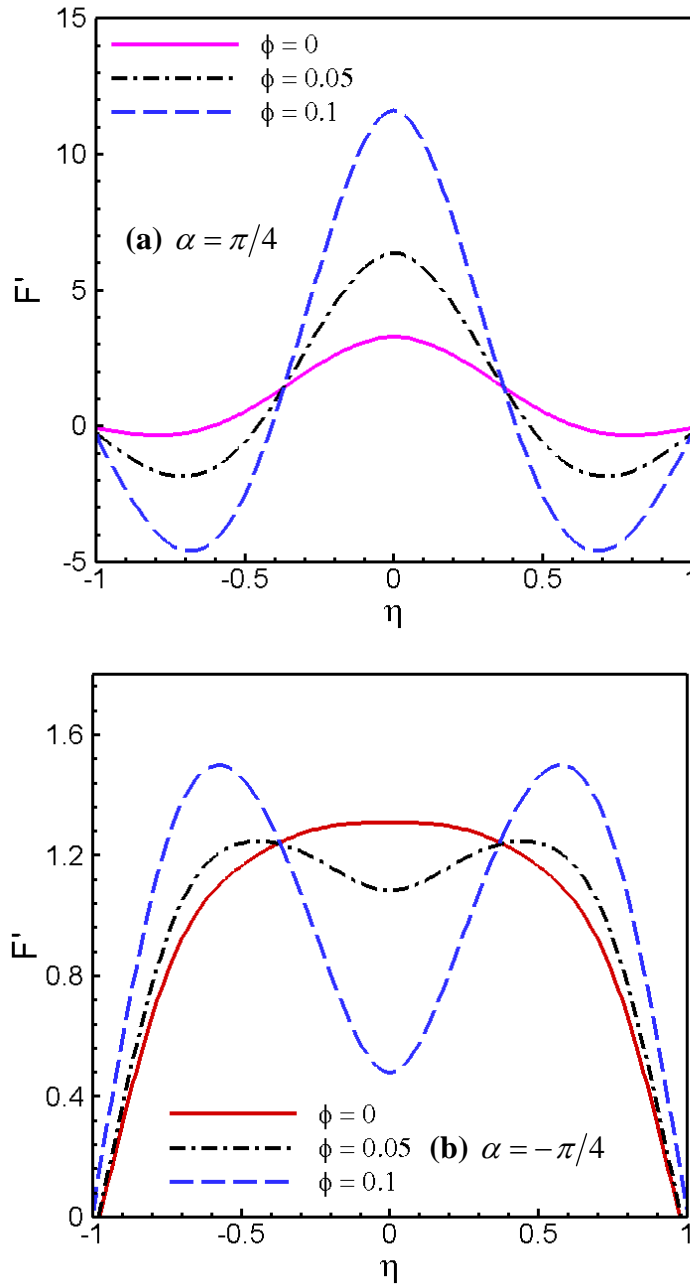


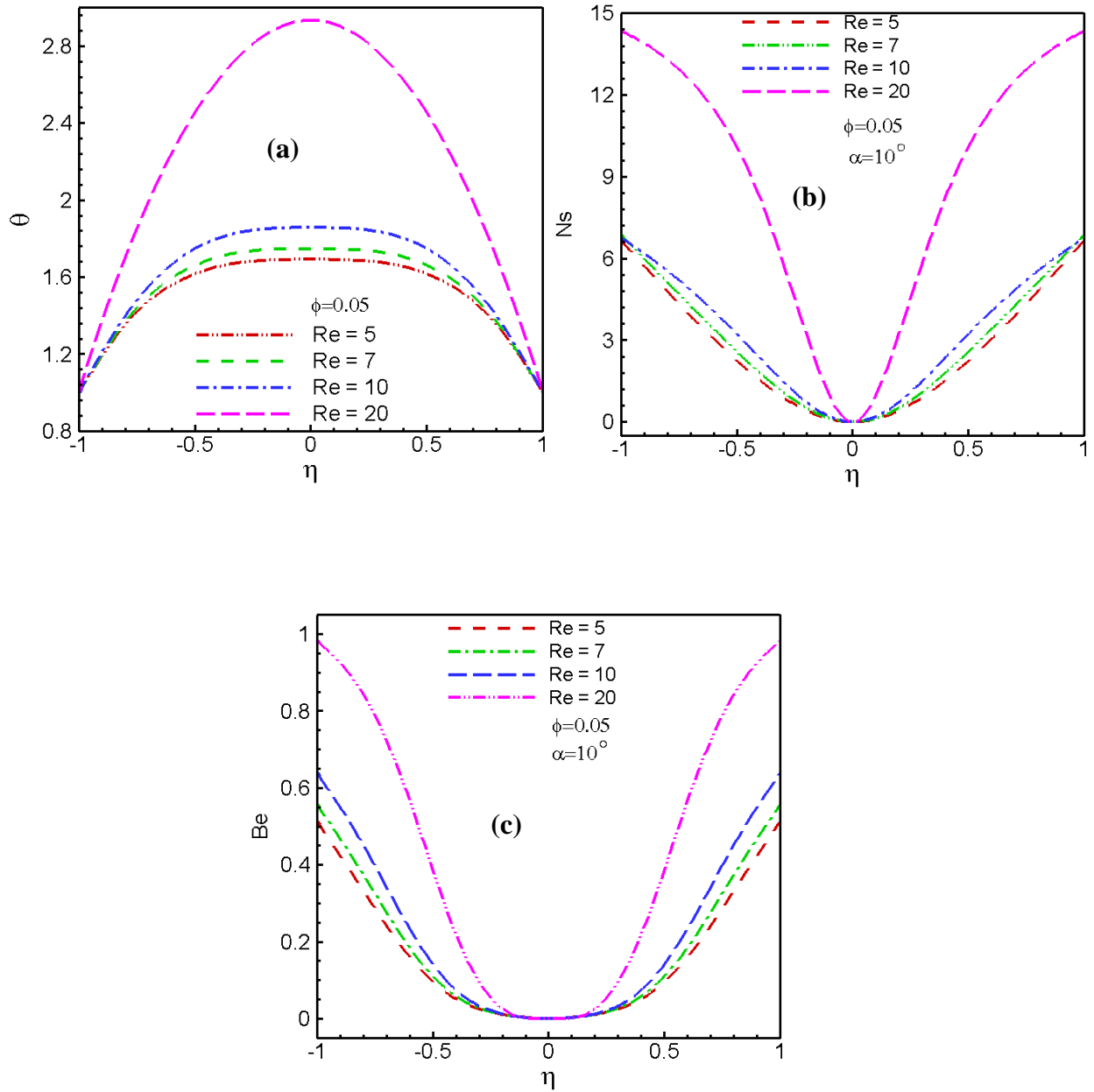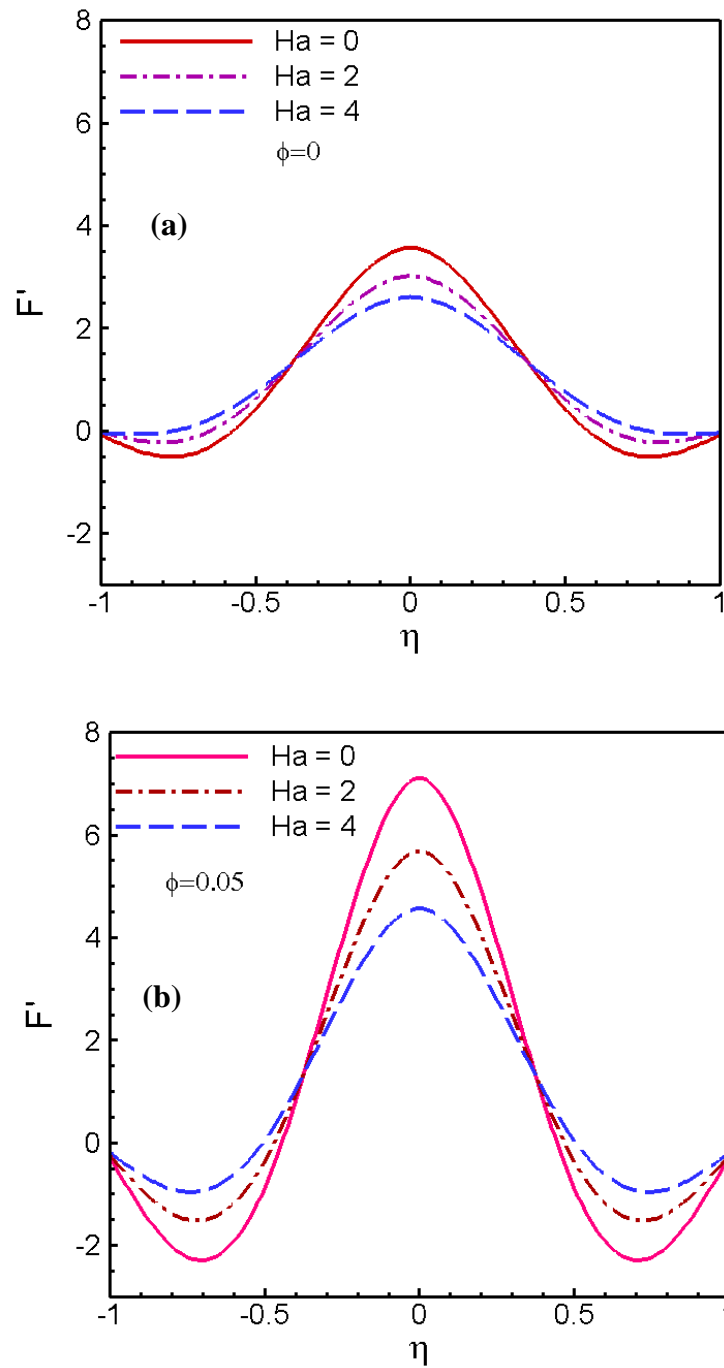**Figure 7.13** Velocity profiles with different values of $\phi$ (a) divergent channel and (b) convergent channel at $\mathrm{Re} = 7, Ha = 1$ for Cu-water nanofluid.

Figures 7.14 (a, b) explain the variations of dimensionless temperature with increasing nanoparticle volume fraction $\phi$ for both divergent and convergent channel respectively. A

150

definite and uniform rise in temperature is seen in Figure 7.14(a) for divergent channel because of an increase in the gap between the walls. This explains also the influence of higher thermal conductivity and specific heat.
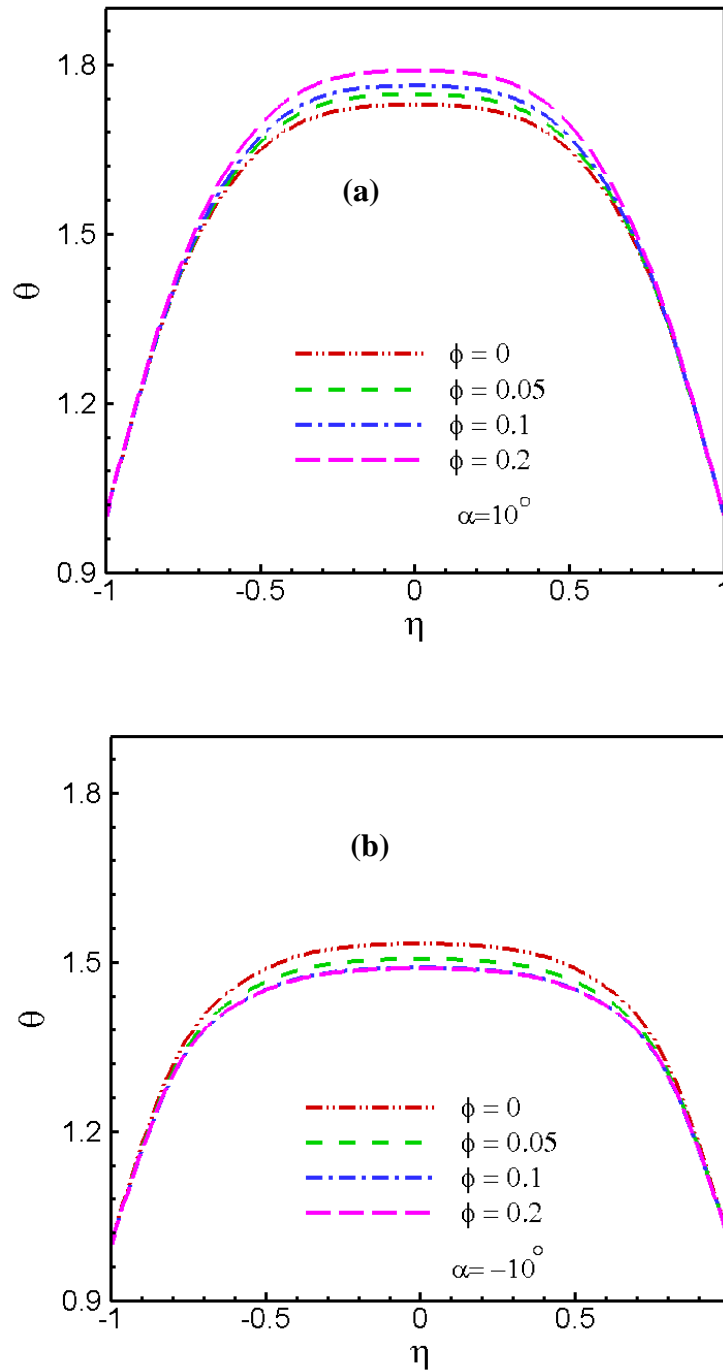


**Figure 7.14** Temperature profiles for different values of $\phi$ (a) in divergent channel and (b) in convergent channel at $Pr = 7.1, Ec = 0.1, Re = 7$ and $Ha = 1$ .
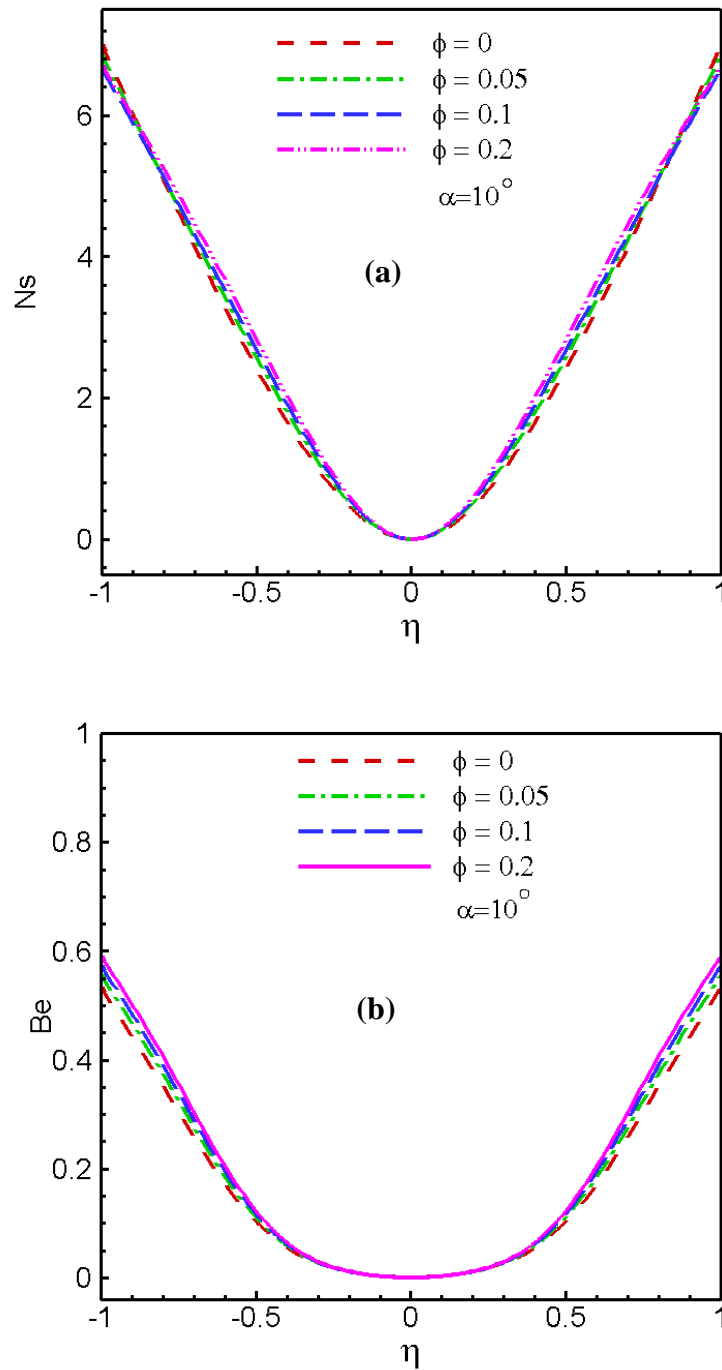
**Figure 7.15** Effect of nanoparticles volume fraction on (a) Entropy rates and (b) Bejan profiles respectively at $Ec = 0.1, \mathrm{Pr} = 7.1,$ and $Ha = 1$ .

Also, copper nanoparticles are much more efficient to control the rise in temperature for various practical situations as compared to pure base fluid. The temperature field in

convergent channel presented by Figure 7.14 (b) is decreasing uniformly by the positive change of $\phi$. Since the gap between the walls reduces rapidly towards the sink at $r = 0$, which produces reduction of temperature at the centerline region. Figures 7.15 (a, b) depict the entropy generation with Bejan number with the control of nanoparticles volume fraction correspondingly. The properties of total entropy rate $N_s$ in Figure 7.15 (a) is almost similar as in Figures 7.8(b) and 7.10(b), whereas the effect of $\phi$ on $N_s$ is insignificant in the divergent channel. It can be noted from Figure 7.15(b) that the dominant effect of heat transfer irreversibility enhances due to the escalating values of $\phi$. As it is already discussed previously that the higher thermal conductivity and specific heat of nanofluid generates more heat transfer.

### 7.5.5 Effect of Eckert number

The effect of Eckert number on temperature field within the channel for convergent and divergent is discussed in Figures 7.16(a, b). Eckert number describes the effects due to the dissipation term in energy equation. Since Eckert number is the ratio of the square of maximum velocity and specific heat. As a result, when the value of Eckert number increases, the fluid flow rate along the centerline becomes more faster. It is noticed from Figure 7.16 (a, b) that the fluid temperature increases successively with increasing values of viscous heating parameter $Ec$ for both convergent and divergent channels. Furthermore, due to the higher thermal conductivity coefficient of the nanofluid, the heat is more intensely transferred. The consequences of Eckert number on irreversibility of the system is analysed in Figures 7.17 (a, b). The entropy generation rate $N_s$ increases promptly and symmetrically near the two hot walls with the growing values of $Ec$ due to viscous dissipation effect as seen in Figure 7.17 (a). Moreover, the positive variation of Eckert number has a key impact on the dominant effect of heat transfer irreversibility at the two heated walls shown in Figure 7.17(b).
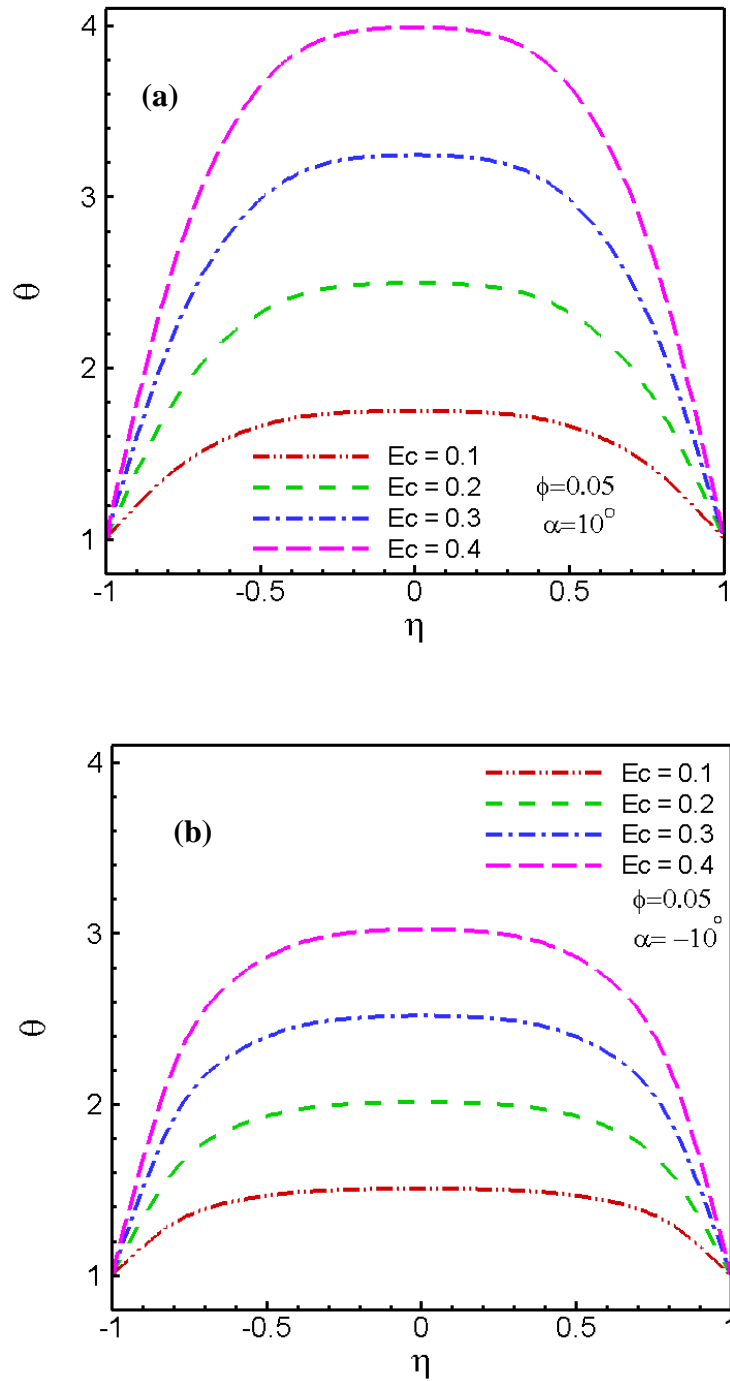
**Figure 7.16** Temperature profiles for different values of Eckert number *Ec* (a) in divergent channel and (b) in convergent channel at $\mathrm{Pr} = 7.1, \mathrm{Re} = 7$ and $Ha = 1$ .
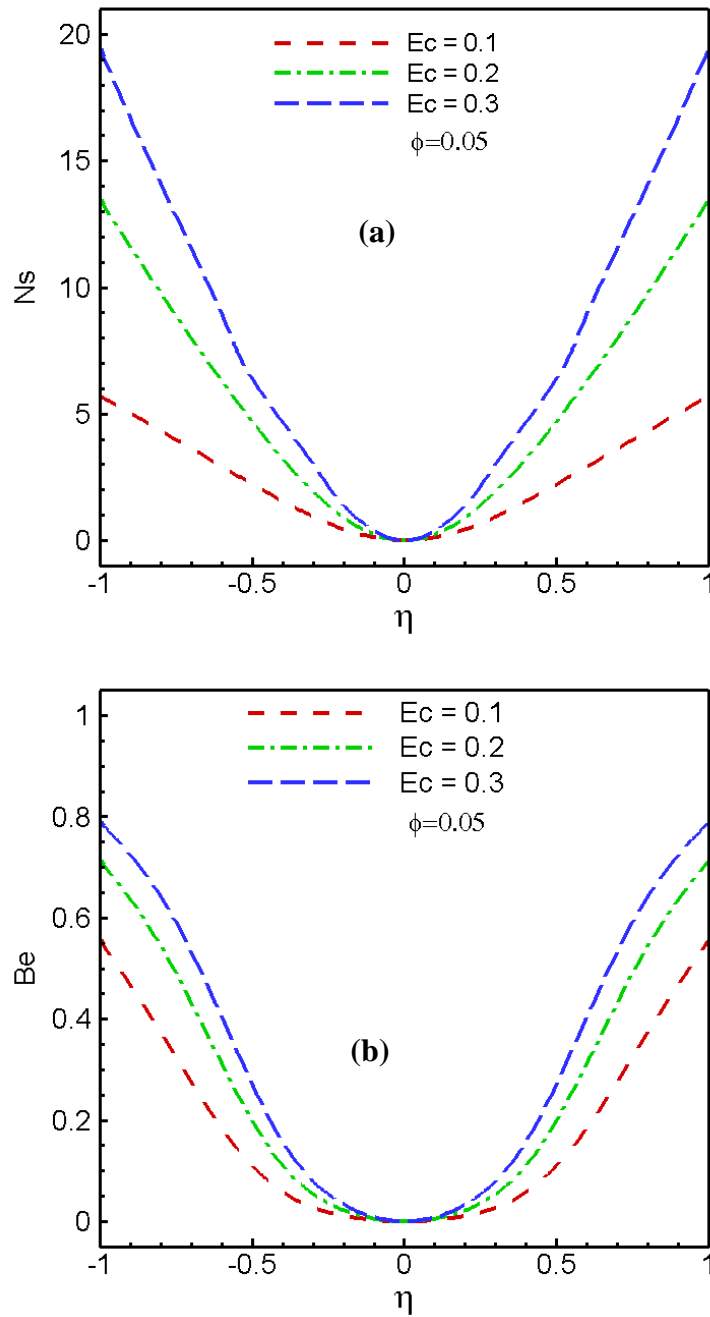
**Figure 7.17** Effect of Eckert number *Ec* on (a) Entropy rates and (b) Bejan profiles respectively

at $\alpha = 10°, \mathrm{Pr} = 7.1$, and $Ha = 1$ .

## 7.7 Conclusion

The entropy generation of magnetohydrodynamic Jeffry-Hamel flow with three different types of nanoparticles as water is the base fluid is investigated using a special type of

Hermite-Padé approximation technique. A comparison is made between the available results and the present approximate solutions. The influences of various physical parameters on the velocity field, temperature distribution and entropy generation rate with Bejan profile are discussed in detail. The basic conclusions are as follows:

➢ The dominating singularity behaviour is a branch point singularity with the critical exponent half for both the wall divergence semi-angle $\alpha$ and flow Reynolds number *Re* is found with the effect of various types of nanoparticles volume fraction. The critical relationships among the parameters with the effect of nanofluid coincide with the conjecture of classical Jeffery-Hamel flow.

➢ Increasing channel semi angle and Reynolds number leads to enrichment of fluid centerline velocity and flow reversal near the walls in the divergent channel for both base fluid and nanofluid. Increasing Hartmann number reduces fluid flow in the channel centerline and produces the backflow reduction near the walls for both base fluid and nanofluid. The velocity increases as nanoparticles volume fraction increases along the centerline whereas increasing volume fraction generates backflow near the walls. Behaviour of the flow for changing of the physical parameters in convergent channel is quite opposite to the one seen in divergent channel.

➢ The increasing values of the pertinent physical parameters namely channel angle, flow Reynolds number, Eckert number enhances temperature field along the channel centerline region. Also temperature increases uniformly as nanoparticles volume fraction increases.

➢ Entropy generation rate is higher near the hot solid walls in comparison to the channel centerline region. Fluid friction irreversibility dominates the entropy generation absolutely near the channel centerline while the heat transfer irreversibility dominates at the hot solid walls. Heat transfer irreversibility is the sole contributor to the total entropy generation at the hot solid walls. Nanofluid enhances the dominant effect of heat transfer irreversibility in the entropy generation of the system.

# Conclusion and Recommendations

## 8.1 Conclusion

The thesis has investigated numerically the stability of a steady magnetohydrodynamic flow of viscous incompressible nanofluids through channel. The governing partial differential equations for mass, momentum and energy are derived according to the physical model of the problem. These governing equations with boundary conditions are then made dimensionless form using suitable transformations. The resulting dimensionless nonlinear differential equations are solved numerically using power series with Hermite-Padé approximation method.

> ➢ The dominating singularity behaviour of the flow as well as the existence of the dual solution branches of the systems are examined to study the stability of the fluid flow.

> ➢ The irreversibility of the system due to the effect of governing physical parameters and the influences of the parameters on the velocity and temperature distributions are discussed in detail.

A general conclusion on the works is presented below in brief:

> ❖ The thermal stability conditions for dual solution branches are analysed with the effect of Radiation parameter in both solid and porous surfaces for parallel channel. As the thermal conductivity variation parameter exceeds the critical value, the solution of local rate of heat transfer has two branches, namely, an upper branch and a lower branch.

> ❖ It is found that at the lower solution branch which is physically acceptable, the value of Nusselt number decreases with the increase of radiation parameter. It is observed

that suction/injection of fluid exerts a significant influence on the thermal stability condition.

❖ Next, in convergent-divergent channel, the dominating singularity behaviour as a branch point singularity with the critical exponent half for both the channel semi-angle and flow Reynolds number is found numerically and shown in bifurcation diagrams with the effect of nanoparticles volume fraction.

❖ The critical relationships among the parameters with the effect of nanofluid coincide with the conjecture of classical Jeffery-Hamel flow.

▪ Increasing Hartmann number and nanoparticles solid volume fraction cause the reduction of fluid velocity near the centerline uniformly in parallel channel.

▪ An increase in the thermal conductivity variation parameter advances fluid velocity and reduces temperature distribution along the centerline region of the channel.

▪ Radiation parameter reduces both fluid velocity and temperature distribution due to faster heat loss.

▪ At the region of the left porous wall in parallel channel, there occurs backflow as the porosity parameter increases.

▪ For the regions of the flow field adjacent to the porous walls, the total entropy generation rate is dominated by the effects of fluid friction and it is dominated at the centerline region by the effects of heat transfer.

▪ Hence the suction/injection of fluid exerts a significant influence on the velocity and temperature distributions, which transitively affects the entropy generation within the channel.

● Increasing channel semi angle and flow Reynolds number lead to enrichment of fluid centerline velocity and produce flow reversal near the walls in the convergent-divergent channel for both base fluid and nanofluid.

- Increasing Hartmann number produces backflow reduction at the two walls for convergent-divergent channel and large values of Hartmann number is required for decline of the backflow.

- The velocity increases as nanoparticles volume fraction increases along the centerline of the channel whereas increasing volume fraction generates backflow near the walls.

- Behaviour of the flow for changing of the physical parameters in convergent channel is quite opposite to the one seen in divergent channel.

- The increasing values of the pertinent physical parameters namely channel angle, flow Reynolds number, Eckert number, Prandtl number enhance temperature field along the channel centerline region. Also temperature increases uniformly as nanoparticles volume fraction increases.

- Entropy generation is higher near the walls in comparison to the centerline region in convergent-divergent channel. Fluid friction irreversibility dominates the entropy generation absolutely near the channel centerline while the heat transfer irreversibility dominates at the hot solid walls. It is found that Nanofluid enhances the dominant effect of heat transfer irreversibility at the hot walls.

We numerically provide a guidance on the concepts of magnetohydrodynamic stability of several channel flows for nanofluid using Hermite-Padé approximation that should be chosen for many problems in fluid mechanics and similar subjects. The computational cost of the series coefficients of the solution is very high in these problems. Hermite-Padé approximation technique could produce better and accurate results if more terms of the series were computed using highly powerful computer.

## 8.2 Relevancy of the Work to Physical Applications

➢ The three dimensional stability analysis of noncohesive particles under two-dimensional flow in the downstream hydraulic geometry of alluvial channels, in terms of bank-full width, average flow depth, mean flow velocity, and channel slope.

The flow conditions may unstable for meandering to braided, sand-bed and gravel-bed rivers with flow depths and channel widths varying. The conditions can be analytically defined by combining four governing equations: flow rate, resistance to flow, secondary flow, and particle mobility.

➢ The stability analysis of a river channel by investigating the role of phase shift angle between the secondary current and the channel axis displacement. The secondary currents perpendicular to the primary direction of motion form a helical motion in which the water in the upper part of the river is driven outward, whereas the water near the bottom is driven inward in a bend. The instability arises and transition from straight to meandering and then from meandering to braiding occurs when phase shift angle is reduced. Therefore any factor that triggers the formation of secondary currents will have a major contribution in interfering with the stability of a river channel. Some of these factors are: (i) change in slope; (ii) change in channel width; and (iii) formation of ripples among others.

## 8.3 Possible Future Works based on this Thesis

The present study can be extended by considering the following cases:

- Temperature dependent physical properties like viscosity, Prandtl number with different physics like heat generation/absorption, stress work may be considered.
- The study can be extended considering velocity and temperature slip effects.
- One can consider steady three-dimensional flow, unsteady two-dimensional flow and unsteady three-dimensional flow.
- Considering stretchable, porous wall of the convergent-divergent channel, this work can be extended.
- Investigation can be carried out on the interaction of magnetic field and nanofluids for turbulent flow.

# References

Arpaci, V. S., Selamet, A. and Kao, S. H., (2000): "Introduction to Heat Transfer", Prentice-Hall, New York.

Abiodun, O. A., Basant, K. J. and Andrew, O., (2011): "Entropy generation under the effect of suction/injection", Applied Mathematical Modelling, Vol. 35, pp. 4630-4646.

Axford, W. I., (1961): "The Magnetohydrodynamic Jeffrey–Hamel problem for a weakly conducting fluid", Q. J. Mech. Appl. Math., Vol. 14, pp. 335–351.

Alam, M. S. and Khan, M. A. H., (2010): "Critical behaviour of the MHD flow in convergent-divergent channels", Journal of Naval Architecture and Marine Engineering, Vol. 7, No. 2, pp. 83 - 93.

Banks, W. H. H., Drazin, P. G. and Zaturska, M. B., (1988): "On perturbation of Jeffery-Hamel flow", Journal of Fluid Mechanics., Vol. 186, pp. 559-581.

Berman, A. S., (1953): "Laminar flow in channels with porous walls", Journal of Applied Physics, Vol. 24, No. 9, pp. 1232-1235.

Bejan, A., (1996): "Entropy-generation minimization", CRC Press, New York.

Bejan, A., (1979): "A study of entropy generation in fundamental convective heat transfer", J. Heat Transfer, Vol. 101, pp. 718-725.

Brezinski, C., (1990): "History of Continued fraction and Pade′ Approximants." Springer, Berlin.

Blanch, G., (1964): "The numerical evaluation of continued fractions", SIAM Rev., Vol. 6, pp. 383-421.

Bender, C. and Orszag, S. A., (1978): "Advanced Mathematical Methods for Scientists and Engineers", Mcgraw-Hill, New York.

Baker, G. A. Jr. and Graves-Morris, P., (1996): "Pade' Approximants", Second edition, Cambridge University Press, Cambridge.

Batchelor, K., (1967): "An Introduction to Fluid Dynamics", Cambridge University Press, Cambridge.

Cha, J. E., Ahn, Y. C. and Kim, M. H., (2002): "Flow measurement with an electromagnetic flow meter in two-phase bubbly and slug flow regimes", Flow Measurement and Instrumentation, Vol. 12, No. (5-6), pp. 329–339.

Chawla, T. C. and Chan, S. H., (1980): "Combined radiation and convection in thermally developing Poiseuille flow with scattering", J. Heat Transfer, Vol. 102, pp. 297–302.

Cogly, A. C. L., Vincenti, W. G. and Gilles, E. S., (1968): "Differential approximation for radiative heat transfer in a nonlinear equations grey gas near equilibrium", Am. Inst. Aeronaut. J., Vol. 6, pp. 551-553.

Choi, S. U. S., (1995): "Enhancing thermal conductivity of fluids with nanoparticles", In Proceedings of the 1995 ASME International Mechanical Engineering Congress and Exposition, Vol. 66, San Francisco, USA, pp. 99–105.

Chang, L. C., Yang, K. T. and Lloyd, J. R., (1983): "Radiation-natural convection interaction in two-dimensional complex enclosure", J. Heat Transfer, Vol. 105, pp. 89–95.

Chen, C. K., Chen, B. S. and Liu, C. C., (2014): "Heat transfer and entropy generation in fully-developed mixed convection nanofluid flow in vertical channel", Int. J. Heat Mass Transfer, Vol. 79, pp. 750-758.

Cha, J. E., Ahn, Y. C. and Kim, M. H., (2002): "Flow measurement with an electromagnetic flow meter in two-phase bubbly and slug flow regimes," Flow Measurement and Instrumentation, Vol. 12, No. (5-6), pp. 329–339.

Choi, S. U. S., (2009): "Nanofluids: from vision to reality through research", Journal of Heat Transfer, Vol. 131, No. 3, pp. 1-9.

Choi, S. U. S., Zhang, Z. G. and Keblinski, P., (2004): "Nanofluids in Encyclopedia of Nanoscience and Nanotechnology", American Scientific, Vol. 6, pp. 757-737.

Das, S. R., Choi, S. U. S. and Patel, H. E., (2006): "Heat transfer in nanofluids-a review. Heat Transfer Engineering", Vol. 27, No. 10, pp. 3-19.

Drazin, P. G. and Tourigny, Y., (1996): "Numerically study of bifurcation by analytic continuation of a function defined by a power series", SIAM Journal of Applied Mathematics, Vol. 56, pp. 1-18.

Das, S. K., Choi, S. U. S., Yu, W. and Pradeep, T., (2007): "nanofluids: Science and

Technology", Wiley, New York.

Drazin, P. G., (2002): "Introduction to Hydrodynamic Stability", Cambridge University Press, U.S.A.

Esmaili, Q., Ramiar, A., Alizadeh, E. and Ganji, D. D., (2008): "An approximation of the analytical solution of the Jeffery–Hamel flow by decomposition method", Physics Letters A, Vol. 372, pp. 3434–3439.

Fraenkel, L. E., (1962): "Laminar flow in symmetrical channels with slightly curved walls. I: On the Jeffery-Hamel solutions for flow between plane walls", Proceeding of the Royal Society of London, Vol. 267, pp. 119 - 138.

Goerke, A. R., Leung, J. and Wickramasinghe, S. R., (2002): "Mass and momentum transfer in blood oxygenators", Chemical Engineering Science, Vol. 57, No. 11, pp. 2035-2046.

Guttmann, A. J., (1981): "Asymptotic Analysis of Power Series Expansions", Academic Press.

Hamel, G., (1916): "Spiralförmige Bewgungen Zäher Flüssigkeiten", Jahresbericht der Deutschen Math. Vereinigung, Vol. 25, pp. 34-60.

Hamadiche, M., Scott, J. and Jeandel, D., (1994): "Temporal stability of Jeffery-Hamel flow", J. Fluid Mech, Vol. 268, pp. 71-88.

Hermite, C., (1893): "Sur la généralisation des fractions continues algébriques", Annali di Mathematica Pura e Applicata, Vol. 21, No. 2, pp. 289-308.

Jafari, A., Zamankhan, P., Mousavi, S. and Kolari, P., (2009): "Numerical investigation of blood flow, Part II: in capillaries", Communications in Nonlinear Science and Numerical Simulation, Vol. 14, No. 4, pp. 1396-1402.

Jeffery, G. B., (1915): "The two-dimensional steady motion of a viscous fluid", Philosophical Magazine, Vol. 6, pp. 455-465.

Joneidi, A. A., Domairry, G. and Babaelahi, M., (2010): "Three analytical methods applied to Jeffery–Hamel flow", Commun. Nonlinear Sci. Numer. Simulat, Vol. 15, pp. 3423–3434.

Kay, W. M., (1966): "Convective heat and mass transfer", Mc-Graw Hill, New York.

Khan, M. A. H., (2002): "High-Order Differential Approximants", Journal of Computational and Applied Mathematics, Vol.149, pp. 457-468.

Khovanskii, A. N., (1963): "The application of Continued Fractions and their Generalizations to problems in Approximation Theory", P. Noordhoff N. V., Groninger.

Khan, M. A. H., (2001): "Singularity analysis by summing power series", Ph.D. Thesis, University of Bristol, U. K.

Kwak, K. and Kim, C., (2005): "Viscosity and thermal conductivity of copper nanofluid dispersed in ethylene glycol", Korea–Aust. Rheol. J., Vol. 17, pp. 35–40.

Kaufui, V. W. and Omar, D. L., (2010): "Applications of Nanofluids: Current and Future", Advances in Mechanical engineering, Article ID 519659, 11 pages.

Kayvan, S., Navid, K. and Seyed-Mohammad, T., (2007): "Magnetohydrodynamic (MHD) flows of viscoelastic fluids in converging-diverging channels", International Journal of Engineering Science, Vol.45, No.11, pp. 923-938.

Liu, M., Lin, M. C., Huang, I. and Wang, C., (2005): "Enhancement of thermal conductivity with carbon nanotube for nanofluids", International Communication in Heat and Mass Transfer, Vol. 32, No. 9, pp. 1202-1210.

Masuda, H., Ebata, A., Teramea, K. and Hishinuma, N., (1993): "Alternation of thermal conductivity and viscosity of liquid by dispersing ultra-fine particles", Netsu Bussei, Vol. 4, pp. 227-233.

Moreau, R., (1990): "Magnetohydrodynamics", Kluwer Academic Publishers, Dordrecht.

Makinde, O. D., (2003): "Magneto-hydrodynamic stability of plane-Poiseuille flow using multi-deck asymptotic technique", Math. Comput. Model, Vol. 37, No. (3-4), pp. 251–259.

Makinde, O. D. and Motsa, S. S., (2001): "Hydromagnetic stability of plane Poiseuille flow using Chebyshev spectral collocation method", J. Ins. Math. Comput. Sci., Vol. 12, No. 2, pp. 175–183.

Makinde, O. D., (2008): "Thermal criticality in viscous reactive flows through channels with a sliding wall: An exploitation of the Hermite-Padé approximation method", Math. and Comp. Modelling, Vol. 47, pp. 312-317.

Makinde, O. D., (2009): "Hermite-Padè approach to thermal radiation effect on inherent irreversibility in a variable viscosity channel flow" Comp. and Math. with Applications, Vol. 58, pp. 2330-2338.

Makinde, O. D., (2008): "Entropy-generation analysis for variable-viscosity channel flow with non-uniform wall temperature", Appl. Energy, Vol. 85, pp. 384–393.

Mah, W. H., Hung, Y. M. and Guo, N. Q., (2012): "Entropy generation of viscous dissipative nanofluid in microchannels", Int. J. Heat Mass Transfer, Vol. 55, No. (15-16), pp. 4169-4182.

Makinde, O. D. and Eegunjobi, A. S., (2013): "Effects of convective heating on entropy generation rate in a channel with permeable walls", Entropy, Vol. 15, pp. 220-233.

Motsa, S. S., Sibanda, P., Awad, F. G. and Shateyi, S., (2010): "A new spectral-homotopy analysis method for the MHD Jeffery–Hamel problem", Computers & Fluids, Vol. 39, pp. 1219–1225.

Moghimia, S. M., Ganji, D. D., Bararnia, H., Hosseini, M. and Jalaal, M., (2011): "Homotopy perturbation method for nonlinear MHD Jeffery–Hamel Problem", Computers and Mathematics with Applications, Vol. 61, pp. 2213–2216.

Moradi, A., Alsaedi, A., Hayat, T., (2013): "Investigation of Nanoparticles effect on the Jeffery-Hamel Flow", Arab J. Sci. Eng., Vol. 38, pp. 2845-2853.

Makinde, O. D., (1997): "Steady flow in a linearly diverging asymmetrical channel", Computer Assisted Mechanics and Engineering Sciences, Vol. 4, pp. 157 - 165.

Makinde, O. D. and Mhone P. Y., (2006): "Hermite-Pade' Approximation approach to Hydromagnetic flows in convergent-divergent channels", Applied Mathematics and Computations, Vol. 181, No. 2, pp. 966 – 972.

Makinde, O. D. and Mhone, P. Y., (2007): "Temporal stability of small disturbances in MHD Jeffery-Hamel flows", Computers & Mathematics with Application, Vol. 53, pp.128 – 136.

Makinde, O. D., (2008): "Effect of arbitrary magnetic Reynolds number on MHD flows in convergent-divergent channels" International Journal of Numerical Methods for Heat & Fluid Flow, Vol. 18, No. 6, pp. 697 - 707.

Moradi, A., Alsaedi, A. and Hayat, T., (2015): "Investigation of heat transfer and viscous dissipation effects on the Jeffery-Hamel flow of nanofluids", Thermal Science, Vol. 19, No. 2, pp. 563-578.

Oztop, H. F. and Abu-Nada, E., (2008): "Numerical study of natural convection in partially heated rectangular enclosures filled with nanofluids", Int. J. Heat Fluid Flow, Vol. 29, pp. 1326–1336.

Patra, R., Das, S. and Jana, R. N., (2014): "Radiation effect  on MHD fully developed mixed convection in a vertical channel with asymmetric heating", J. Applied Fluid Mechanics, Vol. 7, No. 3, pp. 503-512.

Pinarbasi, A., Coskun, O. and Selim, D., (2011): "Influence of variable thermal conductivity and viscosity for nonisothermal fluid flow", Physics of Fluids, Vol. 17, No. 3, pp. 109-114.

Padé, H., (1892): "Sur la représentation approchée d'une fonction pour des fractions rationnelles", Ann. Sci. École Norm. Sup. Suppl., Vol. 9, pp. 1-93.

Rahman, M. M., (2004): "A New Approach to Partial Differential Approximants", M. Phil thesis, Bangladesh University of Engineering & Technology, Dhaka.

Rosenhead, L., (1940): "The steady two-dimensional radial flow of viscous fluid between two inclined plane walls", Proc. R. Soc. A, Vol. 175, pp. 436-467.

Sadri, R., (1997): "Channel entrance flow", Ph.D. thesis, Dept. Mechanical Engineering, the University of Western Ontario.

Sadik, K., Almila, G., Yazicioglu, and Arif, C. G., (2011):   "Effect of variable thermal conductivity and viscosity on single phase convective heat transfer in slip flow", Heat and Mass Transfer, Vol.47, No. 8, pp. 879-891.

Sheikholeslami, M., Soleimani, S., Gorji-Bandpy, M., Ganji, D. and Seyyedi, S., (2012): "Natural convection of nanofluids in an enclosure between a circular and a sinusoidal cylinder in the presence of magnetic field", Int. Com. in Heat and Mass transfer, Vol. 39, No. 9, pp. 1435-1443.

Sahin, A. Z., (1999): "Effect of variable viscosity on the entropy generation and pumping power in a laminar fluid flow through a duct subjected to constant heat flux", Heat Mass Transfer, Vol. 35, pp. 499-506.

Senthilraja, S., Karthikeyan, M. and Gangadevi, R., (2010): "Nanofluid applications in future automobiles: comprehensive review of existing data", Nano-Micro let. Vol. 2, pp. 306-310.

Sheikholeslami, M., Ganji, D. D., Ashorynejad, H. R. and Rokni, H. B., (2012): "Analytical investigation of Jeffery-Hamel flow with high magnetic field and nanoparticle by Adomian decomposition method", Appl. Math. Mech. Engl. Ed., Vol.33, pp. 25–36.

Sheikholeslami, M., Ganji, D. D. and Rokni, H. B., (2013): "Nanofluid flow in a semi-porous channel in the presence of uniform magnetic field", Int. J. of Engineering, Vol. 26, No. 6, pp. 653-662.

Syed, T. M., Khan, U., Ahmed, N. and Sikander, W., (2015): "A study of Velocity and Temperature slip effects on flow of water based nanofluids in Converging and Diverging Channels", Int. J. Appl. Comput. Math, DOI 10.1007/s40819-015-0032-z.

Sobey, I. J. and Drazin, P. G., (1986): "Bifurcations of two-dimensional channel flows", Journal of Fluid Mechanics, Vol. 171, pp. 263 – 287.

Tyler, T., Shenderova, O., Cunningham, G., Walsh, J., Drobnik, J. and McGuire, G., (2006): "Thermal transport properties of diamond based nanofluids and nanocomposites, Diamond and related Materials", Vol. 15, No. (11-12), pp. 2078-2081.

Tendler, M., (1983): "Confinement and related transport in extrap geometry," Nuclear Instruments and Methods in Physics Research, Vol. 207, No. (1-2), pp. 233–240.

Tourigny, Y. and Drazin, P. G., (2000): "The asymptotic behavior of Algebraic approximants" Proc. Roy. Soc. London A, Vol. 456, pp. 1117-1137.

Tabanfar, S. and Modest, M. F., (1987): "Combined radiation and convection in absorbing, emitting, nongray gas-particulate tube flow", J. Heat Transfer, Vol. 109, pp. 478–484.

Van Dyke, M., (1975): "Computer extension of perturbation series in fluid mechanics", SIAM J. Appl. Math., Vol. 28, pp. 720-734.

Wernert, V., Schaf, O., Ghobarkar, H. and Denoyel, R., (2005): "Adsorption properties of zeolites for artificial kidney applications", Microporous and Mesoporous materials, Vol. 83, No. 1, pp. 101-113.

Wang, L. and Fan, J., (2010): "Nanofluids Research: key issues", Nanoscale Research Letters, Vol. 5, pp. 1241-1252.

Yasir, K., Qingbiao, W., Naeem, F. and Ahmet, Y., (2011): "The effects of variable viscosity and thermal conductivity on a thin film flow over a shrinking/stretching sheet", Computers & Mathematics with Applications, Vol. 61, No. 11, pp.3391-3399.

Yu, W., France, D. M., Routbort, J. L. and Choi, S. U. S., (2008): "Review and comparison of nanofluid thermal conductivity and heat transfer enhancements", Heat Transfer Engineering, Vol. 29, No. 5, pp. 432-460.

Yan, J. F. and Liu, J., (2008): "Nanocryosurgery and its mechanisms for enhancing freezing efficiency of tumor tissues", Nanomedicine, Vol. 4, No. 1, pp. 9-87.